Helwan
University
Faculty of Computers and Information
Computer Science Department

# Automatic Detection of Landmarks and Abnormalities in Eye Fundus Images

**Dissertation submitted to the Faculty of Computers and Information in partial fulfillment of the requirements for the award of the degree of**
**Doctor of Philosophy in Computer Science**

**Submitted By**

**Ali Mohamed Nabil Allam**

**Supervisors**

**Professor Aliaa Abdel-Halim Youssif**
Professor of Computer Science, Dean
Faculty of Computers and Information
Helwan University

**Professor Atef Zaki Ghalwash**
Professor of Computer Science, Ex-Dean
Faculty of Computers and Information
Helwan University

**2017**

---

The research described in this dissertation was carried out at the Faculty of Computers & Information – Helwan University, Cairo, Egypt.

# Abstract

The eye fundus is the only organ of the central nervous system that can be photographed directly, as it can be seen through the eye's pupil. Thereby, computer vision systems are developed with the aim of localizing and analyzing the eye fundus landmarks, namely the optic disc, blood vessels, and macula. Particularly, the optic disc segmentation is a key element in screening systems which facilitates the detection of lesions that affect the interior surface of the eye (i.e. fundus), such as glaucoma and diabetic retinopathy.

Thereby, this research aimed to provide an automated technique for detecting and segmenting the optic disc via color fundus image photography. It reviewed, categorized and compared the optic disc detection algorithms and methodologies in the literature, giving a description of each of them, highlighting their key points and performance measures. In a similar way, the research also reviewed the algorithms of detecting and segmenting the lesions that indicate the presence of some of the retinal diseases within the eye fundus images. Accordingly, the scope of this research focused on two primary goals, as noticed from the title of this dissertation: 1. Detecting and segmenting the optic disc landmark and 2. Detecting and segmenting the bright abnormalities.

Hence, the first part of this research proposed an automated technique for segmenting the optic disc, a structural landmark in all eye fundus images. First, the fundus image was preprocessed in order to estimate the approximate location of the optic disc, excluding the positions that doubtfully contain the optic disc. Consequently, the top candidates for the optic disc were nominated based on the spatial characteristics of the optic disc, and then these candidates were ranked according to their circularity strengths. Afterwards, the vessels density within each candidate was computed and then weighted according to the candidate's strength, in which the top-scoring candidate was chosen to be the segmented optic disc.

Using MATLAB, the proposed approach for segmenting the optic disc was implemented and evaluated over nine diverse datasets containing a total of 1937 images of heterogeneous imaging settings. The segmentation algorithm proved its effectiveness by detecting the optic disc correctly in 1835 images achieving a total sensitivity of 94.73% which was comparable to the results achieved by the other approaches. But more importantly, the implementation

of the segmentation algorithm was automated regardless of the extreme heterogeneity of the tested datasets; as no image-dependent parameters were tuned, nor predefined templates were used for the sake of customizing the proposed algorithm over certain datasets.

The second part of this research also proposed an automated technique for detecting and segmenting the abnormalities that may be confused with the optic disc due to their similar look and appearance, such as exudates and cotton wool spots. Initially, the fundus image was preprocessed by transforming it into the $L^*a^*b^*$ color space which has the ability to quantify and decouple the chromaticity (color information) of the fundus image. Next, the fundus image was partitioned into clusters based on the chromaticity information via the unsupervised k-means algorithm. Among the clustered images, the one having the highest mean intensity was chosen to be the best cluster containing the bright objects like the optic disc, hard exudates, and cotton wool spots, etc. Using this selected cluster, a threshold value was estimated via statistic-based metrics, and subsequently applied in order to remove any non-bright clustered pixels and preserve only the relatively bright ones within the image. Finally, the optic disc was excluded and erased from the thresholded image along with the pixels connected to it, leaving out only the pixels that represent the bright abnormalities.

The aforementioned approach for segmenting bright abnormalities was implemented and evaluated over a total of 1419 images retrieved from three specific datasets: DIARETDB0, DIARETDB1, and MESSIDOR, which are the only ones among all the datasets that provided the ground truths of the different types of abnormalities occurring in diabetic retinopathy. The proposed system correctly detected the bright abnormalities, such as hard exudates and cotton wool spots, achieving an average sensitivity and specificity of 85.08% and 56.77%, respectively, over the 1419 fundus images.

# Declaration

I declare that the work in this dissertation was carried out in accordance with the *Regulations of Helwan University*. The work is original except where indicated by special reference in the text and no part of the dissertation has been submitted for any other degree.

The dissertation has not been presented to any other academic institute for examination either in the Arab Republic of Egypt or abroad.

**Ali M. N. Allam**

## List of Scholarly-Indexed Publications

**In International Conference Proceedings:**

**[1]** A. M. N. Allam, A. A. Youssif, and A. Z. Ghalwash, “Optic Disc Segmentation by Weighting the Vessels Density within the Strongest Candidates,” in *Proceedings of 2016 SAI Computing Conference*, pp. 91-99, London, United Kingdom, July 2016. DOI: 10.1109/SAI.2016.7555967
Accessible at: http://ieeexplore.ieee.org/document/7555967/

**In Peer-reviewed International Journals:**

**[2]** A. M. N. Allam, A. A. Youssif and A. Z. Ghalwash, “Segmentation of Exudates via Color-based K-means Clustering and Statistical-based Thresholding,” *Journal of Computer Science,* Science Publications, vol. 13, no. 10, pp. 524-536, October 2017. DOI: 10.3844/jcssp.2017.524.536
Accessible at: http://thescipub.com/PDF/jcssp.2017.524.536.pdf

**[3]** A. M. N. Allam, A. A. Youssif and A. Z. Ghalwash, “Automatic Segmentation of Optic Disc in Eye Fundus Images: A Survey,” *Electronic Letters on Computer Vision and Image Analysis,* vol. 14, no. 1, pp. 1-20, Barcelona, Spain, September 2015. DOI: 10.5565/rev/elcvia.680
Accessible at: http://elcvia.cvc.uab.es/article/view/680

# Acknowledgments

I would like to express my deep appreciation to all those who gave me the support to complete this research. I am sure that my success in finishing this work would make them proud and delighted.

Foremost, I wish to express my deepest gratitude and recognition to my supervisor and mentor, Professor Aliaa Youssif. Her encouragement, advice and example, on both a professional and personal level since the first day I stepped into Helwan University, provided a sterling impetus on my own professional development for which I will always be indebted.

I also owe my supervisor, Professor Atef Ghalwash, great thanks and appreciation for his support and for providing me with additional encouragement through the high standards and perseverance he set in his own scientific endeavors. Thank you so much dear professor.

My special thanks go to my bosses at work, Professor Tareq Abdeen and Dr. Nermeen Magdi, as well as my ex-boss Dr. Essam Elfakharany. You all deserve gratitude for creating a unique atmosphere of trust and cooperation on both academic and non-academic bases.

Special appreciation and thanks is also due to my true friends, Ahmad Maher, Ahmad Yehia, Hussein Mowafak, Karim Tarek, and Mohamad Halawa, for their moral support which made me pass all the hard times. Thank you guys for this wonderful and endless friendship.

Finally, saving the best for last, I wish to give my heartfelt gratitude and love to my father (may Allah bless his soul), my mother and my brother for their encouragement and support throughout my whole life. Your continuous and limitless support will be deeply cherished all my life through. Words would never express my gratitude.

**Thanks to all.**

**Ali Allam**

# Table of Contents

# List of Figures

# List of Tables

# Glossary & Abbreviations

**Age-related Macular Degeneration (AMD)**: a deterioration or breakdown of the eye's ***macula*** among people aged 50 and more. There are two types of macular degeneration: dry and wet. The most common type is the dry AMD where tiny yellow or white pieces of fatty protein called ***drusen*** form under the ***retina***. Wet macular degeneration occurs when abnormal ***blood vessels*** begin to grow underneath the retina (i.e. ***neovascularization***). These vessels can leak fluid and blood, which may lead to swelling and damage of the macula (i.e. ***macular edema***).

**Aneurysms / Microaneurysms (MA):** small bulges in ***blood vessels*** of the ***retina*** that often leak fluid.

**Arteriosclerosis:** a series of changes in the ***retina*** characterized by bleeding in the retina, thick fluid oozing from the retina, impaired oxygenation of the retina, an abrupt reduction of blood flow to the heart muscle that may cause dying off of tissue, and hardening of the walls of the little arteries (arterioles) in the eye.

**Blood Vessels (BV) / Vasculature:** the two main types of blood vessels responsible for the eye's blood supply are the arteries and veins. Arteries carry fresh blood from the heart and lungs to the eye while veins take away the blood that has been used by the eye and return it to the lungs and heart to be refreshed with oxygen and other nutrients. The arteries appear brighter and slightly narrower than the veins.

**Drusen:** tiny yellow or white pieces of fatty protein usually scattered around the ***fovea*** which is caused by ***age-related macular degeneration***.

**Exudates (EX):** deposits of cholesterol or other fats from the blood that have leaked into the ***retina***. There are two types of exudates: hard exudates and soft exudates (also called cotton wool spots).

**Fovea:** a depression in the ***retina*** that contains only cones (not rods) and that provides accurate focused eyesight.

**Glaucoma:** a disease that damages the eye’s optic nerve and can result in vision loss and blindness. It is characterized by the cupping of the ***optic disc*** which becomes ischemic due to the imbalance between the intraocular pressure and the perfusion pressure in the ***blood vessels*** of the ***retina***.

**Hemorrhages (HM):** a disorder of the eye in which bleeding leaks into the ***retina*** forming tiny blood spots.

**Macula:** a part of the eye close to the center of the ***retina*** responsible for central vision which allows us to see objects with great detail.

**Macular Edema**: swelling or thickening of the ***macula*** caused by fluid leaking from the retinal ***blood vessels***. The macula does not function properly when it is swollen.

**Neovascularization (NV):** abnormal formation of new small ***blood vessels*** which contributes to visual loss in several ocular diseases, the most common of which are ***proliferative diabetic retinopathy***, ***age-related macular degeneration***, and ***retinopathy of prematurity***.

**Non-proliferative Diabetic Retinopathy (NPDR):** the earliest stage of diabetic retinopathy. With this condition, damaged ***blood vessels*** in the ***retina*** begin to leak extra fluid causing ***macular edema***, and small amounts of blood into the eye (i.e. ***microaneurysms***). Sometimes, deposits of cholesterol or other fats from the blood may leak into the retina (i.e. ***exudates***).

**Optic Disc (OD) / Optic Nerve Head (ONH):** a circular area where the optic nerve enters the ***retina***; it does not contain receptors itself, and is thus the blind spot of the eye.

**Proliferative Diabetic Retinopathy (PDR):** a disease that mainly occurs when many of the ***blood vessels*** in the ***retina*** close, preventing enough blood flow. In an attempt to supply blood to the area where the original vessels closed, the retina responds by growing new blood vessels (i.e. ***neovascularization***). However, these new blood vessels are abnormal and do not supply the retina with proper blood flow. The new vessels are also often accompanied by scar tissue that may cause the retina to wrinkle or detach (i.e. retinal detachment).

**Retina:** the tissue where the image is projected since it receives images formed by the lens and converts them onto signals that reach the brain by the means of the optic nerve. It contains light sensitive cells called cones and rods, which are responsible for daytime and night vision, respectively.

**Retinopathy of Prematurity:** a disease that affects immature ***vasculature*** in the eyes of premature babies. It can be mild with no visual defects, or it may become aggressive with new blood vessel formation (i.e. ***neovascularization***) and progress to retinal detachment and blindness.

# Chapter 1. Introduction

Ophthalmologists can diagnose eye diseases using images of the eye fundus which is photographed directly through the eye's pupil via a specialized low-power microscope with an attached camera. Thereby, computer vision systems are developed in order to localize and analyze fundus landmarks, namely the optic disc (i.e. optic rim and optic cup), the retinal blood vessels (i.e. arteries and veins), and the macular region (i.e. macula and fovea). This computer-aided image analysis, in turn, facilitates the detection of retinal lesions and abnormalities that result in slight-to-major changes of the eye fundus, such as exudates, aneurysms, hemorrhages, neovascularization, macular edema, notching, etc.

## 1.1. Ophthalmological Background

### 1.1.1. Eye Anatomical Structure

Fundus, Latin for the word "bottom", is an anatomical term referring to the portion of an organ opposite from its opening. Hence, the fundus of the eye is the interior surface of the eye, opposite the lens, and which includes the retina, optic disc, blood vessels, macula and fovea [1]. Moreover, the eye fundus is the only organ of the central nervous system of the human body that can be imaged directly since it can be seen and captured through the pupil of the eye [1], [2].

Therefore, numerous numbers of fundus images are analyzed by ophthalmologists all over the world, and over the past two decades, experts have been applying digital image processing techniques to ophthalmology with the main aim of improved diagnosis of various diseases that affect the eye such as glaucoma, diabetic retinopathy, neovascularization, age-related macular degeneration, arteriosclerosis, etc.

Figure 1-1 illustrates the anatomical structure of the human eye [3], in which some of the functions performed by the interior surface of the human eye are described below:

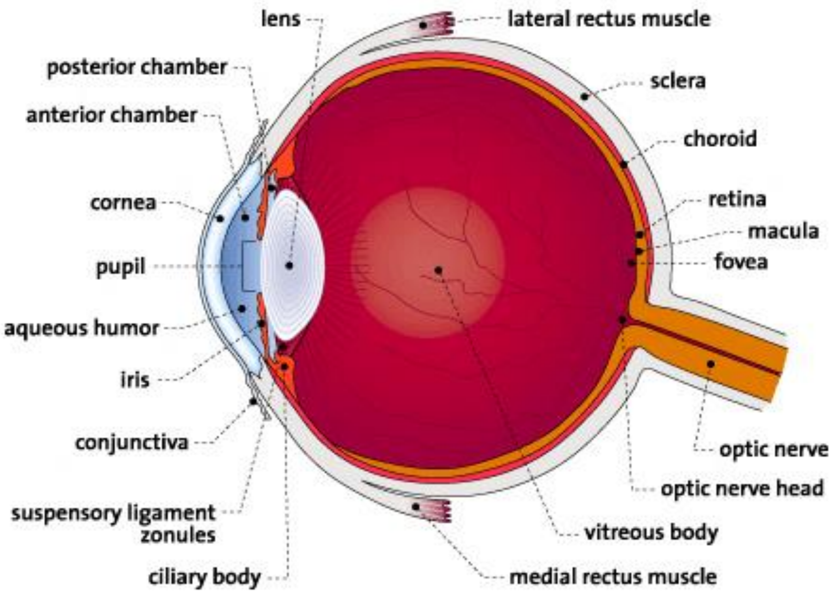

**Figure 1-1. Anatomical structure of the human eye**

i. **Retina:** contains light sensitive cells called cones and rods, which are responsible for daytime and night vision, respectively; the retina is the tissue where the image is projected since it receives images formed by the lens and converts them onto signals that reach the brain by the means of the optic nerve.
ii. **Optic Nerve Head (ONH):** commonly referred to as the optic disc and sometimes as the optic papilla. It is a circular area where the optic nerve enters the retina coming from the brain, and which does not contain receptors itself, and is thereby the blind spot of the eye.
iii. **Macula and Fovea:** the macula it is a part of the eye close to the center of the retina which allows us to see objects with great detail. The fovea is a depression in the retina that contains only cones (not rods), and which provides accurate focused eyesight.
iv. **Blood Vessels:** like the rest of the human body, arteries and veins are the two main types of blood vessels responsible for the eye's blood supply. Arteries carry fresh blood from the heart and lungs to the eye while veins take away the blood that has been used by the eye and return it to the lungs and heart to be refreshed with oxygen and other nutrients.

### 1.1.2. Imaging Modalities

An imaging modality, in general, is an imaging system which uses a particular technique in order to detect different physical signals arising from a patient and produce images. The following modalities belong to the broad category of ophthalmological photography [4], [5]:

i. **Color Fundus Photography:** the interior surface of the eye (i.e. retina, vasculature, optic disc and macula) is captured using a specialized low-power microscope with an attached camera. Moreover, in stereo fundus photography, image intensities represent the amount of reflected light from two or more different view angles for depth resolution.

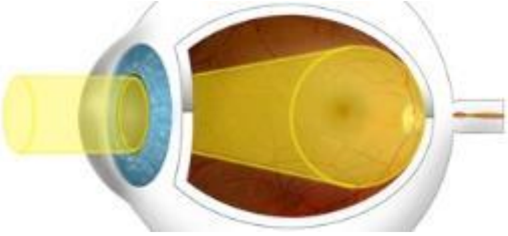

**Figure 1-2. Fundus photography**

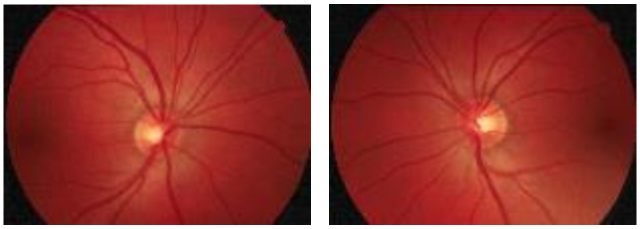

**Figure 1-3. Images produced via fundus photography**

ii. **Fluorescein Angiography (FA) / Indocyanine Green Angiography (ICG):** a grayscale image is produced where the blood flow within both, the retina and the choroid, is captured by injecting fluorescein dye and indocyanine dye, respectively, in the blood vein.

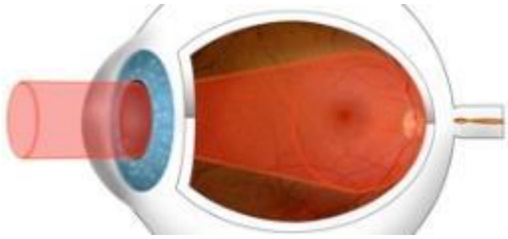

**Figure 1-4. Fluorescein / ICG angiography**

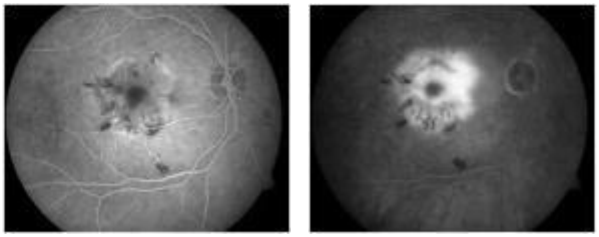

**Figure 1-5. Images produced via angiography**

iii. **Fundus Auto Fluorescence (FAF):** the retina is illuminated with blue light which causes certain cellular components to glow without injecting any dye in the blood veins.

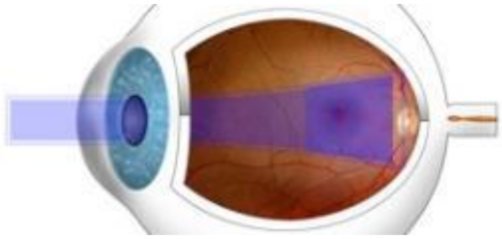

**Figure 1-6. Fundus auto fluorescence (FAF)**

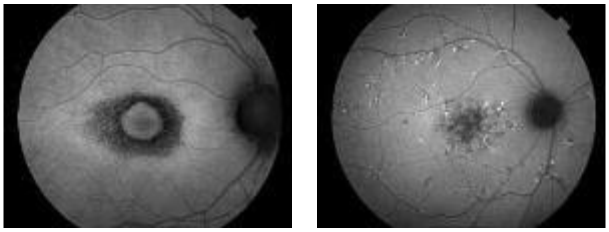

**Figure 1-7. Images produced via FAF**

iv. **Confocal Scanning Laser Ophthalmoscopy (CSLO):** commercially, this imaging modality is known as Heidelberg Retina Tomography (HRT). It uses a special laser beam that is focused on the surface of the optic nerve in order to precisely capture a 3D image of the optic disc and the surrounding retina. HRT is a powerful diagnostic tool for glaucoma in particular.

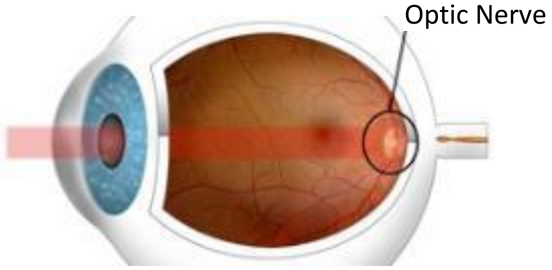

**Figure 1-8. Heidelberg Retina Tomography**

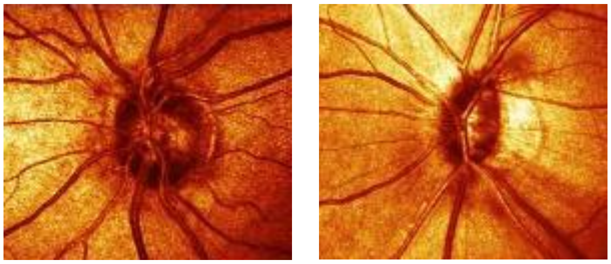

**Figure 1-9. Images produced via HRT**

v. **Optical Coherence Tomography (OCT):** Precisely, OCT is not literally considered a *"fundus imaging"* modality, as it is analogous to ultrasound except that it utilizes light instead of sound. OCT scan is used to capture the thickness of the retinal tissue by measuring the flight time of the originated backscatter. Thereby, it is well-suited to monitor pathological conditions such as macular edema which leads to the swelling or thickening of the macula.

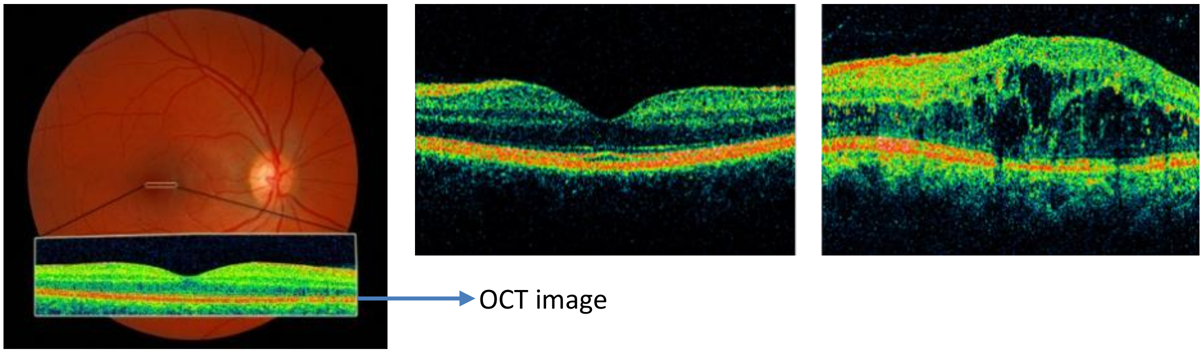

**Figure 1-10. Images produced via OCT**

### 1.1.3. Eye Fundus Image

While the function performed by each part of the fundus was described in section 1.1.1, the following text briefly describes the semblance and characteristics of each of these fundus landmarks. Figure 1-11 shows a labeled color fundus image of a healthy human eye (i.e. without lesions), produced via color fundus photography.

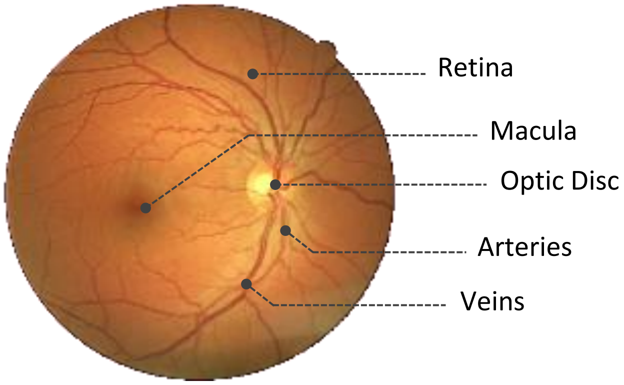

**Figure 1-11. Color fundus image**

i. **Retina:** the color of the retina varies naturally according to the color of the light employed; however, the color of the fundus may be described as ranging from orange to vermillion [2].
ii. **Optic Nerve Head (Optic Disc):** it is located towards the left-side or the right-side of a fundus image. It is round or vertically oval in shape, measuring about one-tenth to one-sixth the fundus diameter (about 2mm). It typically appears as a bright yellowish or whitish area where large blood vessels are found in the vicinity of the optic disc [2], [6].
iii. **Macula & Fovea:** the fovea, which falls at the center of the area known as the macula, is an oval-shaped, blood vessel-free reddish spot. It is approximately 5mm away from the center of the optic disc (equal to about 2.5 times the diameter of the optic disc) [2].
iv. **Blood Vessels:** the major branches of the retinal vasculature originate from the center of the optic disc to the four quadrants of the retina. In the macular region, all the vessels arch around, sending only small branches towards the vascular fovea area. The arteries appear with a brighter red color and are slightly narrower than the veins [2].

## 1.2. Motivation of Fundus Image Processing

The majority of works dealing with fundus image processing can be classified into two broad categories:

### 1.2.1. Automated Segmentation of Landmarks

The process of locating and subdividing an image into its constituent regions or objects is called segmentation. Hence, the eye fundus is being segmented in order to locate and isolate the fundus landmarks, namely the optic disc, macular region, and retinal blood vessels.

i. **Optic disc segmentation:** the optic disc is a key landmark in retinal images, and shows changes related to diseases including glaucoma and diabetic retinopathies. The optic disc also serves as a landmark in order to locate other fundus features such as the macula and central blood vessels [6] as discussed earlier in section 1.1.3.

ii. **Macula segmentation:** locating the macula is important in detecting related diseases such as age-related macular degeneration and macular edema [7].

iii. **Vessels segmentation:** analyzing the shape, size, and color of the blood vessels in the retina is important for detecting diseases of blood circulation such as neovascularization, arteriosclerosis and occlusion.

### 1.2.2. Automated Detection of Abnormalities

Identifying the abnormalities within the eye fundus assists ophthalmologists to diagnose, predict and monitor the progress of, the disease that a patient suffers from.

i. **Disease diagnosis:** refers to detecting the abnormal symptoms in the retina such as exudates, aneurysms and hemorrhages in order to diagnose diseases that affect the eye such as diabetic retinopathy, glaucoma, macular edema, etc.

ii. **Disease prediction:** refers to the early observation of retinal disorders that may lead to other serious pathological conditions or vision loss (blindness).

iii. **Disease progress monitoring:** concerned with comparing the changes of the states in the eye fundus at particular intervals of time in order to observe either the improvement or deterioration of some disease.

## 1.3. Architecture of Fundus Image Processing

Figure 1-12 overviews the general high-level architecture of fundus image processing showing the data which is employed, the steps which are followed and the procedures which are applied in processing the eye fundus images [8].

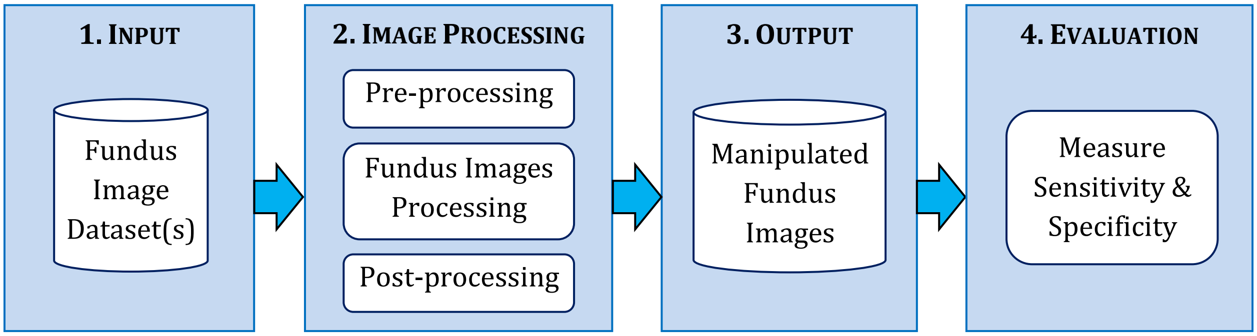

**Figure 1-12. Architecture of fundus image processing**

Each of the four modules of the shown architecture is briefly described below, and then reviewed in detail in the subsequent sections:

**i. Input – fundus image datasets** (section 1.3.1): refers to one set or more of fundus images that constitute the input data to be processed.

**ii. Image Processing** (section 1.3.2): this is the backbone of the system architecture which is composed usually of three sub-processes in order to manipulate the raw fundus images and convert it to a set of meaningful images (e.g. diagnosing a fundus image that suffers from a particular disease):

- Preprocessing: a preliminary step that normally aims to enhancing and preparing the input image (e.g. contrast, sharpness and illumination of the image, etc.).
- Fundus images processing: the main objective of processing the fundus image normally aims to the segmentation of the image which is the process of isolating particular regions of interest within the image [9]. Regions of interest (ROI) may include retinal abnormalities (e.g. exudates, hemorrhages, aneurysms, etc.), and may also include the retinal landmarks (e.g. optic disc, macula, and vascular tree) as discussed earlier at section 1.2.
- Post-processing: refers to the last processing step that aims to describing, marking or classifying (i.e. annotating) the objects that were segmented in the fundus image.

**iii. Output – manipulated fundus images** (section 1.3.3): the output set of images which refers to the fundus images after being enhanced, processed and then annotated.

**iv. Evaluation** (section 1.3.4): the accuracy of experimental results is usually measured by two main metrics, sensitivity and specificity. Sensitivity is the true positive rate of detecting the ROI, whereas specificity is the true negative of confirming the absence of the ROI.

### 1.3.1. Fundus Image Datasets

Table 1-1 is an alphabetical list of the most widely used datasets of fundus images employed for image processing, which are described in detail at section 2.1, on the next chapter. The table differentiates between each dataset and another from the perspective of: 1. the size of the dataset, 2. field of view (FOV) which indicates the observable extent of the captured fundus, 3. image size, 4. images format, and 5. the ground truth provided with the dataset. The ground truth provides the means of evaluating the experimental results achieved by some algorithm using the true results provided usually by medical experts.

**Table 1-1. Fundus images datasets**

| Dataset Name, (Release Date) | Dataset Size | FOV | Image Size (pixels) | Images Format | Ground Truth |
|---|---|---|---|---|---|
| ARIA, (2006) [10], [11] | 143 images (three sets) | 50° | 768×576 | TIFF | OD, BV and Fovea |
| DIARETDB0 [12] (2006) | 130 images | 50° | 1500×1152 | PNG | MA, HM, HE, CWS and NV |
| DIARETDB1 (2007) [13] | 89 images | 50° | 1500×1152 | PNG | MA, HM, HE, CWS and NV |
| DRIONS-DB, (2008) [14] | 110 images | - | 600×400 | JPG | OD |
| DRIVE, (2004) [15] | 40 images (two sets) | 45° | 565×584 (both sets) | TIFF | BV |
| HRF, (2009) [16] | 45 images (three sets) | 45° | 3504×2336 (all three sets) | JPG | BV |
| MESSIDOR, (2014) [17] | 1200 images (three sets) | 45° | Set (1): 1440×960<br>Set (2): 2240×1488<br>Set (3): 2304×1536 | TIFF | Grading of Diabetic Retinopathy and Macular Edema |
| ONHSD, (2004) [18] | 99 images | 45° | 760×570 | BMP | OD |
| STARE, (2000) [19] | 397 images | 35° | 700×605 | PPM | OD and BV |

**FOV**≡ field of view, **OD**≡ optic disc, **BV**≡ blood vessels, **MA**≡ microaneurysms, **HM**≡ hemorrhages, **HE**≡ hard exudates, **CWS**≡ cotton wool spots, **NV**≡ neovascularization

### 1.3.2. Image Processing Functions

As mentioned before, image processing is the main module of the system architecture which includes three sub-components in order to manipulate the dataset of the captured retinal images and convert it to a set of meaningful images. The input image is first enhanced, then segmented, and finally annotated. Software packages such as MATLAB®, OpenCV®, and ImageJ® provide powerful means for implementing these image processing functions. The following part briefly overviews the main image processing functions that can be used for the enhancement and segmentation of images, which will be discussed later in details at Chapter 2 within the context of the literature review.

**Step (1) – Preprocessing: Image Enhancement**

Image enhancement is the initial process of manipulating a raw image so that the result would be more suitable than the original for a specific application or further processing [9]. Below are some of the major enhancements that can be applied either solely or combined together with one another:

i. **Color image processing:** since the captured fundus image is a full-color image, it is obvious that color image processing techniques are strongly needed. For example, color splitting can be used to view and process each of the red, green, blue channels independently from one another [20]. Also, conversion between the (RGB) and (HIS, HSV, L*a*b*) color models is very useful in many situations; unlike the RGB color space, HSI, HSV, and Lab models decouple the color (chromaticity) and gray-scale (intensity) information, HSI and HSV represent the intensity within the (I) and (V) layers, respectively, while chromaticity is represented within both the Hue (H) and Saturation (S) layers. As for the L*a*b* color space, the L* represents the luminosity (intensity), while the a* and b* layers represent the chromaticity. Therefore, it is sometimes more useful to process an image using color models such as HSI, HSV, or L*a*b* color models rather than the RGB model [9].

ii. **Contrast enhancement:** when the contrast of the captured image is too low, it is difficult to detect and isolate objects of interest. Therefore, brightening or darkening a low-contrast image can be achieved by stretching (spreading) the histogram of that image through approaches such as histogram equalization and histogram specification. Moreover, in order to stretch the contrast of a full-color image, it is logical to spread the color intensities uniformly, leaving the colors themselves unchanged; therefore, as mentioned in the previous paragraph, the HSI color space is ideally suitable for color histogram processing [9].

iii. **Luminosity equalization:** the non-uniform illumination in the retina makes the typical analysis of retinal images impractical and useless. Thus, in order to overcome the uneven illumination, each pixel of the image is corrected and equalized [6], [21].

iv. **Filtering:** spatial linear filters (e.g. mean filter) as well as non-linear filters (e.g. median filter) are used for image smoothing and noise removal. Conversely, first derivative filters (e.g. Prewitt and Sobel filters) as well as second derivative filters (e.g. Laplacian filter) are used for image sharpening (i.e. deblurring) as well as the detection of edges, lines and points. Moreover, an image can be also filtered in the frequency domain in order to smoothen and sharpen it via using low-pass filters and high-pass filters, respectively [9].

v. **Background subtraction:** masks are created and used to exclude the background of the image from further calculations and processing. In other words, only the pixels belonging to the semi-oval retina are included for processing [6].

vi. **Morphological processing:** this technique can be applied as an image enhancement technique as well as an image segmentation technique. The two fundamental operations of morphological processing are dilation and erosion; in which dilation leads to thickening the original object, whereas erosion is an inverse procedure in which an object is thinned. Moreover, erosion and dilation can be applied together after one another and in a reversed order as well, in order to achieve opening and closing, respectively. Opening generally removes small objects from an image while preserving the shape and size of large objects in the image; whereas closing generally merges narrow breaks or gaps and eliminates small holes in the image [20], [9].

vii. **Datasets conversion:** a scale factor is calculated and used to convert the spatial resolution between datasets with different field of views (FOVs). For instance, a scale factor of 0.76 is used to convert between the STARE and DRIVE datasets [21] which have FOVs of 35 and 45 degrees, respectively.

**Step (2) – Processing: Image Segmentation**

As stated previously, the main objective of processing the fundus image typically aims to the segmentation of the objects within an image. Segmentation is an essential step prior to the classification and description of the lesions or landmarks in a fundus image. The main methods of image segmentation reviewed in the literature are:

i. **Region-based methods:** the objective of such methods is to produce connected regions, based on similarity, that are as large as possible (i.e. produce as few regions as possible) allowing some flexibility within each region [20]. For example, region-growing, as its name implies, groups the seed pixels or sub-regions into larger similar regions based on predefined criteria of growth (such as specific ranges of color) [9].

ii. **Boundary-based methods:** the objective of such methods is to determine a closed boundary, based on differences and discontinuities, such that an inside object (e.g. optic disc) and an outside boundary (edge) can be defined [20]. Gradient operators (e.g. Prewitt and Sobel kernels), the Laplacian, Laplacian of Gaussian (LoG), Difference of Gaussians (DoG) and the Canny edge detector are some of the methods of detecting image boundaries (edges) [9].

iii. **Color-based methods:** in order to segment an image based on color, the segmentation technique can be carried out on either the HSI color space or the RGB color space. It is intuitive to use the HSI space because color is conveniently represented in the hue plane (H), and saturation (S) is typically used as a masking image in order to isolate further regions of interest in the hue image, while the intensity (I) is used less frequently for segmentation of color images because it carries no color information. However, better results can be obtained using the RGB color vectors by measuring and comparing the Euclidean distance between an RGB pixel and a specified color range [9].

iv. **Active contour (snakes):** the main aim of active contour models or snakes is to evolve a curve in order to detect objects in an image. For instance, starting with an initial curve around the object to be segmented within an image, the curve (i.e. snake) is pulled toward nearby features (i.e. local minima) such as lines and edges, locating them accurately [22], [23].

v. **Matched filters:** a matched filter describes the expected appearance of a desired object or region of interest for purposes of comparative modeling. Thus, the segmentation process is carried out by isolating the region (pixels) having the least accumulated difference compared to the matched filter [6].

vi. **Thresholding:** an image is easily and speedily segmented by selecting a threshold which partitions images directly into regions based on intensity values and/or properties of these values. Global thresholding and local thresholding are two types of thresholding that may be applied to an image; global thresholding is a segmentation technique that uses a constant threshold over the entire image, whereas local (variable) thresholding uses a variable threshold that changes over an image based on the properties of a neighborhood (e.g. average intensities of a neighborhood) [9].

vii. **Morphological Watershed:** the watershed transform is a powerful segmentation tool that aims to isolate and separate the touching objects within an image. Segmenting an image via watershed is a two-step process; first, finding the markers and the segmentation criterion used to split the regions which is most often the contrast or gradient. Second, performing a marker-controlled watershed with these two elements in order to control over-segmentation [9], [24], [25].

**Step (3) – Post-processing: Image Description**

After the eye fundus image has been preprocessed and segmented, either the external boundary or the internal skeleton of the recognized region is marked, classified or annotated with the appropriate description, automatically.

### 1.3.3. Manipulated Fundus Images

The manipulated fundus images constitute the output dataset which refers to the fundus images after being enhanced, processed and then annotated. These manipulated fundus images are compared to the ground truth in order to evaluate the accuracy of experimental work as explained in the following section.

### 1.3.4. Evaluation Metrics

The experimental work is typically assessed using the sensitivity and specificity measures which are also sometimes referred to as recall and precision, respectively. Sensitivity is a measure that reflects the probability of a positive response for the cases in which the landmark or abnormality is present, whereas specificity is the probability of negative response for the cases in which the landmark or abnormality is absent. The higher the sensitivity and specificity values was, the better the diagnosis [13]. These two evaluation metrics, sensitivity and specificity, can be computed as follows:

$$\boldsymbol{Sensitivity} = \frac{\boldsymbol{T_P}}{\boldsymbol{T_P + F_N}} \qquad \textbf{\textit{Equation 1-1}}$$

$$\boldsymbol{Specificity} = \frac{\boldsymbol{T_N}}{\boldsymbol{T_N + F_P}} \qquad \textbf{\textit{Equation 1-2}}$$

where,

$\boldsymbol{T_P}$ (true positive): correct response to detecting the presence of an object (i.e. hit).

$\boldsymbol{T_N}$ (true negative): correct response to identifying the absence of an object (i.e. correct rejection).

$F_P$ (false positive): incorrect response to identifying the absence of an object (i.e. false alarm).

$F_N$ (false negative): incorrect response to detecting the presence of an object (i.e. miss).

$T_P + F_N$: total number of objects that are present.

$T_N + F_P$: total number of objects that are non-present.

## 1.4. Research Work

The research work proposed within this dissertation is concerned to be S.M.A.R.T. [26]; that is to be **s**pecific, **m**easurable, **a**chievable, **r**elevant and **t**ime-constrained. The following figure illustrates and highlights the scope of this research done within each stage of fundus image processing:

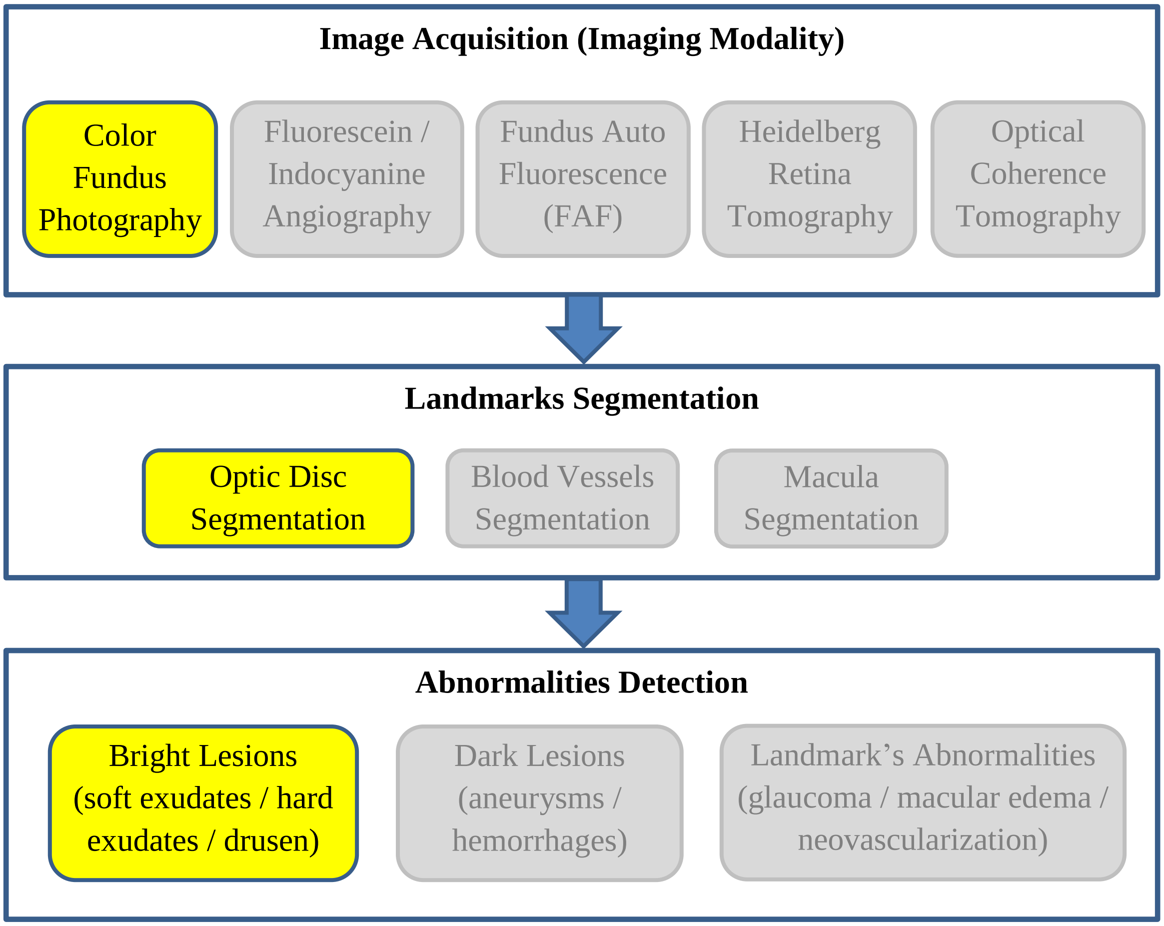

**Figure 1-13. Scope of research work**

### 1.4.1. Aims and Objectives of Research

This research aims mainly to detect and segment one of the major landmarks in the fundus images which is the optic nerve head (i.e. optic disc). It also aims to the detection of particular lesions associated with retinal pathological conditions which significantly change the normal appearance and semblance of the fundus. Therefore, in order to reach the aforementioned aims, the main objectives of this research are to:

i. Employ a dataset of fundus images that act as a test bed on which digital image processing techniques are applied and assessed.
ii. Exploit image processing techniques that enhance the original fundus images in order to make them more suitable for further image processing.
iii. Investigate and propose image processing techniques in order to isolate and localize fundus landmarks, namely the optic disc.
iv. Identify the bright abnormal features in the fundus with respect to the normal fundus anatomy in order to detect the lesions that the eye fundus suffers from.
v. Examine the efficiency of the achieved results using the ground truth of the employed dataset in order to assess the proposed techniques compared to other ones.

### 1.4.2. Research Methodology

The research methodology is mainly based on employing many of the publicly available image datasets. The chosen datasets act as a benchmark in order to provide robust evaluations and consistent comparisons against other methods using the ground truth accompanied with the dataset. The ground truth provides a means of evaluating the experimental results achieved by some algorithm using the true results provided usually by ophthalmologists on an image set.

### 1.4.3. Organization of Dissertation

This research is organized into five main chapters followed by a glossary of the medical terminologies mentioned in the dissertation, and ended with the appendices that present additional information not directly included within the research, as well as a list of references cited in the research. Chapter 2 is mainly concerned with reviewing pertinent literature related to various aspects of medical image analysis research, particularly in the field of ophthalmology. The chapter reviews and compares the methods and algorithms used to enhance fundus images, as well as the techniques used for the detection of retinal abnormalities and the segmentation of fundus landmarks. Following the literature review, Chapter 3 presents the proposed system architecture and describes each of its components along with the proposed methods, techniques and algorithms used to carry out and implement these components. Chapter 4 lays out the experimental results obtained during the course of this work. At the end of this research, Chapter 5 forms the conclusion obtained by the research and outlines a direction for the work that could be done in the future.

# Chapter 2. Literature Review

This chapter presents a review of the pertinent literature that runs along a parallel vein to this research. The literature review starts with presenting the most widely used image datasets, passing through the evaluation metrics used for segmentation assessment, and ending with a detailed review of the image preprocessing and segmentation approaches for segmenting the key landmark of the eye fundus, the optic disc. It also reviews the methods of detecting abnormalities occurring within the eye fundus image which in turn help in diagnosing eye diseases.

## 2.1. Fundus Image Datasets

The fundus images are considered the raw material to be enhanced, segmented and evaluated. The image datasets are normally accompanied with a ground truth which acts as a benchmark for comparing and evaluating the achieved experimental results using the true results of that image set. Table 1-1 provided a brief description of the most widely used publicly available datasets, which are described in more details in the following subsections:

### 2.1.1. ARIA

- **Dataset description:** ARIA (Automated Retinal Image Analysis) [10], [11] aimed to provide an automated image analysis platform for predicting eye diseases. The dataset contained a total of 143 images with FOV of 50 degrees at resolution of 768×576, which were stored as uncompressed TIFF files. The dataset was organized into three groups (subsets), including 23 images of age-related macular degeneration, 61 healthy images, and 59 diabetic images.
- **Ground truth:** Two image analysis experts traced out the blood vessels in the images of all three subsets. Besides, the locations of the optic disc and fovea were also marked in 120 images within the healthy and diabetic groups, as shown in the following figure.

**Figure 2-1. Example of a fundus image and its associated ground truth in ARIA**

### 2.1.2. DIARETDB0

- **Dataset Description:** DIARETDB0 (Standard Diabetic Retinopathy Database Calibration Level 0) [12] contained 130 fundus images, of which 22 were normal and 108 contained signs of diabetic retinopathy. The fundus images were captured using a digital fundus camera of 50° field of view in which each image was of size of 1500×1152 pixels in PNG format.
- **Ground truth:** Each fundus image had a corresponding text file that listed the types of abnormalities occurring in that image, accompanied with a labeled image that marked these abnormalities within 50 images of the whole dataset. These abnormalities included the five main indicators of diabetic retinopathy, namely, the red small dots, hemorrhages, hard exudates, soft exudates, and neovascularization. This ground truth of DIARETDB0 was aggregated and illustrated at Appendix A.1 in a tabular layout.

```
redsmalldots hemorrhages hardexudates n/a n/a
```

**Figure 2-2. Example of a fundus image and its associated ground truth in DIARETDB0**

### 2.1.3. DIARETDB1

- **Dataset Description:** DIARETDB0 was furtherly extended by another dataset, DIARETDB1 (Standard Diabetic Retinopathy Database Calibration Level 1) [13]. DIARETDB1 contained 89 color fundus images of which 84 contained signs of diabetic retinopathy, and 5 only were considered as non-diabetic fundus images. The fundus images were acquired and stored using the same imaging settings used in its predecessor, DIARETDB0.
- **Ground truth:** Each fundus image was associated with a corresponding xml file that showed all finding types occurring in an image, observed by four different experts with a certainty/confidence degree (i.e. high, medium, low), as well as their location coordinates. Similar to DIARETDB0, these finding types included the five main indicators of diabetic retinopathy. Besides, the optic disc was occasionally marked by some of the experts within some of the images. Appendix A.2 illustrates an excerpt of the ground truth which was restructured and aggregated in a more readable tabular format.

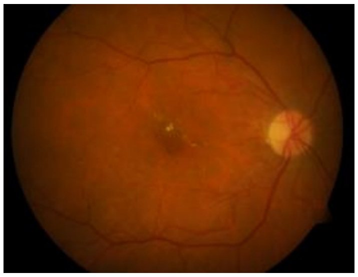

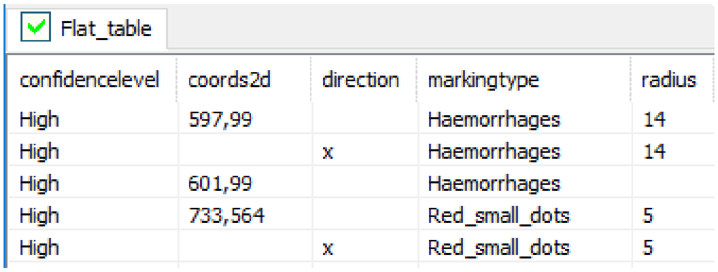

| confidencelevel | coords2d | direction | markingtype | radius |
|---|---|---|---|---|
| High | 597,99 |  | Haemorrhages | 14 |
| High |  | x | Haemorrhages | 14 |
| High | 601,99 |  | Haemorrhages |  |
| High | 733,564 |  | Red_small_dots | 5 |
| High |  | x | Red_small_dots | 5 |

**Figure 2-3. Example of a fundus image and its associated ground truth in DIARETDB1**

### 2.1.4. DRIONS-DB

- **Dataset description:** DRIONS-DB (Digital Retinal Images for Optic Nerve Segmentation Database) [14] was created for benchmarking optic nerve segmentation in fundus images. The images were acquired with a color analogical fundus camera, and they were digitized using a high-resolution scanner. The database was composed of 110 images of size of 600×400 pixels.
- **Ground truth:** For each image, two experts manually segmented the contour of the optic disc. Each contour was marked as a sequence of 36 points and was stored in a separate text file. A MATLAB script was also provided to graphically show the experts' segmentations using the textual data stored in the text file.

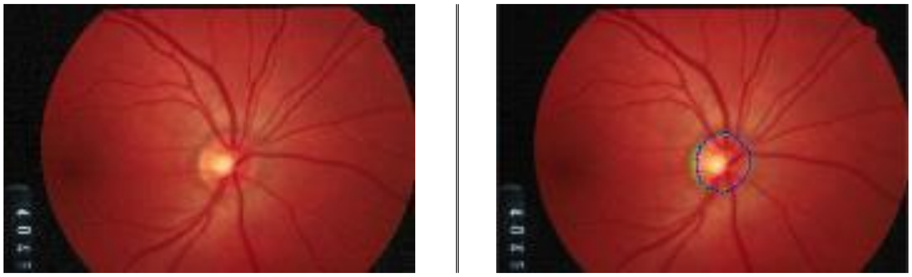

**Figure 2-4. Example of a fundus image and its associated ground truth in DRIONS-DB**

### 2.1.5. DRIVE

- **Dataset description:** DRIVE database (Digital Retinal Images for Vessel Extraction) [15] was mainly developed for the segmentation of blood vessels in retinal images. The dataset contained 40 images in each image was captured at 565×584 pixels with a FOV of 45 degrees. For this database, the images were cropped around the FOV, and for each image, a mask image was provided in order to delineate the FOV.
- **Ground truth:** the dataset of 40 images was divided into a training set and a test set, each of which contained 20 images. For the training images, a single manual segmentation of the

vasculature was provided. For the test cases, two manual segmentations were available: one to be used as gold standard, whereas the other one to be used for comparing computer-generated segmentations against those of an independent human observer. The DRIVE's website also provided a result browser in order to explore the database by viewing images and segmentations for a small set of algorithms that had been implemented.

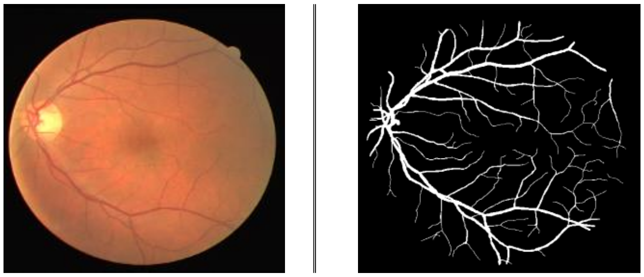

**Figure 2-5. Example of a fundus image and its associated ground truth in DRIVE**

### 2.1.6. HRF

- **Dataset description:** HRF (High-Resolution Fundus) image database [16] was established in order to evaluate the algorithms which localize the macula, optic disc, or differentiate between arteries and veins. The database contained a total of 45 images divided into three subsets; 15 images of healthy patients, 15 images of patients with diabetic retinopathy and 15 images of glaucomatous patients. Each image was of size of 3504×2336 pixels captured using a fundus camera with a field of view of 45 degrees.
- **Ground truth:** Each image, as mentioned above, was classified either as a normal fundus image, a diabetic fundus image, or a glaucomatous fundus image. Also, binary gold standard vessel segmentation images were available for each image, along with a spreadsheet that shows the spatial properties of the papilla (i.e. optic disc) within each fundus image.

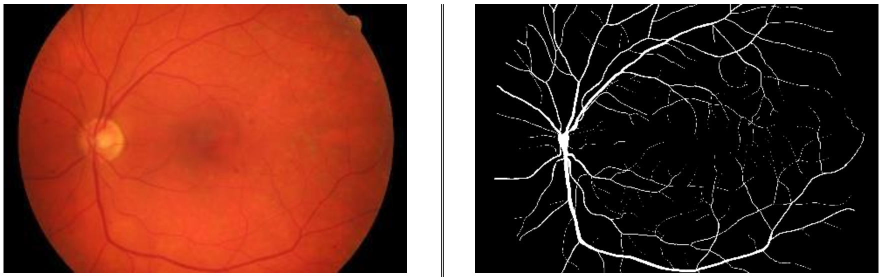

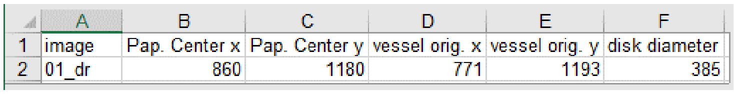

| | A | B | C | D | E | F |
|---|---|---|---|---|---|---|
| 1 | image | Pap. Center x | Pap. Center y | vessel orig. x | vessel orig. y | disk diameter |
| 2 | 01_dr | 860 | 1180 | 771 | 1193 | 385 |

**Figure 2-6. Example of a fundus image and its associated ground truth in HRF**

### 2.1.7. MESSIDOR

- **Dataset description:** MESSIDOR database [17] (Méthodes d'Evaluation de Systèmes de Segmentation et d'Indexation Dédiées à l'Ophtalmologie Rétinienne) was established to facilitate studies on computer-assisted diagnoses of diabetic retinopathy. The dataset contained 1200 images packaged in three sets. Each set was divided into four subsets, each of which containing 100 images in TIFF format. The images were captured using a camera with a 45-degree field of view at 1440×960, 2240×1488 and 2304×1536 pixels. 800 images were acquired with pupil dilation (one drop of Tropicamide at 0.5%) and 400 images were captured without dilation.
- **Ground truth:** each subset was associated with a spreadsheet that included two diagnoses: the retinopathy grade and the risk grade of macular edema, provided by medical experts for each image. The retinopathy grade was classified into four grades (grade 0, 1, 2 and 3) according to three main factors, namely the number of microaneurysms, number of hemorrhages, and the presence of neovascularization. Whereas, hard exudates have been used to classify the risk of macular edema into three grades (grade 0, 1 and 2).

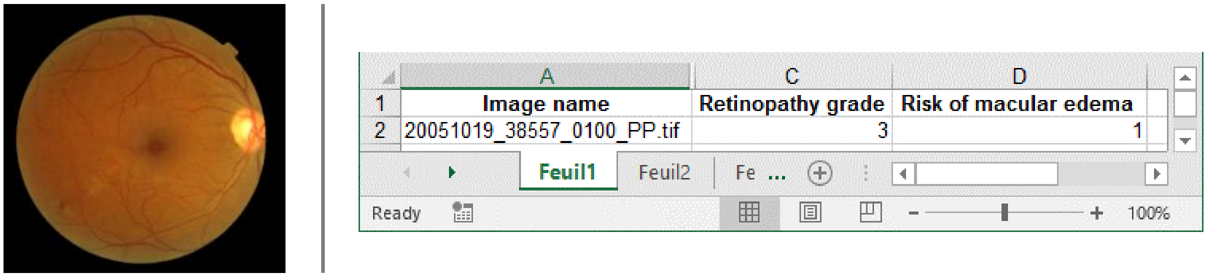

|  | A | C | D |
|---|---|---|---|
| 1 | Image name | Retinopathy grade | Risk of macular edema |
| 2 | 20051019_38557_0100_PP.tif | 3 | 1 |

**Figure 2-7. Example of a fundus image and its associated ground truth in MESSIDOR**

### 2.1.8. ONHSD

- **Dataset description:** ONHSD dataset (Optic Nerve Head Segmentation Dataset) [18] contained 99 fundus images taken from both, the left and right eyes of 50 patients. It is observed that the dataset missed one right-eye image out of the 50 eye pairs. Besides, 96 images had discernible optic discs which were acquired using a fundus camera with a field angle lens of 45 degrees and size of 760×570 pixels.
- **Ground truth:** the center of the optic disc has been marked up by a clinician. Then, four clinicians marked the optic disc edge where it intersected with radial spokes (at 15 degree angles) radiating from the nominated center.

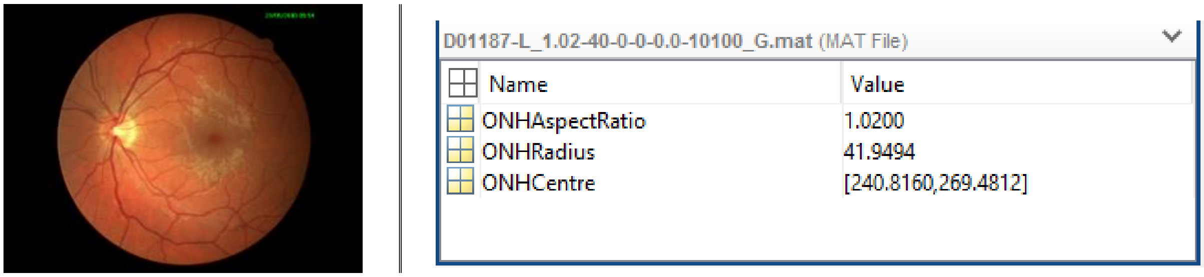
D01187-L_1.02-40-0-0-0.0-10100_G.mat (MAT File)

| Name | Value |
|---|---|
| ONHAspectRatio | 1.0200 |
| ONHRadius | 41.9494 |
| ONHCentre | [240.8160,269.4812] |

**Figure 2-8. Example of a fundus image and its associated ground truth in ONHSD**

### 2.1.9. STARE

- **Dataset description:** STARE dataset (Structured Analysis of the Retina) [19] contained 397 fundus images which were captured using a fundus camera with a field of view (FOV) of 35 degrees. Each image was of size of 700×605 pixels, in which the images were cropped at the top and the bottom of the FOV. It is worth to mention that some of the fundus images were occasionally missed within the provided dataset, namely images (47), (108), (109), (144) and (167).
- **Ground truth:** each image within the dataset was diagnosed by one or more of thirteen different clinical diagnoses. Also, blood vessel segmentation experimental work was provided including 20 hand-labeled images, along with the experimental results, and a demo. Moreover, the dataset was accompanied with a subset of 81 fundus images that marked the location of the optic disc within each image.

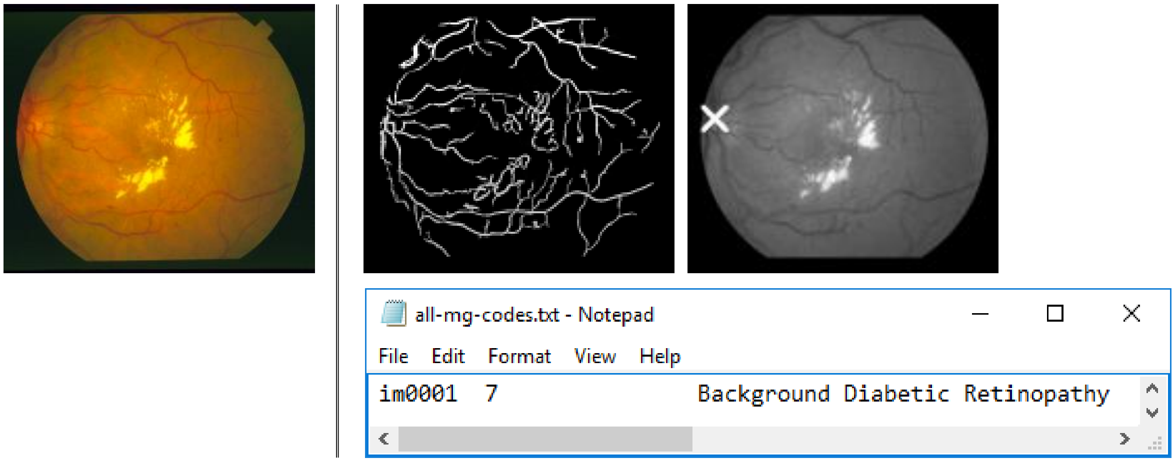

```
im0001   7              Background Diabetic Retinopathy
```

**Figure 2-9. Example of a fundus image and its associated ground truth in STARE**

## 2.2. Evaluation Metrics

Although the evaluation of an algorithm typically comes at the final stage of a detection or segmentation algorithm, yet the metrics used for evaluation are reviewed here in advance, in order to provide a concrete understanding of the results achieved by the segmentation algorithms in the literature that will be reviewed afterwards.

In medical diagnosis, the region of interest “ROI” (e.g. landmark or abnormality) is usually classified into two classes: present or absent; in which the response given by a human observer (expert) or a computer process is: positive or negative. Therefore, the detection of the abnormality or landmark is normally depicted in the terms presented in Table 2-1.

**Table 2-1. Signal detection indices and derived evaluation metrics**

| | **Present ROI** | **Absent ROI** |
|---|---|---|
| **Positive Response** | Hit ($T_P$) | False alarm ($F_P$) |
| **Negative Response** | Miss ($F_N$) | Correct rejection ($T_N$) |
| | **SENS =** $\frac{T_P}{T_P+F_N}$ | **SPEC =** $\frac{T_N}{T_N+F_P}$ |

The $T_P$ and $T_N$ indices refer to a “correct response” for identifying the presence and the absence of the ROI, respectively. Thus, the true positive index ($T_P$) indicates the correct positive response of a human observer or computer for the ROI that is present within the fundus image, whereas the true negative index ($T_N$) indicates the correct negative response for a ROI that is not present. Conversely, the $F_P$ and $F_N$ indices refer to an “incorrect response”. The false positive index ($F_P$) indicates the incorrect positive response for the ROI that is not present, whereas the false negative index ($F_N$) indicates the incorrect negative response for the ROI that is present.

### 2.2.1. Sensitivity and Specificity

Derived from the four aforementioned indices as shown in Table 2-1, two main statistical metrics are computed in order to evaluate the detection of the regions of interest ROI (i.e. landmarks or abnormalities). These two evaluation metrics are: sensitivity and specificity.

Sensitivity is a measure that reflects the probability of a positive response for the cases where the ROI is present, whereas specificity is the probability of negative response for the cases in which the ROI is absent. Both, sensitivity and specificity are expressed either as a ratio or a percentage given by the equation shown in Table 2-1, in which sensitivity is sometimes referred to as detection rate or true positive rate (TPR), whereas specificity is sometimes referred to as the true negative rate (TNR) [27].

### 2.2.2. Segmentation Accuracy

Typically, the spatial features of an object of interest such as its size, shape and area are the parameters that are commonly used in order to evaluate the segmentation accuracy of an object of interest. Moreover, these features also have clinical significance because they help in diagnosing diseases, as well as assessing the effect of treatment. Therefore, the main requirement needed to evaluate the segmentation results is the presence of the ground truth indicating the true features of the segmented object (i.e. its true size, shape or area). Thus, once the ground truth data is available, a variety of metrics can be used to evaluate the segmentation accuracy.

These evaluation metrics include the Hausdorff distance and the degree of overlap, which are relatively easy to compute and at the same time are not limited to certain geometrical patterns [28]. Other pixel-wise metrics such as the Euclidean distance is sometimes used to measure similarity, but the main drawback of such metric is that the similarity is estimated according to the distance between only two certain pixels such as the distance between the centroid of two optic discs.

**(i) Hausdorff Distance**

The intuition behind Hausdorff distance is to measure the similarity between two sets. So, if these sets have close Hausdorff distance, they are considered to look alike. Thereby, the Hausdorff distance $h(A,B)$ is used to measure the similarity between two contours of the same object (e.g. optic disc), in which one contour $A$ is defined by a human expert while the other contour $B$ is generated by a computer process. The Hausdorff distance is computed as follows [28], [29].

Let $A = \{a_1, a_2, \dots a_m\}$ and $B = \{b_1, b_2, \dots b_m\}$ be the set of points on the two contours in which each point represents a pair of x and y coordinates. Then, the distance of a point $a_i$ to the closest point on curve $B$ is defined as

$$d(a_i,B) = \min_j \|b_j - a_i\| \qquad \textit{Equation 2-1}$$

Similarly, the distance of a point $b_j$ to the closest point on curve $A$ is given by

$$d(b_j,A) = \min_i \|a_i - b_j\| \qquad \textit{Equation 2-2}$$

Finally, the Hausdorff distance is the maximum of the above distances between the two contours.

$$h(A,B) = \max\left[\max_i\{d(a_i,B)\}\ ,\ \max_j\left\{d\left(b_j,A\right)\right\}\right] \qquad \textit{Equation 2-3}$$

**(ii) Overlap Score**

The degree of overlap between two areas $\boldsymbol{G}$ and $\boldsymbol{E}$ encompassed by contours $\boldsymbol{A}$ and $\boldsymbol{B}$, respectively, is defined as the ratio of the intersection and the union of these two areas, where $\boldsymbol{G}$ is the ground truth human-defined area and $\boldsymbol{E}$ is the experimental computer-generated area. The degree of overlap is computed as follows [28], [30], [31]:

$$\boldsymbol{OL} = \frac{\boldsymbol{G} \cap \boldsymbol{E}}{\boldsymbol{G} \cup \boldsymbol{E}} \qquad \textit{\textbf{Equation 2-4}}$$

If there is an exact overlap between both contours, the ratio will be 1, whereas the ratio is given by 0 if there is no overlap between the two contours.

## 2.3. Preprocessing: Fundus Image Enhancement

Unfortunately, the raw digital fundus images are not always ready for immediate processing because of their poor quality due to factors such as the patient's movement and iris color, as well as imaging conditions such as non-uniform illumination. Therefore, an image should be first prepared in order to make it more suitable for further processing in terms of facilitation, accuracy and speed. The following subsections present the main preprocessing functions of fundus images.

### 2.3.1. Mask Generation

The captured fundus image consists of a semi-oval region of interest (ROI) on a dark background which is never really pure black. Therefore, masks are created and used in order to exclude the dark background of the image from further calculations and processing; in other words, only the pixels belonging to the semi-oval fundus region are included for manipulation. The mask image is a binary image in which the background pixels are assigned the value of "zero" and pixels within the ROI are assigned the value of "one" to produce a color image without noisy pixels in the background, while the ROI is left unchanged [6], [21], as shown in Figure 2-10.

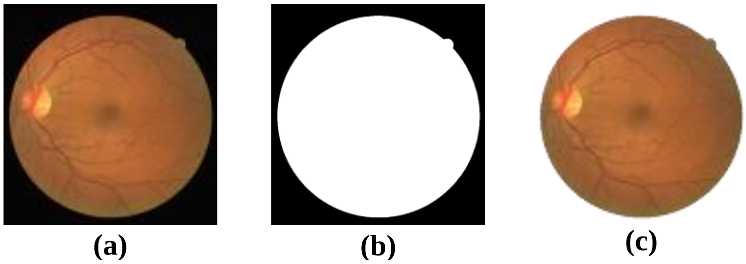

**Figure 2-10. (a)** A color image, **(b)** its corresponding mask, and **(c)** its excluded background

However, some of the publicly available retinal datasets, such as DRIVE, HRF, DIARETDB0 and DIARETDB1 are accompanied with these corresponding mask images, but many of the other datasets, and intuitively the real-time images as well, do not include such mask images. Therefore, the retinal images should be manipulated in some way in order to generate their corresponding binary mask images.

For instance, in their procedure of detecting the anatomical structures in fundus images, Gagnon *et al.* [32] generated the binary mask image using pixel value statistics outside the ROI of the fundus image which were calculated for each of the three color bands. Consequently, a 4-sigma thresholding was applied such that pixels, with intensity value above that threshold, were considered to belong to the ROI. Finally, results for all bands were combined through logical operations and region connectivity test in order to identify the largest common connected mask, since ROI size was not always the same for each band due to different color response of the camera.

Also, Goatman *et al.* [33] automatically generated the masks by the simple thresholding of the green channel of the retinal image followed by a 5×5 median filtering in order to exclude the dark surrounding region. On the other hand, Haar [21] created the mask by thresholding the red channel of the retinal image using a threshold value that was determined empirically, and then the thresholded image was morphologically processed via the opening, closing and erosion operators through a 3×3 square kernel. In the same direction, Hashim *et al.* [34] generated the binary mask by convolving the red channel with a Gaussian low-pass filter, in which the resultant image was thresholded using Otsu's global threshold.

### 2.3.2. Conversion between heterogeneous datasets

A digital fundus camera using a field of view (FOV) of 35°, such as the one used in the STARE dataset, displays a smaller area of the retina than a camera using a FOV of 45°, such as the one used in the DRIVE dataset, which is obviously smaller than that of DIARETDB1 whose FOV is 50°, as described earlier in Table 1-1 as well as Section 2.1. A scale factor computed by Haar [21] was used to convert the spatial resolution (i.e. magnification) between datasets having different field of views. The scale factor was based on the FOV-trigonometry, which is illustrated in Figure 2-11:

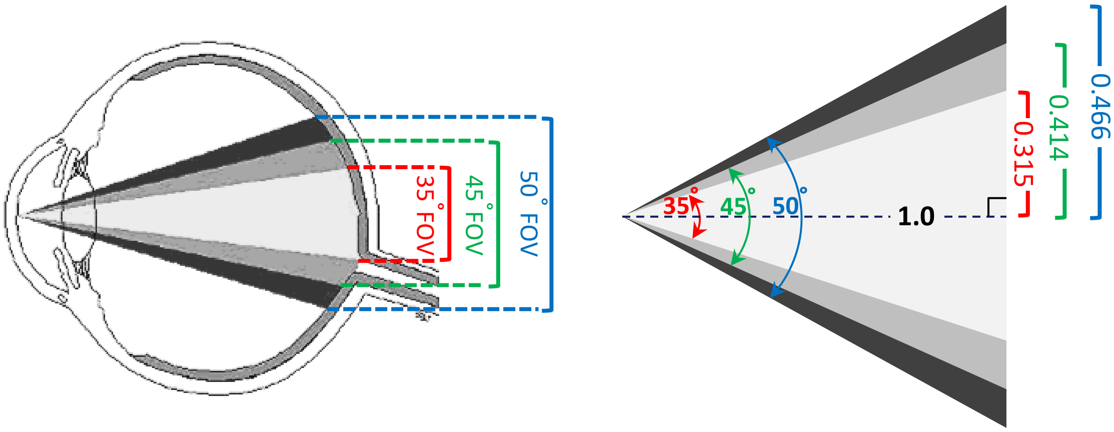

**Figure 2-11. The FOV trigonometry used for computing the scale factor**

Hence, the following equation was used to convert between images with 35° FOV (e.g. STARE) and 45° FOV (e.g. DRIVE), based on the trigonometry of the FOV:

$$scale = \frac{\tan(35/2)}{\tan(45/2)} = \frac{0.315}{0.414} = 0.76 \qquad \textit{Equation 2-5}$$

### 2.3.3. Color Channels Processing

Like any color image, the fundus image consists of three color channels in which the green channel has the highest contrast, whereas the red channel tends to be saturated and it is the brightest channel, while the blue channel tends to be empty [35], as noticed in Figure 2-12.

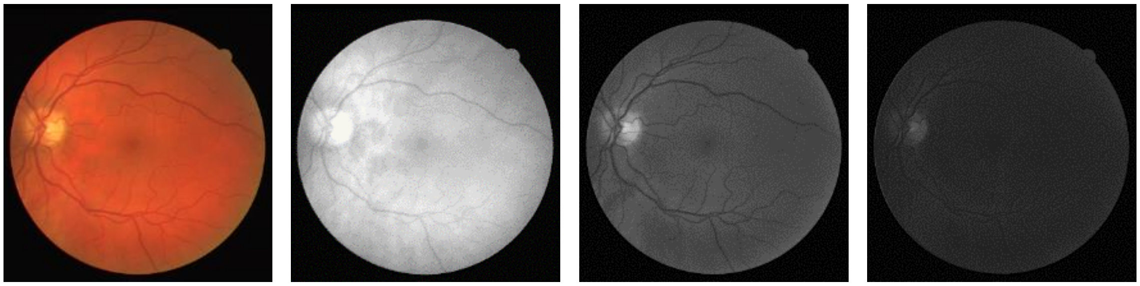

**(a)** **(b)** **(c)** **(d)**

**Figure 2-12. (a)** Full-color image split into its **(b)** red, **(c)** green and **(d)** blue channels

Since it provides the highest contrast, the green channel was heavily used by most algorithms, discarding the red component in some cases which are so-called "red-free images", and ignoring the blue component in most of the algorithms. Therefore, the green channel was heavily utilized for miscellaneous purposes such as detecting different retinal landmarks and several abnormalities due to its high contrast within retinal images. For instance, Goldbaum *et al.* [36] and Odstrcilik *et al.* [16] convolved the green plane with matched filters with the purpose of segmenting retinal blood vessels, while Yang *et al.* [37] utilized the green band to detect microaneurysms although they normally appear as small red spots. Also, Hoover and Goldbaum [35] located the optic disc using only the green band of the retinal image, whereas Staal *et al.* [15] used the green channel for the extraction of image ridges in color fundus images, while Niemeijer *et al.* [38] localized both the optic disc and fovea simultaneously using only the green plane of the color fundus image.

Moreover, Salem and Nandi [39] utilized the green channel image intensity as one of the feature components of the feature vector created for segmenting the retinal vessels. Similarly, Soares *et al.* [40] utilized the "inverted" green band to construct the feature vector. Related to the latter approach, many algorithms such as [41], [42], [43], [44], [45] exploited the "inverted green channel" so that the blood vessels appear brighter than the background, as shown in Figure 2-13.

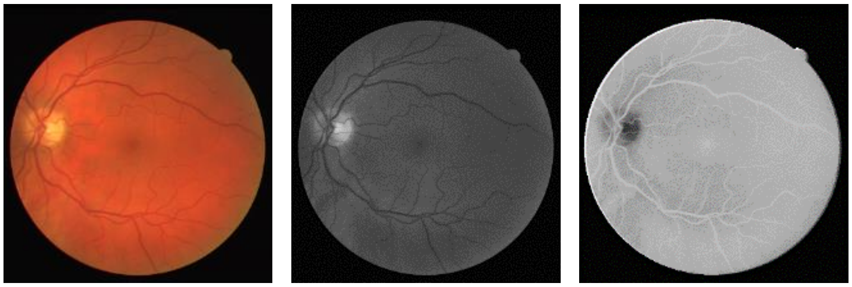

**(a)** **(b)** **(c)**

**Figure 2-13. (a)** Reference color image **(b)** Green channel **(c)** Inverted green channel

However, even though the green channel as well as its complement were solely utilized in most approaches and for various purposes as mentioned in the previous paragraph, yet the red channel was also exploited sometimes in combination with the green band. For instance, Aquino *et al.* [31] observed that the optic disc appeared in the red field as a well-defined white shape, brighter than the surrounding area, and therefore, the optic disc segmentation was performed in parallel on the red and green bands and the better of the two segmentations was ultimately selected. Also, Al-Rawi *et al.* [46] showed that using the red band or even the blue band was comparable to using the green band in vessels segmentation with matched filtering. Moreover, Lu [30] and Hashim *et al.* [34] combined intensity information from the red and green channels together by calculating a modified intensity channel component using a weighted average, in which a higher weight was given to the red channel in order to keep the image variation across the optic disc boundary but suppress that across the retinal vessels.

### 2.3.4. Color Normalization

Another major preprocessing task in retinal images is color normalization which does not aim to find the true color of an image, but in fact color normalization algorithms transform the color of an image so as to be invariant with respect to the color of illumination, without losing the ability to differentiate between the objects or regions of interest [33]. The most commonly-used algorithms for color normalization are the gray-world normalization, comprehensive normalization, histogram equalization and histogram specification.

Gray-world normalization assumes that the changes in the illuminating spectrum can be modeled by three multiplicative constants applied to the red, green and blue channels, respectively. The new color of any pixel is calculated by dividing each color channel by its respective mean value, removing the dependence on the multiplicative constant. Comprehensive normalization, a variation of the gray-world normalization proposed by Finlayson *et al.* [47], is a technique that iteratively applies chromaticity normalization followed by gray-world normalization for four or five iterations, until the change in values is less than a certain tolerance value. On the other hand, histogram equalization is a non-linear transform applied individually to the red, green and blue bands of an image which affects the color perceived. It is a more powerful normalization transformation than the gray-world method. The results of histogram equalization tend to have an exaggerated blue channel and look unnatural due to the fact that in most images the distribution of the pixel values is usually more similar to a Gaussian distribution, rather than uniform [48]. Whereas, histogram specification transforms the red, green and blue histograms to match the shapes of three specific histograms, rather than simply equalizing them, which results in more realistic images than those blueish ones produced by equalization [33].

Both, Goatman *et al.* [33] and Youssif *et al.* [49] evaluated the effectiveness of the aforementioned methods of color normalization which aim to reduce color variations among different retinal images. According to the assessment of Goatman, histogram specification was found to be the most effective normalization method in clustering and discriminating four different types of lesions, namely the cotton wool spots, hard exudates, blot hemorrhages, and drusen. Moreover, histogram specification had the advantage that it produced more realistic looking images since it did not exaggerate the contribution of the blue channel like the other methods, as shown in Figure 2-14, whereas comprehensive normalization was not found to perform much better than gray-world normalization in discriminating the lesions.

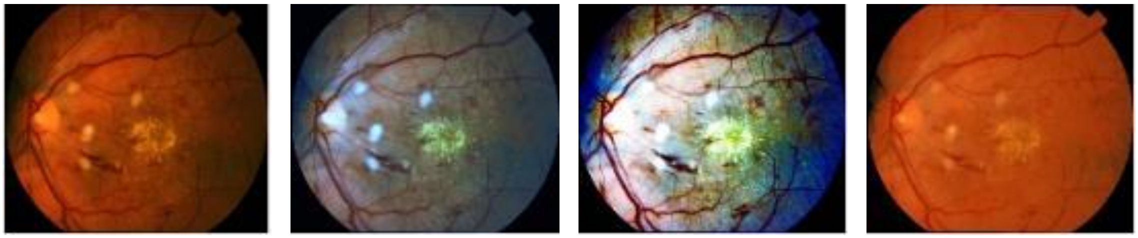

**(a)** **(b)** **(c)** **(d)**

**Figure 2-14. Effect of color normalization on abnormal retinal images**
**(a)** Reference image **(b)** Gray-world normalization
**(c)** Histogram equalization **(d)** Histogram specification

However, from a different perspective in evaluating normalization techniques as observed by Youssif *et al.* [49], histogram specification recorded the worst result in discriminating the vessels from non-vessels, while histogram equalization was found be the most effective method by showing a clear separation between clusters of vessels and non-vessels, whereas comprehensive normalization, compared to gray-world normalization, showed more intense clusters and a narrower overlap between objects scattered in both clusters, as shown in Figure 2-15.

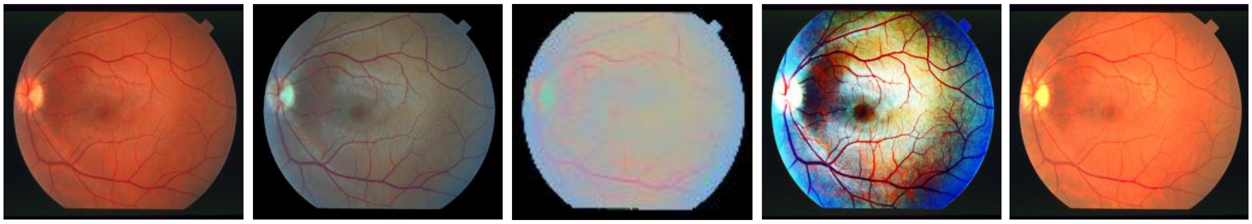

**(a)** **(b)** **(c)** **(d)** **(e)**

**Figure 2-15. Effect of color normalization on retinal vessels**
**(a)** Reference image (STARE: im0255.ppm)
**(b)** Gray-world normalization **(c)** Comprehensive normalization
**(d)** Histogram equalization **(e)** Histogram specification

### 2.3.5. Contrast Enhancement

Contrast enhancement is the process of either darkening or brightening a low-contrast intensity image by spreading the range of intensities so that it spans a wider range of intensity levels, as noticed in the next figure. Hence, some of the color normalization techniques, such as histogram equalization and histogram specification which were applied to the three color channels, may be also utilized to enhance the contrast of an image using one gray-level channel, typically the green channel, the one which provides the highest contrast between vessels and non-vessels as mentioned before.

Figure 2-16 illustrates the contrast of an image in the green band whose contrast was enhanced via histogram equalization (HE) and contrast-limited adaptive histogram equalization (CLAHE). The reference image of the preceding figure (Figure 2-15) was used again in the following figure, in order to clarify the visual difference between contrast enhancement and color normalization.

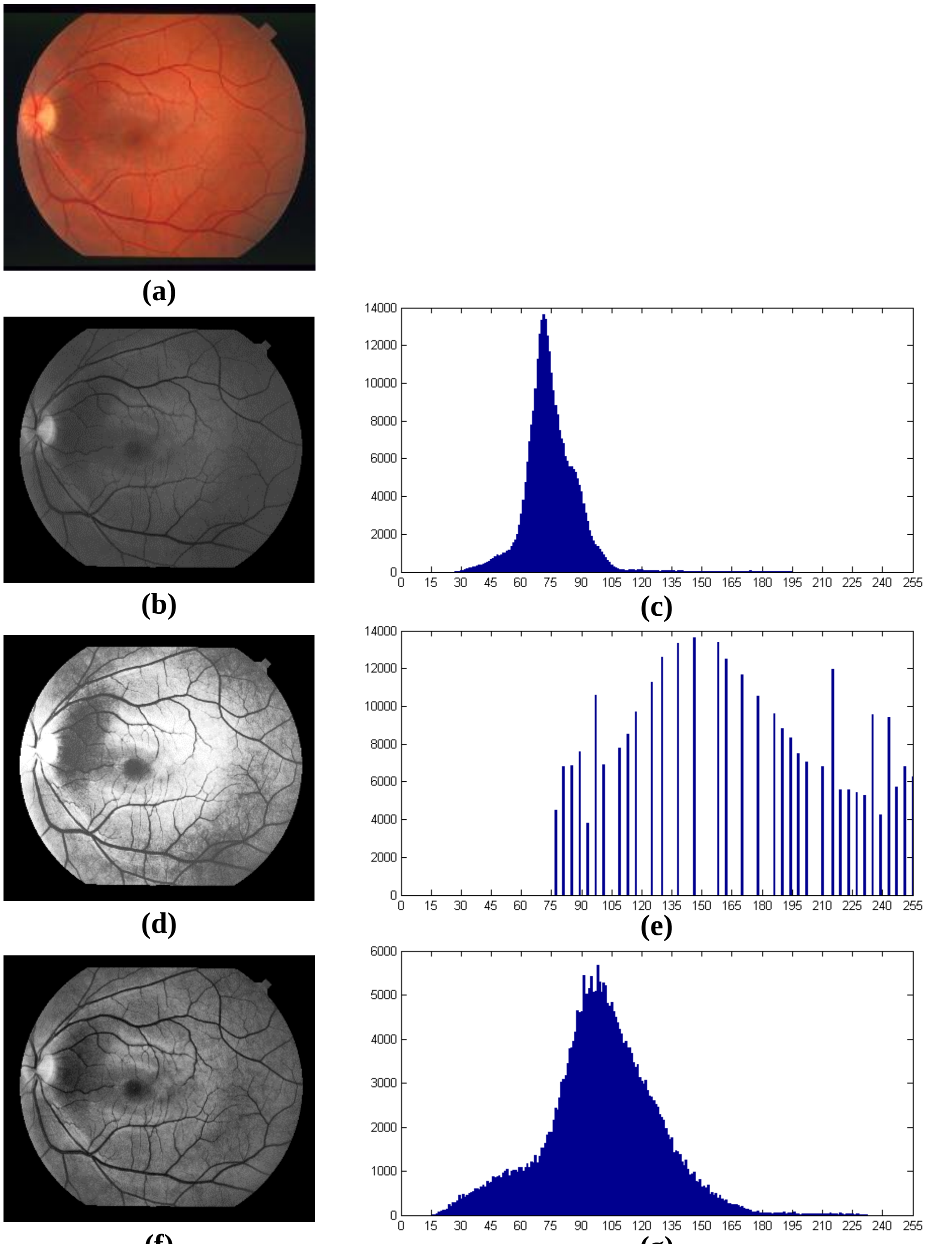

Total no. of pixels: **423,500**
No. of pixels in ROI: **295,700**
No. of gray levels: **168**
Lowest intensity value: **(27)**
Highest intensity value: **(194)**
Most frequent intensity: **(71)**
No. of its occurrences: **13,635**

Total no. of pixels: **423,500**
No. of pixels in ROI: **295,700**
No. of gray levels: **35**
Lowest intensity value: **(77)**
Highest intensity value: **(255)**
Most frequent intensity: **(146)**
No. of its occurrences: **13,635**

Total no. of pixels: **423,500**
No. of pixels in ROI: **295,700**
No. of gray levels: **217**
Lowest intensity value: **(16)**
Highest intensity value: **(232)**
Most frequent intensity: **(98)**
No. of its occurrences: **5,681**

**Figure 2-16. Contrast enhancement using HE and CLAHE**
**(a)** Original color image (STARE: im0255.ppm)
**(b)** Green channel of the original image **(c)** Corresponding histogram of (b)
**(d)** Histogram equalization of the green channel **(e)** Corresponding histogram of (d)
**(f)** CLAHE of the green channel **(g)** Corresponding histogram of (f)

The main drawback of using histogram equalization (HE) in contrast enhancement is its dependence on the global statistics of an image, which may lead to noise amplification as well as the absence of many gray levels, as noticed in the previous figure. This in turn results in a washed-out appearance in some parts of the image due to over enhancement, while other parts around the periphery may not be enhanced enough [9], [50].

Adaptive histogram equalization (AHE) was applied by Wu *et al.* [51] and also exploited by Youssif *et al.* [6] in enhancing the contrast. AHE differs from the ordinary histogram equalization (HE) in the respect that the adaptive method computes several histograms, each of which corresponds to a distinct section (i.e. tile) of an image in order to redistribute the lightness values of the image. Therefore, it is suitable for improving the local contrast of an image and bringing out more detail, however noise may be still amplified as the ordinary histogram equalization.

Fadzil *et al.* [52], Krishnan *et al.* [53] and Maruthusivarani *et al.* [54] enhanced the contrast of the retinal image using contrast-limited adaptive histogram equalization (CLAHE) which is an improved variation of the AHE that limits the amplification of noise produced by the AHE.

Sinthanayothin *et al.* [55] presented a technique for enhancing the contrast of color images rather than intensity images using the adaptive local contrast enhancement, which was also utilized by Osareh *et al.* [56], Haar [21] and Park *et al.* [57]. This technique first transformed the components of the three color bands RGB into the HSI color model, which allowed the intensity component to be processed without affecting the perceived relative color values of the pixels. Consequently, the contrast of the intensity was enhanced by a locally adaptive transformation that depended on the mean and standard deviation using a small running square window. Finally, the processed HSI image was converted back into an RGB image with an enhanced contrast. Figure 2-17 illustrates the effect of the local color contrast enhancement.

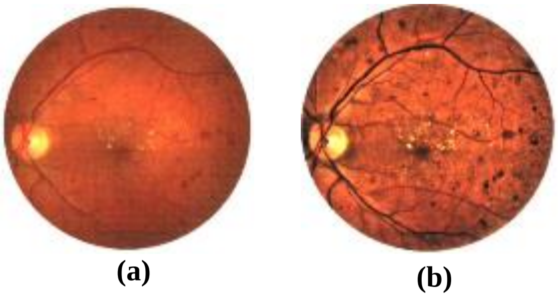
**(a)** **(b)**

**Figure 2-17. Local color contrast enhancement**
**(a)** Original image **(b)** Contrast-enhanced color image

Rather than spreading the range of intensities in order to enhance the contrast, other more complex methods based on enhancing ridges, were exploited for contrast enhancement. For example, unsharp masking can increase either the sharpness or local contrast because both are forms of increasing differences between pixel values. Unsharp masking, based on spatial high-pass filtering, emphasizes high-frequency components of the image by subtracting an unsharp (blurred) version of the original image, which in turn improves the contrast, but amplifies the noise. However, Polesel *et al.* [58] proposed a technique that reduced noise amplification in digital images via adaptive unsharp masking.

Similar to the previous approach of increasing sharpness, each of the curvelet and contourlet transforms were used for enhancing edges. Both transforms differ from the wavelet transform in the respect of two additional features: directionality (i.e. the ability to capture different orientations) and anisotropy (i.e. the ability to capture smooth contours). Accordingly, the contourlet transform, presented by Do and Vetterli [59], was exploited by Feng *et al.* [60] and Rezatofighi *et al.* [61] in order to increase the contrast of blood vessels as well as the retinal lesions. Also, Miri and Mahloojifar [62] used the discrete curvelet transform to enhance the image ridges which, as mentioned before, play an important role in enhancing the image contrast.

Figure 2-18 provides a visual comparison between all the aforementioned techniques of contrast enhancement.

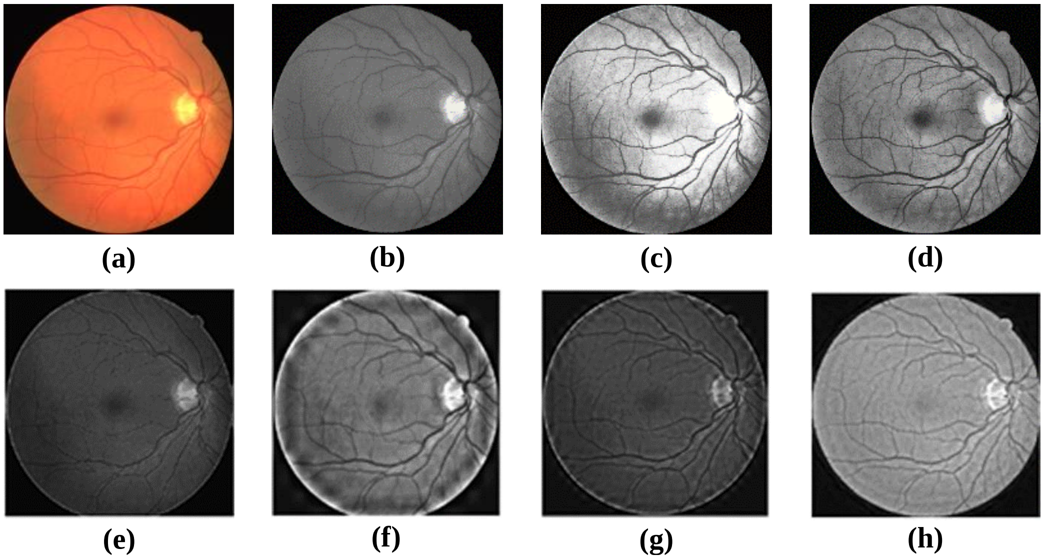

**Figure 2-18. Comparison between different techniques of contrast enhancement**
**(a)** Reference image **(b)** Green channel **(c)** HE **(d)** CLAHE
**(e)** Unsharp masking **(f)** Wavelet **(g)** Contourlet **(h)** Curvelet

### 2.3.6. Non-uniform Illumination Correction

The improper light focus of an imaging system may decrease the brightness of the retinal image around the peripheral region compared to the center of the retina, causing a non-uniform illumination referred to as vignetting, as shown by the images of Figure 2-19.

**Figure 2-19. Examples of non-uniform illumination**

Therefore, in order to overcome vignetting, Hoover and Goldbaum [35] presented an illumination equalization technique to enhance the image, in which each pixel *I(r,c)* in the image was corrected as follows:

$$\boldsymbol{I_{eq}(r,c) = I(r,c) + m - A(r,c)} \qquad \textbf{\textit{Equation 2-6}}$$

where $\boldsymbol{m}$ is the desired average intensity (128 in an 8-bit gray-scale image) and $\boldsymbol{A(r,c)}$ is local average intensity of the pixels within a window of size $N \times N$. This equalization technique was also employed by other algorithms such as [6] and [21] on the green band of the retinal images in order to adjust uneven illumination.

Using an alternative approach for equalization, Yang *et al.* [37] corrected the non-uniform illumination of an image via dividing the green band image by an over-smoothed version of it using a spatially large median filter. Figure 2-20 shows the equalized images in the green bands using the two methods (reproduced from [49]).

**(a)** **(b)** **(c)**

**Figure 2-20. Illumination equalization**
**(a)** Source image (STARE: im0255.ppm) **(b)** Hoover’s method **(c)** Yang’s method

Recently, Odstcilik *et al.* [16] preprocessed the green band of the color fundus image using a B-spline-based illumination correction method. The non-uniform illumination correction was applied together with contrast enhancement, in which a multiplicative illumination model was used to produce the corrected image $\boldsymbol{G}$, as follows:

$$\boldsymbol{G = \frac{I}{b} - \ b^{max} + 128} \qquad \textbf{\textit{Equation 2-7}}$$

where the term $\boldsymbol{I}$ refers to the original intensity image and $\boldsymbol{b}$ is the background illumination model obtained by approximating the low-pass filtered image by a two-dimensional B-spline function, while the term ($\boldsymbol{b^{max} + 128}$) ensures that the mean value of the reconstructed image will be approximately 128 (for images with 256 grey levels).

## 2.4. Segmentation of Eye Fundus Landmarks

In general, detecting and locating the main anatomical structures of the eye fundus, such as the optic disc, the macula, the fovea and the major blood vessels, is considered an essential step toward detecting abnormalities and analyzing lesions in the fundus images. Thus, these segmented fundus landmarks may be exploited to establish a coordinate system (retinal model) of the eye fundus which in turn may be used to determine the spatial relationship of lesions, edema and hemorrhages with reference to the optic disc and macula.

### 2.4.1. Motivation of Optic Disc Detection

The optic disc acts as a landmark for locating the macula and tracking the blood vessels. Moreover, detecting the optic disc and analyzing its spatial structure also serves as an indicator of various ophthalmologic pathologies such as diabetic retinopathy and glaucoma. As because of the similarity and confusion between exudates and the optic disc (Figure 2-21b), diabetic retinopathy can be diagnosed by isolating and omitting the optic disc which improves the identification of exudates, one of the main retinal abnormalities occurring in diabetic retinopathy [6], [63].

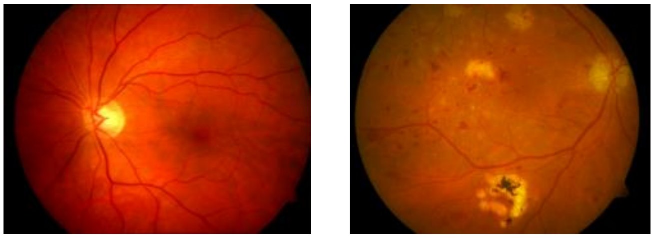

**(a)** **(b)**

**Figure 2-21.** **(a)** Healthy fundus image **(b)** Diabetic fundus (containing exudates)

Besides, both the cup-to-disc ratio and the ISNT rim thickness rule (Inferior > Superior > Nasal > Temporal) are two intrapapillary indicators used to diagnose glaucoma which is characterized by the cupping of the optic disc, as well as the thinning of the Inferior and Superior rims (i.e. notching), as discussed later at section 2.5.1. The pathology of glaucoma is characterized by the cupping of the optic disc which becomes ischemic due to the imbalance between the intraocular pressure and the perfusion pressure in the vessels of the retina [2], as shown in Figure 2-22.

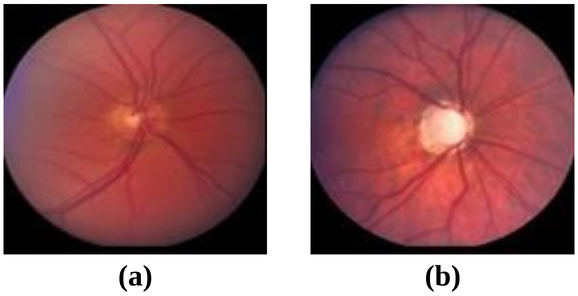

**Figure 2-22. (a)** Normal optic disc **(b)** Glaucomatous optic disc

### 2.4.2. Properties of the Optic Disc

The optic disc is found towards the right-hand side or the left-hand side of the fundus image for the right-eye and left-eye, respectively. It is round or vertically oval in shape, measuring about one-tenth to one-sixth the width of the image, and typically appears as a bright yellowish or white area. Also, the optic disc appears as the convergent area of the vascular tree of blood vessels [2], [6], [55], [64], [65]. In addition, the process of locating the optic cup aims only to identifying the centroid of the optic disc, whereas detecting the optic rim (neuroretinal rim) aims to identifying the boundary between the retina and the optic disc [6]. Figure 2-23 distinguishes the optic cup and the optic rim within the optic disc.

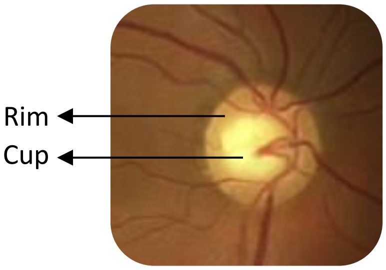

**Figure 2-23. The cup and the rim of the optic disc**

### 2.4.3. Literature of Optic Disc Segmentation

A comprehensive survey of optic disc segmentation was presented by Allam *et al.* [8], through which the main methods reviewed in the literature were categorized and distinguished, as follows:

#### i. Property-based methods

Such techniques exploit few or all of the main characteristics of the optic disc listed in the previous section, namely its brightness, relative width, roundness, location within the fundus image, or the existence of blood vessels in its vicinity. In the early work of the optic disc detection, Goldbaum *et al.* **[36]** utilized many of these properties in order to jointly locate the optic disc. They combined three properties of the optic disc: the convergence of blood vessels at the optic disc, the appearance of the optic disc as a bright region, and entrance of large vessels above and below the optic disc.

Also, Sinthanayothin *et al.* [55] located the optic disc by identifying the area with the highest variation in intensity of adjacent pixels using a window whose size was equal to that of the optic disc. Their approach correctly detected the optic disc with sensitivity and specificity of 99.1% on a local dataset composed of 112 TIFF fundus images.

Similarly, based on the brightness and roundness of the optic disc, Park *et al.* [66] also presented a method with a successful detection percentage of 90.25% using an approach that included thresholding, detection of object roundness, and detection of circles.

Also, Chrástek *et al.* [67] applied an averaging filter to the green-band image, and roughly located the optic disc at the point with the highest average intensity with a success rate of 97.3% on a local dataset.

Walter and Klein [68] approximated the centroid of the optic disc as the center of the largest and brightest connected object in the fundus. Their method successfully detected optic disc in all images of a local dataset composed of 30 images, and achieved a success rate of 58% on the STARE dataset.

Carmona *et al.* [14] proposed a genetic algorithm in order to obtain an ellipse that approximated the optic disc. First, they obtained a set of hypothesis points that exhibited the geometric properties and intensity levels similar to the optic disc contour pixels. The genetic algorithm was used next to find an ellipse containing the maximum number of hypothesis points in an offset of its perimeter. The results of their algorithm showed that 96% of the 110 retinal images had less than five pixels of discrepancy.

Using the Circular Hough Transform, Abdel-Ghafar *et al.* [69] detected the optic disc by finding the largest circular object. Similarly, Zhu *et al.* [2], [70] also used the Hough Transform to detect the circles in which the best-fitting circle for the optic disc was chosen by using a method of intensity-based selection. They achieved a successful detection rate of 90% on the DRIVE dataset and 44.4% on the STARE dataset.

A circular transformation was designed by Lu [30] to capture both the circular shape of the optic disc as well as the image variation across the optic disc boundary, simultaneously. The variation of each pixel within the retinal image was measured along multiple evenly-oriented radial line segments of specific length. The pixels with the maximum variation along all radial line segments were determined, which were then exploited to locate both the center and the boundary of the optic disc. Experimental results showed that the center of the optic disc was accurately detected in 99.75%, 97.5%, and 98.77% of the STARE, ARIA and MESSIDOR datasets, respectively. Also, the boundary of the optic disc was accurately segmented in 93.4% and 91.7% of the STARE dataset and the ARIA dataset, respectively.

Zubair *et al.* [71] detected the optic disc by increasing its contrast using preprocessing techniques such as CLAHE, contrast stretching transformation, and extended minima transformation. Using the contrasted image, the optic disc was localized by using morphological erosion and dilation in order to remove all non-optic disc regions that are not of the size of the optic disc. Finally, after taking negative of the image, the resultant image obtained was subtracted from the resized green-channel component to get an optic disc free image, with an accuracy of 98.65% on the MESSIDOR dataset.

Yu and Yu [72] localized the optic disc via a technique of detecting the brightest pixels iteratively, as to be robust against the existence of any bright lesions such as hard exudates. They also set thresholds for the area of the optic disc and its circularity in order to select the optic disc over other nominees. They reported that their approach achieved a detection rate of 95%, although only 40 “selected-images” of the STARE dataset were tested, which means that this rate might have been degraded if the whole dataset had been used.

As a concluding observation, it was obvious that all the aforementioned property-based methods achieved good results in normal fundus images that contained no abnormalities, but most of these approaches usually failed to detect the optic disc in pathological images where abnormalities, such as large exudates, had been confused with the optic disc due to their similar appearance.

### ii. Convergence of blood vessels

Instead of relying on the properties of the optic disc, an alternative approach to detect the optic disc is to exploit the information provided by the vascular tree of the retina, since the optic disc is considered as the convergence point of the few major blood vessels that split into many smaller vessels throughout the retina [6].

Taking advantage of this spatial relationship between the optic disc and blood vessels, Hoover and Goldbaum [35] developed a voting-type algorithm called fuzzy convergence in order to detect the origination of the blood-vessel network (i.e. convergence point) which was considered as the center of the optic disc in a fundus image. The input to their algorithm was a binary segmentation of the blood vessels, in which each vessel was modeled by a fuzzy segment that contributed to a cumulative voting image. The output of the algorithm was a convergence image which was thresholded to identify the strongest point(s) of convergence. This technique successfully detected 89% of the normal and abnormal images in the STARE dataset.

The Hough Transform was utilized by Haar [21] in two different ways. In the first method, the Hough Transform was applied only to the pixels on or close to the binary image of the retinal vasculature obtained by [15], in which the binary image was dilated on order to increase the number of optic disc candidates. This approach achieved a success rate of 96.3% on a local dataset and 71.6% on the STARE dataset. In the second alternative method, the Hough Transform was applied only to the brightest 0.35% of the fuzzy convergence image produced by Hoover and Goldbaum [35], in which dilation was applied again to the convergence image to fill the gaps created by small vessels. This approach achieved a success rate of 97.4% on a local dataset and 65.4% on the STARE dataset.

Fleming *et al.* [73] detected the approximate region of the optic disc using an elliptical shape of the major retinal vessels which was formed using the Generalized Hough Transform. The approximate location of the optic disc was then refined via the Circular Hough Transform achieving a success rate of 98.4% of the 1056 retinal images, in which the positional accuracy was better than 50% of the diameter of the optic disc.

Ying *et al.* [74] proposed an algorithm that differentiates the optic disc from other bright regions such as hard exudates, in which the optic disc was detected based on its high fractal dimension of the converging pattern of blood vessels. With its location known, the optic disc was correctly segmented via local histogram analysis in 97.5% of the images of the DRIVE dataset.

Based on tensor voting for analyzing vessel structures, Park *et al.* [57] proposed a method to identify the location of the optic disc. The vessel patterns were first extracted by tensor voting in equalized images, and then the position of the optic disc was identified by mode detection which was based on mean-shift procedure. Their approach was tested with 90 images from the STARE dataset, which achieved 100% success rate on 40 normal images and 84% on pathological images.

In the work of Rangayyan *et al.* [2], [75], the blood vessels were first detected using Gabor filters, and then phase portrait modeling was applied to detect the convergence points of the vessels, in which the best-fitting circle for the optic disc was chosen by using an intensity-based condition. This approach achieved success rates of 100% and 69.1% for the DRIVE and STARE datasets, respectively.

### iii. Model-based methods (template-matching)

This type of methods is based on comparing a template image (model) with a set of candidates in order to determine the best-matching candidate. Lalonde *et al.* [29] implemented a Hausdorff-based template matching technique using edge maps, guided by pyramidal decomposition for large-scale object tracking where small bright lesions (e.g. exudates) disappear, creating fewer optic disc candidates. The edge map regions were matched to a circular template with different radii using the Hausdorff distance, and the region having the largest number of overlapped template pixels was considered the optic disc. This approach correctly detected the center of the optic disc in 93% of a dataset of 40 images.

Another model-based approach was proposed by Osareh *et al.* [76] who created a gray-level template image by averaging the optic disc region of 25 images whose colors were normalized using histogram specification. The center of the optic disc was located by using the generated template along with gray-scale morphological filtering and active-contour modeling in which the normalized correlation coefficient was used to find the most similar match between the template and all the candidate pixels, with an average accuracy of 90.32% in detecting the boundary of the optic disc of 75 images of the retina.

Also, Li and Chutatape [77] created an optic disc model (disc-space) by applying Principal Component Analysis (PCA) to a training set of 10 intensity normalized images that were manually cropped around the optic disc. The candidate regions with the highest 1% gray-level were selected and matched to the disc-space, in which the optic disc was successfully detected in 99% of a local dataset, as the region with the smallest Euclidean distance to its projection onto the disc-space.

Also, the method proposed by Foracchia *et al.* [78] for detecting the optic disc was based on a preliminary detection of the major retinal vessels. They proposed a geometrical model to describe the general direction of retinal vessels at any given position using the coordinates of the optic disc center which were two model parameters estimated by the means of a simulated annealing optimization technique. The position of the optic disc was correctly located in 97.53% of the STARE images using the common vertex of the two model parameters (i.e. the convergence point for the blood vessels).

Lowell *et al.* [18] designed a detection filter (i.e. template) for the optic disc which was composed of a Laplacian of Gaussian filter with a vertical channel carved out of the middle corresponding to the major blood vessels exiting the optic disc vertically. This template was then correlated to the intensity component of the fundus image using full Pearson-R correlation. The optic disc was successfully detected in 99% of the images in a local dataset.

A method presented by Haar [21] was based on fitting the vascular orientations on a directional model (DM), using a training set of 80 images of vessel segmentations. For all the pixels in each vessels image, the orientation was calculated to form a directional vessel map, in which the DM was created by averaging, at each pixel, all the corresponding orientation values in the directional maps. At the end, each pixel in an input vasculature was aligned to the center of the optic disc, and the pixel having the minimal distance to both DMs was selected as the optic disc location. This method detected the optic disc successfully in 99.5% of the images in a local dataset and 93.8% of the STARE dataset.

Inspired by the aforementioned work, Youssif *et al.* [6] proposed another model-based approach by matching the expected directional pattern of the retinal blood vessels found in the vicinity of the optic disc. They obtained a vessels direction map of the retinal vessels that were segmented using 2D Gaussian matched filter. The minimum difference between the matched filter and the vessels directions at the surrounding area of each of the optic disc candidates achieved a successful detection rate of 100% on the DRIVE dataset and 98.77% on the STARE dataset.

Niemeijer *et al.* [38] formulated the problem of finding a certain position in a retinal image as a regression problem. A k-nearest neighbor classifier (k-NN) was trained to predict the distance to the optic disc given a set of measurements of the retinal vasculature obtained around a circular template placed at a certain location in the image. The method was trained with 500 images for which the location of the optic disc was known, where the point with the lowest predicted distance to the optic disc was selected as the optic disc center. This supervised method was tested using 600 images of which 100 images contained gross abnormalities, and successfully located the optic disc in 99.4% of the normal images and 93% of the pathological images.

Aquino *et al.* [31] presented a template-based methodology that used morphological and edge detection techniques followed by the Circular Hough Transform to obtain an approximate circular optic disc boundary. Their methodology required an initial pixel located within the optic disc, and for this purpose, a location procedure based on a voting-type algorithm was utilized and succeeded in 99% of the cases. The algorithms were evaluated on the 1200 images of the MESSIDOR dataset, achieving a success rate of 86%.

Lu [79] used another technique for the detection of the optic disc in a way different than the one he used in [30] (previously reviewed in the *property-based methods*). In the proposed technique, the retinal background surface was first estimated through an iterative smoothing procedure. Afterwards, multiple optic disc candidates were detected through the difference between the retinal image and the estimated retinal background surface. Finally, the real optic disc was selected through the combination of the difference image and the directional retinal blood vessel which was based on the observation that the retinal blood vessels were mostly oriented vertically as they exit the optic disc. The proposed technique was evaluated over four datasets DIARETDB0, DIARETDB1, DRIVE and STARE giving an accuracy of 98.88%, 99.23%, 97.50% and 95.06%, respectively.

Instead of creating an image and using it as a template, Dehghani *et al.* [64] constructed three histograms as a template for localizing the center of the optic disc using four retinal images from the DRIVE dataset, in which each histogram represented one color channel. Then, an 80×80 window was moved through the retinal image to obtain the histogram of each channel. Finally, they calculated the correlation between the histogram of each channel in the moving window and the histograms of its corresponding channel in the template. The DRIVE, STARE, and a local dataset composed of 273 images were used to evaluate their proposed algorithm, in which the success rate was 100%, 91.36% and 98.9%, respectively.

Zhang and Zhao [80] proposed a method for detecting the optic disc accurately in an efficient way. First, the algorithm identified a number of possible vertical windows (x-coordinates) for the optic disc according to three characteristics of retinal vessels, which are: (1) the high density of vessels at optic disc vicinity, (2) compactness of the vertical vascular segments around the optic disc center, and (3) the uniform distribution of vessels. Consequently, the y-coordinate of the optic disc is identified according to the vessels direction via parabola curve fitting using the General Hough Transform. The proposed method was tested on four datasets: DIARETDB0, DIARETDB1, DRIVE and STARE, in which the optic disc was correctly detected in all images of each dataset, except only one image in the STARE dataset.

Table 2-2 chronologically summarizes the aforementioned methods of optic disc localization.

**Table 2-2. List of optic disc detection methods**

| # | Approach | Dataset | SENS | ACC |
|---|---|---|---|---|
| **1** | Goldbaum et al., 1996 [36]: vessels convergence, OD brightness, and large vessels entrance | None | - | - |
| **2** | Sinthanayothin et al., 1999 [55]: High intensity variation | Local dataset (112 images)<br>STARE (81 images)[1] | 0.9911<br>0.4200 | -<br>- |
| **3** | Lalonde et al., 2001 [29]: Hausdorff template matching & pyramidal decomposition | Local dataset (40 images)<br>STARE (81 images)[1] | 1.0000<br>0.7160 | 0.9300<br>- |
| **4** | Walter & Klein, 2001 [68]: Largest brightest connected object | Local dataset (30 images)<br>STARE (81 images)[1] | 0.9000<br>0.5802 | -<br>- |
| **5** | Chrástek et al., 2002 [67]: Highest average intensity | Local dataset (261 images) | 0.9732 | 0.8171 |
| **6** | Osareh et al., 2002 [76]: Averaged OD-images template matching | Local dataset (75 images)<br>STARE (81 images)[1] | 0.9032<br>0.5800 | -<br>- |
| **7** | Hoover & Goldbaum, 2003 [35]: Fuzzy convergence of blood vessels | STARE (81 images) | 0.8888 | - |
| **8** | Foracchia et al., 2004 [78]: Geometrical model of vessel structure | STARE (81 images) | 0.9753 | - |
| **9** | Li & Chutatape, 2004 [77]: Template matching via Principal Component Analysis | Local dataset (89 images) | 0.9888 | 0.9400 |
| **10** | Lowell et al., 2004 [18]: Laplacian of Gaussian template & full Pearson-R correlation | Local dataset (90 images) | 0.9889 | - |
| **11** | Haar, 2005 [21]: Hough Transform applied to the pixels close to the retinal vasculature | STARE (81 images)<br>Local dataset (191 images) | 0.7160<br>0.9634 | -<br>- |
| **12** | Haar, 2005 [21]: Hough Transform applied to the fuzzy convergence image | STARE (81 images)<br>Local dataset (191 images) | 0.6543<br>0.9738 | -<br>- |
| **13** | Haar, 2005 [21]: Fitting the vasculature orientations on a directional model | STARE (81 images)<br>Local dataset (191 images) | 0.9948<br>0.9383 | -<br>- |

---

[1] Additional results for the STARE dataset were obtained from the comparative study done by Haar, 2005.

| # | Approach | Dataset | SENS | ACC |
|---|---|---|---|---|
| **14** | Park et al., 2006 [66]: Brightness and roundness detection | DRIVE (40 images) | 0.9025 | - |
| **15** | Abdel-Ghafar & Morris, 2007 [69]: Circular Hough Transform | None | - | - |
| **16** | Fleming et al., 2007 [73]: Elliptical form of blood vessels | Local dataset (1056 images) | 0.9840 | - |
| **17** | Park et al., 2007 [57]: Tensor voting and adaptive mean-shift | STARE (90 images) | 0.8444 | - |
| **18** | Ying et al., 2007 [74]: Fractal dimension of blood vessels and local histogram analysis | DRIVE (40 images) | 0.9750 | - |
| **19** | Carmona et al., 2008 [14]: Approximating elliptical form of optic disc via genetic algorithm | Local dataset (110 images) | 0.9636 | - |
| **20** | Youssif et al., 2008 [6]: Vessels' direction matched filter | DRIVE (40 images)<br>STARE (81 images) | 1.0000<br>0.9877 | -<br>- |
| **21** | Niemeijer et al., 2009 [38]: Vasculature measurements and the k-NN regression | Local dataset (600 images) | 0.9300 | - |
| **22** | Aquino, et al., 2010 [31]: Morphology, edge detection and circular Hough transform | MESSIDOR (1200 images) | 0.8600 | - |
| **23** | Lu, 2010 [79]: Estimation of retinal background surface and directional blood vessel information | DIARETDB0 (130 images)<br>DIARETDB1 (89 images)<br>DRIVE (40 images)<br>STARE (81 images) | 0.9888<br>0.9923<br>0.9750<br>0.9506 | -<br>-<br>-<br>- |
| **24** | Rangayyan et al., 2010 [75]: vessels convergence by Gabor filters and phase portrait modeling | DRIVE (40 images)<br>STARE (81 images) | 1.0000<br>0.6913 | -<br>- |
| **25** | Zhu et al., 2010 [70]: Circle detection via Hough transform | DRIVE (40 images)<br>STARE (81 images) | 0.9000<br>0.4444 | -<br>- |
| **26** | Lu, 2011 [30]: Circular transformation and image variation along multiple radial line segments | ARIA (120 images)<br>MESSIDOR (1200 images)<br>STARE (81 images) | 0.9750<br>0.9975<br>0.9876 | 0.9170<br>-<br>0.9340 |
| **27** | Dehghani et al., 2012 [64]: Histogram-based template matching | DRIVE (40 images)<br>Local dataset (273 images)<br>STARE (81 images) | 1.0000<br>0.9890<br>0.9136 | -<br>-<br>- |
| **28** | Zubair et al., 2013 [71]: Contrast enhancement and morphological transformation | MESSIDOR (1200 images) | 1.0000 | 0.9865 |
| **29** | Yu & Yu, 2014 [72]: Iterative brightest pixels extraction | STARE subset (40 images) | 0.9500 | - |
| **30** | Zhang & Zhao, 2014 [80]: Vessels distribution and directional characteristics | DIARETDB0 (130 images)<br>DIARETDB1 (89 images)<br>DRIVE (40 images)<br>STARE (81 images) | 1.0000<br>1.0000<br>1.0000<br>0.9877 | -<br>-<br>-<br>- |

According to the previous table, the plots for the sensitivity of detecting the optic disc are illustrated in Figure 2-24, Figure 2-25 and Figure 2-26, for the reviewed algorithms over the DRIVE, STARE and other miscellaneous datasets, respectively.

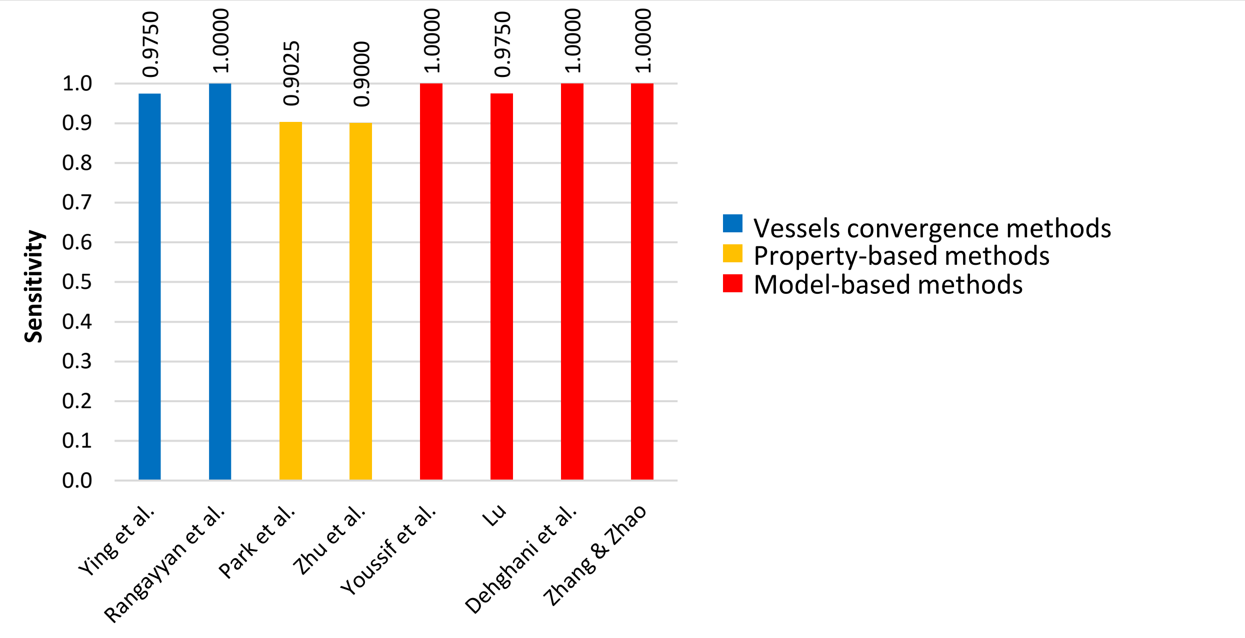

**Figure 2-24. Sensitivity of OD detection algorithms over the DRIVE dataset**

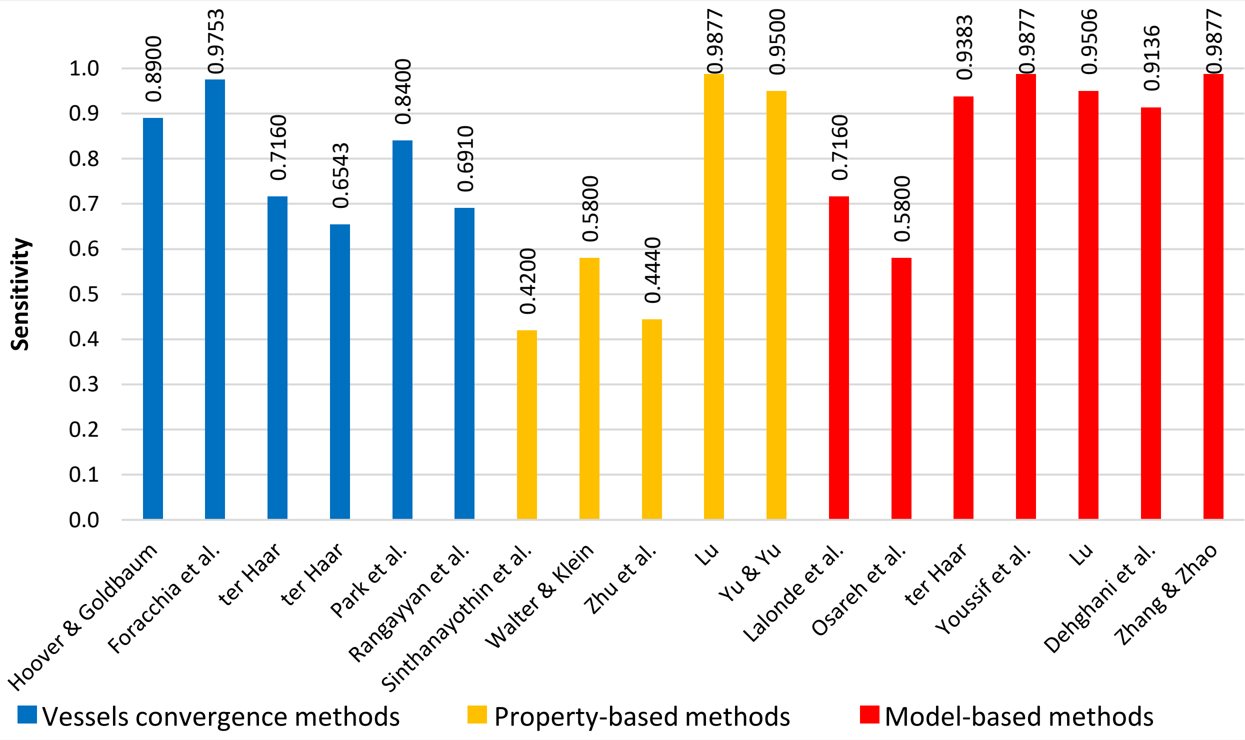

**Figure 2-25. Sensitivity of OD detection algorithms over the STARE dataset**

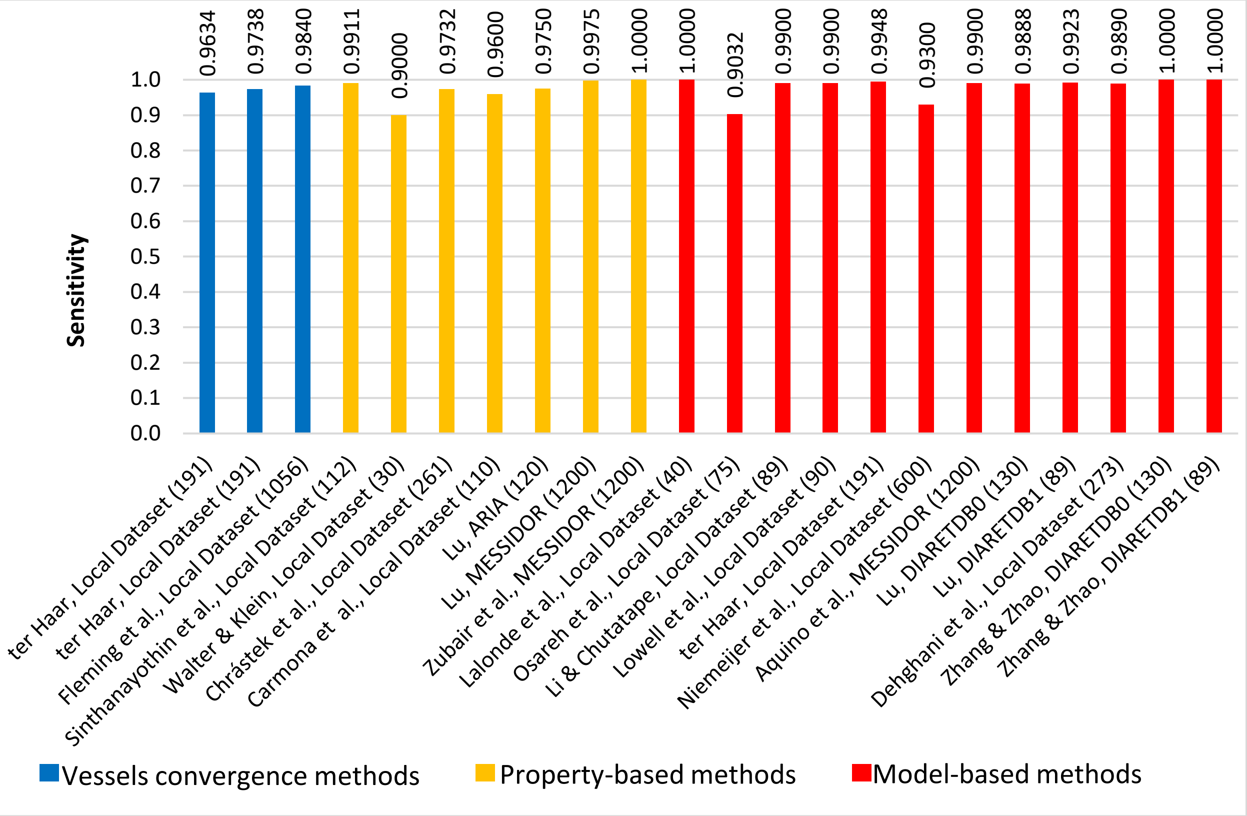

**Figure 2-26. Sensitivity of OD detection algorithms over miscellaneous datasets**

## 2.5. Detection of Eye Fundus Abnormalities

The detection of fundus lesions occurring in the interior surface of the eye, such as microaneurysms, exudates, hemorrhages, neovascularization and optic disc abnormalities, can assist in the diagnosis and treatment of serious ophthalmological diseases such as glaucoma, diabetic retinopathy, and age-related macular degeneration. In 2014, the World Health Organization (WHO) reported that 285 million people were estimated to be visually impaired worldwide: 39 million were blind and 246 had low vision, in which 80% of all visual impairment could be prevented or cured. The WHO also stated that around 90% of the world's visually impaired people lived in low-income settings [81].

The following subsections describe the motivations, clinical indicators, and the literature for two of the most leading causes of visual impairment and blindness: glaucoma and diabetic retinopathy.

### 2.5.1. Motivation of Detecting Glaucoma

Statistically, about 60 million people all over the world were found to have glaucoma in 2010 who were estimated to reach 80 million by 2020 [82], and according to the Egyptian Society for the Glaucomas (ESG), about 0.5% to 1% of the population in Egypt suffer from glaucoma (i.e. more than half a million people) [83]. Moreover, glaucoma presents a great health motivation over other eye diseases, such as cataract and diabetic retinopathy, because the damage that glaucoma causes is permanent and irreversible (i.e. could not be cured). In addition, glaucoma patients lose their vison gradually such that they are often unaware of it until their sight has already been compromised. For this reason, glaucoma is often called the “sneak thief of sight" [84].

### 2.5.2. Clinical Indicators of Glaucoma

Glaucoma is a neuropathy disease that occurs due to the damage and loss of ganglion cells. Typically, there are five main different types of glaucoma: primary open-angle, normal-tension, closed-angle, congenital, and secondary glaucoma [84]. Glaucomatous damage typically affects the intrapapillary region (i.e. inside the optic disc), as well as the peripapillary region (i.e. the optic disc surroundings). Thereby, ophthalmologists agreed that glaucoma can be diagnosed through the following five indicators within the intrapapillary and peripapillary regions [8], [85]:

**i. Cup-to-Disc Ratio (CDR)**

The CDR is defined as the ratio of the vertical diameter of the optic cup to the vertical diameter of the neuroretinal rim which is an important structural indicator for assessing the presence of glaucoma characterized by the cupping of the optic disc, as shown earlier in Figure 2-22. Clinically, glaucoma is suspicious with a CDR more than 0.6. However, the CDR in only one eye is not always a reliable indicator due to the varying cup size among patients. Therefore, a glaucomatous optic cup can be identified more precisely via the cupping asymmetry in the left-and-right eye pair, where the asymmetry ratio is typically more than 0.2 [86], [87].

**ii. ISNT Rule**

However, it is possible to have a healthy optic disc with a large CDR (especially in myopic eyes), and it is also possible to have a glaucomatous optic disc with a normal CDR. So, besides CDR, glaucoma is also diagnosed when the optic cup is tilted (i.e. the neuroretinal rim thickness violates the ISNT rule). The healthy optic disc typically demonstrates a configuration where the inferior neuroretinal rim (i.e. lower rim) is the widest portion of the rim, followed by the superior rim (i.e. upper rim), and then the nasal rim (i.e. inner, nearest the nose), and finally the temporal rim (outer, nearest the temple) which is the narrowest [88], [89], [90], as shown in Figure 2-27.

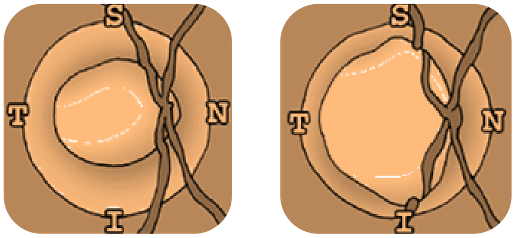

**(a)** **(b)**

**Figure 2-27. Sketch of the ISNT rule for the thickness of the neuroretinal rim**
**(a)** Healthy optic disc in a right eye – follows the ISNT rule
**(b)** Glaucomatous optic disc in a right eye – violates the ISNT rule

### iii. Disc Hemorrhages

Another important clinical indicator of glaucoma is the presence of splinter-like hemorrhages within the optic disc whose existence is more common in normal-tension glaucoma, compared to all other types of glaucoma. Moreover, disc hemorrhaging most often occurs in the same regions of, and also associated with, “Rim Notching” and “Nerve Fiber Layer Defect” (i.e. occurs within the inferior-temporal and superior-temporal regions). Besides, disc hemorrhages may repeatedly appear and disappear at different intervals of time, and accordingly, the color and size of disc hemorrhages depends upon how long they have been present, since they are transient, lasting from two to six months [85], [91]. Figure 2-28 shows different examples of optic disc hemorrhages which have many appearances, depending on how long they have been present.

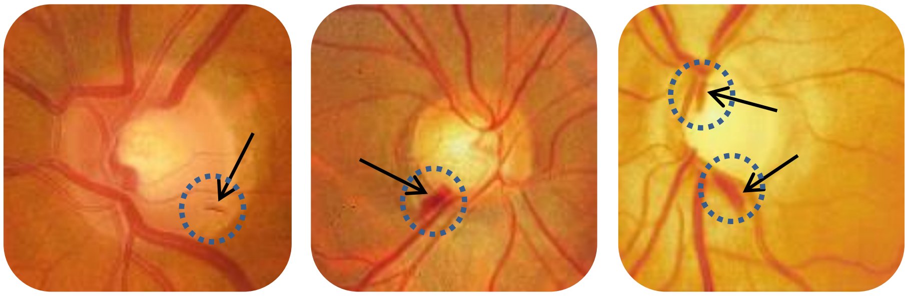

**Figure 2-28. Optic disc splinter hemorrhages**

### iv. Nerve Fiber Layer Defect (NFLD)

The retinal nerve fiber layer (RNFL) is formed by the ganglion cell axons which represents the innermost layer of the eye fundus. Due to the loss of ganglion cells in glaucoma, it is well known that the NFLD precedes and subsequently leads to the enlargement of the optic cup; and hence the NFLD is considered one of the earliest signs of glaucoma [92].

The RNFL is best observed using red-free or green light images where the normal healthy eye has a thick layer of retinal nerve fibers which can be seen as fine bright striations (strips). The RNFL demonstrates a “bright-dark-bright” pattern when viewed up from the superior-temporal region down to the inferior-temporal region. In other words, the retina shines in the regions in which the RNFL is thickest (i.e. superior-temporal and inferior-temporal regions), whereas the area between the disc and the macula (i.e. temporal region) appears darker [85], [86], [93]. Figure 2-29 (a) shows an example of the bright striations around the superior and inferior parts in a healthy retina creating the bright-dark-bright pattern (reproduced from [93]).

On the other hand, the region around the optic disc with NFLD gets darker and changes from stripy-texture to wedge-shaped form. Also, blood vessels appear darker with sharp reflexes in the region of NFLD, as shown in Figure 2-29 (b) [93].

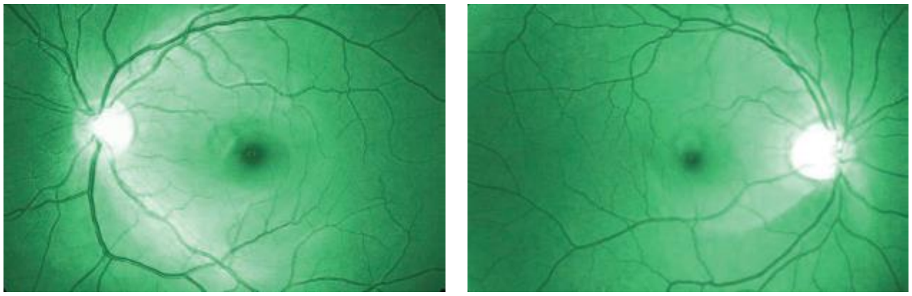

**(a)** **(b)**

**Figure 2-29. Red-free optic disc image showing nerve fiber layer**
**(a)** Normal NFL: bright-dark-bright strip pattern **(b)** NFLD below the optic disc

There are two kinds of NFLD, namely, localized and diffuse. The localized NFLD appears as a wedge-shaped dark area that follows the pattern of the RNFL originating from the optic disc [85], [86]. In such defects, the specificity is very high but the sensitivity is low since these defects are a definite sign of pathology, but can occur in diseases other than glaucoma [86]. Figure 2-30 shows an example of a localized NFLD showing a dark wedge-shaped defect that touches the edge of the optic disc and increases in width toward the periphery.

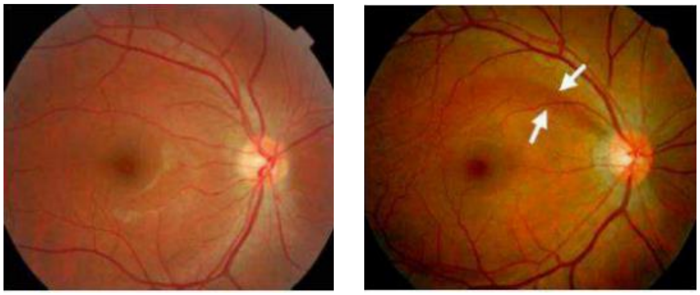

**(a)** **(b)**

**Figure 2-30. Example of localized NFLD**

**(a)** Normal NFL **(b)** Localized NFLD with a dark wedge

On the other hand, diffuse NFLD can be seen in advanced glaucoma. It is usually more difficult to be detected in one eye, but it is easily recognized when both eyes are compared together. In diffuse NFLD, there is a general reduction of the RNFL brightness causing the normal “bright-dark-bright” pattern to be lost and look like a “dark-dark-dark” pattern (i.e. appears completely dark) [85], [86], [93].

### v. Peripapillary Atrophy (PPA)

The peripapillary region, as its name implies, is the area located around the periphery of the papilla (i.e. just outside the optic disc). Thus, the peripapillary atrophy (PPA) refers to the thinning and degeneration of the chorioretinal tissue around the optic disc. Two distinct zones of atrophy, Alpha zone (α) and Beta zone (β) can surround the optic disc, where the Alpha zone is located on the outer periphery of the Beta zone, as shown in Figure 2-31.

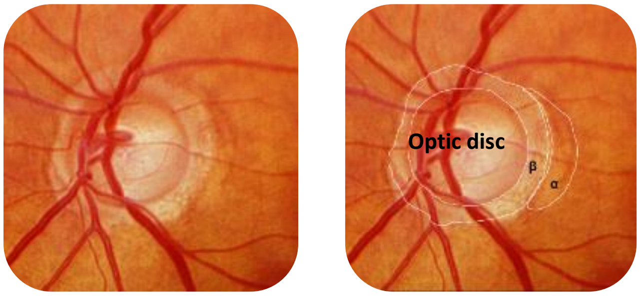

**(a)** **(b)**

**Figure 2-31. Peripapillary atrophy**

(a) Glaucomatous papilla (b) Marked alpha and beta zones

The outer zone alpha (α) is present in almost any eye (i.e. normal and glaucomatous). This zone is characterized by a region of irregular hypopigmentation and hyperpigmentation of the retinal pigment epithelium (RPE). The inner beta zone (β) is more often observed in glaucomatous eyes than in healthy eyes, which is characterized by visible sclera and visible large choroidal vessels, located between the peripapillary ring and alpha zone, showing a complete loss of the RPE. The peripapillary atrophy is located and associated within the region of neuroretinal rim loss, with the atrophy being largest in the corresponding area of thinner neuroretinal rim [85], [94].

Table 2-3 summarizes the main structural indicators described within this section as well as the functional characteristics indicating the presence or the suspect of glaucoma.

**Table 2-3. Glaucoma structural and functional indicators**

| Clinical Indicator | Glaucoma Risk Reference | Viewable in fundus image |
|---|---|---|
| Cup-to-disc ratio (CDR) | Greater than 0.6 | ✓ |
| Left-Right cup asymmetry | Greater than 0.2 | ✓ |
| ISNT irregularity | Thinning of inferior & superior rim (notching) | ✓ |
| Disc hemorrhages | Present at inferior & superior sectors | ✓ |
| Nerve fiber layer defects | Present | ✓ |
| Peripapillary atrophy | Beta zone appears adjacent to rim loss region | ✓ |
| Rim color | Pink (except in very end-stage disease) | ✓ |
| Intraocular pressure (IOP) | Higher than 21 mmHg | × |
| Defect of visual field (VF) | Present | × |
| Myopia (near sightedness) | Present | × |
| Age | Above 60 years | × |
| Ethnicity | African / Hispanic / East Asian | × |
| Family history | Positive | × |

### 2.5.3. Literature of Glaucoma Diagnosis

Fundus images were, and are still, widely used by many ophthalmologists for diagnosing glaucoma instantly and spontaneously, which makes them suitable for large-scale screening. This is because of their fast and low-cost acquisition compared to images captured via other imaging modalities reviewed in section 1.1.2, such as OCT and HRT. Thus, most of the work done for diagnosing glaucoma typically exploited one or more of the main structural characteristics of glaucomatous optic disc described in section 2.5.2. Moreover, some other very few approaches also employed some of the functional features of glaucomatous subjects, such as the visual field defect, myopia and the high intraocular pressure. These functional features are considered an additional source for diagnosing glaucoma, but obviously can never be viewed within the captured fundus images, as previously shown in Table 2-3.

For instance, Song *et al.* [95] utilized a set of fuzzy “if-then” rules that defined a set of criteria for glaucoma diagnosis. That set of diagnosis criteria was based on two structural features of the optic disc which were the NFLD and CDR. Moreover, in order to increase the accuracy of glaucoma diagnosis, the fuzzy set also used two more functional features of the eye which were the visual field test and the intraocular pressure measurement. Using 128 photographs, the authors claimed that their fuzzy set technique obtained sufficient sensitivity and specificity, without reporting quantitative results.

Hayashi *et al.* [96] relied on the detection of NFLD in the fundus images in order to diagnose glaucoma. At the beginning, the blood vessels were removed from the original image using morphological operations. Consequently, the optic disc was detected within the vessels-free image using snakes, which was then transformed into a rectangular array using a polar coordinate read-out. The NFLD regions were finally localized as vertical dark bands by using Gabor filtering. Their proposed technique detected 71% of the NFLD regions within 52 fundus images with an average of 3.2 false positives per image.

Continuing their previous work described in the preceding paragraph, Muramatsu *et al.* [92] again relied on the detection of NFLD for early diagnosis of glaucoma. Similar to their previous work, the major blood vessels were first removed from the fundus image. Afterwards, the images were transformed by creating a set of elliptical curves that represented the estimated paths of the retinal nerves. Consequently, Gabor filtering was applied in order to enhance the contrast of NFLDs, in which the band-like regions darker than the surrounding pixels were selected as NFLD candidates. For each of these initial candidates, six features were used by a neural network to determine the likelihood score of being a true NFLD.

Muramatsu *et al.* [97] again extended their previous work by presenting a technique for detecting the peripapillary atrophy (PPA) which is the other peripapillary feature of glaucoma. The objective of their procedure was to detect the PPA by using a texture analysis based on the gray-level co-occurrence matrix. In a dataset of 26 images, the sensitivity and specificity for detecting moderate-to-severe PPA regions was 73% and 95%, respectively.

Liu *et al.* [98] proposed ARGALI system which automatically measured the CDR for the sake of automated glaucoma risk assessment. They used the variational level-set algorithm to extract and segment the optic disc. Subsequently, the optic cup was segmented using a multi-modal approach in which a color histogram analysis was first performed; afterwards the optic cup boundary was segmented by applying the level-set algorithms, and finally the segmented cup was smoothened using ellipse fitting. At the last stage of ARGALI, a multi-layer neural network was proposed in order to fuse the results obtained via the various modes.

In the same direction, Burana-Anusorn *et al.* [99] presented a technique for measuring the CDR automatically in order to detect glaucoma. For extracting the optic disc, they exploited two methods: Canny edge detection method as well as a variational level-set method. As for the optic cup, it was extracted using color component analysis and threshold level-set method. At the end, ellipse fitting was applied in order to reshape the boundaries of the extracted disc and cup. In a dataset of 44 images, their approach showed that the sensitivity of glaucoma classification was 80%, and the specificity was 93%.

Nayak *et al.* [100] extracted three intrapapillary features for automated glaucoma diagnosis which were CDR, size of optic disc, ISNT ratio. The optic disc and the optic cup were segmented via the red and green planes, respectively, after inpainting the blood vessels using morphological operations. Those three features were used to classify the normal and glaucomatous images using a neural network classifier, achieving a sensitivity and specificity of 100% and 80%, respectively.

Joshi *et al.* [101] proposed a technique for glaucoma diagnosis via an intrapapillary indicator (i.e. CDR). They then extended their work by proposing another technique to detect the peripapillary glaucomatous features (i.e. PPA and NFLD) [102]. In their former work [101], the cup boundary was detected in monocular fundus images based on the vessel-bends at the boundary of the optic cup. The bends in a vessel were robustly detected using a region of support concept. Consequently, a reliable subset of vessels bends, called r-bends, was obtained using a multi-stage selection algorithm, which in turn helped to detect the desired cup boundary using a local spline fitting approach. Moreover, in their latter work for detecting the PPA and NFLD indicators [102], they proposed a detection algorithm based on the salience property associated with these two indicators. They first extracted candidate regions of interest along with the respective adjacent region. Then, they modeled the region of interest as a region that was significantly different from the adjacent image regions, at an appropriate feature level.

Based on the CDR evaluation, Madhusudhan *et al.* [103] presented and tested three different techniques for detecting glaucoma. The proposed methods were multi-thresholding, active contour model (i.e. snakes), and region-growing segmentation. The fundus images were fist preprocessed via illumination correction, blood vessels removal, and optic disc normalization. Afterwards, the disc and cup were segmented and thereby the CDR ratio was measured using each of the three mentioned techniques. Their comparative analysis showed that the region-growing technique achieved the best results with sensitivity and specificity of 94.73% and 100%, respectively.

Cheng *et al.* [104] proposed a superpixel-based classification framework for the optic disc and optic cup segmentation to be used for glaucoma screening. Their approach used the simple linear iterative clustering algorithm to aggregate nearby pixels into superpixels. In order to segment the optic disc, they exploited histograms as well as center surround statistics to classify each superpixel as "disc" or "non-disc". Along with the histograms and center surround statistics, they also included the location information in order to segment the optic cup. Finally, a support vector machine with linear kernel was applied to classify superpixels as "discs" and "non-discs", as well as "cups" and "non-cups". At the end, the CDR was computed for glaucoma screening in two different datasets, achieving areas under curve of 0.8 and 0.822.

Table 2-4 lists the aforementioned methods for glaucoma detection in a chronological order.

**Table 2-4. List of glaucoma detection methods (intrapapillary and peripapillary lesions)**

| | Approach | Glaucoma Indicators | Dataset size | SENS | SPEC | ACC |
|---|---|---|---|---|---|---|
| **1** | Song *et al.*, (2005) [95] | CDR, NFLD, IOP, VF | 128 images | - | - | - |
| **2** | Hayashi *et al.*, (2007) [96] | NFLD | 52 images | 0.7100 | 0.9680 | |
| **3** | Liu *et al.*, (2009) [98] | CDR | 23 images | 0.9500 | | |
| **4** | Nayak *et al.*, (2009) [100] | CDR, ISNT | 61 images | 1.0000 | 0.8000 | 0.9000 |
| **5** | Muramatsu *et al.*, (2010) [92] | NFLD | 162 images | 0.9100 | | |
| **6** | Joshi *et al.*, (2011) [101] | CDR | 138 images | | | |
| **7** | Muramatsu *et al.*, (2011) [97] | PPA | 26 images | 0.7300 | 0.9500 | |
| **8** | Madhusudhan *et al.*, (2011) [103] | CDR | 25 images | 0.9473 | 1.000 | |
| **9** | Joshi *et al.*, (2012) [102] | PPA, NFLD | 139 images | | | |
| **10** | Burana-Anusorn *et al.*, (2013) [99] | CDR | 44 images | 0.8000 | 0.9300 | 0.8900 |
| **11** | Cheng *et al.*, (2013) [104] | CDR | 2326 images | | | |

### 2.5.4. Motivation of Detecting Diabetic Retinopathy

In addition to glaucoma, diabetic retinopathy is another major sight-threatening complication caused by diabetes mellitus. Diabetes harmfully affects the retina (so called diabetic retinopathy), as well as the kidneys (diabetic nephropathy) and the nervous system (diabetic neuropathy) [7], [13]. As reviewed by the WHO in 2016 [105], 2.6% of global blindness could be attributed to diabetic retinopathy, in which the number of people with diabetes had risen from 108 million in 1980 to 422 million in 2014. Moreover, the global prevalence of diabetes among adults over 18 years of age had risen from 4.7% in 1980 to 8.5% in 2014. Accordingly, the greatest emphasis in automated diagnosis had unsurprisingly been given to the detection of diabetic retinopathy.

### 2.5.5. Clinical Indicators of Diabetic Retinopathy

There are no predictable symptoms in the very early stages of diabetic retinopathy (DR), but the severity of diabetic retinopathy increases during the time. Thereby, DR can be classified into four levels according to the grade of severity: (1) mild non-proliferative diabetic retinopathy (NPDR), (2) moderate NPDR, (3) severe NPDR, and (4) proliferative diabetic retinopathy (PDR) [13], [52], [106].

Moreover, the indicators of diabetic retinopathy can be roughly categorized into two classes: “dark lesions” which include microaneurysms and hemorrhages, and “bright lesions” which include hard and soft exudates [50]. Specifically, the mild NPDR typically begins with small changes in the retinal vessels, where the first detectable abnormality is the microaneurysms which are local distensions of the retinal vessels. Microaneurysms eventually rupture to form hemorrhages deep within the retina, which because of their dot-like appearance, they are called "dot-and-blot" hemorrhages. Over time, retinal edema and hard exudates are followed by the increased permeability of the vessels’ walls. The hard exudates are lipid formations leaking from these weak blood vessels. This state of the retinopathy is called moderate NPDR. However, if these abnormalities appear in the central vision area (i.e. macula), it is called diabetic maculopathy. As this state of NPDR progresses, the blood vessels become obstructed resulting in white fluffy patches in the retina called cotton wool spots or soft exudates. When a significant number of hemorrhages, soft exudates, or vascular abnormalities are encountered, the state of the retinopathy is graded as severe NPDR. This severe NPDR can quickly turn into proliferative diabetic retinopathy (PDR) when extensive lack of oxygen causes the development of new fragile vessels (i.e. neovascularization) which is a serious sight-threatening state. The proliferative diabetic retinopathy may cause sudden loss in visual acuity or, in worst case, permanent blindness due to vitreous hemorrhage or detachment of the central retina [13], [106]. Figure 2-32 illustrates these different types of the “dark” and “bright” abnormalities occurring in diabetic retinopathy.

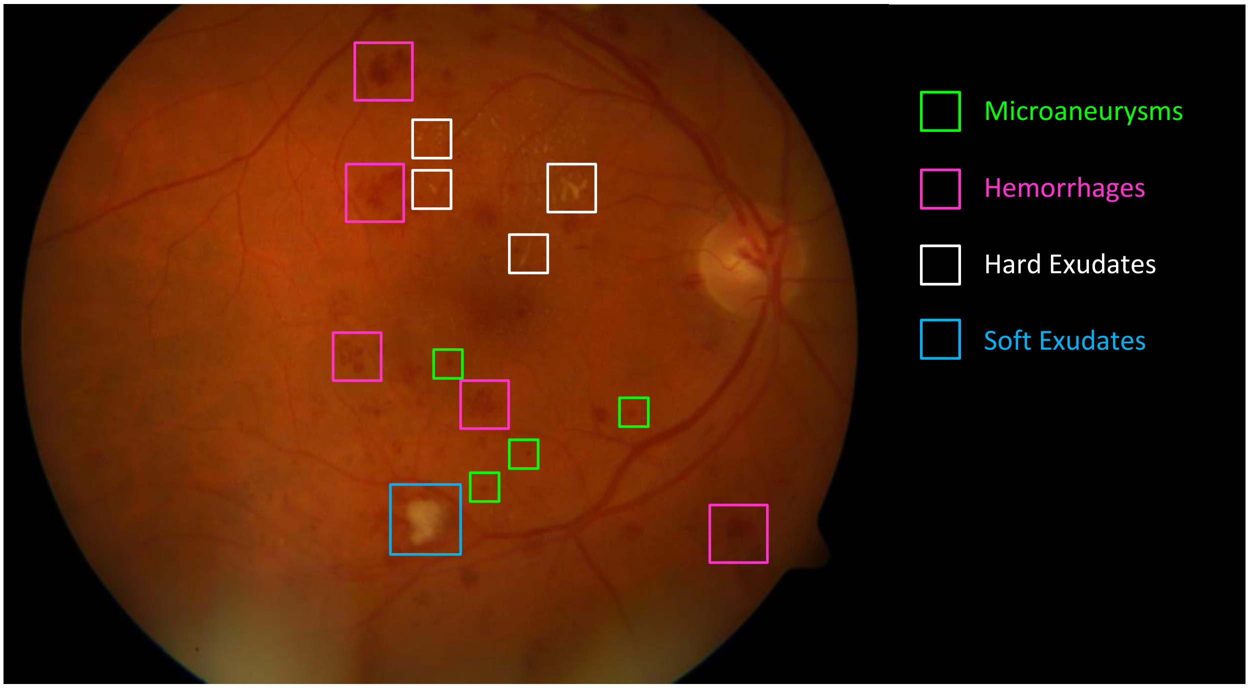

**Figure 2-32. Abnormalities occurring in eye fundus due to diabetic retinopathy**

Table 2-5, as proposed by Wilkinson *et al.* [106], provides a severity grading scale for the different levels of diabetic retinopathy according to the abnormalities observed within the retina.

**Table 2-5. International clinical diabetic retinopathy disease severity scale**

| **Severity Level of Diabetic Retinopathy** | **Observable Abnormalities** |
|---|---|
| Mild NPDR | Microaneurysms only. |
| Moderate NPDR | Microaneurysms and/or soft exudates but less than "Severe NPDR". |
| Severe NPDR | Any of the following and no signs of PDR:<br>1. More than 20 intraretinal hemorrhages in each of four quadrants.<br>2. Definite venous beading in two or more quadrants.<br>3. Prominent intraretinal microvascular abnormalities in one or more quadrants. |
| Proliferative DR | One or more of the following:<br>1. Definite neovascularization<br>2. Vitreous/pre-retinal hemorrhage |

### 2.5.6. Literature of Diabetic Retinopathy Diagnosis

As mentioned earlier in section 1.2.2, eye fundus abnormalities are identified either for diagnosing or for monitoring a disease such as diabetic retinopathy. Moreover, most of the detection systems also aim to detect the fundus landmarks (e.g. optic disc, macula and blood vessels) and then eliminate them to facilitate the detection of abnormalities that have similar appearance in spatial features (e.g. color, size and shape) [13]. As mentioned before in section 2.5.5, non-proliferative diabetic retinopathy is clinically diagnosed via the presence of two categories of lesions: the bright lesions (i.e. hard exudates and soft exudates), and the dark lesions (i.e. microaneurysms and hemorrhages).

#### i. Detection of the bright lesions (exudates)

Harangi *et al.* [107] enhanced the visual appearance of the exudates by eliminating the optic disc as well as improving the contrast of the green channel via CLAHE. Then, they identified the candidate regions containing exudates via morphological closing and reconstruction. Consequently, 56 descriptors were extracted for each candidate pixel to classify them, where the most relevant features were selected to train a boosted naïve Bayes classifier. This approach achieved a sensitivity of 63% over the DIARETDB1 dataset.

Similar to the previous method of preprocessing, Jaafar *et al.* [108] first enhanced the contrast of the green channel using CLAHE. Consequently, the hard exudates were detected by top-down image segmentation to partition the image into two homogeneous regions followed by Canny edge detection and region growing to segment the candidates of hard exudates. These candidates were classified into either “exudates” or “non-exudates” using a rule-based classifier. The proposed method successfully detected the hard exudates in 93.2% of the 106 images picked from the DIARETDB1 and MESSIDOR datasets.

Kumar *et al.* [109] employed histogram analysis to detect exudates. First, the contrast of the image was changed via the nonlinear curve with brightness values of the HSV space, in which gamma correction was applied on each of the red and green components of the image. Then, the exudates candidates were detected using histogram analysis. Finally, multi-channel histogram analysis was performed to eliminate the false positive candidates in the optic disc. This algorithm was tested over a dataset of 158 images achieving a sensitivity and specificity of 88.45% and 95.5%, respectively.

Sopharak *et al.* [110] preprocessed the image in order to enhance its contrast and eliminate the optic disc. Then, they carried out a set of experiments on feature selection and exudate pixel classification using a naïve Bayes classifier, which proved that the best feature set is a combination of six features: (1) the preprocessed pixel intensity, (2) the standard deviation of the preprocessed intensities in a window around the pixel, (3) the pixel's hue, (4) the number of edge pixels in a window around the pixel, (5) the ratio between the size of the pixel's intensity cluster and the optic disc, and (6) the response of the pixel to Gaussian filter derivative. Their approach correctly classified the exudates in 93.38% of a dataset containing 39 images.

Again, in order to prevent confusion with exudates, Sreng *et al.* [111] first detected and eliminated the optic disc through image binarization, ROI-based segmentation and morphological reconstruction. Then, the exudates were detected by applying the maximum entropy thresholding to filter out the bright pixels, and finally, exudates were extracted via morphological reconstruction. This exudates extraction method was tested over 100 fundus images achieving a sensitivity of 91%.

Eadgahi and Pourreza [112] detected and eliminated the blood vessels using bottom-hat transformation and then extracted the bright components of high intensities using the top-hat transformation. After extracting the bright components, their method consequently distinguished the exudates by locating and eliminating the optic disc via its distinctive properties such as its high intensity and its high density of blood vessels. Their method successfully extracted exudates with an average sensitivity of 78.28% over the DIARETDB1 dataset.

Sinthanayothin *et al.* [113] detected the exudates based on a recursive region-growing segmentation algorithm. Their approach clustered similar pixels using the intensity difference as a criterion for recursive region growing to detect two classes of lesions: bright (exudates) and dark (microaneurysms and hemorrhages). Then, a binary image was produced via thresholding in which the regions containing the exudates were overlaid onto the original image. This region-growing technique achieved a sensitivity and specificity of 88.5% and 99.7%, respectively, within a dataset composed of 30 images of which 21 contained exudates.

Li and Chutatape [77] utilized the LUV color space for segmenting exudates. The Canny edge detector was employed along with the region growing algorithm based on three thresholds, namely, the gradient of the pixel, the difference between pixel value and the region's mean value, and the difference between pixel value and seed value. Their approach was tested on a dataset of 35 images achieving a sensitivity and specificity of 100% and 71%, respectively.

Osareh *et al.* [114] normalized the fundus images via histogram specification, and then applied local contrast enhancement on the intensity channel "I" of the HSI color space. Afterwards, they detected the coarse hard exudates regions using fuzzy C-means clustering with Gaussian smoothed histograms for each color channel in the fundus image. In order to classify the segmented regions into exudates and non-exudates, an artificial neural network classifier was employed, after eliminating the optic disc. This method successfully classified exudates in 93% of a dataset composed of 142 images.

Franklin and Rajan [115] preprocessed the fundus images in the LAB color space using CLAHE to enhance its contrast. After eliminating the optic disc, the bright pixels were detected and classified as either "exudates" or "non-exudates" based on their high grey-level variations via employing an artificial neural network that utilized features such as color, size, shape, edge strength and texture. Their algorithm was tested over DIARETDB1 achieving an average sensitivity and specificity of 96.3% and 99.8%, respectively.

Singh *et al.* [116] proposed two independent methods to detect exudates after eliminating the optic disc, and then strategically combined both methods to reduce all possible false positives. The first method transformed the OD-free image into the LAB color space, in which the contrast of the luminance channel was adjusted and then thresholded in order to detect exudates. Whilst, the second method morphologically processed the green channel of the OD-free image by dilating it twice via two different structuring elements, and consequently subtracted the two dilated images in order to detect exudates edges. Finally, both methods were combined using some morphological and logical operators in order to remove noisy false positives. Their algorithm achieved an average sensitivity of 94.87% over a dataset made up of 20 diabetic fundus images.

Roychowdhury *et al.* [117] measured the severity grade of diabetic retinopathy using a machine learning system that classified the bright and red lesions. Their algorithm went through three stages; initially the optic disc and blood vessels were detected and then excluded from further processing. Secondly, the bright lesions were detected and classified into exudates or cotton wool spots, and the red lesions were classified into microaneurysms or hemorrhages. At the end the severity grade was estimated according to the severity scale specified by MESSIDOR project. Among several classifiers, the Gaussian Mixture Model (GMM) classifier proved to be the best in classifying the bright lesions using a set of 30 features, achieving a sensitivity and specificity of 89% and 85%, respectively, over the DIARETDB1 dataset.

To detect the exudates, Rajan *et al.* [118] utilized the orientation scores of the retinal image to form an orientation-enhanced image, from which a binary mask of exudates was obtained by thresholding. First, the 2D orientation-score framework mapped the position and orientation angle of each pixel to a complex scalar, where the information of the edges and oriented structures were given by the imaginary and real parts, respectively. Afterwards, an enhanced image was formed using the real and imaginary parts of the complex scores. Furthermore, the other bright landmarks were removed from the enhanced image to reduce the false positives. Finally, the resultant intensity image was thresholded to obtain the exudates, achieving a sensitivity and specificity of 86.2% and 85%, respectively, over the DIARETDB1 dataset.

Prentasic and Loncaric [119] detected the exudates using deep convolutional neural networks. First, the anatomical structures of the eye fundus were detected. Accordingly, the probability maps of blood vessels, optic disc, parabola fitting and values for the bright border detection were combined all together to get one probability map via weighted summing. Afterwards, the outputs of those probability maps were combined with the output of the deep neural network of exudates in order to reduce the false positive detection and hence improve the detection accuracy. This algorithm achieved a sensitivity of 78% using 50 fundus images from the DRiDB database.

Liu *et al.* [120] presented a location-to-segmentation strategy for segmenting exudates via three stages. First, the fundus image was preprocessed by removing the main vessels and the optic disc to facilitate the detection of the exudate patches at the further stages. In the second stage, the random forest classifier was learned to classify, identify and locate the exudate patches, in which the histograms of completed local binary patterns were extracted to describe the texture structures of the patches. At the final stage, the local variance, the size prior about the exudate regions and the local contrast prior were used to segment the exudate regions out from patches which were classified as exudate patches in the location stage. The algorithm was tested on DIARETDB1, achieving a sensitivity and specificity of 83% and 75%, respectively.

### ii. Detection of the red lesions

The preceding algorithm [117], as mentioned, classified the red lesions into microaneurysms and hemorrhages. A k-NN classifier was employed to do so and scored the best classification results against other various classifiers. The number of microaneurysms and hemorrhages were then utilized to grade the severity level of diabetic retinopathy. The algorithm successfully classified the red lesions within the DIARETDB1 dataset with a sensitivity of 80% and a specificity of 85%.

Similarly, in the work of Sinthanayothin *et al.* [113] for detecting indicators of diabetic retinopathy, they detected the red lesions besides exudates, as described in the previous section. They treated microaneurysms and hemorrhages as one group of lesions, but due to similarities in color, the blood vessels were classified into that same group as well. To overcome that problem, a neural network was used to identify the blood vessels and extract them from the image. Their algorithm achieved a sensitivity of 77.5% and specificity of 88.7% in detecting red lesions within 30 fundus images of which 14 of them contained microaneurysms or hemorrhages.

Fleming *et al.* [121] were able to distinguish microaneurysms against other dots that occurred within the retina via contrast normalization. Their approach showed that the contrast was best normalized using watershed transform which derived a region that contained no vessels or other lesions. The dots occurring within blood vessels were then handled successfully using a local vessel detection technique. They tested their algorithm for identifying the images that contained microaneurysms within 1441 images, as well as detecting the microaneurysms themselves in 71 additional images. Images containing microaneurysms were identified with a sensitivity of 85.4% and specificity of 83.1%.

Driven by the motivation of detecting microaneurysms within color fundus images, Niemeijer *et al.* [122] provided the Retinopathy Online Challenge (ROC) database, along with an online competition in which detection systems were submitted and evaluated. Detection algorithms were evaluated via the competition performance metric (CPM) which is the average sensitivity values at several false positives ratios, ⅛, ¼, ½, 1, 2, 4, and 8. Although the ROC database is publicly available, yet the online submission and evaluation are no longer possible at the time being (closed in 2016). Below are the microaneurysms detection systems that achieved the top-five CPM scores on the ROC database throughout the online competition.

Achieving the first rank at the ROC competition with a CPM score of 0.464, Wang *et al.* [123] proposed an integrated method for microaneurysms detection. First, candidates were identified via a dark object filtering process. Then, their cross-section profiles along multiple directions were processed via singular spectrum analysis. The correlation coefficient between each processed profile and a typical microaneurysm profile was measured and used as a scale factor to adjust the shape of the candidate profile, in order to increase the difference in their profiles between true microaneurysms and non-microaneurysm candidates. A set of statistical features of those profiles was then extracted for a k-NN classifier.

Also, Antal and Hajdu [124] proposed a detection system called DRSCREEN which combined previous preprocessing methods and different candidate extractor techniques using optimal voting scheme. Consequently, the selection of optimal ensembles, preprocessing and candidate extractor pairs were optimized using simulated annealing. The final microaneurysms were then found by fusing the candidates of the pairs which were considered as optimal ensemble. This ensemble-based approach was tested over the ROC dataset, achieving a CPM score of 0.434. Over the MESSIDOR dataset, the performance of the algorithm was also assessed achieving a sensitivity and specificity of 0.76 and 0.88, respectively.

Dai *et al.* [125] detected microaneurysms in fundus images using a two-stage approach: extraction and classification. In the first stage, the vessels were removed and the candidate microaneurysms were localized by analyzing the gradient vectors of the images. Next, these candidates were classified into “true-microaneurysms” and “non-microaneurysms” using several features. Since the extracted candidates were extremely class-imbalanced, the class-imbalanced classifier RUSBoost was exploited to effectively classify those candidates into “true-microaneurysms” and “non-microaneurysms”. The proposed method achieved CPM of 0.433 on the ROC database, and 0.321 on the DIARETDB1 database.

Lazar and Hajdu [126] detected microaneurysms by analyzing directional cross-section profiles centered on the candidate pixels of an inverted-green blurred image. First, peak detection was applied on each profile, and consequently a set of values describing the size, height, and shape of the peak were calculated. The statistical values of these attributes (e.g. orientation of the cross-section changes) composed the feature set for a Naïve Bayes classifier in order to exclude false candidates. Finally, the algorithm calculated the final score of the remaining candidates based on the obtained feature values. The proposed method achieved an overall CPM score of 0.423 on the ROC dataset.

Fegyver [127] proposed a method based on the analysis of the concentration gradient. The algorithm applied a set of features based on gradient directions and lengths. This set of features was utilized to train a Naïve Bayes classifier in order to identify true microaneurysms. The algorithm achieved a CPM of 0.422, scoring the fifth rank on the ROC competition.

Table 2-6 chronologically lists the aforementioned methods for detecting the bright and red lesions occurring in diabetic retinopathy.

**Table 2-6. List of diabetic retinopathy detection methods (bright and dark lesions)**

| | Approach | DR Indicators | Dataset | SENS | SPEC | ACC |
|---|---|---|---|---|---|---|
| **1** | Sinthanayothin *et al.*, (2002) [113] | Exudates | Local dataset (30 images) | 0.8850 | 0.9970 | - |
| | | Red lesions | Local dataset (30 images) | 0.7750 | 0.8870 | - |
| **2** | Osareh *et al.*, (2003) [114] | Exudates | Local dataset (142 images) | 0.9300 | 0.9410 | - |
| **3** | Li & Chutatape, (2004) [77] | Exudates | Local dataset (35 images) | 1.0000 | 0.7100 | - |
| **4** | Fleming *et al.*, (2006) [121] | Microaneurysms | Local dataset (1441) | 0.8540 | 0.8310 | - |
| **5** | Sopharak *et al.*, (2008) [110] | Exudates | Local dataset (39 images) | 0.9338 | 0.9814 | 0.9338 |
| **6** | Jaafar *et al.*, (2011) [108] | Exudates | Mixed dataset (236 images) | 0.9320 | 0.9920 | 0.9940 |
| **7** | Harangi *et al.*, (2012) [107] | Exudates | DIARETDB1 (89 images) | 0.6300 | - | - |
| **8** | Antal & Hajdu, (2012) [124] | Microaneurysms | MESSIDOR (1200 images) | 0.7600 | 0.8800 | 0.8200 |
| | | | ROC dataset (100 images) | 0.4340 | - | - |
| **9** | Eadaghi & Pourreza, (2012) [112] | Exudates | DIARETDB1 (89 images) | 0.7828 | - | - |
| **10** | Fegyver, (2012) [127] | Microaneurysms | ROC dataset (100 images) | 0.4220 | - | - |
| **11** | Kumar *et al.*, (2013) [109] | Exudates | Mixed dataset (158 images) | 0.8845 | 0.9550 | - |
| **12** | Lazar & Hajdu, (2013) [126] | Microaneurysms | ROC dataset (100 images) | 0.4230 | | |
| **13** | Sreng *et al.*, (2013) [111] | Exudates | Local dataset (100 images) | 0.9100 | - | - |
| **14** | Franklin & Rajan, (2014) [115] | Exudates | DIARETDB1 (89 images) | 0.9630 | 0.9980 | 0.9970 |
| **15** | Roychowdhury *et al.*, (2014) [117] | Bright lesions | DIARETDB1 (89 images) | 0.8900 | 0.8500 | - |

| | Approach | DR Indicators | Dataset | SENS | SPEC | ACC |
|---|---|---|---|---|---|---|
| | | Red lesions | DIARETDB1 (89 images) | 0.8000 | 0.8500 | - |
| **16** | Singh *et al.*, (2015) [116] | Exudates | Local dataset (20 images) | 0.9487 | - | - |
| **17** | Dai *et al.*, (2016) [125] | Microaneurysms | DIARETDB1 (89 images) | 0.3210 | - | - |
| | | | ROC dataset (100 images) | 0.4330 | - | - |
| **18** | Wang et al., (2016) [123] | Microaneurysms | ROC dataset (100 images) | 0.4640 | - | - |
| **19** | Rajan et al., (2016) [118] | Exudates | DIARETDB1 (89 images) | 0.8620 | 0.8500 | - |
| **20** | Prentasic & Loncaric (2016) [119] | Exudates | DRiDB (50 images) | 0.7800 | - | - |
| **21** | Liu et al., (2017) [120] | Exudates | DIARETDB1 (89 images) | 0.8300 | 0.7500 | - |

# Chapter 3. System Architecture

Based on the literature pertaining to the segmentation and detection of the landmarks and abnormalities within the eye fundus images, this chapter hereby presents the proposed system architecture. The block diagram shown in Figure 3-1 illustrates the proposed architecture of segmenting the optic disc and the bright abnormalities, showing the data that was employed, the steps that were followed and the procedures that were applied in manipulating the eye fundus images [128].

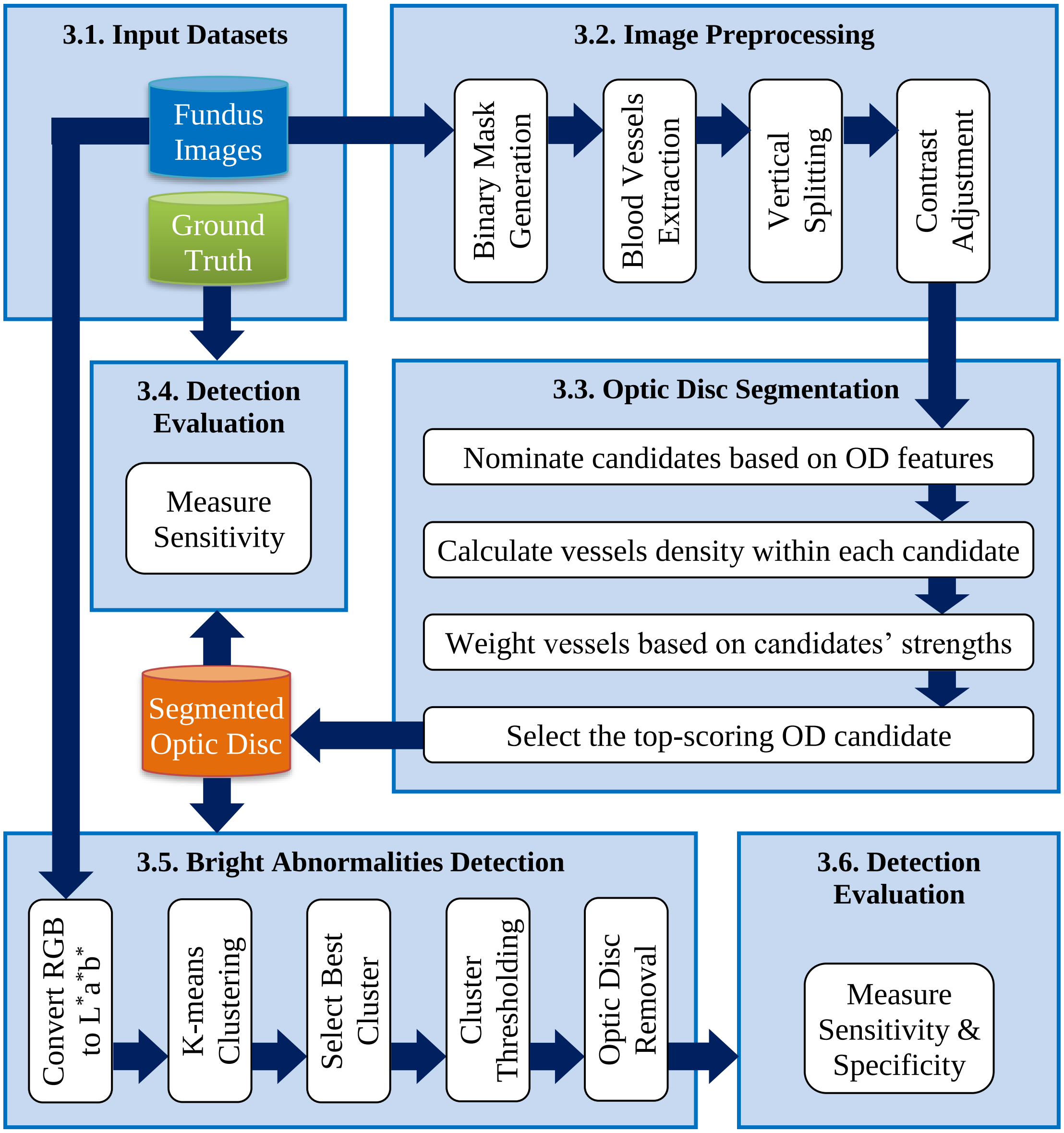

**Figure 3-1. Block diagram of the proposed system architecture**

Each of the block components for this proposed architecture is clarified in detail at the subsequent sections. Figure 3-2 shows the corresponding algorithm proposed to segment the optic disc and the bright lesions within miscellaneous fundus images from diverse image datasets.

For the sake of organization and clarity, each step in the algorithm is numbered in a way that is typically consistent with the numbering of this chapter, as well as the numbering of the previous block diagram.

```
For each of the employed datasets:
3.1 Input Datasets: retrieve all the fundus images within the dataset
3.2. Preprocessing the fundus images
    3.2.1. Generate the binary mask for the ROI and mask out the dark background
    3.2.2. Roughly extract the blood vessels using Canny edge detector
    3.2.3. Split the extracted vasculature into two vertical halves
    3.2.4. Adjust the contrast of the intensity image of the selected half
3.3. Optic Disc Segmentation
    3.3.1. Nominate the OD candidates based on their brightness, size, and roundness
    3.3.2. Calculate the vessels density within each candidate
    3.3.3. Weight the vessels density within each candidate based on their strengths
    3.3.4. Select the segmented optic disc based on the top-scoring candidate
3.4. Evaluation: calculate the sensitivity of detecting the optic disc
3.5. Bright Abnormalities Detection
    3.5.1. Transform the fundus image from RGB into L*a*b* color space
    3.5.2. Perform K-means clustering based on chromaticity
    3.5.3. Select the best cluster having the brightest average intensity
    3.5.4. Threshold the intensity image of the selected cluster
    3.5.5. Remove the optic disc and the pixels connected to it
3.6. Evaluation: calculate the sensitivity/specificity of detecting the bright abnormalities
```

**Figure 3-2. Algorithm of the proposed method**

## 3.1. Input Dataset: fundus images and ground truth

As mentioned before, the fundus images are the raw material to be utilized in the proposed system. These fundus images are accompanied with the ground truth which were exploited in this research to evaluate the results. Table 1-1 showed a list of nine publicly available datasets, which were all used for implementing and assessing the proposed screening system. For consistency and coding reasons, all fundus images within each dataset were renamed serially as im (1), im (2), im (3), etc., in order to facilitate the process of retrieving the images within the given datasets.

## 3.2. Fundus Image Preprocessing

Since the raw digital fundus images are not always ready for immediate segmentation, therefore, an image was first preprocessed in order to make it more suitable for further segmentation. For instance, not all datasets are accompanied with the binary mask that defines the region of interest (i.e. semi-oval fundus), neither all datasets include the vasculature tree of the fundus images, which is also a vital component in the process of localizing the optic disc. Table 3-1 illustrates the availability of such supplementary images within each of the utilized datasets.

**Table 3-1. Availability of supplementary images within different datasets**

| | Dataset | Fundus Binary Mask | Vessels Binary Map |
|---|---|---|---|
| 1 | ARIA | × | ✓ |
| 2 | DIARETDB0 | ✓ | × |
| 3 | DIARETDB1 | ✓ | × |
| 4 | DRIONS-DB | × | × |
| 5 | DRIVE | ✓ | ✓ |
| 6 | HRF | ✓ | ✓ |
| 7 | MESSIDOR | × | × |
| 8 | ONHSD | × | × |
| 9 | STARE | × | ✓ |

Therefore, the following subsections present the main preprocessing steps utilized in the proposed segmentation system, which intuitively started with generating the binary masks and extracting the vascular map.

### 3.2.1. Binary Mask Generation

Masks are usually generated and then exploited in order to furtherly process only the region of interest, and exclude the dark background. Our proposed segmentation method adopted the masking technique presented by Haar [21]. As illustrated in Figure 3-3, the binary mask was created by thresholding the red channel of the fundus image using an empirical threshold ($T=35$). Afterwards, the thresholded image was morphologically processed through opening, closing and erosion operators using a 3×3 square structuring element (kernel). It is worth to mention that this technique succeeded in omitting unimportant artifacts appearing in some datasets (e.g. date, time, batch number, etc.). These artifacts were imprinted on the captured fundus images, most likely for labeling and documentation purposes, such as the images of ONHSD and DRIONS-DB datasets.

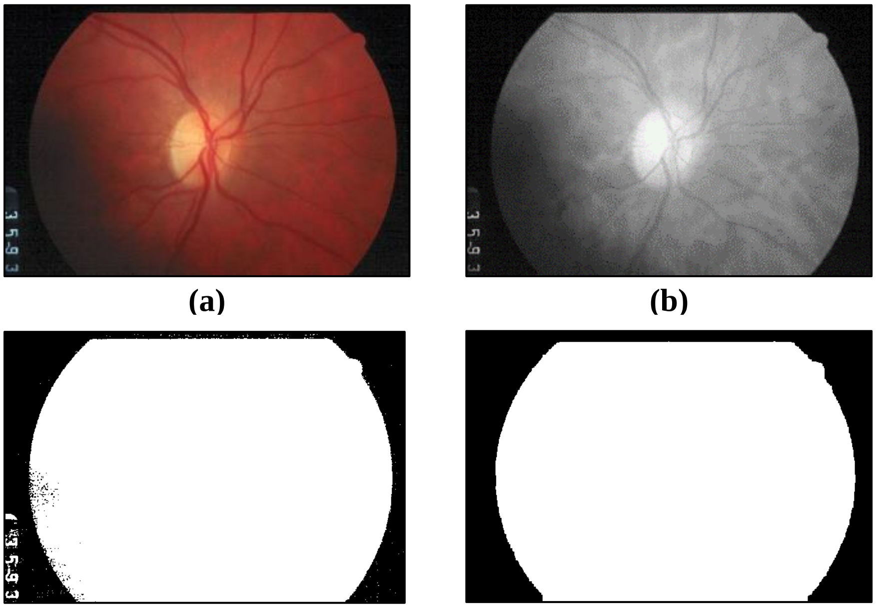

**Figure 3-3. Mask generation technique**
**(a)** Reference image (DRIONS-DB) **(b)** Red channel image
**(c)** Thresholded binary image (*T=35*) **(d)** Resultant mask via morphological processing

### 3.2.2. Blood Vessels Extraction

The vasculature tree of the fundus images was roughly extracted via the Canny edge detector using the intensity image specified by the mask, as shown in Figure 3-4.

**Figure 3-4. Blood vessels extraction using Canny edge detector**
**(a)** Reference image (DRIVE) **(b)** Intensity image **(c)** Extracted blood vessels

This process of extracting the vascular tree of the fundus image would be furtherly benefited twice. First, it would be utilized to split the fundus into two vertical halves indicating which half contains the optic disc (section 3.2.3). Secondly, these detected retinal vessels would be used to calculate the density of vessels within each of the segmented optic disc candidates (section 3.3.2). In brief, the Canny edge detector algorithm consisted the following four basic steps:

**Step (1):** The intensity image was smoothed with a 5×5 Gaussian filter in order to remove noise. The equation for the Gaussian filter kernel is computed as:

$$G(x, y) = \frac{1}{2\pi\sigma^2} e^{-\frac{x^2+y^2}{2\sigma^2}} \qquad \textbf{\textit{Equation 3-1}}$$

Thus, the kernel of a 5×5 Gaussian filter with a standard deviation of $\sigma = 1.4$ is given by:

$$B = \frac{1}{159} \bullet \begin{bmatrix} 2 & 4 & 5 & 4 & 2 \\ 4 & 9 & 12 & 9 & 4 \\ 5 & 12 & 15 & 12 & 5 \\ 4 & 9 & 12 & 9 & 4 \\ 2 & 4 & 5 & 4 & 2 \end{bmatrix} \qquad \textbf{\textit{Equation 3-2}}$$

**Step (2):** The smoothened image was filtered with a Sobel kernel in both horizontal and vertical directions to get the first derivative in horizontal direction ($G_x$) and vertical direction ($G_y$). From these two images, the gradient magnitude (i.e. edge strengths) as well as the gradient direction for each pixel was computed as follows:

$$Gradient\ Magnitude\ (G) = \sqrt{{G_x}^2 + {G_y}^2} \qquad \textbf{\textit{Equation 3-3}}$$

$$Gradient\ Direction\ (\theta) = tan^{-1}\left(\frac{G_y}{G_x}\right) \qquad \textbf{\textit{Equation 3-4}}$$

**Step (3):** Non-maxima suppression, which is an edge thinning technique, was applied to the gradient magnitude image. The purpose of this step was to convert the blurred edges in the image of the gradient magnitudes into sharp edges. Basically, this is done by preserving all local maxima in the gradient image, and deleting everything else.

**Step (4):** Double thresholding and connectivity analysis were used to detect and to link edges, respectively. Hence, edge pixels stronger than the high threshold were marked as “strong”, whereas edge pixels weaker than the low threshold were suppressed, and edge pixels between the two thresholds were marked as “weak”. Finally, the strong edges were immediately included in the final vessels map, while weak edges were included only if they were connected to strong edges.

### 3.2.3. Vertical Splitting

As mentioned previously, the optic disc is typically located towards the left-hand side or the right-hand side of the fundus, and specifically, from which the major blood vessels originate. Thus, the optic disc is normally located at one of the vertical halves containing more blood vessels (as noticed before in Figure 3-4, for example). Thereby, the binary vasculature, which was extracted in the previous step, was split into two vertical halves (i.e. left and right). The half containing more blood vessels (i.e. greater number of white pixels) was selected for further image processing whereas the other one having less vessels was excluded and neglected, as shown in Figure 3-5.

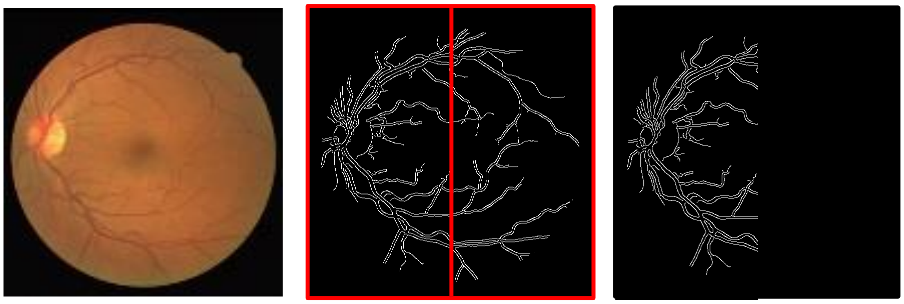

**(a)** **(b)** **(c)**

**Figure 3-5. Vertical splitting**
**(a)** Original image **(b)** Left and right extracted vessels **(c)** Selected half

Figure 3-6 shows the algorithm for splitting the blood vessels image (BV_Image) into two vertical halves, and thereby selecting the half containing more blood vessels than the other.

```
Left_Half ← CountWhitePixels ( BV_Image [ 1 : end ] [ 1 : end/2 ] )
Right_Half ← CountWhitePixels ( BV_Image [ 1 : end ] [ end/2 + 1 : end ] )
if ( Left_Half ≥ Right_Half )
    New_Image [ ] [ ] ← Original_Image [ 1 : end ] [ 1 : end/2 ]
elseif ( Right_Half > Left_Half )
    New_Image [ ] [ ] ← Original_Image [ 1 : end ] [ end/2 + 1 : end ]
endif
```

**Figure 3-6. Pseudo code of splitting the image into two vertical halves**

This splitting algorithm killed two birds with one stone. First, it greatly reduced all further processing-time to about 50%. Secondly, it reduced the number of false candidates of the optic disc which might occur in the excluded half. As shown in Figure 3-7, those false candidates might result from artifacts that are similar to the optic disc such as bright lesions, or might also sometimes occur due to non-uniform illumination (i.e. vignetting effect). Moreover, this procedure also classified whether the fundus image was a left-eye or a right-eye, although the proposed system did not intentionally aim to discover such information and did not even exploit that furtherly.

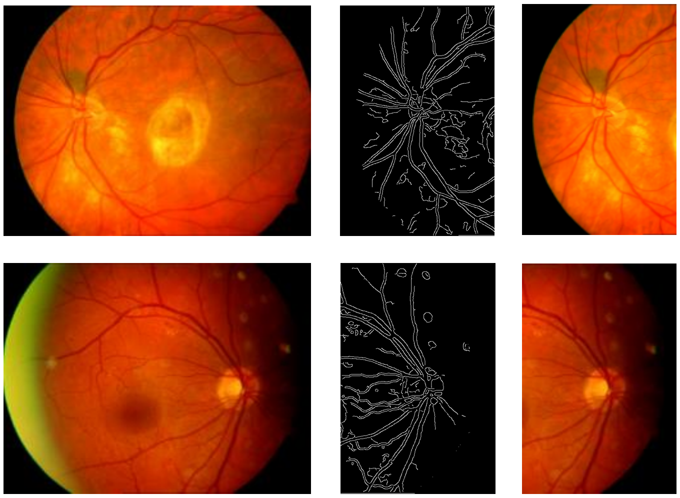

**Figure 3-7. Example of reducing false candidates of the optic disc via vertical splitting**
**Upper row:** excluded bright lesion occurring at the right half of the fundus image
**Lower row:** excluded uneven illumination occurring at the left edge of the fundus image

### 3.2.4. Contrast Adjustment

Approaching towards the process of segmenting the optic disc, the contrast of fundus image was first adjusted in order to improve and facilitate the segmentation process. At the beginning, the color fundus image was converted to a grayscale image by eliminating the hue and saturation information while retaining the luminance. Consequently, the intensity pixels in this grayscale image were mapped to new values such that 1% of the data was saturated at low and high intensities of the grayscale image. This increased the contrast of the output image, as shown in Figure 3-8.

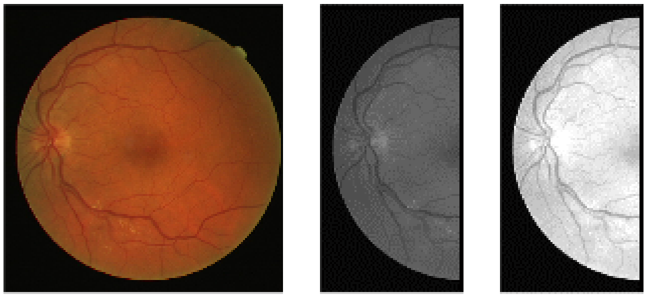

**(a)** **(b)** **(c)**

**Figure 3-8. Contrast adjustment**
**(a)** Original image **(b)** Intensity image of selected half
**(c)** Adjusted contrast of intensity image

Table 3-2 shows sample images for each of the previous preprocessing steps within the various datasets.

Table 3-2. Sample images of preprocessing the fundus images in different datasets

| Dataset Sample | Fundus Image | Mask Generation | Vessels Extraction | Vertical Splitting |
|---|---|---|---|---|
| Dataset: ARIA<br>Image title: im (18)<br>Filename: aria_a_13_2 |  | 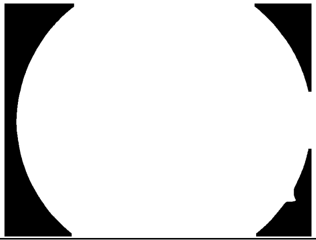 |  | 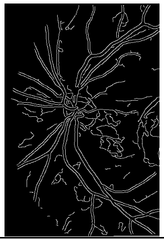 |
| Dataset: DIARETDB0<br>Image title: im (9)<br>Filename: image009 |  | 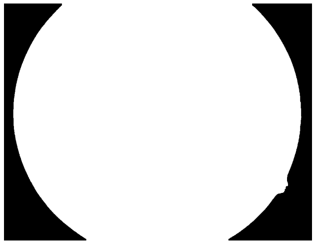 | 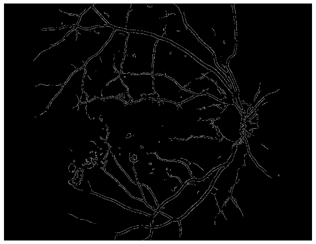 | 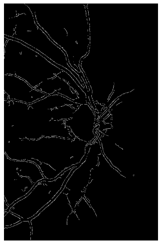 |
| Dataset: DIARETDB1<br>Image title: im (33)<br>Filename:<br>diaretdb1_image033 | 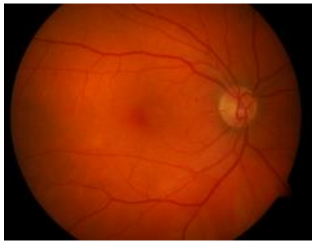 | 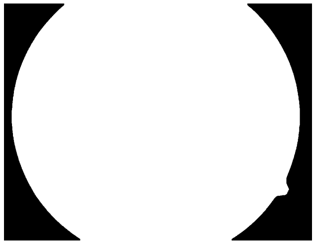 | 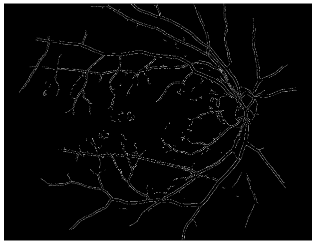 |  |
| Dataset: DRIVE<br>Image title: im (2)<br>Filename: 02_test |  | 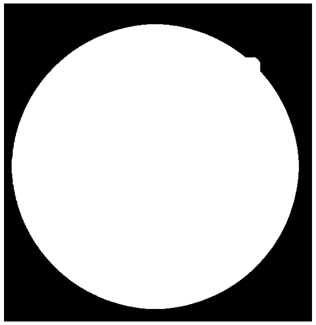 | 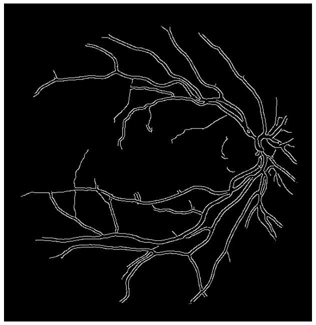 | 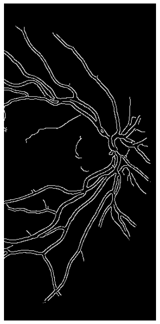 |

| Dataset Sample | Fundus Image | Mask Generation | Vessels Extraction | Vertical Splitting |
|---|---|---|---|---|
| Dataset: DRIONS-DB<br>Image title: im (13)<br>Filename: image_013 |  | 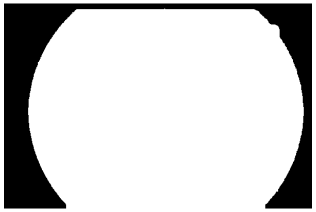 | 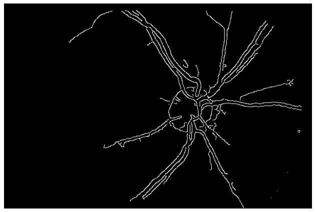 | 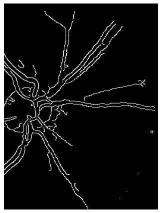 |
| Dataset: HRF<br>Image title: im (2)<br>Filename: 01_g | 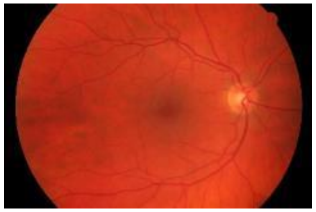 | 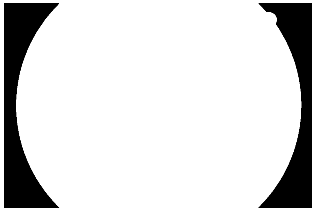 |  |  |
| Dataset: MESSIDOR<br>Image title: im (5)<br>Filename:<br>20051020_43906_0100_PP |  | 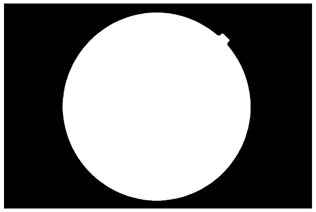 | 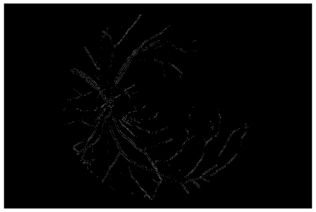 |  |
| Dataset: ONHSD<br>Image title: im (6)<br>Filename: D106154-R |  | 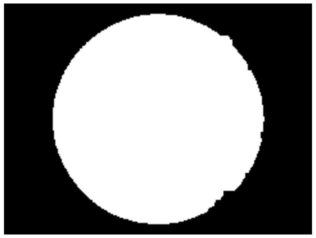 | 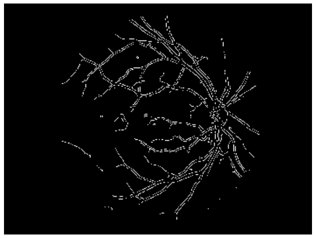 | 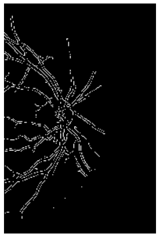 |
| Dataset: STARE<br>Image title: im (43)<br>Filename: im0043 |  | 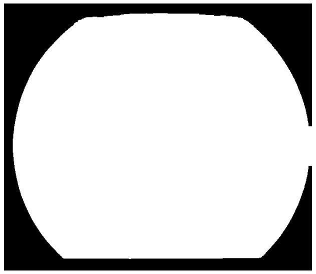 | 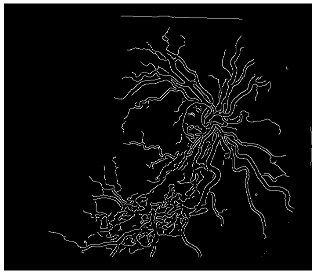 | 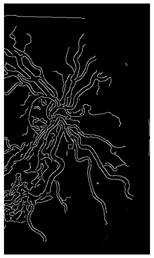 |

## 3.3. Optic Disc Segmentation

This module is the backbone of the system architecture. First, the top three candidates for the optic disc were detected and then ranked according to their circularity strengths. Consequently, the vessels density within each candidate was calculated and then weighted with respect to the candidate strength. Finally, the top-scoring candidate was chosen to be the segmented optic disc. The following subsections illustrates in details how that whole segmentation process was carried out.

### 3.3.1. Nominating Optic Disc Candidates

Identifying the optic disc candidates (nominees) is the vital step that greatly affects the accuracy of the whole segmentation process. Thereby, the objective of this step was to automatically nominate the top three candidates of the optic disc based on a vector of its main spatial features: its brightness, relative size, roundness, and before all, its approximate location within the fundus (i.e. left-side or right-side). Since the approximate location of the optic disc had been already determined previously during splitting the fundus image into two vertical halves, therefore this step was only concerned with the other three features:

- ***Brightness***: the contrasted intensity image was converted to a binary image by thresholding it at *t=255*, in order to detect only the bright (white) objects in the fundus image.
- ***Size***: as mentioned before, the optic disc constitutes one-tenth to one-sixth of the width of the whole fundus image. Accordingly, the algorithm automatically estimated the radius range of the optic disc relative to the width (i.e. diameter) of the fundus image, rounded to the greater integer. The radius range (min-to-max) was estimated via the following equations:

$$minRadius = ceiling\left(\frac{fundusWidth}{10} \times \frac{1}{2}\right) \qquad \textbf{\textit{Equation 3-5}}$$

$$maxRadius = ceiling\left(\frac{fundusWidth}{6} \times \frac{1}{2}\right) \qquad \textbf{\textit{Equation 3-6}}$$

- ***Circularity***: because the optic disc is normally round or vertically oval in shape, the algorithm first applied some morphological opening operators in order to structurally enhance the circular objects in the thresholded image. Consequently, the Circular Hough Transform (CHT) was utilized in order to detect and localize all the circular shapes specified by the estimated size range of radii.

Based on this vector of features, the best-three matching objects were chosen as the top candidates of the optic disc, and were then ranked according to their circularity strengths. Table 3-3 shows sample images for the process of nominating the top-three ranked optic discs within a given fundus image. The red, green and blue markings represent the strongest, moderate and weakest candidates, respectively. For the sake of clarity and continuity, the sample images that are shown in the following table are the same ones that were previously illustrated therein Table 3-2.

**Table 3-3. Sample images of the top-ranked optic disc candidates**

| Dataset Sample | Fundus Image | Vertical binary map of vessels and bright objects | Top-three ranked OD candidates |
|---|---|---|---|
| Dataset: ARIA<br>Image title: im (18)<br>Filename: aria_a_13_2 |  |  | 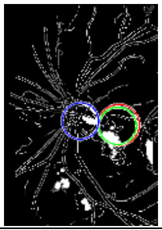 |
| Dataset: DIARETDB0<br>Image title: im (9)<br>Filename: image009 |  | 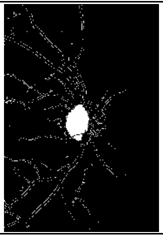 | 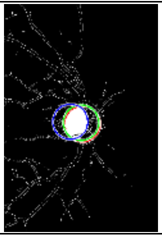 |
| Dataset: DIARETDB1<br>Image title: im (33)<br>Filename:<br>diaretdb1_image033 | 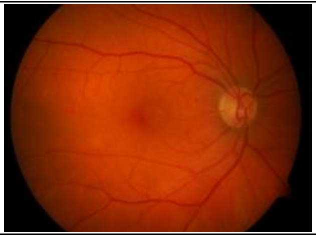 | 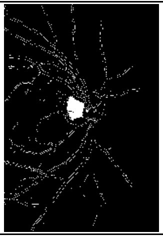 | 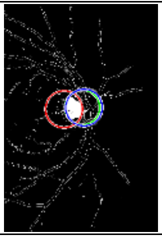 |
| Dataset: DRIVE<br>Image title: im (2)<br>Filename: 02_test |  | 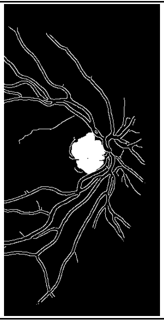 |  |
| Dataset: DRIONS-DB<br>Image title: im (13)<br>Filename: image_013 | 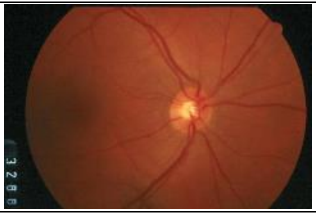 | 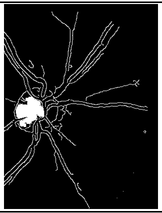 | 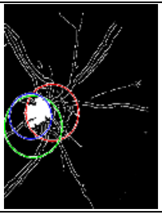 |

| Dataset Sample | Fundus Image | Vertical binary map of vessels and bright objects | Top-three ranked OD candidates |
|---|---|---|---|
| Dataset: HRF<br>Image title: im (2)<br>Filename: 01_g |  |  | 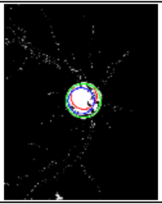 |
| Dataset: MESSIDOR<br>Image title: im (5)<br>Filename: 20051020_43906_0100_PP | 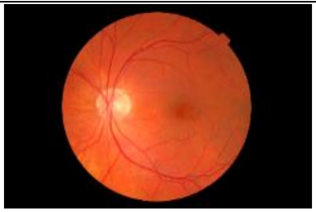 | 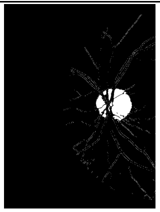 | 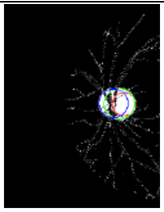 |
| Dataset: ONHSD<br>Image title: im (6)<br>Filename: D106154-R |  | 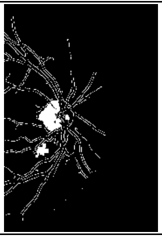 | 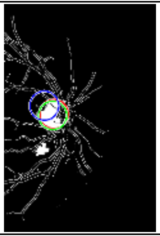 |
| Dataset: STARE<br>Image title: im (43)<br>Filename: im0043 |  |  | 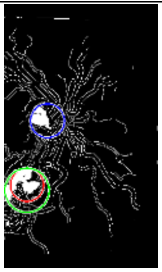 |

### 3.3.2. Calculating Vessels Density

Recalling the fact that the major blood vessels radiate from the center of the optic disc, the vessels density within each candidate was calculated in order to determine how much blood vessels each candidate possessed. For each of the three optic disc candidates, the corresponding vessels density was calculated via the following equation:

$$Density = \frac{Size\ (BV)}{Size\ (OD\ Candidate)}$$

***Equation 3-7***

where, ***Size (BV)*** is the number of pixels of the blood vessels inside the detected candidate, and ***Size (OD Candidate)*** is the number of pixels of the optic disc candidate (i.e. area of the oval).

### 3.3.3. Weighting Vessels Density

Having the top three ranked candidates of the optic disc, as well as the vessels density within each candidate, the vessels density was weighted accordingly. First, each candidate was assigned a weight based on its circularity strength. These weights were determined empirically as $w_1 = 1.2$, $w_2 = 1.1$, *and* $w_3 = 1.0$, for the strongest, moderate and weakest candidates, respectively. Consequently, the calculated vessels densities were weighted according to the candidates' strengths, as follows:

$$\boldsymbol{Score_1 = w_1 \times Density_1} \qquad \textbf{\textit{Equation 3-8}}$$

$$\boldsymbol{Score_2 = w_2 \times Density_2} \qquad \textbf{\textit{Equation 3-9}}$$

$$\boldsymbol{Score_3 = w_3 \times Density_3} \qquad \textbf{\textit{Equation 3-10}}$$

The notion behind weighting the vessels density within each optic candidate was to interchangeably promote or demote these candidates based on twofold criteria: their circularity strengths and their vessels density. For example, a weak candidate may be promoted over other highly-weighted stronger candidates because of being significantly the densest (i.e. richest) in blood vessels. On the other hand, a strongly-circled candidate may be given the advantage of achieving the highest score due to weighting, even if the other weaker candidates had higher density of vessels.

### 3.3.4. Selecting the Segmented Optic Disc

The final step in the segmentation process was selecting one of the candidates to be the segmented optic disc. Each of the figures from Figure 3-9 to Figure 3-14 are snapshots of the segmentation system for selecting the optic disc candidate within healthy and pathological images from various datasets. The top three candidates of the optic disc in a fundus image are: the red circle (strongest candidate), the green circle (moderate candidate), and the blue circle (weakest candidate).

Figure 3-9 and Figure 3-10 show examples of how the strongest candidate (red circle) was selected. In Figure 3-9 (*ARIA: "aria_c_46_12"*), for instance, the red candidate was promoted and selected to be the optic disc as a result of weighting, although the other two candidates had denser blood vessels. Also, Figure 3-10 (*STARE: "im0008.ppm"*) shows a good example of how vertical splitting succeeded in excluding the right half which contained a false candidate (i.e. large round bright lesion) that looked like the optic disc, and which would have probably led to a wrong response in segmenting the optic disc if not excluded.

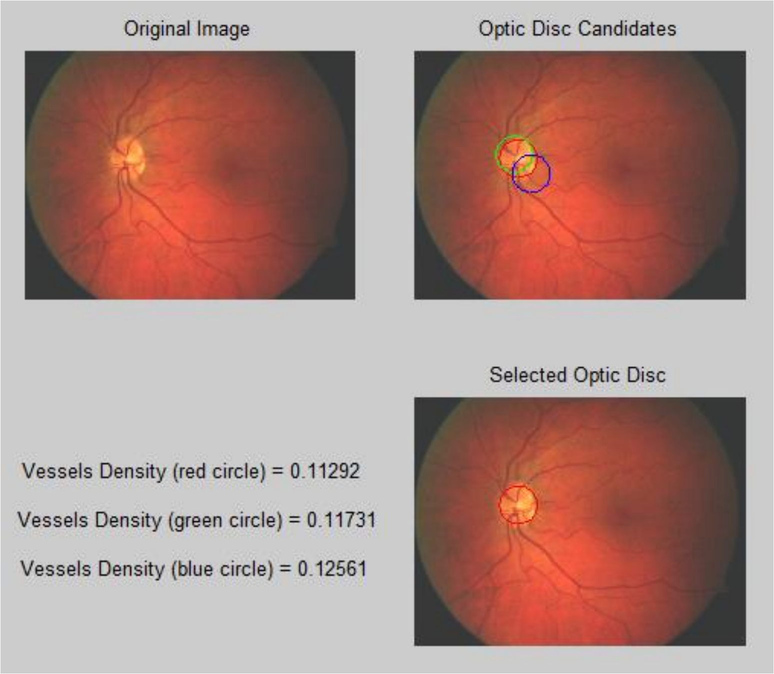

Vessels Density (red circle) = 0.11292

Vessels Density (green circle) = 0.11731

Vessels Density (blue circle) = 0.12561

**Figure 3-9. Example of selecting the strongest candidate in a healthy image**

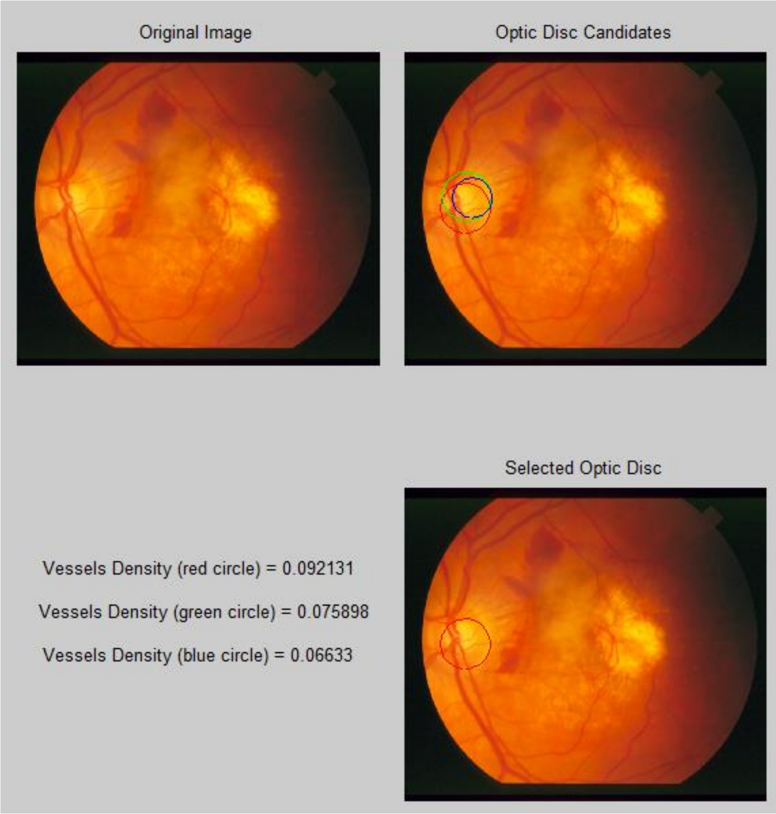

Vessels Density (red circle) = 0.092131

Vessels Density (green circle) = 0.075898

Vessels Density (blue circle) = 0.06633

**Figure 3-10. Example of selecting the strongest candidate in a pathological image**

Figure 3-11 demonstrates the twofold importance of the vessels density together with the candidates' weights in order to accurately localize the optic disc via the moderate candidate.

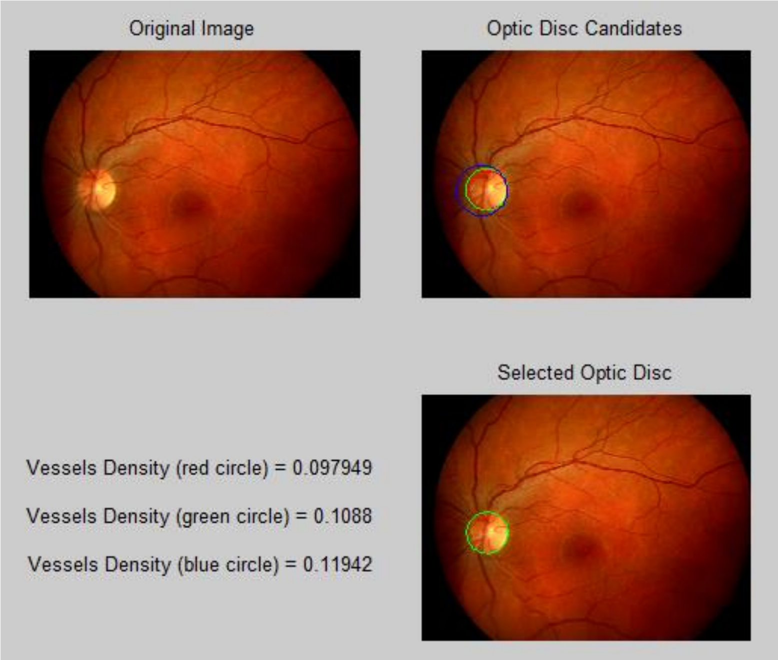

Vessels Density (red circle) = 0.097949

Vessels Density (green circle) = 0.1088

Vessels Density (blue circle) = 0.11942

**Figure 3-11. Example of selecting the moderate candidate in a healthy image**

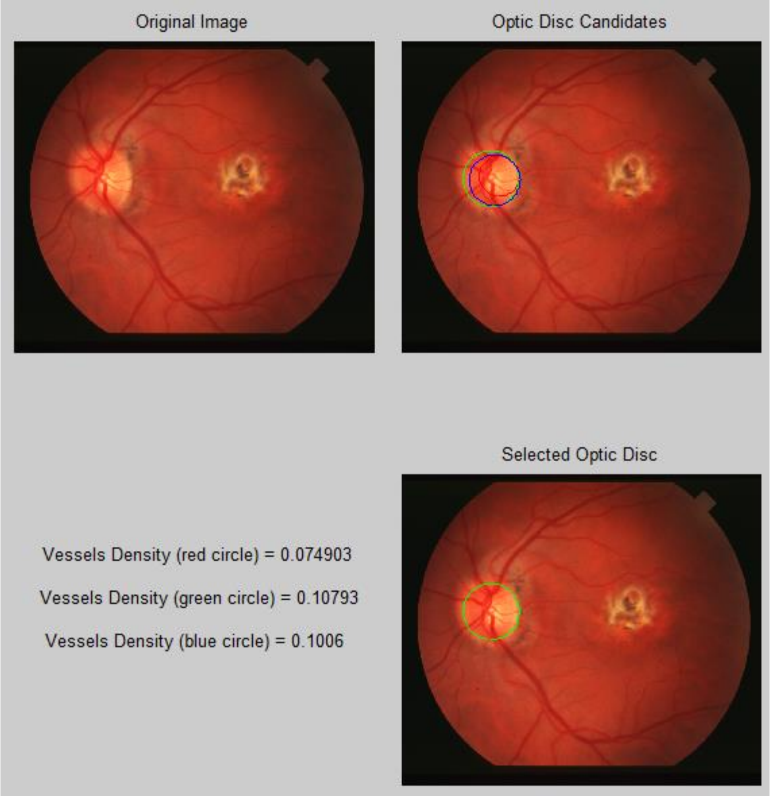

Vessels Density (red circle) = 0.074903

Vessels Density (green circle) = 0.10793

Vessels Density (blue circle) = 0.1006

**Figure 3-12. Example of selecting the moderate candidate in a pathological image**

As noticed, although the green circle in Figure 3-11 (*ARIA: “aria_c_24_12”*) was not the one with the densest vessels nor the highest weight among the two other candidates, yet this green candidate was weighted in such a way that it scored a value surpassing those scored by both, the strongest and the densest candidates. Also, Figure 3-12 (*STARE: “im0011.ppm”*) shows how the circular bright lesion was excluded as a result of vertical splitting.

The examples of Figure 3-13 (*DRIVE: “03_test”*) and Figure 3-14 (*STARE: “im0043.ppm”*) illustrate how the blue circle was promoted over the two other stronger candidates, and was chosen to be the segmented optic disc although it was the weakest candidate. This happened because neither of the two other stronger candidates were weighted highly enough to achieve a score greater than that achieved by the weak (blue) candidate. In other words, the high density of blood vessels within the blue candidate resulted in achieving the highest overall score in spite of being assigned the lowest weight, based on *Equation 3-10*.

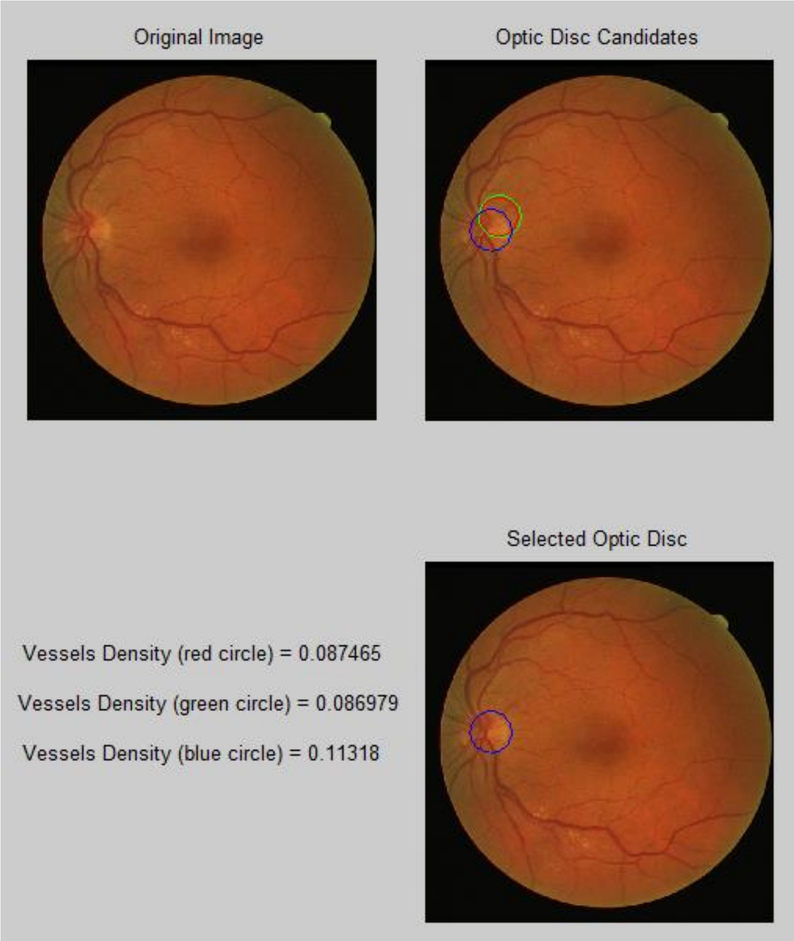

Vessels Density (red circle) = 0.087465

Vessels Density (green circle) = 0.086979

Vessels Density (blue circle) = 0.11318

**Figure 3-13. Example of selecting the weakest candidate in a healthy image**

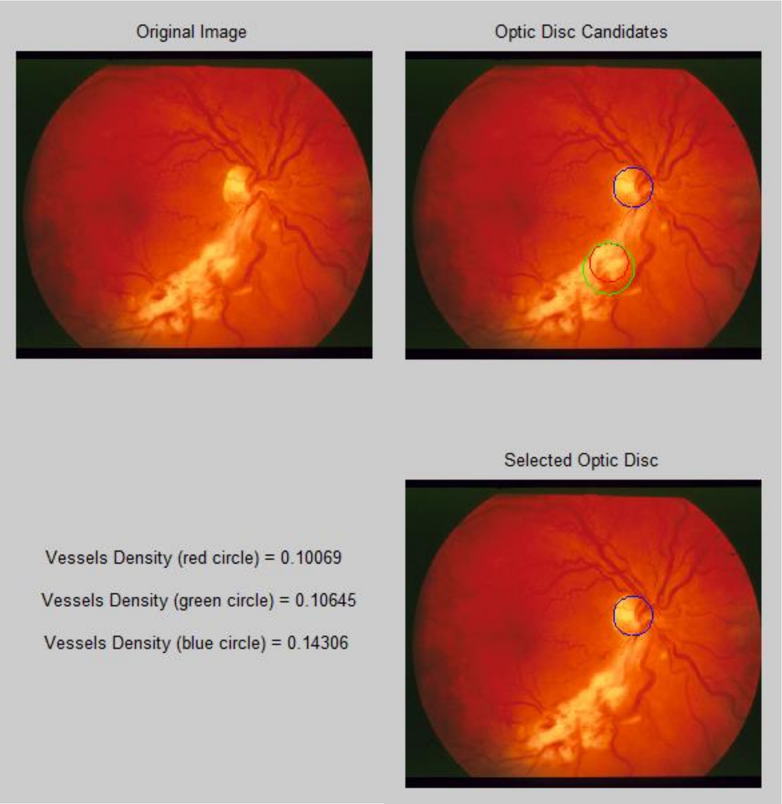

Vessels Density (red circle) = 0.10069

Vessels Density (green circle) = 0.10645

Vessels Density (blue circle) = 0.14306

**Figure 3-14. Example of selecting the weakest candidate in a pathological image**

## 3.4. Evaluation of Optic Disc Detection

In order to evaluate the proposed segmentation algorithm, the produced segmentations were compared against the provided ground truths. The evaluation of the algorithm was measured via the "*sensitivity*" which is the true positive rate of detecting the optic disc. Figure 3-15 to Figure 3-18 show samples from different datasets of fundus images and their corresponding ground truth representations of the optic disc. It is worth to mention that the ground truth is not always represented in the same manner within all datasets; even some datasets (e.g. HRF, DIARETDB0, DIARETDB1) represent this ground truth textually, rather than showing it graphically, as shown in Figure 3-18. The quantitative results of segmenting the optic disc are shown in details on the next chapter within the context of the experimental results.

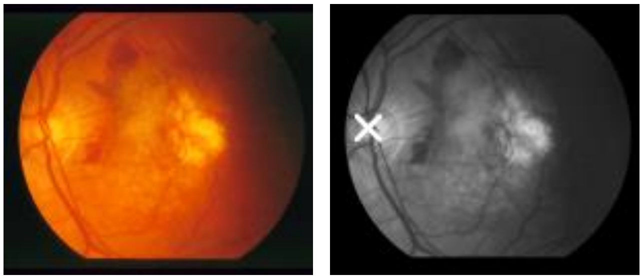

Figure 3-15. Example of the fundus image and its optic disc ground truth in STARE

Figure 3-16. Example of the fundus image and its optic disc ground truth in ARIA

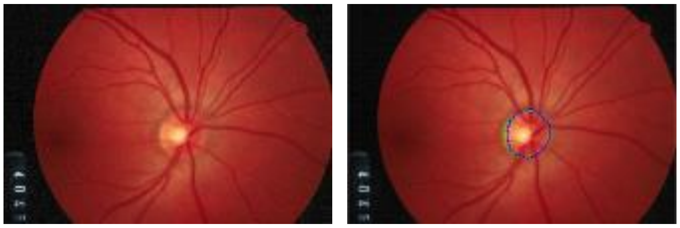

Figure 3-17. Example of the fundus image and its optic disc ground truth in DRIONS-DB

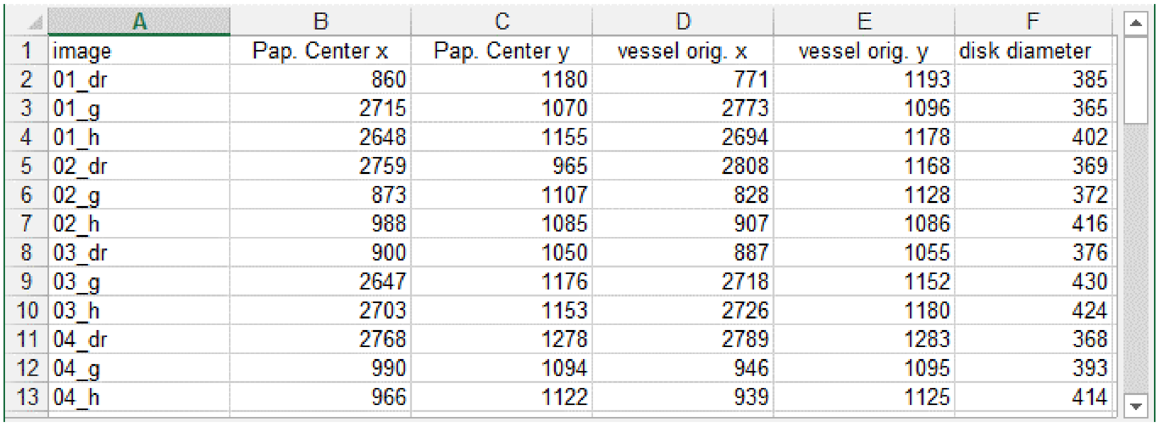

|  | A | B | C | D | E | F |
|---|---|---|---|---|---|---|
| 1 | image | Pap. Center x | Pap. Center y | vessel orig. x | vessel orig. y | disk diameter |
| 2 | 01_dr | 860 | 1180 | 771 | 1193 | 385 |
| 3 | 01_g | 2715 | 1070 | 2773 | 1096 | 365 |
| 4 | 01_h | 2648 | 1155 | 2694 | 1178 | 402 |
| 5 | 02_dr | 2759 | 965 | 2808 | 1168 | 369 |
| 6 | 02_g | 873 | 1107 | 828 | 1128 | 372 |
| 7 | 02_h | 988 | 1085 | 907 | 1086 | 416 |
| 8 | 03_dr | 900 | 1050 | 887 | 1055 | 376 |
| 9 | 03_g | 2647 | 1176 | 2718 | 1152 | 430 |
| 10 | 03_h | 2703 | 1153 | 2726 | 1180 | 424 |
| 11 | 04_dr | 2768 | 1278 | 2789 | 1283 | 368 |
| 12 | 04_g | 990 | 1094 | 946 | 1095 | 393 |
| 13 | 04_h | 966 | 1122 | 939 | 1125 | 414 |

Figure 3-18. Snapshot of the spreadsheet for the optic disc ground truth in HRF

## 3.5. Bright Abnormalities Detection

The proposed detection system adopted a two-stage approach for segmenting the bright abnormalities. First, the fundus image was partitioned into clusters based on its chromaticity information extracted from the $L^*a^*b^*$ color space. At the second stage, the pixels within the brightest cluster were thresholded in order to remove the relatively non-bright pixels and preserve only the brightest ones within the cluster.

Besides, the bright yellowish optic disc is usually clustered together with the other bright yellowish abnormalities found in the fundus image, such as hard exudates, cotton wool spots and retinal drusen. Therefore, this bright yellowish landmark (i.e. optic disc) was removed from the fundus image in order to improve the detection of such bright abnormalities and thereby avoid the false responses. In other words, the notion behind detecting and erasing the optic disc from the fundus image is to preserve only the extra abnormal objects, if any exist, so that the bright lesions would not be misclassified or confused with the optic disc [129].

### 3.5.1. Transform RGB Image into $L^*a^*b^*$ Color Space

Abnormalities such as hard exudates and cotton wool spots are mainly characterized by their bright yellowish color. But on the other hand, such abnormalities have varying sizes (i.e. small-to-medium), irregular shapes, and no specific locations within the fundus. Therefore, the proposed detection method relied mainly on the color properties, and nothing more else, to detect and segment such abnormalities.

Compared to the RGB color space, the $L^*a^*b^*$ model has the ability to quantify and decouple the chromaticity (i.e. real color information) of the fundus image. The $L^*a^*b^*$ color space consists of a luminosity layer ($L^*$), and the two chromaticity layers ($a^*$) and ($b^*$), which represent the red-to-green and yellow-to-blue values, respectively. Hence, all the color information of the fundus image is represented at the ($a^*$) and ($b^*$) layers.

Accordingly, the RGB fundus image was initially transformed into the $L^*a^*b^*$ color space in order to facilitate the detection of the hard exudates and the cotton wool spots based on their yellowish color. In other words, the ($a^*$) and ($b^*$) color layers were extracted from the $L^*a^*b^*$ fundus image, and were exploited to classify objects within the fundus image. The RGB image was transformed into the $L^*a^*b^*$color space as follows:

$Let\ C = \{R, G, B\}$

**Step (1):** Each of the R, G, B values was normalized into the range of [0,1], by dividing each by the maximum intensity limit (i.e. 255).

$$C' = \frac{C}{255}$$ ***Equation 3-11***

**Step (2):** Gamma-correction was applied on each of the R, G, B values. The gamma-corrected R, G, B values, were computed via the following formula:

$$C = \begin{cases} \dfrac{C'}{12.92} & , C' \leq 0.03928 \\ \left[\dfrac{C' + 0.055}{1.055}\right]^{2.4} & , otherwise \end{cases}$$ ***Equation 3-12***

**Step (3):** R, G, B were converted into the X, Y, Z components defined by the CIE color standard.

$$X = 0.4124 * R \; + \; 0.3576 * G \; + \; 0.1805 * B$$ ***Equation 3-13***

$$Y = 0.2126 * R \; + \; 0.7152 * G \; + \; 0.0722 * B$$ ***Equation 3-14***

$$Z = 0.0193 * R \; + \; 0.1192 * G \; + \; 0.9505 * B$$ ***Equation 3-15***

**Step (4):** $L^*$, $a^*$, $b^*$ values were calculated using the X, Y, Z components, as follows.

$$L^* = 116 \times f\left(\frac{Y}{Y_n}\right) - 16$$ ***Equation 3-16***

$$a^* = 500 \times \left[f\left(\frac{X}{X_n}\right) - f\left(\frac{Y}{Y_n}\right)\right]$$ ***Equation 3-17***

$$b^* = 200 \times \left[f\left(\frac{X}{X_n}\right) - f\left(\frac{Z}{Z_n}\right)\right]$$ ***Equation 3-18***

where, $X_n = 0.95047$, $Y_n = 1.0000$, $Z_n = 1.08883$, and

$$f(w) = \begin{cases} \sqrt[3]{w} & w > 0.008856 \\ 7.787w + \dfrac{16}{116} & otherwise \end{cases}$$ ***Equation 3-19***

### 3.5.2. Perform K-means Clustering

After extracting the ($a^*$) and ($b^*$) layers that represent the chromaticity of the fundus image, the pixels in the image were partitioned and classified into five disjoint clusters via the unsupervised K-means clustering algorithm according to their color, such that the colors of the objects within each cluster are as close as possible to each other, and as far as possible from colors within other clusters, as illustrated in Figure 3-19. The number of clusters was chosen empirically, as the yellowish objects were best grouped together and best isolated from other objects.

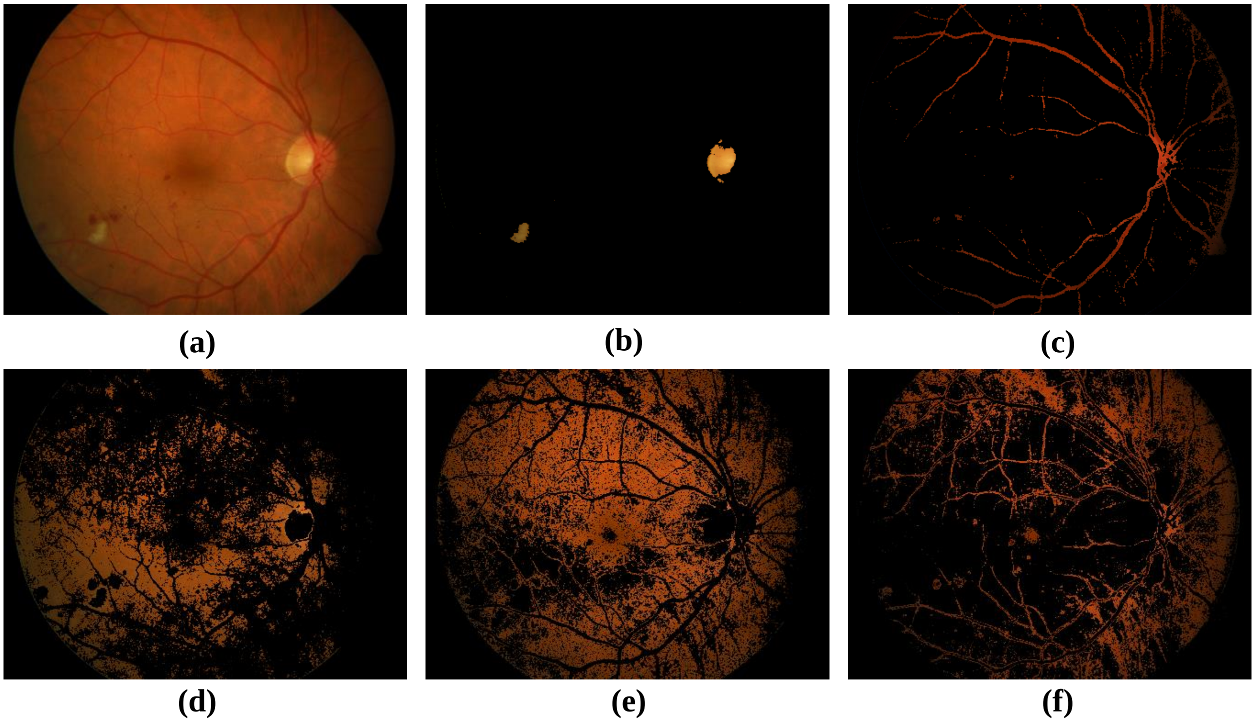

**Figure 3-19. Color-based clustering using k-means method**
**(a)** Reference image (DIARETDB0: image009.png) partitioned and classified into:
**(b)** 1st Cluster **(c)** 2nd Cluster **(d)** 3rd Cluster **(e)** 4th Cluster **(f)** 5th Cluster

Each cluster is defined by its centroid as well as its member objects. The centroid for each cluster is the value to which the sum of distances from all the objects in that cluster is minimized. Once the grouping is done, the process is repeated a number of times in order to calculate the new centroid of each cluster and subsequently reassign the member objects to the cluster having the closest distance to the new centroid. Thus, this color-based clustering algorithm using the k-means method worked as follows:

**Step (1):** Initialize the number of clusters ($k=5$), and randomly specify the cluster centroids ($c_k$).

**Step (2):** Based on the chromaticity value of each pixel $p(x,y)$, measure the cosine distance ($d$) between the cluster centroid and each pixel of the image, as follows:

$$d = \|p(x,y) - c_k\| \qquad \textit{Equation 3-20}$$

**Step (3):** Assign each pixel to the closest centroid according to the distance ($d$) computed in the previous step.

**Step (4):** Calculate the new cluster centroids using the equation given below:

$$c_k = \frac{1}{k} \sum_{x \in c_k} \sum_{y \in c_k} p(x,y) \qquad \textit{Equation 3-21}$$

**Step (5):** Replicate steps (2 to 4) to avoid local minima clustering or empty clusters.

**Step (6):** Reshape the cluster pixels into the image.

### 3.5.3. Select the Best Cluster

Among the five clusters that were created via the k-means algorithm at the preceding step, it was important to automatically find the best cluster, which is the one having the highest average intensity of clustered pixels. The notion behind considering such cluster, is that the exudates as well as the optic disc usually fall within the same cluster due to their similar bright color, and which in turn, leads to having the highest mean intensity among other clusters due to their bright color. Therefore, the cluster with the highest mean intensity was selected to be furtherly processed and manipulated, as shown in Figure 3-20. Thus, this intensity-based choice puts the screening system on the right track for segmenting the bright abnormalities, such as hard exudates and cotton wool spots, within the fundus image.

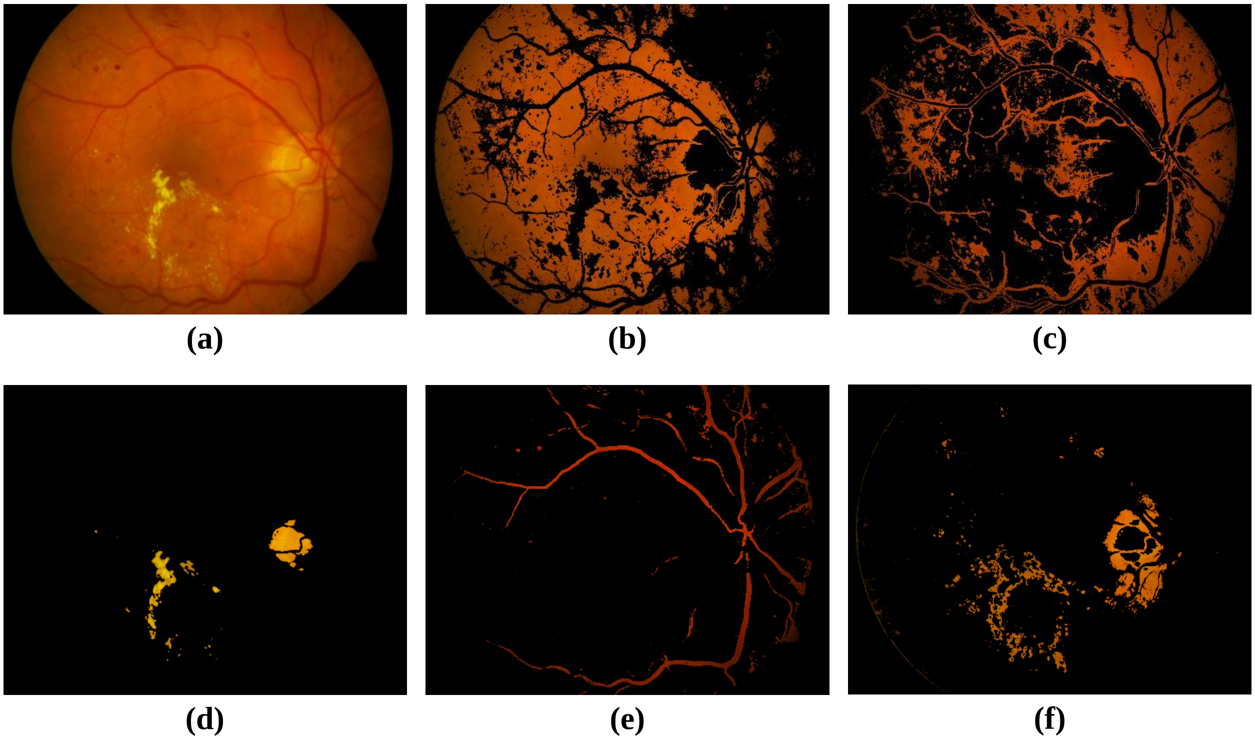
**(a)** **(b)** **(c)**
**(d)** **(e)** **(f)**

**Figure 3-20. The highest mean intensity cluster**
**(a)** Reference image (DIARETDB1: image019.png) **(b)** 1st Cluster **(c)** 2nd Cluster
**(d)** 3rd cluster (the best cluster) **(e)** 4th Cluster **(f)** 5th Cluster

Figure 3-21 illustrates the pseudo code for detecting and selecting the cluster having the highest mean intensity of foreground (non-zero) pixels among the five clustered images.

```
Using clusteredImages[1..5]
Initialize bestCluster to 1
Extract the intensity of the first cluster: I ← Intensity (clusteredImages[bestCluster])
Get the intensity values of its foreground pixels: Values ← Find (I > 0)
Calculate the mean value of the foreground pixels: Mean ← Sum (Values) / Size (Values)
for each of the other clusters: j = 2 to 5
    Extract the intensity of the $j^{th}$ cluster: I ← Intensity (clusteredImages[j])
    Get the intensity values of its foreground pixels: Values ← Find(I > 0)
    if ( Sum (Values) / Size (Values) > Mean )
        bestCluster ← j
        Mean ← Sum (Values) / Size (Values)
    endif
end for
selectedCluster ← clusteredImages[bestCluster]
```

**Figure 3-21. Pseudo code of selecting the best cluster**

### 3.5.4. Estimate a Threshold based on Order-Statistic Metrics

After selecting the best cluster, the proposed detection system automatically computed a threshold value ($\boldsymbol{\theta_t}$) that was estimated via order-statistic properties of the selected cluster intensity image ($\boldsymbol{I_c}$). This threshold value was computed as the difference between the highest non-zero value of $\boldsymbol{I_c}$ and the median of the non-zero values of $\boldsymbol{I_c}$. Thus, the threshold value was estimated via statistic-based metrics, using the following equation:

$$\boldsymbol{\theta_t = maximum\left(\boxed{I_c}\right) - median\left(\boxed{I_c}\right)}$$

***Equation 3-22***

where, $\boxed{\boldsymbol{I_c}}$ is the foreground image (i.e. non-zero pixels) of the cluster intensity image $\boldsymbol{I_c}$. The notion behind using the median metric is because of its resistance to outliers, as well as its appropriateness for skewed distributions.

Consequently, the estimated threshold value $\boldsymbol{\theta_t}$ was applied to the intensity cluster image in order to remove the relatively non-bright pixels and preserve only the bright ones within the cluster including those that belong to the optic disc, as illustrated in Figure 3-22.

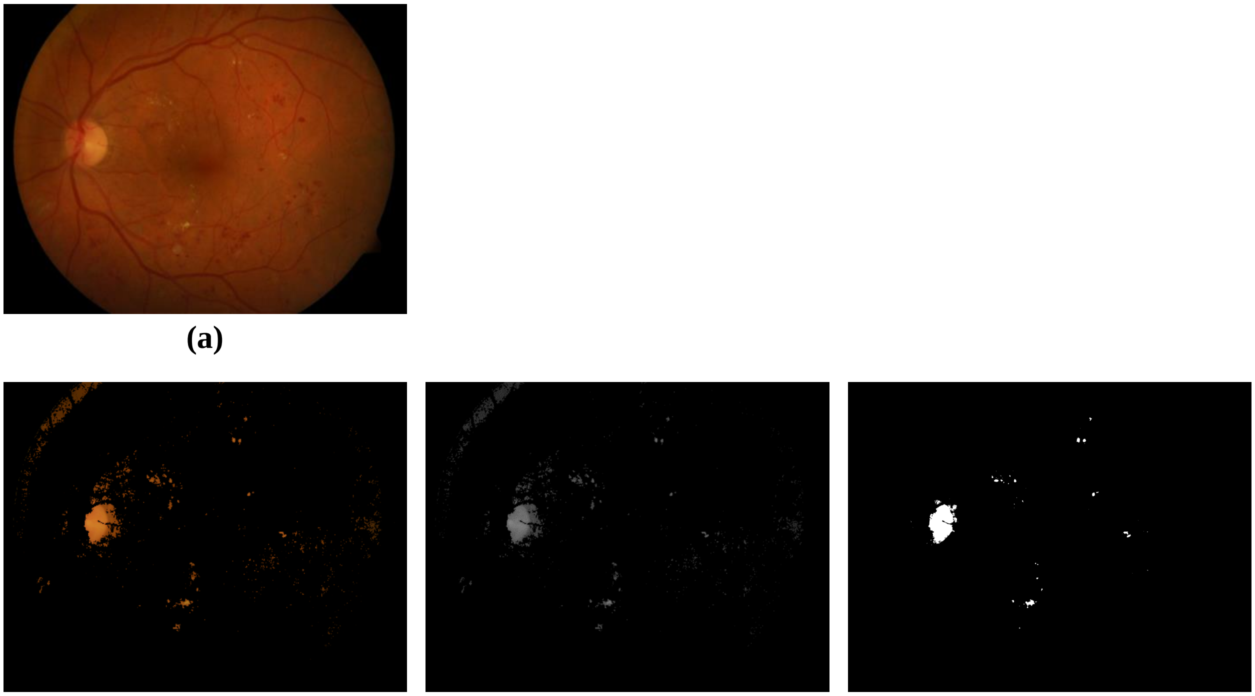

**Figure 3-22. Applying statistic-based thresholding to the selected cluster**
**(a)** Reference image (DIARETDB0: image101.png)
**(b)** Selected best cluster **(c)** Intensity image of best cluster **(d)** Thresholded image

### 3.5.5. Remove the Optic Disc and its Connected Pixels

The optic disc pixels were then eliminated from the fundus image in order to facilitate the detection of the bright lesions that look like the optic disc. Moreover, because the optic disc might had been segmented inaccurately, the pixels connected to the optic disc were most likely part of the optic disc region itself. Accordingly, the optic disc and the pixels connected to it were also removed from the previously thresholded image, leaving out only the additional clustered pixels, as illustrated in Figure 3-23. Thereby, this resultant OD-free image eventually reduced the false response of detecting the bright lesions within the fundus image.

.

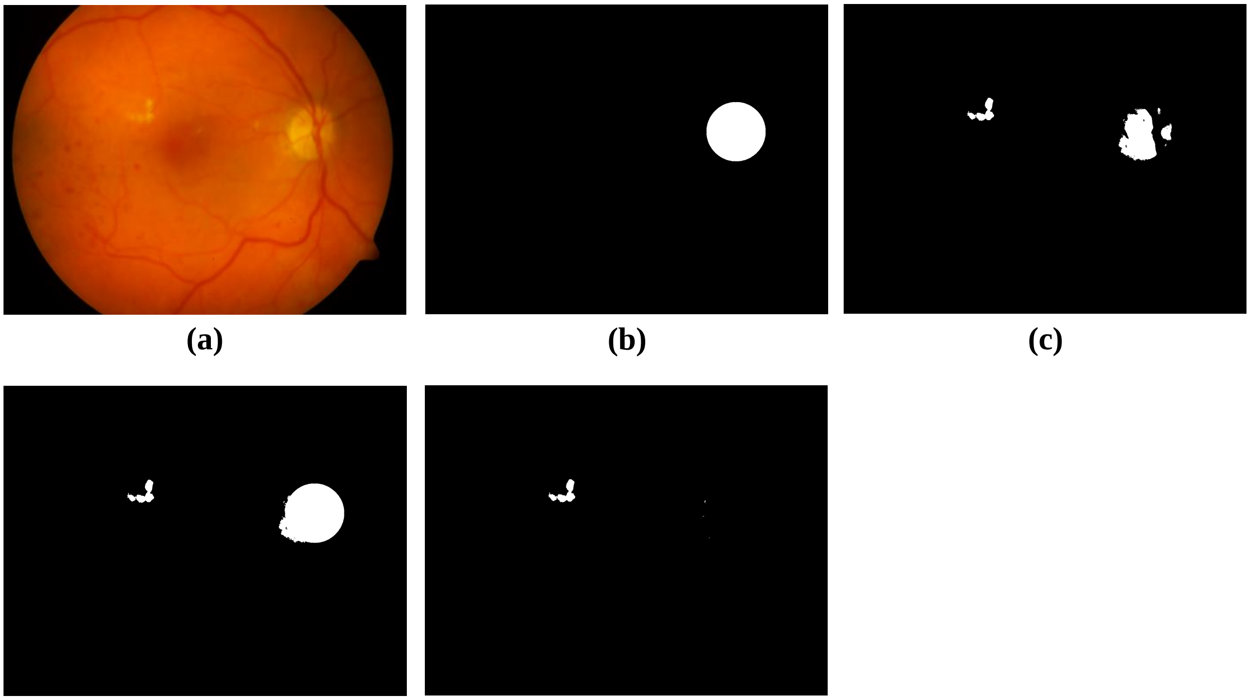

**(a)** **(b)** **(c)**

**(d)** **(e)**

**Figure 3-23. Excluding the optic disc region from the thresholded image**
**(a)** Reference image **(b)** Binary optic disc **(c)** Thresholded image
**(d)** Combining images (b) and (c) **(e)** Removal of the optic disc and its connected pixels

Hence, the final step for segmenting the abnormal pixels was inpainting the internal skeleton of those remaining objects in the original image, after removing the optic disc and the objects connected to it, as exemplified in Figure 3-24.

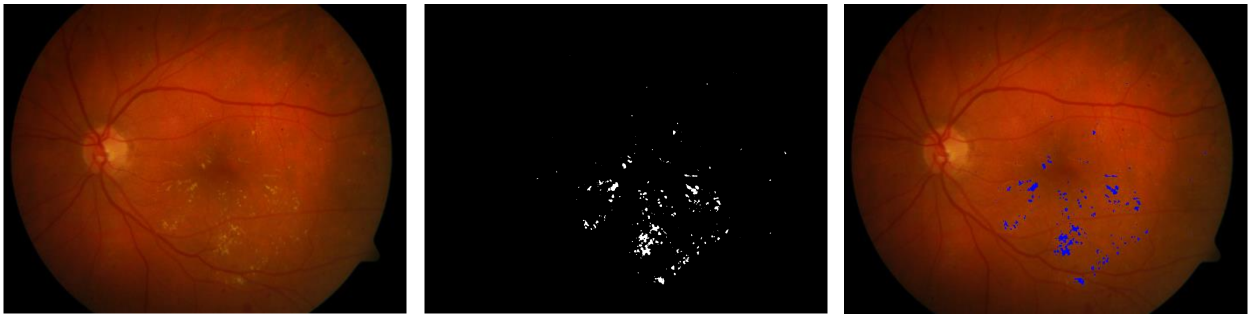

**(a)** **(b)** **(c)**

**Figure 3-24. Inpainting bright abnormalities within fundus image**
**(a)** Reference image **(b)** Abnormal binary pixels **(c)** Segmented abnormalities

Table 3-4, Table 3-5 and Table 3-6 show examples for each of the abovementioned stages of segmenting the abnormalities within DIARETDB0, DIARETDB1 and MESSIDOR, respectively.

Table 3-4. Sample images of segmenting the bright abnormalities in DIARETDB0

| Dataset Sample | Fundus Image | Selected Cluster | OD-Free Thresholded Image | Segmented Abnormalities |
|---|---|---|---|---|
| Dataset: DIARETDB0<br>Image title: im (8)<br>Filename: image008 |  | 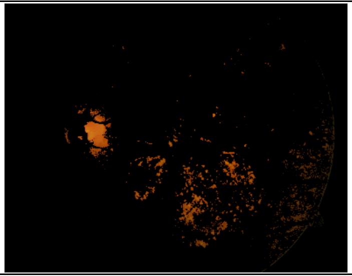 | 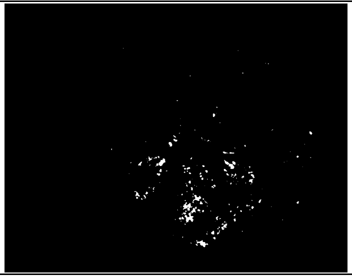 |  |
| Dataset: DIARETDB0<br>Image title: im (19)<br>Filename: image009 |  | 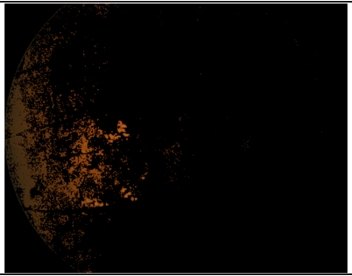 |  |  |
| Dataset: DIARETDB0<br>Image title: im (104)<br>Filename: image104 |  | 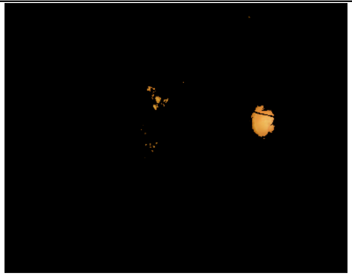 |  | 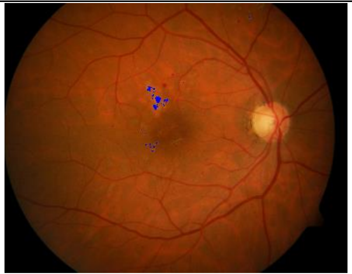 |
| Dataset: DIARETDB0<br>Image title: im (109)<br>Filename: image109 | 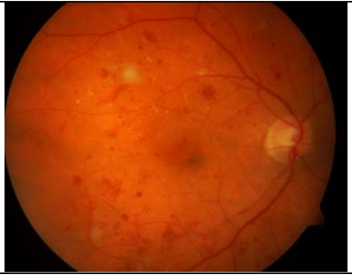 | 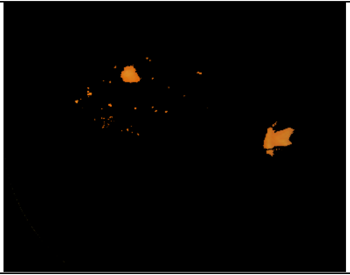 |  | 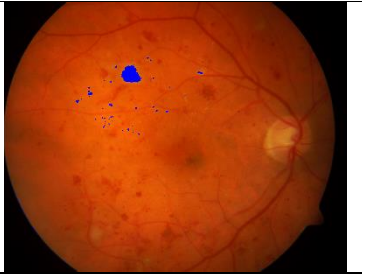 |

Table 3-5. Sample images of segmenting the bright abnormalities in DIARETDB1

| Dataset Sample | Fundus Image | Selected Cluster | OD-Free Thresholded Image | Segmented Abnormalities |
|---|---|---|---|---|
| Dataset: DIARETDB1<br>Image title: im (1)<br>Filename: image001 | 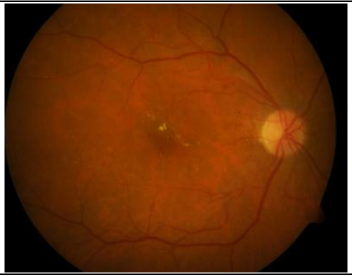 | 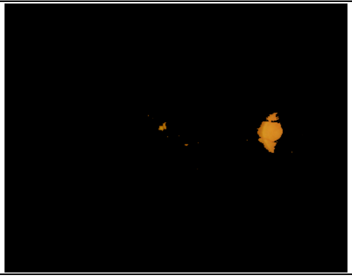 |  | 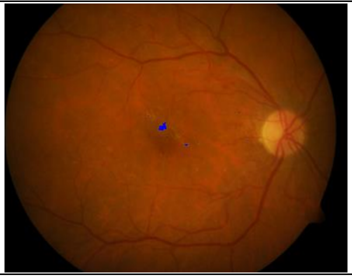 |
| Dataset: DIARETDB1<br>Image title: im (5)<br>Filename: image005 |  | 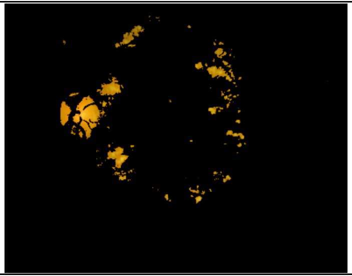 | 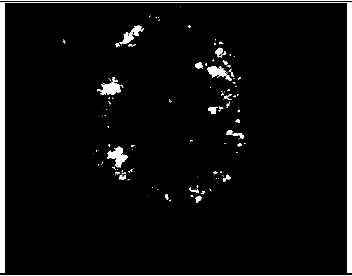 |  |
| Dataset: DIARETDB1<br>Image title: im (16)<br>Filename: image016 |  | 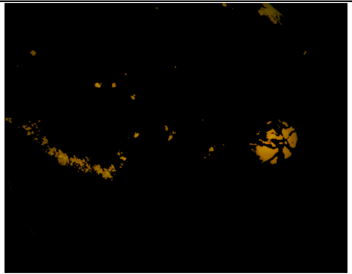 | 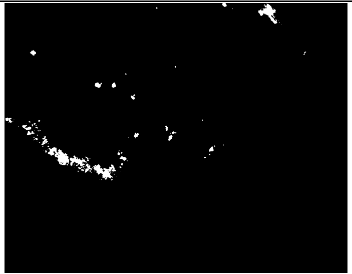 | 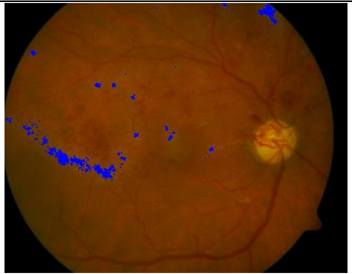 |
| Dataset: DIARETDB1<br>Image title: im (64)<br>Filename: image064 |  | 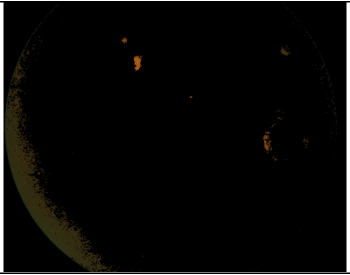 |  |  |

Table 3-6. Sample images of segmenting the bright abnormalities in MESSIDOR

| Dataset Sample | Fundus Image | Selected Cluster | OD-Free Thresholded Image | Segmented Abnormalities |
|---|---|---|---|---|
| Dataset: MESSIDOR<br>Image title: im (29)<br>Filename:<br>20051020_53178_0100_PP | 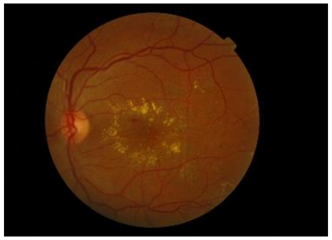 | 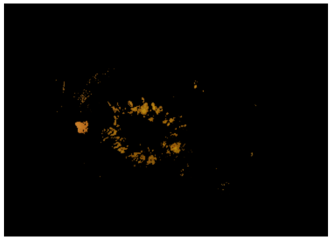 | 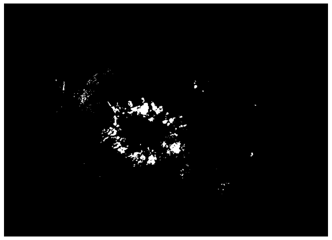 | 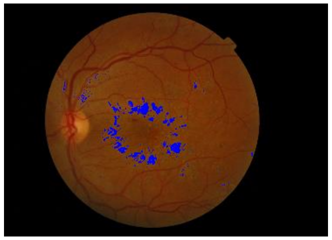 |
| Dataset: MESSIDOR<br>Image title: im (343)<br>Filename:<br>20060529_57430_0100_PP | 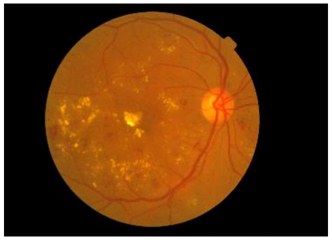 | 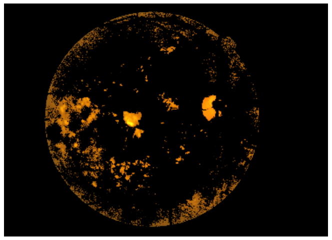 | 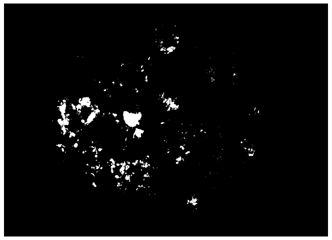 | 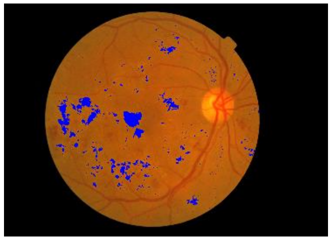 |
| Dataset: MESSIDOR<br>Image title: im (577)<br>Filename:<br>20060410_44248_0200_PP | 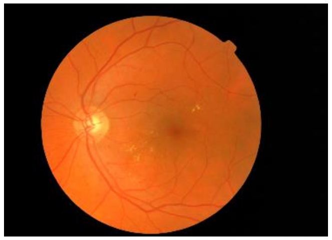 |  |  | 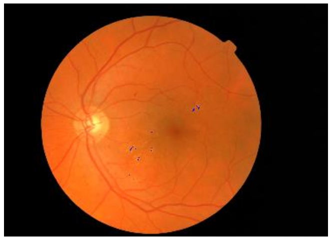 |
| Dataset: MESSIDOR<br>Image title: im (1031)<br>Filename:<br>20051202_51488_0400_PP | 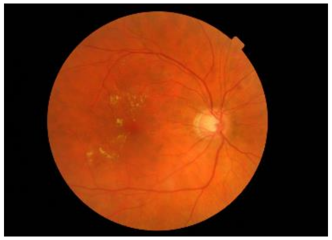 | 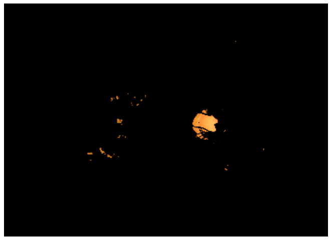 |  |  |

## 3.6. Evaluation of Bright Abnormalities Detection

In order to evaluate the proposed algorithm of segmenting the bright abnormalities, the produced segmentations were compared against the ground truths provided by the employed datasets. The evaluation of the segmentation algorithm was measured via two metrics: the “*sensitivity*” which is the rate of correctly detecting the presence of bright abnormalities, as well as the “*specificity*” which is the rate of correctly confirming the absence of such abnormalities within the exploited fundus images.

The ground truth of the abnormalities of diabetic retinopathy occurring within DIARETDB0, DIARETDB1 and MESSIDOR, is shown at appendices A.1, A.2, and A.3, respectively. Additionally, the quantitative results of detecting and segmenting the bright abnormalities are shown in details on the next chapter within the context of the experimental results.

# Chapter 4. Experimental Results

## 4.1. Experimental Environment

The proposed algorithm was implemented via MATLAB R2013a using the “Image Processing Toolbox” and the “Statistics Toolbox”, under a platform of Windows 10 Pro with an i5-3230M Processor of 2.60 GHz. The proposed system was tested in a unique environment composed of nine miscellaneous datasets of a total of 1937 images having extremely diverse properties (e.g. spatial size, quality, FOV, format, etc.). The reason behind employing a huge set of heterogeneous images was to examine the effectiveness and robustness of the proposed algorithm over any image.

## 4.2. Optic Disc Segmentation Results

Due to the space limitations and the size constraints in this research, it is not practically possible to include all the graphical segmentations for that huge number of tested images herein this text. Thereby, ten sample images from each dataset were chosen to be presented showing some of the correct/true and incorrect/false responses for the optic disc segmentation within each dataset. The samples chosen to be presented here within this text represent the various situations where the optic disc might be found (e.g. normal fundus, pathological fundus, indiscernible optic disc, poor-quality images, etc.). The following tables, from Table 4-1 to Table 4-9, show these ten sample results of each of the nine datasets previously listed within Table 1-1. The quantitative results for all the images in each dataset is listed at Appendix B.

**Table 4-1. Sample results of the optic disc segmentations within ARIA**

| | Reference Image | Optic Disc Candidates | Segmented Optic Disc | Response |
|---|---|---|---|---|
| im (2) |  |  |  | Correct |
| im (10) |  |  | 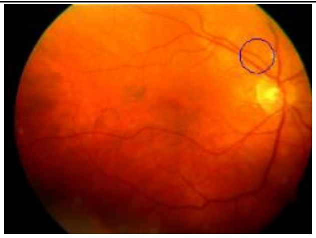 | Incorrect |

|  | **Reference Image** | **Optic Disc Candidates** | **Segmented Optic Disc** | **Response** |
|---|---|---|---|---|
| im (17) | 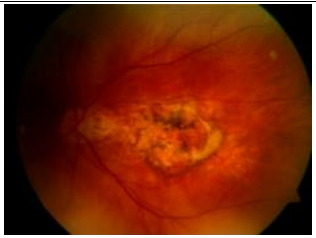 |  |  | Incorrect |
| im (18) |  | 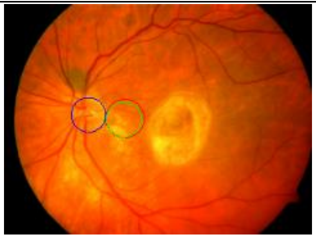 | 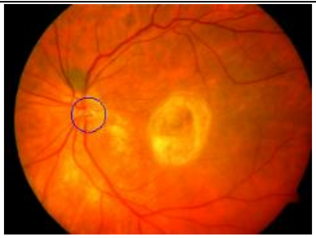 | Correct |
| im (21) | 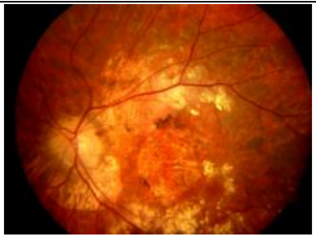 |  |  | Correct |
| im (50) | 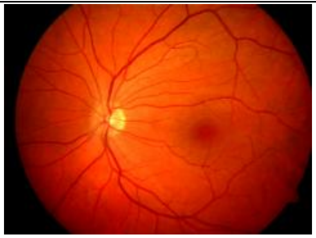 | 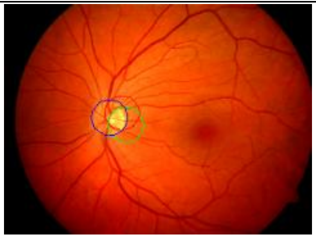 | 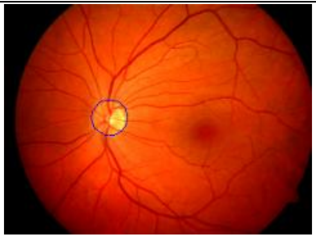 | Correct |
| im (62) |  | 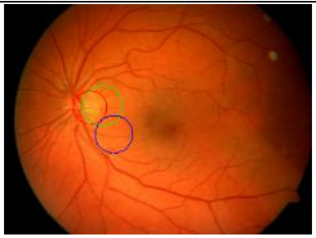 |  | Correct |
| im (77) |  |  |  | Correct |
| im (113) | 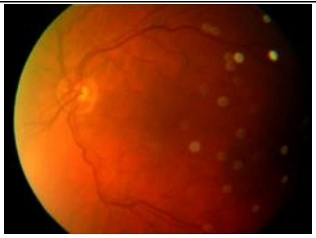 |  |  | Correct |

| | Reference Image | Optic Disc Candidates | Segmented Optic Disc | Response |
|---|---|---|---|---|
| im (129) | 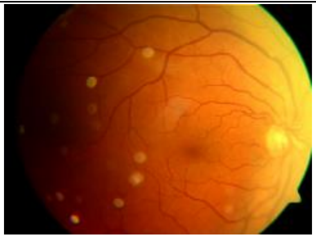 | 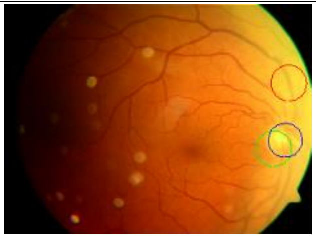 |  | Correct |

Table 4-2. Sample results of the optic disc segmentations within DIARETDB0

| | Reference Image | Optic Disc Candidates | Segmented Optic Disc | Response |
|---|---|---|---|---|
| im (16) |  |  |  | Correct |
| im (35) |  |  |  | Incorrect |
| im (36) |  |  |  | Correct |
| im (44) |  |  |  | Correct |
| im (45) |  |  |  | Correct |

|  | Reference Image | Optic Disc Candidates | Segmented Optic Disc | Response |
|---|---|---|---|---|
| im (50) |  |  |  | Correct |
| im (59) |  |  |  | Incorrect |
| im (114) |  |  |  | Correct |
| im (118) |  | 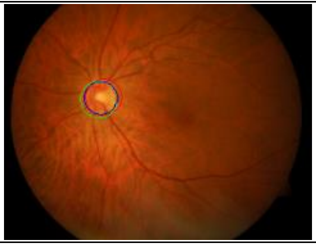 |  | Correct |
| im (127) |  |  |  | Correct |

**Table 4-3. Sample results of the optic disc segmentations within DIARETDB1**

|  | Reference Image | Optic Disc Candidates | Segmented Optic Disc | Response |
|---|---|---|---|---|
| im (5) |  |  | 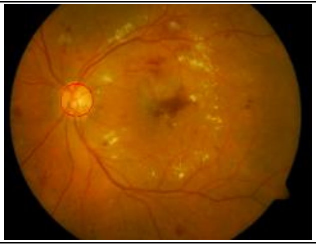 | Correct |

|  | **Reference Image** | **Optic Disc Candidates** | **Segmented Optic Disc** | **Response** |
|---|---|---|---|---|
| im (15) |  |  |  | Correct |
| im (23) | 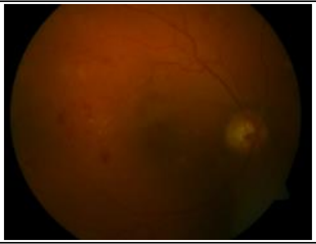 | 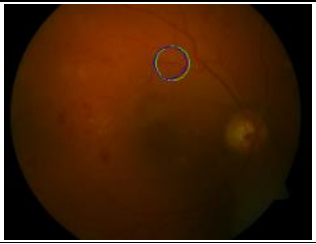 | 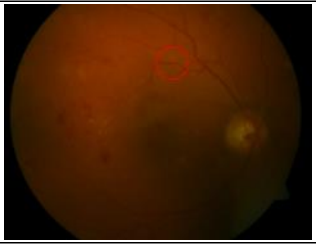 | Incorrect |
| im (27) |  |  |  | Correct |
| im (29) |  | 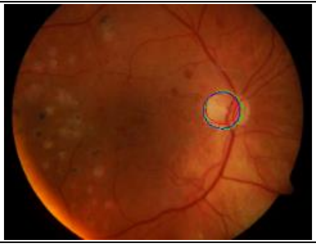 | 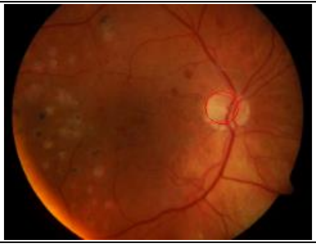 | Correct |
| im (42) |  | 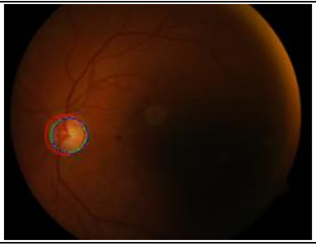 |  | Correct |
| im (71) |  |  | 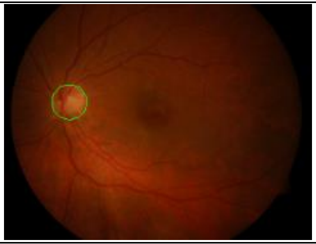 | Correct |

| | Reference Image | Optic Disc Candidates | Segmented Optic Disc | Response |
|---|---|---|---|---|
| im (82) |  |  |  | Correct |
| im (86) |  |  |  | Incorrect |

**Table 4-4. Sample results of the optic disc segmentations within DRIONS-DB**

| | Reference Image | Optic Disc Candidates | Segmented Optic Disc | Response |
|---|---|---|---|---|
| im (31) |  | 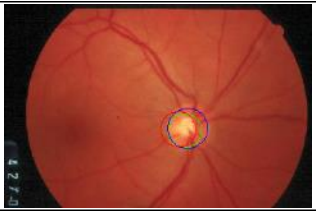 | 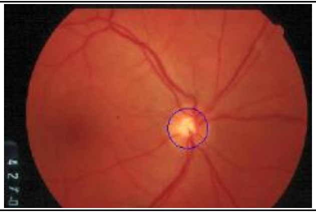 | Correct |
| im (55) |  | 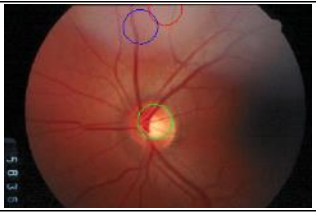 | 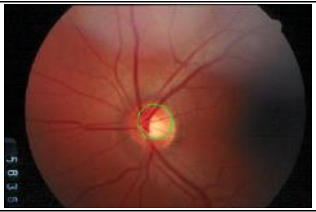 | Correct |
| im (57) |  | 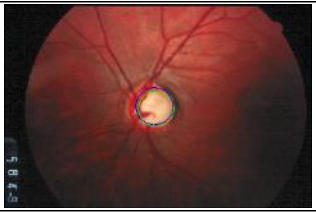 |  | Correct |
| im (67) |  |  |  | Correct |

|  | Reference Image | Optic Disc Candidates | Segmented Optic Disc | Response |
|---|---|---|---|---|
| im (81) |  | 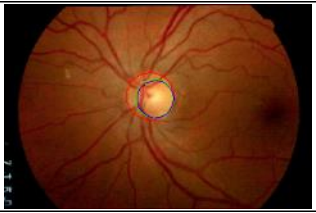 |  | Correct |
| im (90) |  | 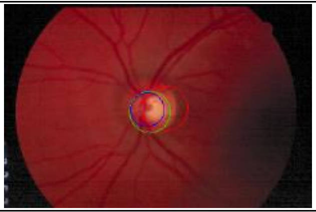 | 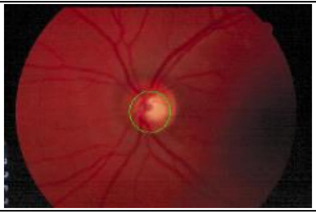 | Correct |
| im (96) |  |  |  | Correct |
| im (103) |  |  |  | Correct |
| im (104) |  |  |  | Correct |

**Table 4-5. Sample results of the optic disc segmentations within DRIVE**

|  | Reference Image | Optic Disc Candidates | Segmented Optic Disc | Response |
|---|---|---|---|---|
| im (3) |  |  |  | Correct |

| | Reference Image | Optic Disc Candidates | Segmented Optic Disc | Response |
|---|---|---|---|---|
| im (4) |  | 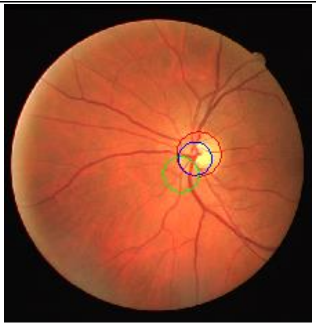 |  | Correct |
| im (6) |  | 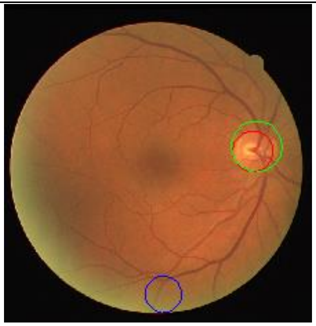 | 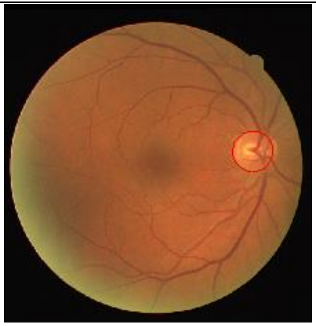 | Correct |
| im (21) |  | 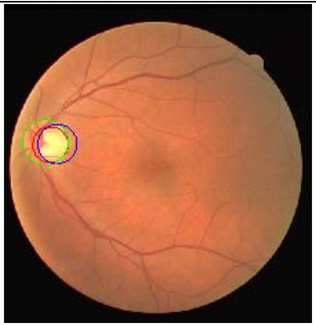 | 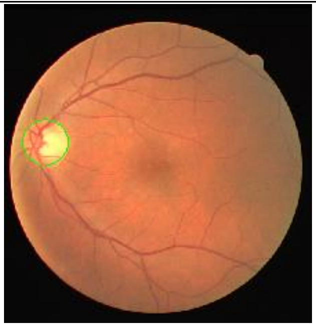 | Correct |
| im (23) |  |  | 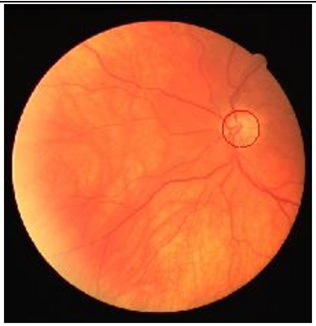 | Correct |
| im (26) |  |  |  | Correct |

|  | Reference Image | Optic Disc Candidates | Segmented Optic Disc | Response |
|---|---|---|---|---|
| im (30) |  |  |  | Correct |
| im (31) |  |  |  | Correct |
| im (34) |  |  |  | Incorrect |

**Table 4-6. Sample results of the optic disc segmentations within HRF**

|  | Reference Image | Optic Disc Candidates | Segmented Optic Disc | Response |
|---|---|---|---|---|
| im (7) | 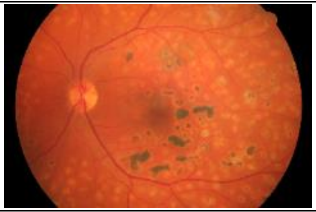 |  |  | Correct |
| im (10) |  |  |  | Correct |

| | **Reference Image** | **Optic Disc Candidates** | **Segmented Optic Disc** | **Response** |
|---|---|---|---|---|
| im (15) |  | 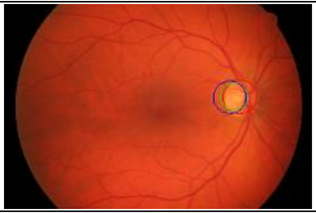 | 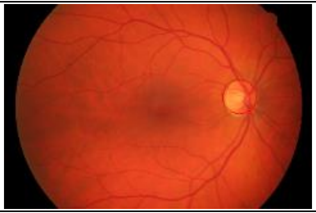 | Correct |
| im (16) |  |  |  | Correct |
| im (25) |  |  |  | Correct |
| im (26) |  |  | 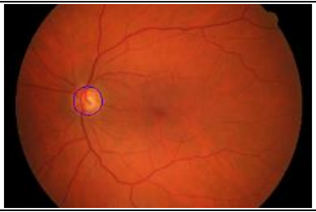 | Correct |
| im (35) |  | 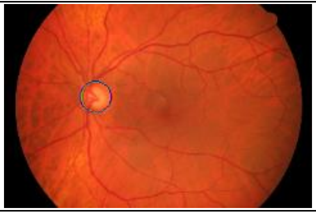 |  | Correct |
| im (37) |  |  |  | Incorrect |
| im (42) |  | 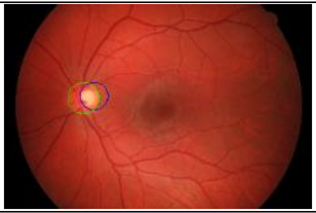 | 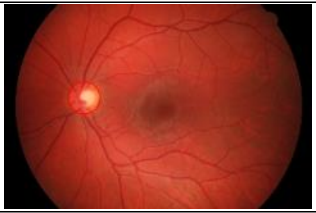 | Correct |

**Table 4-7. Sample results of the optic disc segmentations within MESSIDOR**

| | Reference Image | Optic Disc Candidates | Segmented Optic Disc | Response |
|---|---|---|---|---|
| im (18) |  | 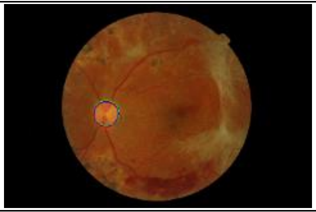 | 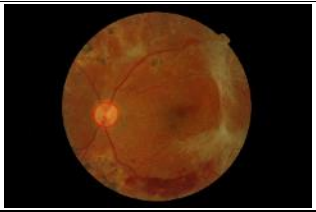 | Correct |
| im (32) |  |  |  | Correct |
| im (77) |  | 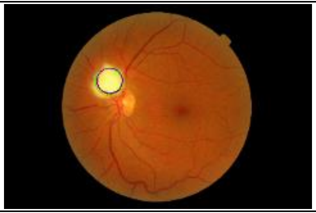 |  | Incorrect |
| im (269) | 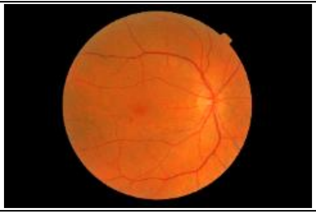 | 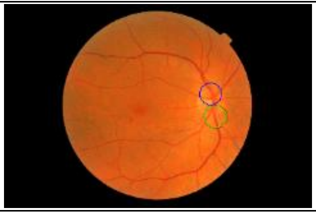 | 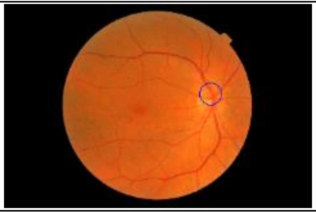 | Correct |
| im (281) |  |  |  | Correct |
| im (453) |  | 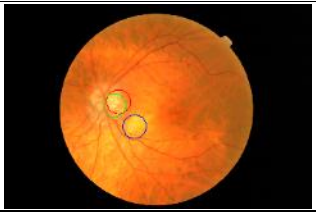 |  | Correct |
| im (486) |  |  | 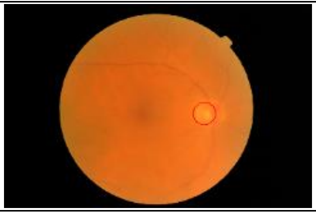 | Correct |

|  | Reference Image | Optic Disc Candidates | Segmented Optic Disc | Response |
|---|---|---|---|---|
| im (1096) |  |  | 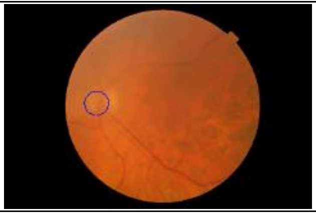 | Correct |
| im (1199) |  | 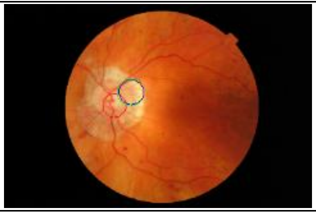 | 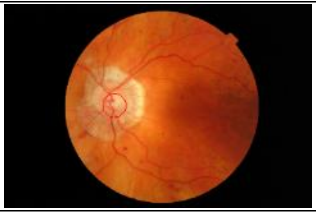 | Correct |

**Table 4-8. Sample results of the optic disc segmentations within ONHSD**

|  | Reference Image | Optic Disc Candidates | Segmented Optic Disc | Response |
|---|---|---|---|---|
| im (4) |  | 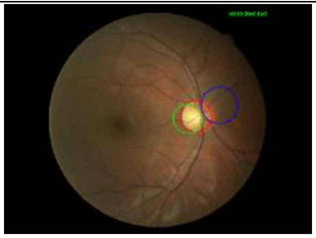 |  | Correct |
| im (24) |  | 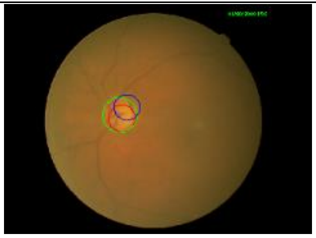 |  | Correct |
| im (36) | 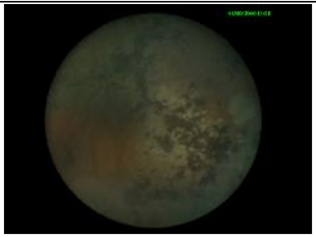 |  |  | Incorrect |
| im (51) |  | 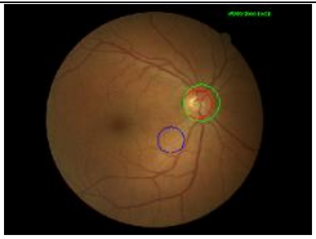 |  | Correct |

|  | Reference Image | Optic Disc Candidates | Segmented Optic Disc | Response |
|---|---|---|---|---|
| im (53) |  | 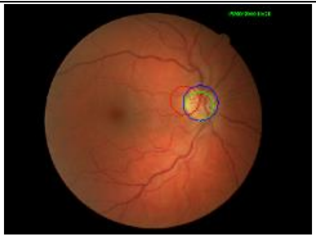 | 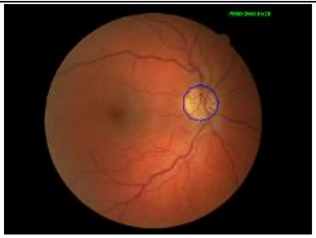 | Correct |
| im (64) |  |  |  | Correct |
| im (73) |  |  |  | Correct |
| im (74) |  |  |  | Incorrect |
| im (95) |  |  |  | Correct |

**Table 4-9. Sample results of the optic disc segmentations within STARE**

|  | Reference Image | Optic Disc Candidates | Segmented Optic Disc | Response |
|---|---|---|---|---|
| im (8) |  |  | 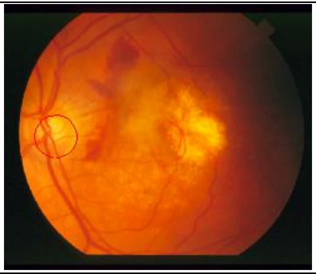 | Correct |

| | **Reference Image** | **Optic Disc Candidates** | **Segmented Optic Disc** | **Response** |
|---|---|---|---|---|
| im (18) | 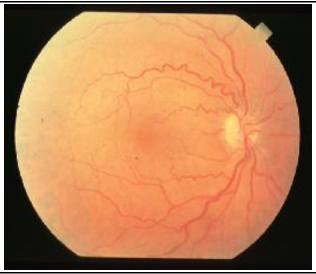 | 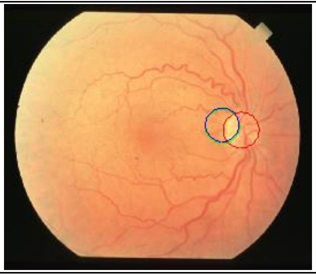 | 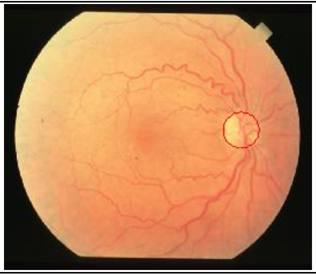 | Correct |
| im (21) |  |  |  | Incorrect |
| im (24) |  | 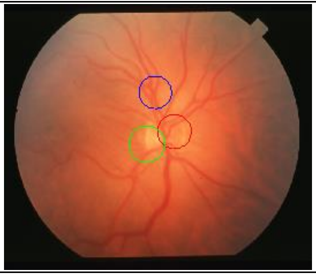 | 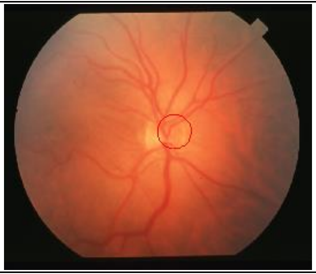 | Correct |
| im (41) | 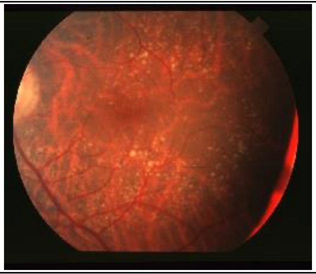 | 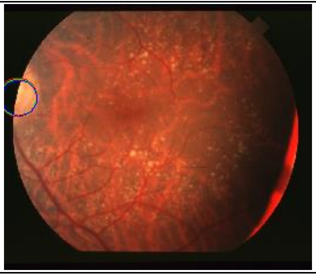 | 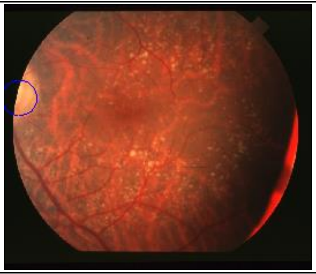 | Correct |
| im (43) |  |  | 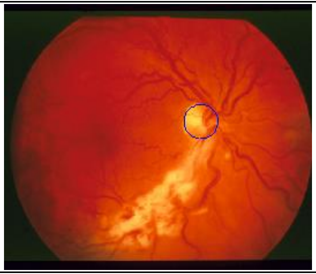 | Correct |
| im (44) |  | 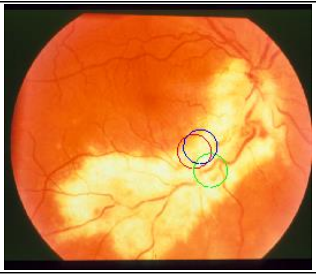 |  | Incorrect |

| | Reference Image | Optic Disc Candidates | Segmented Optic Disc | Response |
|---|---|---|---|---|
| im (45) |  |  | 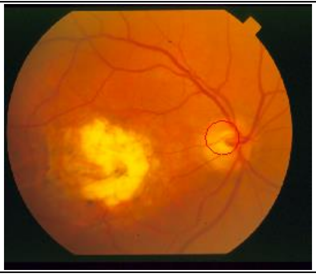 | Correct |
| im (47) |  | 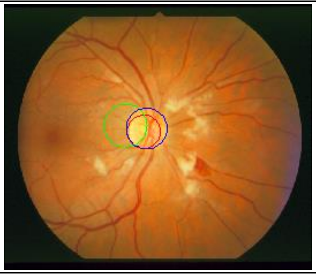 |  | Correct |

Table 4-10 aggregates and compares the results achieved by our proposed segmentation approach over the nine different datasets, mainly in terms of the sensitivity and the processing time. More detailed results are found at Appendix B.

**Table 4-10. Results of the proposed method for segmenting the optic disc**

| # | Dataset | No. of images | Correct responses | SENS | Total processing time (in sec.) | Average processing time per image | No. of pixels per image |
|---|---|---|---|---|---|---|---|
| **1** | ARIA | 143 | 121 | **0.8462** | 78.1165 | 0.5463 | 442,368 |
| **2** | DIARETDB0 | 130 | 117 | **0.9000** | 174.4838 | 1.3848 | 1,728,000 |
| **3** | DIARETDB1 | 89 | 79 | **0.8876** | 122.7492 | 1.3792 | 1,728,000 |
| **4** | DRIONS-DB | 110 | 110 | **1.0000** | 40.2961 | 0.3663 | 240,000 |
| **5** | DRIVE | 40 | 39 | **0.9750** | 14.4641 | 0.3616 | 329,960 |
| **6** | HRF | 45 | 43 | **0.9556** | 296.2217 | 6.5827 | 8,185,344 |
| **7.1** | MESSIDOR (set1) | 400 | 394 | **0.9850** | 933.4118 | 2.3335 | 1,382,400 |
| **7.2** | MESSIDOR (set2) | 400 | 389 | **0.9725** | 440.6891 | 1.1017 | 3,333,120 |
| **7.3** | MESSIDOR (set3) | 400 | 390 | **0.9750** | 731.8618 | 1.8297 | 3,538,944 |
| **8** | ONHSD | 99 | 94 | **0.9495** | 56.5776 | 0.5715 | 433,200 |
| **9** | STARE | 81 | 59 | **0.7284** | 45.9078 | 0.5668 | 423,500 |
| **ALL DATASETS** | | 1937 | 1835 | **0.9473** | 2934.7796 | 1.5183 | N/A |

Table 4-11 along with Figure 4-1 show a comparison of the proposed technique against the main optic disc detection methods reviewed in section 2.4.3.

**Table 4-11. Comparison of the proposed method of segmenting the optic disc against others**

| # | Detection Approach | Dataset(s) | SENS |
|---|---|---|---|
| **1** | Goldbaum *et al.*, (1996) [36]: Vessels convergence, optic disc brightness, and entrance of large vessels | None | - |
| **2** | Walter & Klein, (2001) [68]: Largest brightest connected object | Local dataset<br>STARE[1] | 0.9000<br>0.5802 |
| **3** | Hoover & Goldbaum, (2003) [35]: Fuzzy convergence of vessels | STARE | 0.8888 |
| **4** | Foracchia *et al.*, (2004) [78]: Geometrical model of vessel structure | STARE | 0.9753 |
| **5** | Li & Chutatape, (2004) [77]: Template matching via PCA | Local dataset | 0.9888 |
| **6** | Haar, (2005) [21]: Hough Transform applied to the pixels on or close to the retinal vasculature | Local dataset<br>STARE | 0.9634<br>0.7160 |
| **7** | Fleming et al., (2007) [73]: Elliptical form of blood vessels | Local dataset | 0.9840 |
| **8** | Youssif *et al.*, (2008) [6]: Vessels' direction matched filter | DRIVE<br>STARE | 1.0000<br>0.9877 |
| **9** | Aquino *et al.*, (2010) [31]: Morphological operators, edge detection and circular Hough transform | MESSIDOR | 0.8600 |
| **10** | Rangayyan *et al.*, (2010) [75]: Vessels convergence by Gabor filters and phase portrait modelling | DRIVE<br>STARE | 1.0000<br>0.6913 |
| **11** | Zhu *et al.*, (2010) [70]: Circle detection via Hough transform | DRIVE<br>STARE | 0.9000<br>0.4444 |
| **12** | Lu, (2011) [30]: Circular transformation and image variation along multiple radial line segments | ARIA (partial)<br>MESSIDOR<br>STARE | 0.9750<br>0.9975<br>0.9876 |
| **13** | Yu & Yu, (2014) [72]: Iterative brightest pixels extraction | STARE subset | 0.9500 |
| **14** | Zhang & Zhao, (2014) [80]: Vessels distribution and directional characteristics | DIARETDB0<br>DIARETDB1<br>DRIVE<br>STARE | 1.0000<br>1.0000<br>1.0000<br>0.9877 |
| **15** | ***Proposed Method: Weighting vessels density within the strongest optic disc candidates*** | **ARIA**<br>**DIARETDB0**<br>**DIARETDB1**<br>**DRIONS-DB**<br>**DRIVE**<br>**HRF**<br>**MESSIDOR**<br>**ONHSD**<br>**STARE** | **0.8462**<br>**0.9000**<br>**0.8876**<br>**1.0000**<br>**0.9750**<br>**0.9556**<br>**0.9775**<br>**0.9495**<br>**0.7284** |

---

[1] Additional results for the STARE dataset were obtained from the comparative study done by Haar [21].

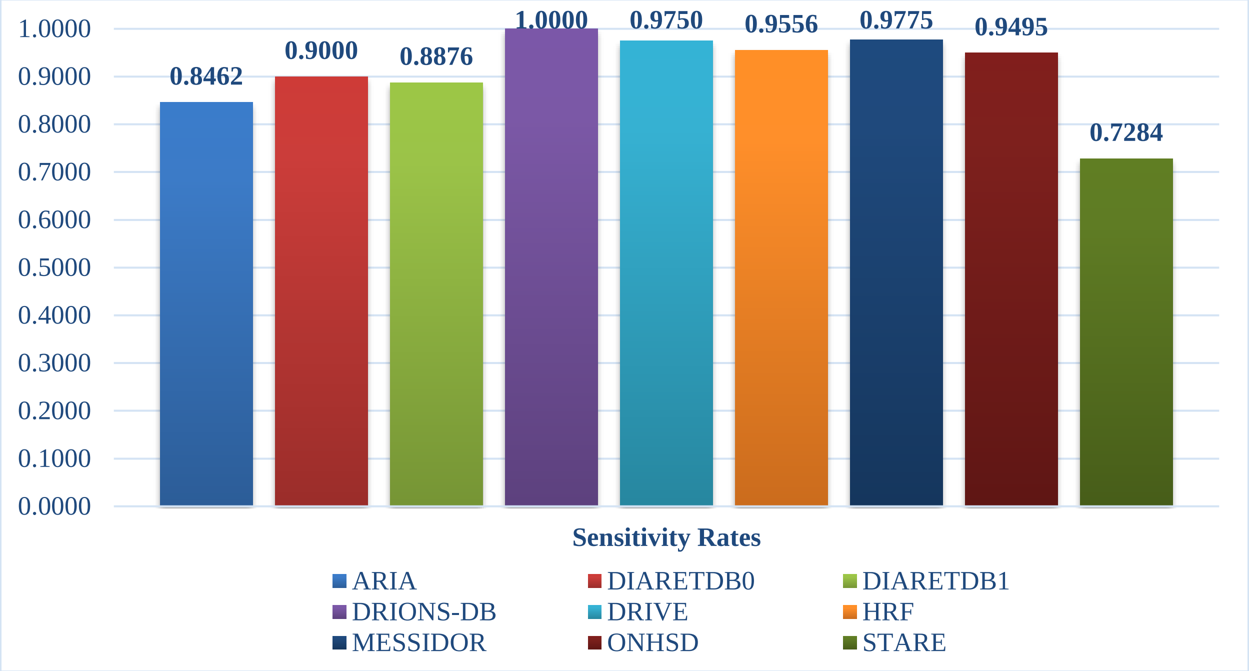

**Figure 4-1. Sensitivity rates of detecting the optic disc in the proposed system**

## 4.3. Abnormalities Detection Results

It is worth to mention that not all the datasets that were employed in our approach of detecting the optic disc, were reutilized to detect the abnormal features within eye fundus images. There are two reasons behind not using all the datasets; first, abnormalities are not normally present in every human eye, which is obviously not the case in the optic disc which is a landmark that exists in any eye fundus image. Second, even though abnormalities occur within some fundus images of the employed datasets, yet the ground truth of these abnormalities are not always provided by the datasets in order to evaluate the proposed screening system.

Among the employed datasets, some of them specify the fundus images that are diagnosed to be suffering from diabetic retinopathy, namely ARIA, DIARETDB0, DIARETDB1, HRF, MESSIDOR and STARE. But only a few of these datasets indicate and specify the clinical signs of diabetic retinopathy within each image (e.g. microaneurysms, hemorrhages, exudates, cotton wool spots, and neovascularization).

Therefore, in order to diagnose diabetic retinopathy and detect its abnormal clinical signs, our proposed system utilized a total of 1419 images from three specific datasets: DIARETDB0 (130 images), DIARETDB1 (89 images), and MESSIDOR (1200 images), which are the only ones among all the datasets that provide the ground truths of the different types of abnormalities occurring in diabetic retinopathy. The ground truths of DIARETDB0, DIARETDB1 and MESSIDOR were aggregated and restructured in a tabular layout, and illustrated at Appendices A.1, A.2, and A.3, respectively.

Again, it is practically infeasible to include all the visual segmentations for that huge number of tested images herein this research. So, the three following tables (Table 4-12, Table 4-13 and Table 4-14) show 30 sample results within each of DIARETDB0, DIARETDB1, and MESSIDOR, respectively, for the proposed system of segmenting the bright abnormalities. These sample results in each table were grouped and sorted by the different types of responses (i.e. 15 true positives, 5 true negatives, 5 false positives, and 5 false negatives).

**Table 4-12. Sample results of segmenting the bright abnormalities within DIARETDB0**

| | Reference Image | Selected Cluster | Bright Abnormalities | Response |
|---|---|---|---|---|
| im (8) |  | 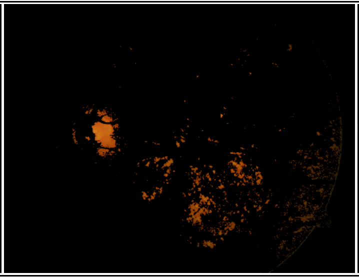 |  | True Positive Response |
| im (9) |  |  | 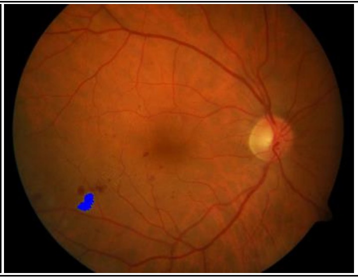 | True Positive Response |
| im (12) |  | 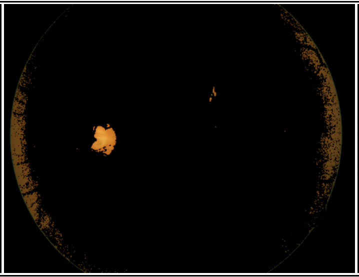 |  | True Positive Response |
| im (14) |  | 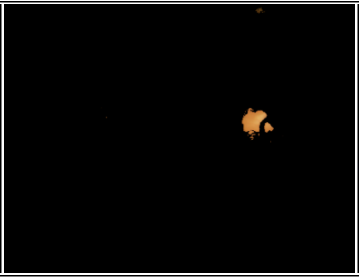 |  | True Positive Response |

|  | Reference Image | Selected Cluster | Bright Abnormalities | Response |
|---|---|---|---|---|
| im (15) |  | 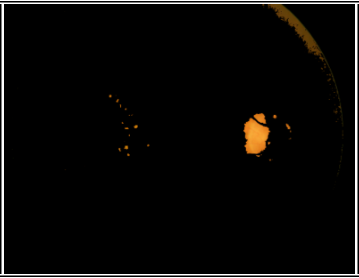 |  | True Positive Response |
| im (16) | 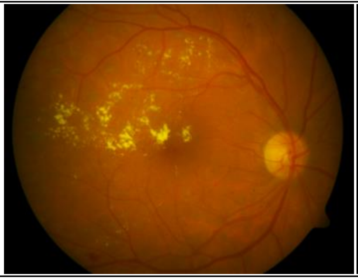 | 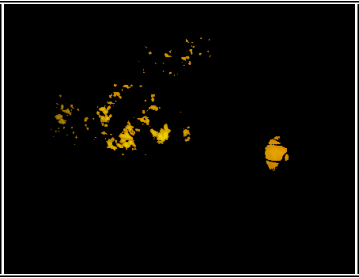 | 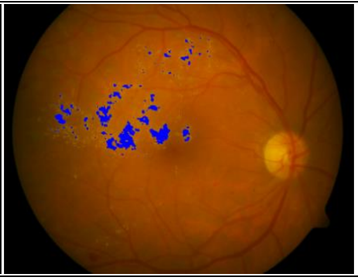 | True Positive Response |
| im (19) |  | 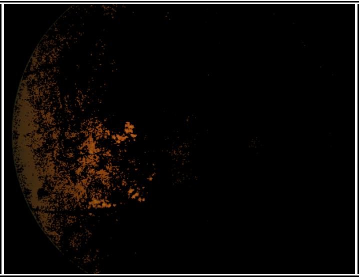 |  | True Positive Response |
| im (34) |  |  |  | True Positive Response |
| im (35) |  | 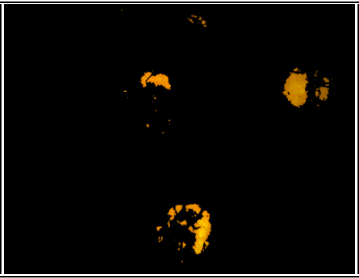 | 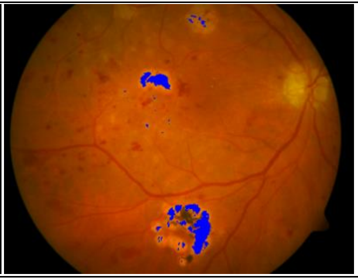 | True Positive Response |
| im (40) |  | 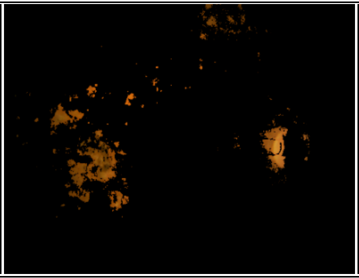 |  | True Positive Response |

|  | Reference Image | Selected Cluster | Bright Abnormalities | Response |
|---|---|---|---|---|
| im (43) |  | 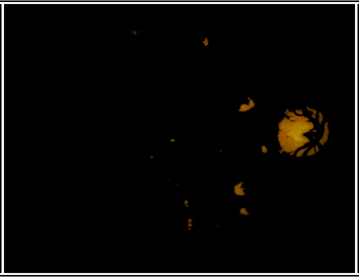 |  | True Positive Response |
| im (100) |  | 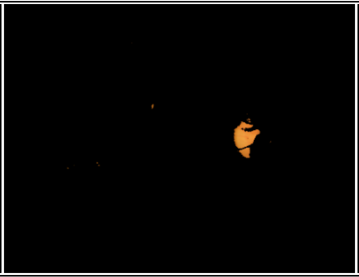 |  | True Positive Response |
| im (103) |  | 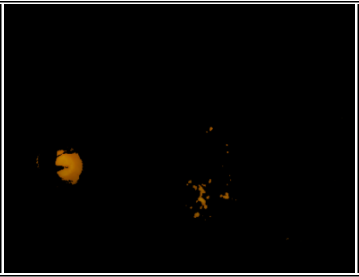 | 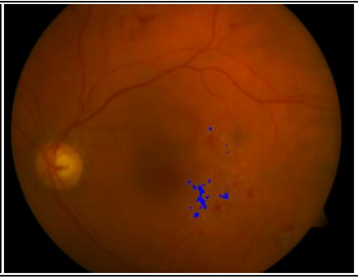 | True Positive Response |
| im (104) |  | 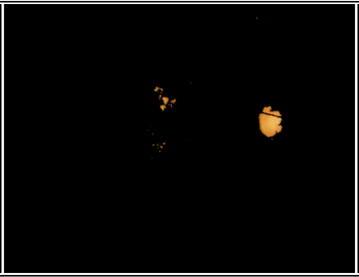 |  | True Positive Response |
| im (109) |  | 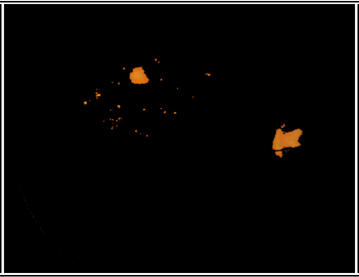 |  | True Positive Response |
| im (49) |  | 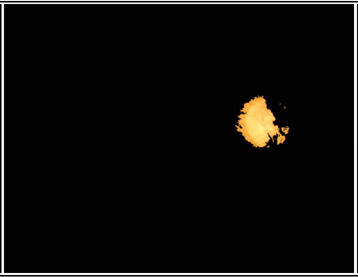 |  | True Negative Response |

| | Reference Image | Selected Cluster | Bright Abnormalities | Response |
|---|---|---|---|---|
| im (95) |  | 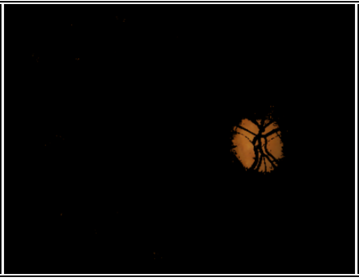 | 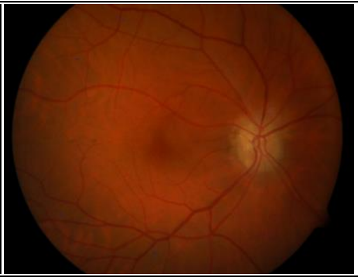 | True Negative Response |
| im (113) |  |  | 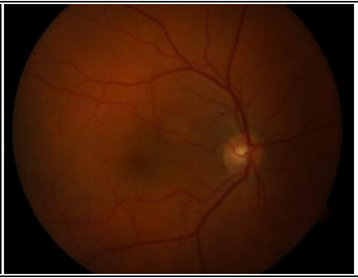 | True Negative Response |
| im (114) |  |  | 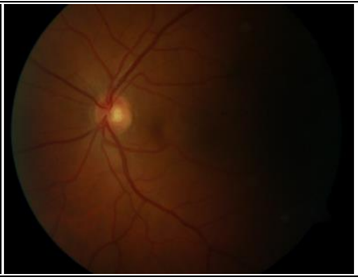 | True Negative Response |
| im (116) |  |  |  | True Negative Response |
| im (63) | 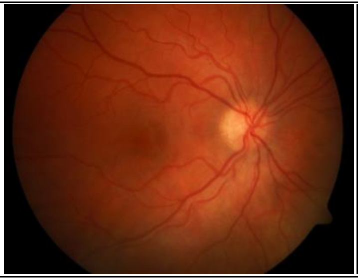 | 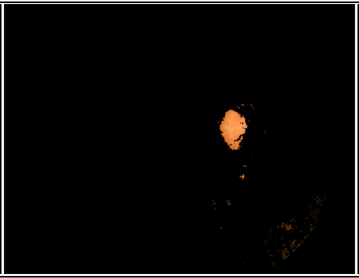 |  | False Positive Response |
| im (75) |  |  | 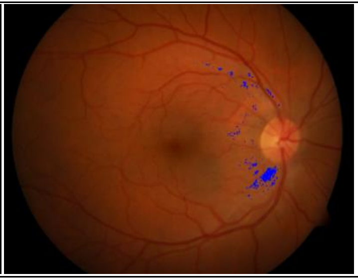 | False Positive Response |

| | Reference Image | Selected Cluster | Bright Abnormalities | Response |
|---|---|---|---|---|
| im (80) |  |  |  | False Positive Response |
| im (97) | 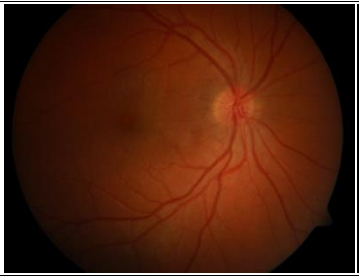 |  | 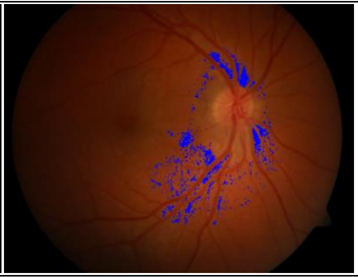 | False Positive Response |
| im (117) |  | 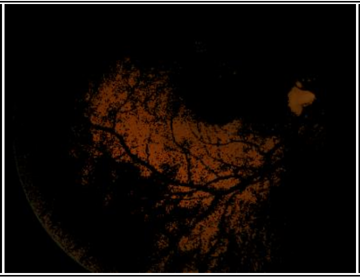 | 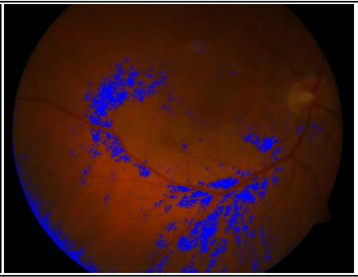 | False Positive Response |
| im (4) |  | 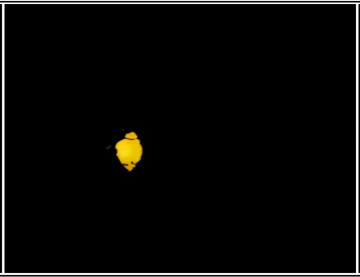 |  | False Negative Response |
| im (23) |  | 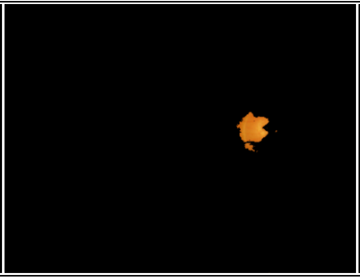 |  | False Negative Response |
| im (54) |  |  | 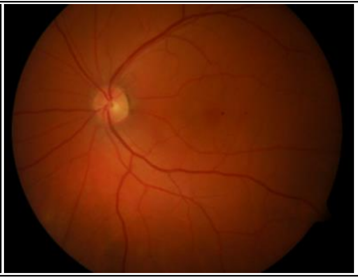 | False Negative Response |

|  | Reference Image | Selected Cluster | Bright Abnormalities | Response |
|---|---|---|---|---|
| im (57) | 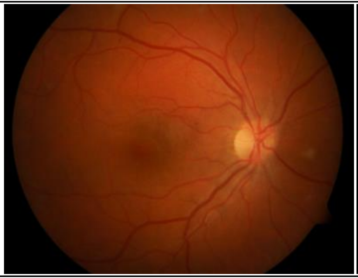 | 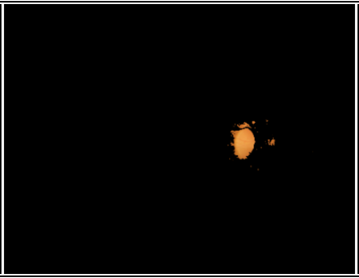 | 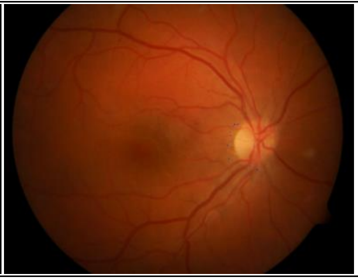 | False Negative Response |
| im (66) | 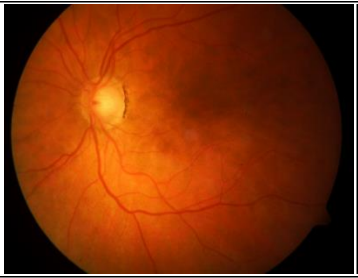 | 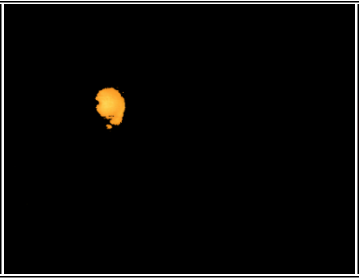 | 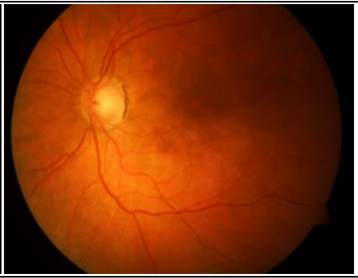 | False Negative Response |

Similarly, the following table also shows the sample results of segmenting the bright abnormalities appearing within the fundus images of DIARETDB1, grouped by the response type.

**Table 4-13. Sample results of segmenting the bright abnormalities within DIARETDB1**

|  | Reference Image | Selected Cluster | Bright Abnormalities | Response |
|---|---|---|---|---|
| im (1) | 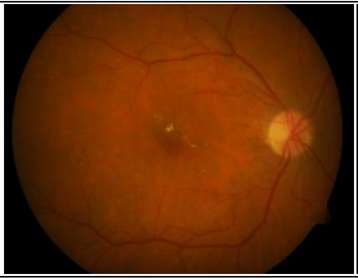 | 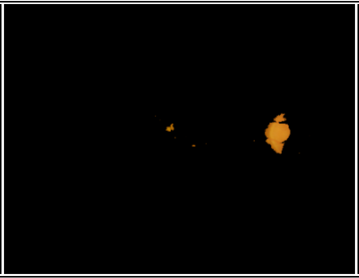 | 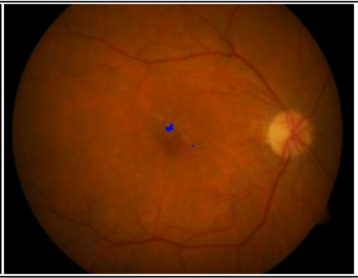 | True Positive Response |
| im (2) |  | 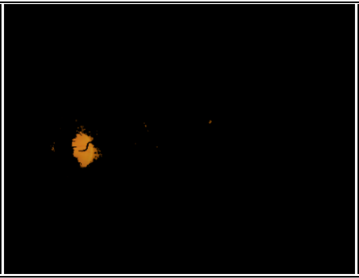 |  | True Positive Response |
| im (5) |  | 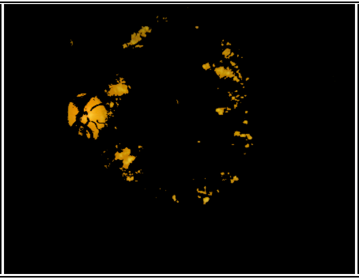 | 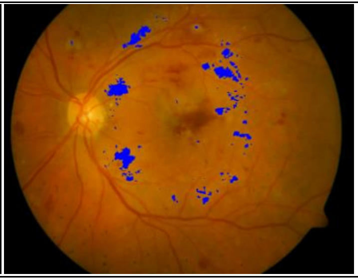 | True Positive Response |

| | Reference Image | Selected Cluster | Bright Abnormalities | Response |
|---|---|---|---|---|
| im (10) |  | 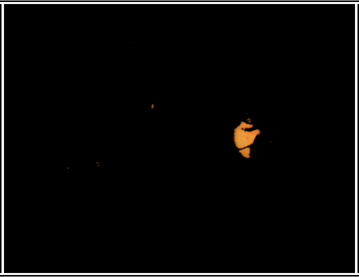 |  | True Positive Response |
| im (15) |  | 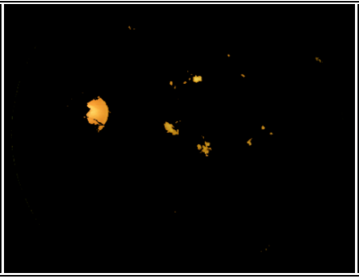 |  | True Positive Response |
| im (16) |  | 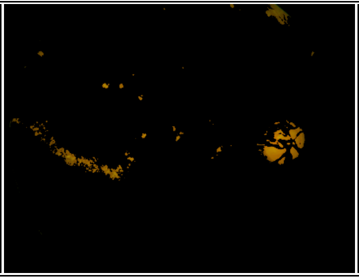 |  | True Positive Response |
| im (18) |  | 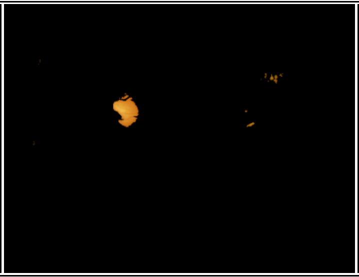 |  | True Positive Response |
| im (19) |  | 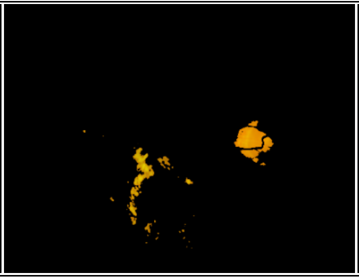 |  | True Positive Response |
| im (20) |  | 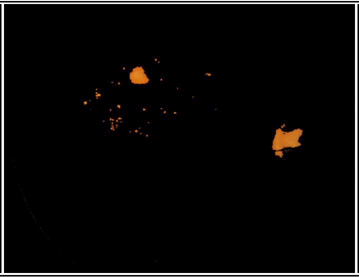 |  | True Positive Response |

|  | Reference Image | Selected Cluster | Bright Abnormalities | Response |
|---|---|---|---|---|
| im (25) |  | 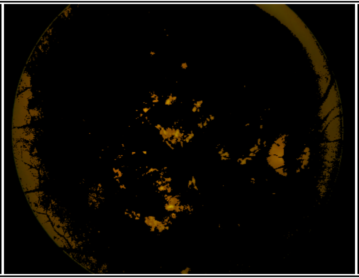 |  | True Positive Response |
| im (26) |  |  | 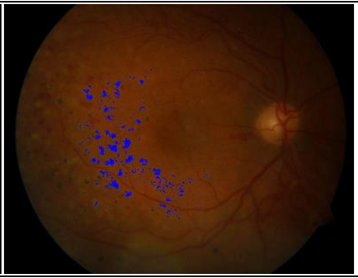 | True Positive Response |
| im (33) | 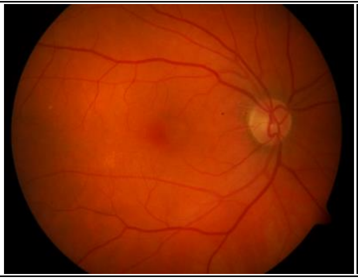 | 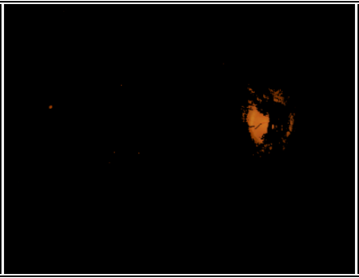 | 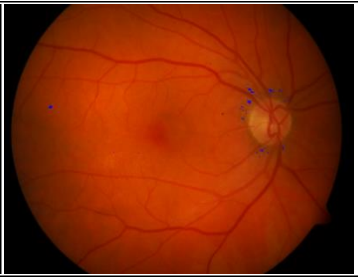 | True Positive Response |
| im (44) | 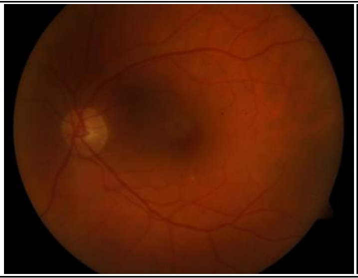 | 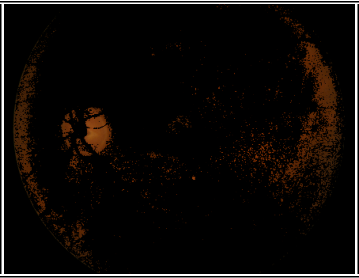 | 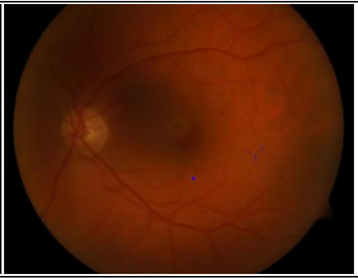 | True Positive Response |
| im (64) |  | 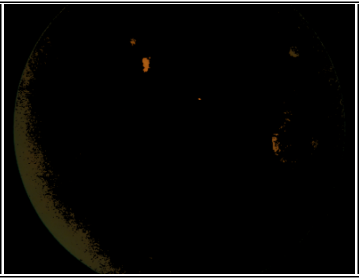 |  | True Positive Response |
| im (84) |  | 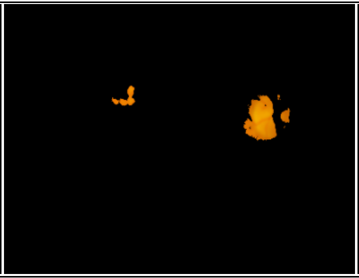 |  | True Positive Response |

| | **Reference Image** | **Selected Cluster** | **Bright Abnormalities** | **Response** |
|---|---|---|---|---|
| im (39) |  |  | 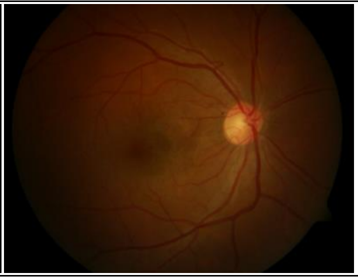 | True Negative Response |
| im (49) |  | 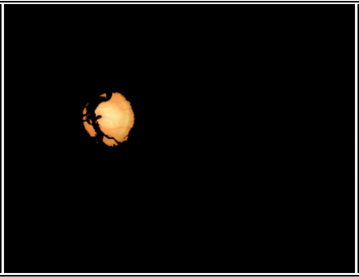 |  | True Negative Response |
| im (61) |  | 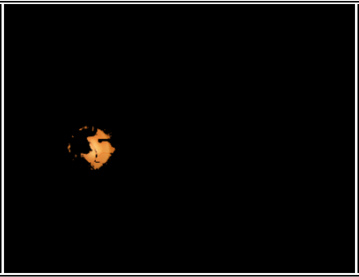 |  | True Negative Response |
| im (74) |  |  |  | True Negative Response |
| im (88) |  | 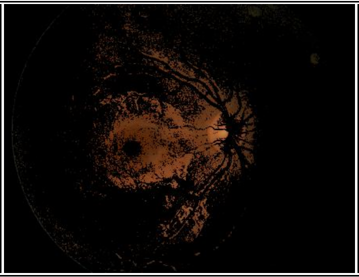 |  | True Negative Response |
| im (40) |  |  |  | False Positive Response |

|  | Reference Image | Selected Cluster | Bright Abnormalities | Response |
|---|---|---|---|---|
| im (68) | 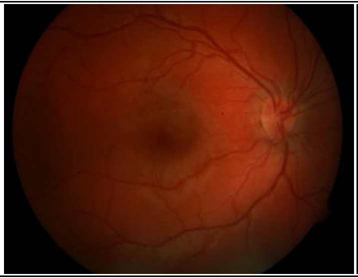 |  | 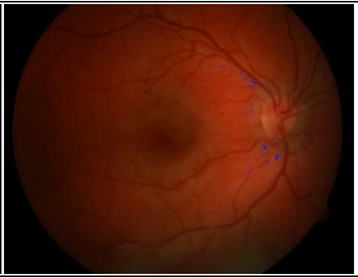 | False Positive Response |
| im (77) | 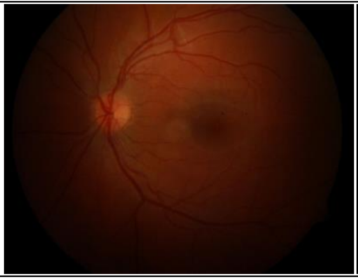 |  | 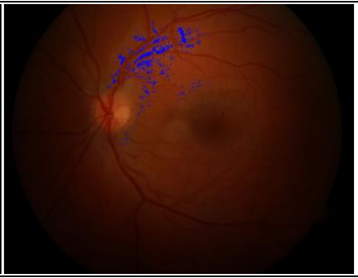 | False Positive Response |
| im (87) |  | 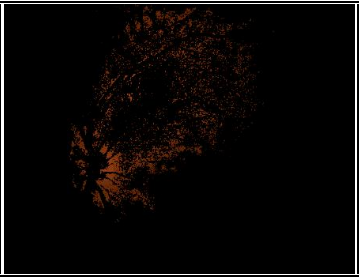 | 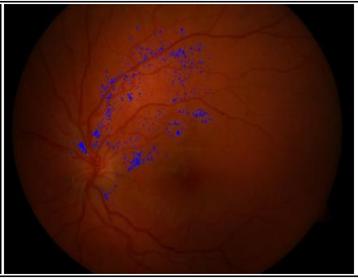 | False Positive Response |
| im (89) |  | 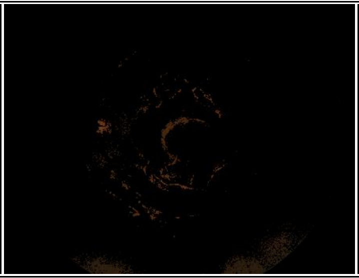 |  | False Positive Response |
| im (34) |  | 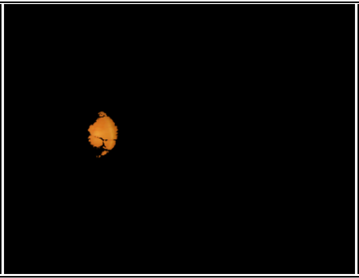 |  | False Negative Response |
| im (54) | 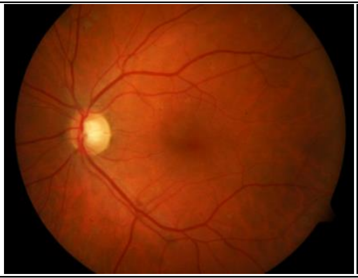 | 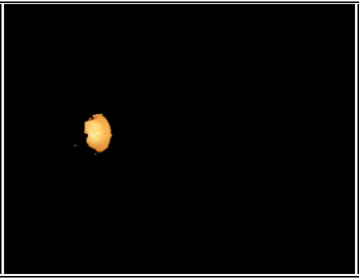 |  | False Negative Response |

|  | Reference Image | Selected Cluster | Bright Abnormalities | Response |
|---|---|---|---|---|
| im (56) | 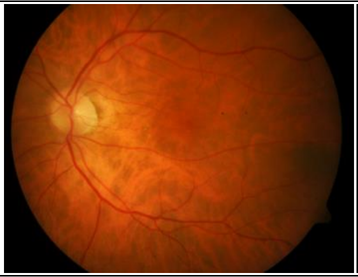 | 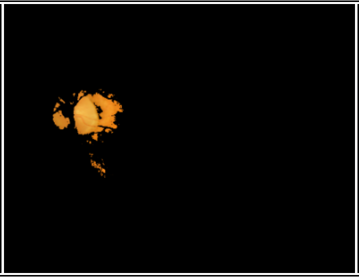 | 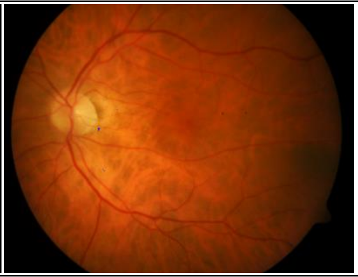 | False Negative Response |
| im (78) |  | 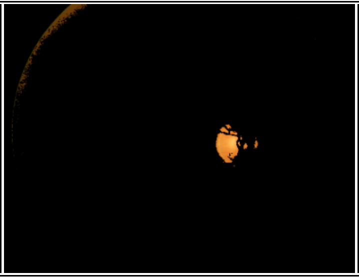 | 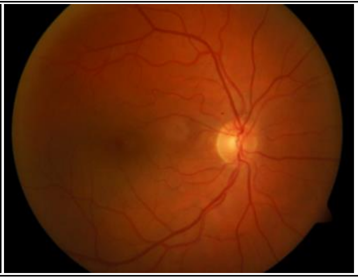 | False Negative Response |
| im (85) |  | 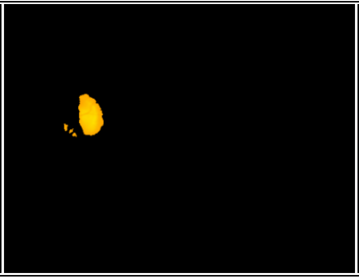 |  | False Negative Response |

Finally, the following table shows the sample results of segmenting the bright abnormalities occurring within the fundus images of MESSIDOR, grouped and sorted by the response type.

**Table 4-14. Sample results of segmenting the bright abnormalities within MESSIDOR**

|  | Reference Image | Selected Cluster | Bright Abnormalities | Response |
|---|---|---|---|---|
| im (29) |  | 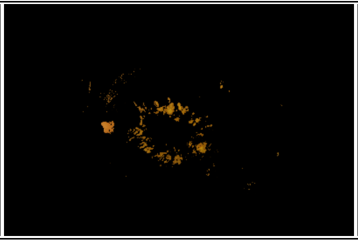 | 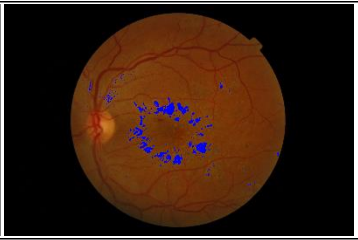 | True Positive Response |
| im (195) |  | 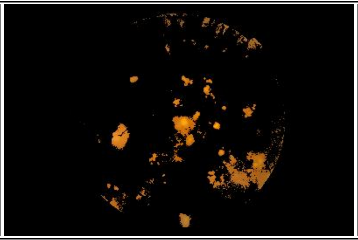 | 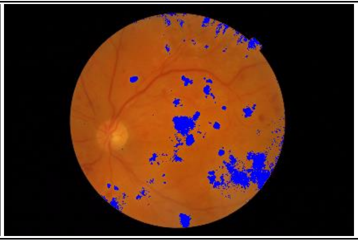 | True Positive Response |

| | Reference Image | Selected Cluster | Bright Abnormalities | Response |
|---|---|---|---|---|
| im (301) |  | 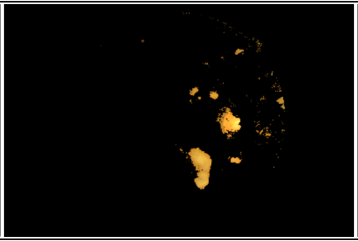 | 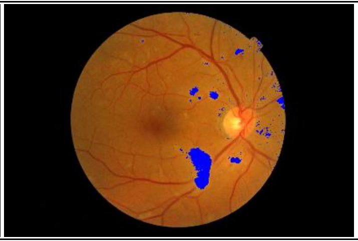 | True Positive Response |
| im (343) |  | 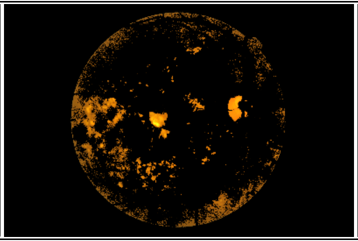 | 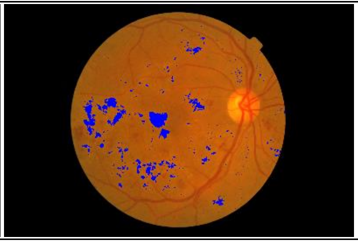 | True Positive Response |
| im (346) |  | 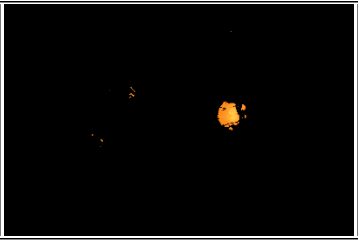 |  | True Positive Response |
| im (360) |  | 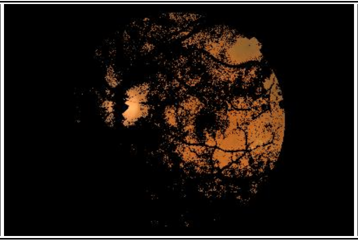 |  | True Positive Response |
| im (362) |  | 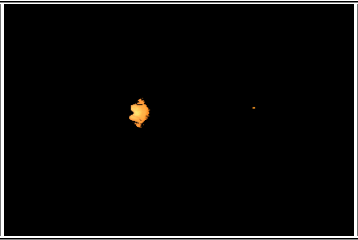 |  | True Positive Response |
| im (378) |  | 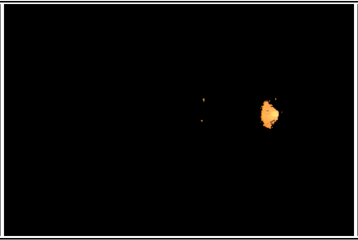 | 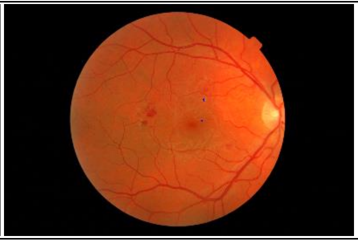 | True Positive Response |
| im (435) |  | 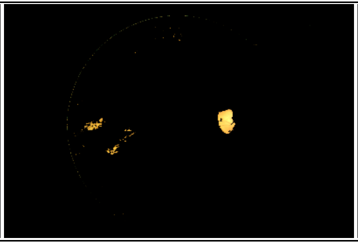 | 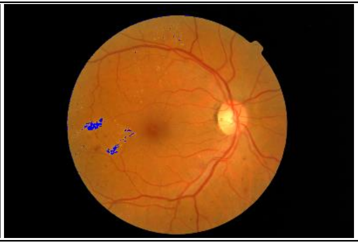 | True Positive Response |

| | Reference Image | Selected Cluster | Bright Abnormalities | Response |
|---|---|---|---|---|
| im (498) |  | 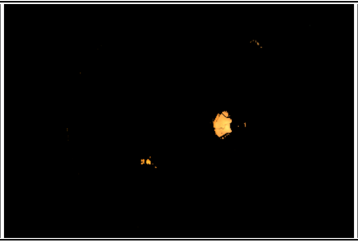 | 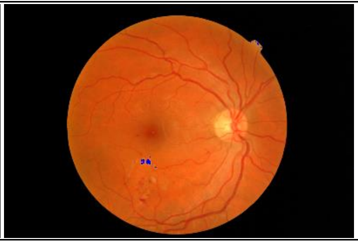 | True Positive Response |
| im (499) |  | 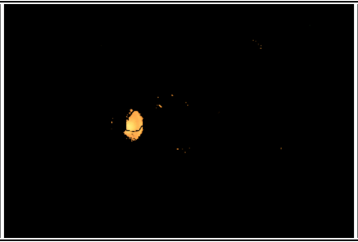 |  | True Positive Response |
| im (577) |  |  |  | True Positive Response |
| im (678) |  |  |  | True Positive Response |
| im (1031) |  | 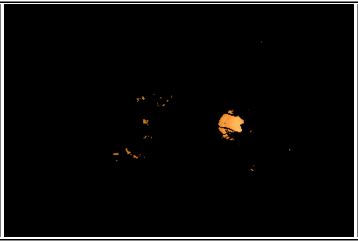 | 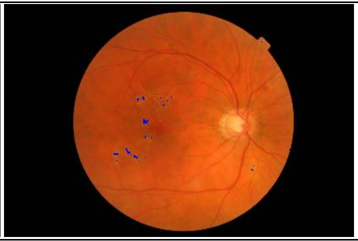 | True Positive Response |
| im (1092) |  | 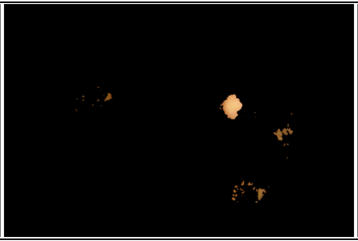 | 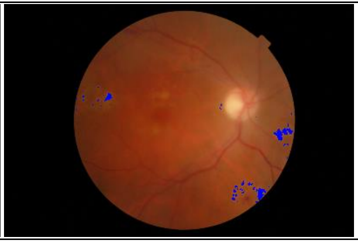 | True Positive Response |

| | Reference Image | Selected Cluster | Bright Abnormalities | Response |
|---|---|---|---|---|
| im (33) |  | 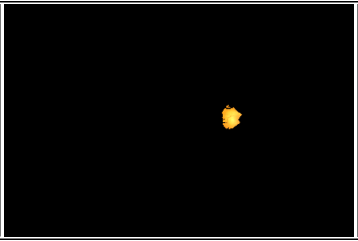 | 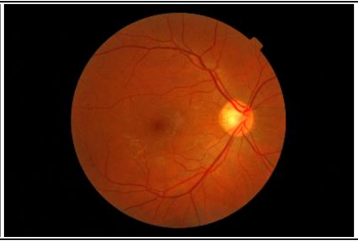 | True Negative Response |
| im (222) | 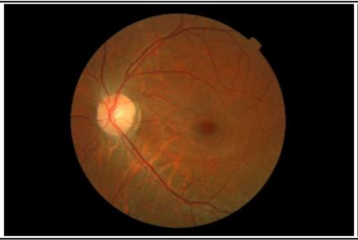 |  | 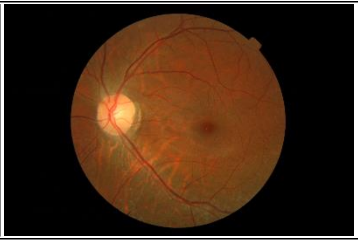 | True Negative Response |
| im (439) | 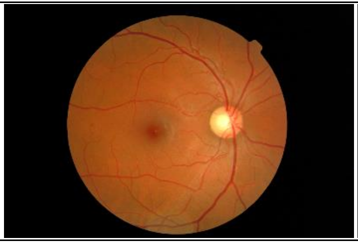 | 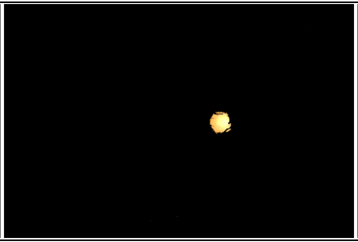 | 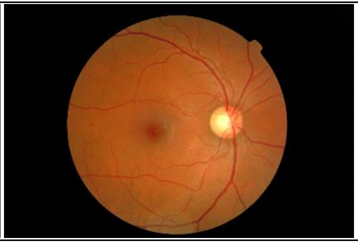 | True Negative Response |
| im (769) |  | 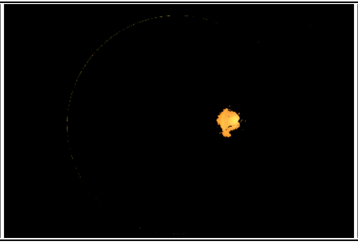 |  | True Negative Response |
| im (924) |  |  |  | True Negative Response |
| im (6) | 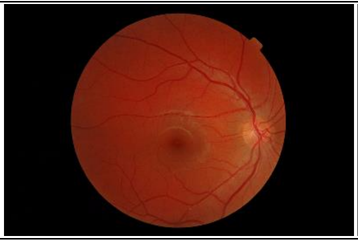 |  | 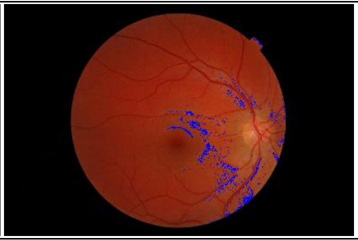 | False Positive Response |
| im (565) |  |  |  | False Positive Response |

|  | Reference Image | Selected Cluster | Bright Abnormalities | Response |
|---|---|---|---|---|
| im (788) | 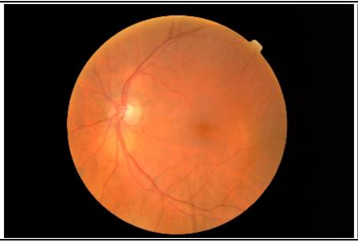 | 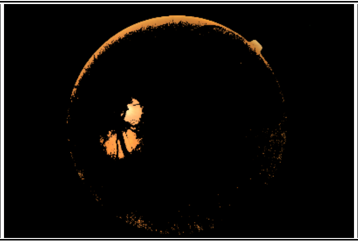 | 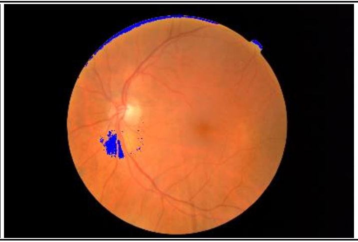 | False Positive Response |
| im (998) |  |  | 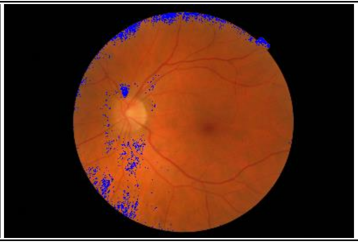 | False Positive Response |
| im (1184) |  |  |  | False Positive Response |
| im (27) | 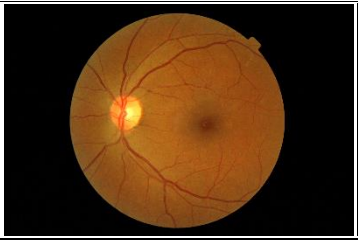 | 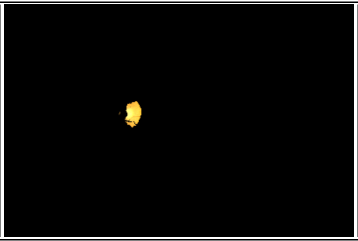 | 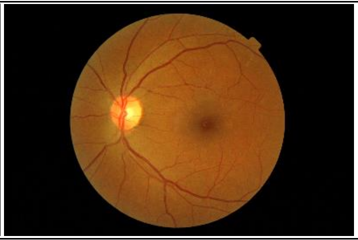 | False Negative Response |
| im (347) |  | 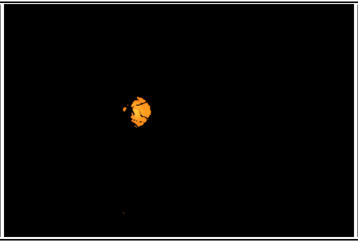 |  | False Negative Response |
| im (656) | 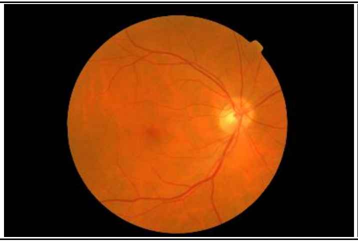 | 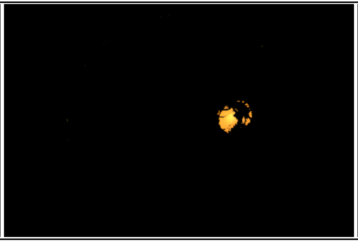 | 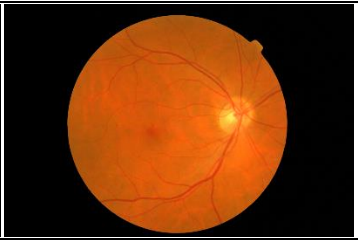 | False Negative Response |

|  | Reference Image | Selected Cluster | Bright Abnormalities | Response |
|---|---|---|---|---|
| im (884) |  |  |  | False Negative Response |
| im (1163) |  | 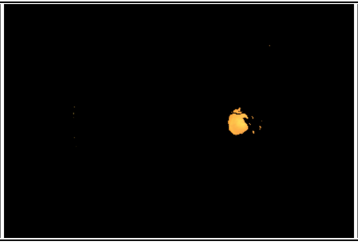 |  | False Negative Response |

Table 4-15 aggregates and compares the results achieved by our proposed segmentation approach over the three different datasets, mainly in terms of the sensitivity and specificity. More detailed results are found at Appendix C.

**Table 4-15. Results of the proposed method for segmenting the bright abnormalities**

| # | Dataset | No. of images | Abnormal Images | Correct responses | SENS | Normal Images | Correct responses | SPEC |
|---|---|---|---|---|---|---|---|---|
| **1** | DIARETDB0 | 130 | 86 | 68 | **0.7907** | 44 | 28 | **0.6364** |
| **2** | DIARETDB1 | 89 | 49 | 40 | **0.8163** | 40 | 29 | **0.7250** |
| **3.1** | MESSIDOR (set1) | 400 | 145 | 130 | **0.8966** | 255 | 143 | **0.5608** |
| **3.2** | MESSIDOR (set2) | 400 | 81 | 70 | **0.8642** | 319 | 159 | **0.4984** |
| **3.3** | MESSIDOR (set3) | 400 | 68 | 57 | **0.8383** | 332 | 203 | **0.6114** |
| **ALL DATASETS** |  | 1419 | 429 | 365 | **0.8508** | 990 | 562 | **0.5677** |

Table 4-16 along with Figure 4-2 show a comparison of the proposed technique against the other methods presented in section 2.5.6 for segmenting the bright abnormalities.

**Table 4-16. Comparison of the methods of segmenting the bright abnormalities**

| | Approach | Dataset(s) | SENS | SPEC | ACC |
|---|---|---|---|---|---|
| **1** | Sinthanayothin *et al.*, (2002) [113] | Local dataset (30 images) | 0.8850 | 0.9970 | - |
| **2** | Osareh *et al.*, (2003) [114] | Local dataset (142 images) | 0.9300 | 0.9410 | - |
| **3** | Li & Chutatape, (2004) [77] | Local dataset (35 images) | 1.0000 | 0.7100 | - |
| **4** | Sopharak *et al.*, (2008) [110] | Local dataset (39 images) | 0.9338 | 0.9814 | 0.9338 |
| **5** | Jaafar *et al.*, (2011) [108] | Mixed dataset (236 images) | 0.9320 | 0.9920 | 0.9940 |
| **6** | Harangi *et al.*, (2012) [107] | DIARETDB1 (89 images) | 0.6300 | - | - |
| **7** | Eadaghi & Pourreza, (2012) [112] | DIARETDB1 (89 images) | 0.7828 | - | - |
| **8** | Kumar *et al.*, (2013) [109] | Mixed dataset (158 images) | 0.8845 | 0.9550 | - |
| **9** | Sreng *et al.*, (2013) [111] | Local dataset (100 images) | 0.9100 | - | - |
| **10** | Franklin & Rajan, (2014) [115] | DIARETDB1 (89 images) | 0.9630 | 0.9980 | 0.9970 |
| **11** | Roychowdhury *et al.*, (2014) [117] | DIARETDB1 (89 images) | 0.8900 | 0.8500 | - |
| **12** | Singh *et al.*, (2015) [116] | Local dataset (20 images) | 0.9487 | - | - |
| **13** | Rajan et al., (2016) [118] | DIARETDB1 (89 images) | 0.8620 | 0.8500 | - |
| **14** | Prentasic & Loncaric (2016) [119] | DRiDB (50 images) | 0.7800 | - | - |
| **15** | Liu et al., (2017) [120] | DIARETDB1 (89 images) | 0.8300 | 0.7500 | - |
| **16** | ***Proposed method: color-based k-means clustering & statistic-based thresholding*** | DIARETDB0 (130 images) | 0.7907 | 0.6364 | - |
| | | DIARETDB1 (89 images) | 0.8163 | 0.7250 | - |
| | | MESSIDOR (1200 images) | 0.8741 | 0.5574 | - |

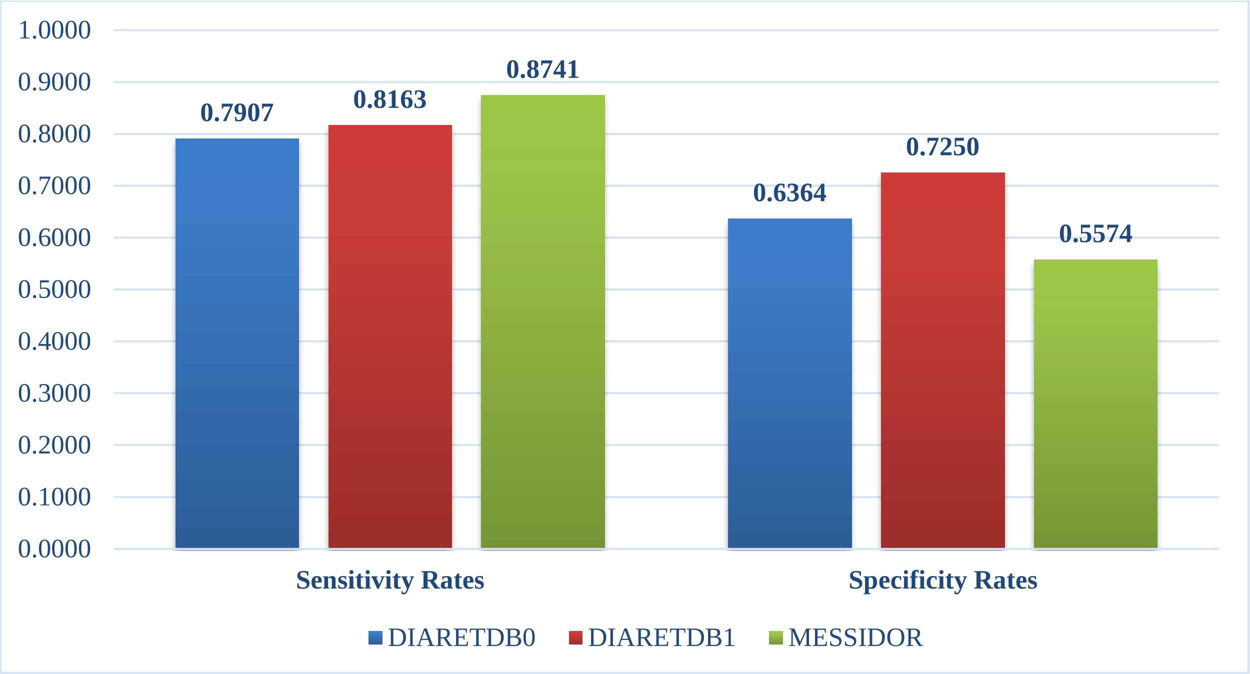

**Figure 4-2. Sensitivity and specificity rates of detecting the bright abnormalities**

# Chapter 5. Conclusion and Future Work

## 5.1. Conclusion & Discussion

The following conclusions were observed from the perspective of each stage of the system proposed for segmenting and detecting the optic disc and the bright abnormalities. Thus, the following subsections conclude and discuss the points of strength and weakness for each of the main components of the proposed system architecture illustrated previously in Figure 3-1.

### 5.1.1. Fundus Image Datasets

From the perspective of the datasets utilized in segmenting the landmarks and abnormalities, STARE and DRIVE datasets were considered the benchmark for most of the segmentation algorithms in the literature. However, other fundus datasets such as DIARETDB0, DIARETDB1, ARIA, and MESSIODOR were also frequently used by some other algorithms in the literature. Thereby, the proposed work exploited all these mentioned datasets and even other more such as DRIONS-DB, ONHSD, and HRF, creating an exceptional and unique experimental environment composed of nine heterogeneous datasets.

It was observed that the proposed algorithm for optic disc segmentation had achieved the best results within the fundus datasets of DRIONS-DB, MESSIDOR and DRIVE. This was intuitively because of the good quality of the images, and the discernibility of optic discs within the fundus images, as well as the absence or rareness of bright abnormalities that looked like the optic disc. On the other hand, STARE dataset recorded the lowest sensitivity rates in segmenting the optic disc compared to the other employed datasets, mainly because of the poor-scanned images in that dataset, as well as the presence of bright lesions within almost all of its images.

### 5.1.2. Fundus Image Preprocessing

Obviously, the preprocessing techniques led to “quicker” and “more accurate” results at the further segmentation stage. For instance, the fundus images in the presented algorithm were initially masked out through a binary image in order to discard the dark background, as well as other unimportant labels, from further unnecessary processing. Although some of the tested datasets were accompanied with these mask images, yet the presented algorithm exploited a technique that created those binary images for the datasets that did not include such masks.

Similarly, some of the datasets also provided binary images of the vasculature tree, while other datasets did not. Therefore, the proposed algorithm extracted the retinal blood vessels which were utilized in splitting the fundus image as well as calculating the vessels density.

In all cases, however, the generated masks as well as the extracted vasculature, that were created via the proposed algorithm, were utilized and they hence replaced the corresponding images provided by those datasets, for the sake of getting accurate and non-misleading experimental results.

Moreover, the vertical splitting approach had proved to be very useful in estimating the initial approximate location of the optic disc. This in turn led to reducing the processing time of the segmentation process by manipulating only half the fundus image rather than the whole image, as well as excluding some parts of the fundus image which might have contained confusing objects that look like the optic disc.

Also, in the process of detecting the bright yellowish abnormalities occurring in the fundus image, the original RGB image was initially converted into the $L^*a^*b$***** color space. This preprocessing transformation was essential in order to get the image partitioned and clustered according to its chromaticity values (i.e. color information).

### 5.1.3. Optic Disc Segmentation

It was obvious, according to the literature review, that the segmentation methods that were solely based on the spatial properties of the optic disc (e.g. its shape, color, size, etc.) achieved good and quick results in normal fundus images that contain no abnormalities. But on the other hand, such approaches usually failed to detect the optic disc in pathological images where abnormalities, such as large exudates, were confused with the optic disc due to their similar appearance. Alternatively, approaches based on vessels-convergence or template matching proved to achieve better sensitivity rates, since the number of false responses were greatly reduced in the presence of other similar abnormal objects. However, such approaches obviously took more processing time and normally required pre-customized templates or image-dependent parameters in order to detect the optic disc.

Thereby, the segmentation approach that was proposed in this research benefited the advantages of these different alternatives, in a simple and straightforward way. It relied on four main features of the spatial properties of the optic disc (i.e. approximate location, roundness, brightness and relative size), and at the same time, it also reduced the number of false candidates in order improve the sensitivity rates within pathological images, and above all, in an automated manner.

The proposed method was tested and evaluated over nine public datasets containing a total of 1937 images. The segmentation algorithm proved its effectiveness by segmenting the optic disc correctly in 1835 images achieving an average sensitivity of 94.73% which was comparable to the results achieved by the other approaches. But more importantly, the implementation of the segmentation algorithm was automated regardless of the extreme heterogeneity of the tested datasets (e.g. spatial size, FOV, image quality, etc.); as no image-dependent parameters were adjusted, nor predefined templates were used for the sake of customizing the proposed algorithm over certain datasets.

However, the false responses for segmenting the optic disc via the proposed approach occurred due to one or more of the following reasons: (1) the poor quality of the images within some of the fundus datasets in which the optic disc was indiscernible, (2) incorrect vertical splitting which led to wrongfully selecting the half that did not contain the optic disc at all, and (3) the presence of too many bright abnormalities in an image that blacked-out and over-confused the appearance of the optic disc.

### 5.1.4. Bright Abnormalities Segmentation

Similar to the optic disc, abnormalities such as hard exudates and cotton wool spots are mainly characterized by their bright yellowish color. But on the contrary to the optic disc, such abnormalities have varying sizes, irregular shapes, and random locations within the fundus. Accordingly, it was impractical for the same approach of detecting the optic disc to be reutilized for extracting those bright abnormalities. Thereby, the proposed detection technique followed a different strategy that relied mainly on the color properties, and nothing more else, in order to detect the bright abnormalities.

The proposed method adopted a two-stage approach for segmenting the bright abnormalities occurring in pathological fundus images. Thus, the overall process of detecting and segmenting those abnormalities was affected by those two stages / factors. The first stage partitioned the fundus image into several clusters, each of which contained the colors that were as close as possible to each other, and as far as possible from colors within the other clusters. Subsequently, the cluster having the brightest objects was selected. Therefore, a wrongfully selected cluster leads to either a false negative response (i.e. deselecting the cluster of abnormal pixels), or a false positive response (i.e. misclassifying the normal pixels as abnormal).

Similarly, the second stage thresholded the selected cluster in order to remove the relatively non-bright pixels and preserve only the bright ones within the cluster. Therefore, an inaccurately estimated threshold also leads to either a false negative response or a false positive response.

The proposed method was tested and evaluated over DIARETDB0, DIARETDB1 and MESSIDOR containing a total of 1416 images. The proposed system correctly detected the bright abnormalities, such as hard exudates and cotton wool spots, achieving comparable average sensitivity and specificity rates of 85.08% and 56.77%, respectively.

### 5.1.5. Evaluation Metrics

From the perspective of evaluating the optic disc segmentation technique, the proposed segmentation algorithm was evaluated in terms of the sensitivity rates (i.e. the true positive rates of detecting the optic disc). It was not applicable to calculate the accuracy of the segmented optic disc, since the ground truth for such spatial information of the optic disc (e.g. x-center, y-center, x-radius, and y-radius) was not provided by the employed datasets. Moreover, the specificity rates were not calculated due to its insignificance, as it is the probability of a negative response for the cases where the optic disc is “absent”, which is obviously an unrealistic case since the optic disc is a structural landmark that exists in any fundus image.

On the other hand, and from the perspective of segmenting the bright abnormalities, both sensitivity and specificity rates were calculated with respect to the presence and the absence of those abnormalities within the employed fundus images.

## 5.2. Future Work

Having a specific research scope and working under time constraints, led this research to disregarding and postponing some research work that could eventually and potentially be done in the future, as an extension and continuation for the current work presented in this research. The following subsections suggest a direction for the work that could be done in the near future within each component of the proposed system architecture.

### 5.2.1. Fundus Image Datasets

From the perspective of the fundus imaging techniques, the recent emergence and commercial release of the smartphone fundus cameras, although not widely-used yet, creates a new, interesting, challenging and broad research area. If such fundus datasets captured by smartphone cameras is publicly available, it would greatly contribute to developing related mobile-based screening systems. Hence, such mobile systems are a great jump towards the “instant” diagnosis and monitoring of eye diseases through the fundus images and videos captured by such smartphone cameras. An example of one type of the commercial smartphone fundus cameras is shown in the following figure.

**Figure 5-1. Example of a smartphone fundus camera**

### 5.2.2. Fundus Image Preprocessing

The vertical splitting procedure that was carried out during preprocessing the fundus image, played a vital role in determining the approximate location of the optic disc, as observed and mentioned before. However, better results would have been achieved if vertical splitting was performed according to prior knowledge of the eye properties, whether it was a right- or left-eye. If this information were available prior to processing the fundus image, it would have been more accurate to vertically split the fundus image accordingly. In other words, the approximate position of the optic disc would have been determined according to the eye type (i.e. right or left), rather than being determined via the amount of blood vessels found at each half.

### 5.2.3. Landmarks and Abnormalities Segmentation

Finally, the system proposed for segmenting the “optic disc” and distinguishing it from the “bright lesions” can be applied likewise on the akin pair of the “blood vessels” and “red lesions”.

This inspiration has been deduced during the process of partitioning the fundus image into several color-based clusters within the presented system. It was observed that the optic disc and the bright lesions were usually grouped within the same cluster, and on the other hand the blood vessels and the red abnormalities were normally grouped together in another cluster, as noticed previously in the images of Figure 3-19(c) and Figure 3-20(e). So, this technique can be exploited and potentially achieve promising results for segmenting the “blood vessels”, as well as detecting and distinguishing the “red / dark abnormalities”.

Also, additional work can be done in the area of classifying the pixels within the segmented landmarks and abnormalities of the fundus image. For example, the pixels of the optic disc can be re-segmented and classified into pixels belonging to either the “optic rim” or the “optic cup”. Similarly, the red abnormalities can be classified into “microaneurysms” and “hemorrhages”. Also, the bright abnormalities can be classified into either “hard exudates”, “soft exudates”, and “drusen”, and so on.

This thorough discrimination between pixels of the segmented objects eventually leads to discovering and grading the severity degree of eye diseases, such as glaucoma and diabetic retinopathy. For instance, glaucoma can be detected and graded through some abnormal indicators within the intra-papillary region (i.e. inside the optic disc itself), such as the large cup-to-disc ratio and the neuroretinal rim that violates the ISNT rule. Also, glaucoma can be detected through abnormalities occurring within the peripapillary region (i.e. the area surrounding the optic disc), such as the defect of the retinal nerve fiber layer, the appearance of optic disc hemorrhages, and the existence of peripapillary atrophy. The literature for glaucoma detection was reviewed within this research as a basis for the potential work to be done and continued for this current work.

# References

[1] K. Mahesh K. and K. Nilesh S., "Review on Fundus Image Acquisition Techniques with Database Reference to Retinal Abnormalities in Diabetic Retinopathy," *International Journal of Computer Applications,* vol. 68, no. 8, pp. 17-27, 2013.

[2] X. Zhu, R. M. Rangayyan and A. L. Ells, "Digital Image Processing for Ophthalmology: Detection of the Optic Nerve Head," in *Synthesis Lectures on Biomedical Engineering,* Morgan & Claypool Publishers, 2011.

[3] L. Segre, "Human Eye Anatomy - Parts of the Eye Explained," February 2013. [Online]. Available: http://www.allaboutvision.com/resources/anatomy.htm. [Accessed 15 July 2013].

[4] M. D. Abràmoff, M. K. Garvin and M. Sonka, "Retinal Imaging and Image Analysis," *IEEE Transactions on Medical Imaging,* vol. 3, pp. 169-208, 2010.

[5] The University of British Columbia, "Ophthalmic Photography," Faculty of Medicine, Department of Ophthalmology & Visual Sciences, [Online]. Available: http://ophthalmology.med.ubc.ca/patient-care/ophthalmic-photography/. [Accessed 22 May 2015].

[6] A. A. A. Youssif, A. Z. Ghalwash and A. A. S. A. Ghoneim, "Optic Disc Detection From Normalized Digital Fundus Images by Means of a Vessels' Direction Matched Filter," *IEEE Transactions on Medical Imaging,* vol. 27, no. 1, pp. 11-18, 2008.

[7] N. Patton, T. M. Aslam, T. MacGillivray, I. J. Deary, B. Dhillon, R. H. Eikelboom, K. Yogesan and I. J. Constable, "Retinal image analysis: Concepts, applications and potential," *Progress in Retinal and Eye Research,* vol. 25, pp. 99-127, 2006.

[8] A. M. N. Allam, A. A. Youssif and A. Z. Ghalwash, "Automatic Segmentation of Optic Disc in Eye Fundus Images: A Survey," *Electronic Letters on Computer Vision and Image Analysis,* vol. 14, no. 1, pp. 1-20, September 2015.

[9] R. C. Gonzalez and R. E. Woods, Digital Image Processing, Pearson Prentice Hall, 2008.

[10] Y. Zheng, M. H. A. Hijazi and F. Coenen, "Automated ‘‘Disease/No Disease’’ Grading of Age-Related Macular Degeneration by an Image Mining Approach," *Investigative Ophthalmology & Visual Science,* vol. 53, no. 13, pp. 8310-8318, November 2008.

[11] D. J. J. Farnell, F. N. Hatfield, P. Knox, M. Reakes, S. Spencer, D. Parry and S. P. Harding, "Enhancement of blood vessels in digital fundus photographs via the application of multiscale line operators," *Journal of Franklin Institute,* vol. 345, no. 7, pp. 748-765, October 2008.

[12] T. Kauppi, V. Kalesnykiene, J. Kamarainen, L. Lensu, I. Sorri, H. Uusitalo, H. Kälviäinen and J. Pietilä, "DIARETDB0: Evaluation Database and Methodology for Diabetic Retinopathy Algorithms," 2006.

[13] T. Kauppi, V. Kalesnykiene, J. Kamarainen, L. Lensu, I. Sorri, A. Raninen, R. Voutilainen, H. Uusitalo, H. Kalviainen and J. Pietila, "DIARETDB1 diabetic retinopathy database and evaluation protocol".

[14] E. J. Carmona, M. Rincón, J. García-Feijoo and J. M. Martínez-de-la-Casa, "Identification of the Optic Nerve Head with Genetic Algorithms," *Artificial Intelligence in Medicine,* vol. 43, no. 3, pp. 243-259, 2008.

[15] J. J. Staal, M. D. Abramoff, M. Niemeijer, M. A. Viergever and B. van Ginneken, "Ridge Based Vessel Segmentation in Color Images of the Retina," *IEEE Transactions on Medical Imaging,* vol. 23, pp. 501-509, 2004.

[16] J. Odstrcilik, R. Kolar, A. Budai, J. Hornegger, J. Jan, J. Gazarek, T. Kubena, P. Cernosek, O. Svoboda and E. Angelopoulou, "Retinal vessel segmentation by improved matched filtering: evaluation on a new high-resolution fundus image database," *IET Image Processing,* vol. 7, no. 4, pp. 373-383, June 2013.

[17] E. Decencière, X. Zhang, G. Cazuguel, B. Lay, B. Cochener, C. Trone, P. Gain, J. Ordonez-Varela, P. Massin, A. Erginay, B. Charton and J. Klein, "Feedback on a Publicly Distributed Database: The Messidor Database," *Image Analysis & Stereology,* vol. 33, no. 3, pp. 231-234, 2014.

[18] J. Lowell, A. Hunter, D. Steel, B. Ryder and E. Fletcher, "Optic Nerve Head Segmentation," *IEEE Transactions on Medical Imaging,* vol. 2, no. 23, 2004.

[19] M. Goldbaum, "The STARE Project," 2000. [Online]. Available: http://www.parl.clemson.edu/~ahoover/stare/index.html. [Accessed 28 July 2013].

[20] G. Dougherty, Digital Image Processing for Medical Applications, New York: Cambridge University Press, 2009.

[21] F. ter Haar, "Automatic localization of the optic disc in digital colour images of the human retina," 2005.

[22] M. Kass, A. Witkin and D. Terzopoulos, "Snakes: Active Contour Models," *International Journal of Computer Vision,* pp. 321-331, 1988.

[23] T. F. Chan and L. A. Vese, "Active Contours Without Edges," *IEEE Transactions on Image Processing,* vol. 10, no. 2, pp. 266-277, 2001.

[24] The MathWorks, Inc., "Marker-Controlled Watershed Segmentation," 2003. [Online]. Available: http://www.mathworks.com/products/demos/image/watershed/ipexwatershed.html. [Accessed 15 August 2013].

[25] S. Beucher, "The Watershed Transformation page," 2010. [Online]. Available: http://cmm.ensmp.fr/~beucher/wtshed.html. [Accessed 15 August 2013].

[26] G. T. Doran, "There's a S.M.A.R.T. way to write management's goals and objectives," *Management Review (AMA Forum)*, vol. 70, no. 11, pp. 35-36, 1981.

[27] P. Macaskill, C. Gatsonis, J. Deeks, R. Harbord and Y. Takwoingi, "Analysing and Presenting Results," in *Cochrane Handbook for Systematic Reviews*, J. Deeks, P. Bossuyt and C. Gatsonis, Eds., The Cochrane Collaboration, 2010.

[28] M. Kallergi, "Evaluation Strategies for Medical-Image Analysis and Processing Methodologies," in *The Electrical Engineering and Applied Signal Processing Series: Medical Image Analysis Methods*, L. Costaridou, Ed., Taylor & Francis Group, 2005.

[29] M. Lalonde, M. Beaulieu and L. Gagnon, "Fast and Robust Optic Disc Detection Using Pyramidal Decomposition and Hausdorff-Based Template Matching," *IEEE Transactions on Medical Imaging*, vol. 20, no. 11, pp. 1193-1200, November 2001.

[30] S. Lu, "Accurate and Efficient Optic Disc Detection and Segmentation by a Circular Transformation," *IEEE Transactions on Medical Imaging*, vol. 30, no. 12, pp. 2126-2133, December 2011.

[31] A. Aquino, M. E. Gegúndez-Arias and D. Marín, "Detecting the Optic Disc Boundary in Digital Fundus Images Using Morphological, Edge Detection, and Feature Extraction Techniques," *IEEE Transactions on Medical Imaging*, vol. 29, no. 11, pp. 1860-1869, November 2010.

[32] L. Gagnon, M. Lalonde, M. Beaulieu and M.-C. Boucher, "Procedure to detect anatomical structures in optical fundus images," in *Proceedings of SPIE, Medical Imaging 2001: Image Processing*, 2001.

[33] K. A. Goatman, A. D. Whitwam, A. Manivannan, J. A. Olson and P. F. Sharp, "Colour Normalisation of Retinal Images," in *Proceedings of Medical Image Understanding Analysis*, 2003.

[34] F. A. Hashim, N. M. Salem and A. F. Seddik, "Preprocessing of Color Retinal Fundus Images," in *IEEE International Japan-Egypt Confernece on Electronics, Communications and Computers*, 6th of October City, 2013.

[35] A. Hoover and M. Goldbaum, "Locating the Optic Nerve in a Retinal Image Using the Fuzzy Convergence of the Blood Vessels," *IEEE Transactions on Medical Imaging*, vol. 22, no. 8, pp. 951-958, 2003.

[36] M. Goldbaum, S. Moezzi, A. Taylor, S. Chatterjee, J. Boyd, E. Hunter and R. Jain, "Automated diagnosis and image understanding with object extraction, object classification, and inferencing in retinal images," in *Proceedings of the IEEE International Conference on Image Processing*, 1996.

[37] G. Yang, L. Gagnon, S. Wang and M.-C. Boucher, "Algorithm for detecting micro-aneurysms in low-resolution color retinal images," in *Proceedings of Vision Interface*, Ottawa, 2001.

[38] M. Niemeijer, M. D. Abramoff and B. van Ginneken, "Fast detection of the optic disc and fovea in color fundus photographs," *Medical Image Analysis*, vol. 13, no. 6, pp. 859-870, December 2009.

[39] N. M. Salem and A. K. Nandi, "Segmentation of Retinal Blood Vessels Using Scale-Space Features and K-Nearest Neighbour Classifier," in *Proceedings of the 2006 IEEE International Conference on Acoustics, Speech and Signal Processing*, Toulouse, 2006.

[40] J. V. B. Soares, J. J. G. Leandro, R. M. Cesar Jr., H. F. Jelinek and M. J. Cree, "Retinal Vessel Segmentation Using the 2-D Gabor Wavelet and Supervised Classification," *IEEE Transactions on Medical Imaging*, vol. 25, no. 9, pp. 1214-1222, September 2006.

[41] E. Ricci and R. Perfetti, "Retinal Blood Vessel Segmentation Using Line Operators and Support Vector Classification," *IEEE Transactions on Medical Imaging*, vol. 26, no. 10, pp. 1357-1365, October 2007.

[42] A. Osareh and B. Shadgar, "Automatic Blood Vessel Segmentation in Color Images of Retina," *Iranian Journal of Science & Technology*, vol. 33, no. B2, pp. 191-206, 2009.

[43] C. A. Lupascu, D. Tegolo and E. Trucco, "FABC: Retinal Vessel Segmentation Using AdaBoost," *IEEE Transactions on Information Technology in Biomedicine*, vol. 14, no. 5, pp. 1267-1274, June 2010.

[44] M. M. Fraz, P. Remagnino, A. Hoppe, S. Velastin, B. Uyyanonvara and S. A. Barman, "A Supervised Method for Retinal Blood Vessel Segmentation Using Line Strength, Multiscale Gabor and Morphological Features," in *2011 IEEE International Confernce on Signal and Image Processing Applications*, Kuala Lumpur, 2011.

[45] M. M. Fraz, P. Remagnino, A. Hoppe and B. Uyyanonvara, "An Ensemble Classification-Based Approach Applied to Retinal Blood Vessel Segmentation," *IEEE Transactions on Biomedical Engineering*, vol. 59, no. 9, pp. 2538-2548, September 2012.

[46] M. Al-Rawi, M. Qutaishat and M. Arrar, "An improved matched filter for blood vessel detection of digital retinal images," *Computers in Biology and Medicine*, vol. 37, pp. 262-267, 2007.

[47] G. D. Finlayson, B. Schiele and J. L. Crowley, "Comprehensive Colour Image Normalization," in *Proceedings of the 5th European Conference in Computer Vision*, Freiburg, 1998.

[48] W. Burger and M. J. Burge, Digital Image Processing - An Algorithmic Introduction Using Java, Springer London, 2008.

[49] A. A. A. Youssif, A. Z. Ghalwash and A. S. Ghoneim, "A Comparative Evaluation of Preprocessing Methods for Automatic Detection of Retinal Anatomy," in *Proceedings of the 5th International Conference on Informatics & Systems*, Cairo, 2007.

[50] A. A. S. A. Ghoneim, "Artificial Intelligence Techniques for Ocular Pattern Classification," Cairo, 2007.

[51] D. Wu, M. Zhang, J. Liu and W. Bauman, "On the Adaptive Detection of Blood Vessels in Retinal Images," *IEEE Transactions on Biomedical Engineering*, vol. 53, no. 2, pp. 341-343, February 2006.

[52] M. H. A. Fadzil, L. I. Izhar, H. Nugroho and H. A. Nugroho, "Analysis of retinal fundus images for grading of diabetic retinopathy severity," *Medical & Biological Engineering & Computing*, vol. 49, no. 6, pp. 693-700, January 2011.

[53] M. R. Krishnan, U. R. Acharya, C. K. Chua, L. C. Min, E. Y. K. Ng, M. M. Mushrif and A. Laude, "Application of Intuitionistic Fuzzy Histon Segmentation for the Automated Detection of Optic Disc in Digital Fundus Images," in *Proceedings of IEEE-EMBS International Conference on Biomedical Health Informatics*, Hong Kong and Shenzhen, 2012.

[54] M. Maruthusivarani, T. Ramakrishnan, D. Santhi and K. Muthukkutti, "Comparison of Automatic Blood Vessel Segmentation Methods in Retinal Images," in *2013 International Confernece on Emerging Trends VLSI Embedded System, Nano Electronics and Telecommunication System*, Tiruvannamalai, 2013.

[55] C. Sinthanayothin, J. F. Boyce, H. L. Cook and T. H. Williamson, "Automated localisation of the optic disc, fovea, and retinal blood vessels from digital colour fundus images," *British Journal of Ophthalmology,* vol. 4, no. 83, pp. 902-910, 1999.

[56] A. Osareh, M. Mirmehdi, B. Thomas and R. Markham, "Classification and Localisation of Diabetic-Related Eye Disease," in *Proceedings of 7th European Conference on Computer Vision*, Copenhagen, 2002.

[57] J. Park, K. N.T. and G. Lee, "Optic Disc Detection in Retinal Images using Tensor Voting and Adaptive Mean-Shift," in *2007 IEEE International Conference on Intelligent Computer Communication and Processing,* 2007.

[58] A. Polesel, G. Ramponi and V. J. Mathews, "Adaptive Unsharp Masking for Contrast Enhancement," in *Proceedings of the IEEE International Conference on Image Processing*, 1997.

[59] M. N. Do and M. Vetterli, "The Contourlet Transform: An Efficient Directional Multiresolution Image Representation," *IEEE Transactions on Image Processing,* vol. 14, no. 12, pp. 2091 - 2106, December 2005.

[60] P. Feng, Y. Pan, B. Wei, W. Jin and D. Mi, "Enhancing retinal image by the Contourlet transform," *Pattern Recognition Letters,* vol. 28, p. 516–522, 2007.

[61] S. H. Rezatofighi, A. Roodaki and H. Ahmadi Noubari, "An Enhanced Segmentation of Blood Vessels in Retinal Images Using Contourlet," in *30th Annual International Conference of the IEEE Engineering and Medicine Biology Society*, Vancouver, 2008.

[62] M. S. Miri and A. Mahloojifar, "Retinal Image Analysis Using Curvelet Transform and Multistructure Elements Morphology by Reconstruction," *IEEE Transactions on Biomedical Engineering,* vol. 58, no. 5, pp. 1183-1192, May 2011.

[63] G. Schaefer and A. Clos, "Image Analysis for Exudate Detection in Retinal Images," in *Biocomputation and Biomedical Informatics: Case Studies and Applications,* Medical Information Science Reference, 2010, pp. 198-203.

[64] A. Dehghani, H. A. Moghaddam and M. Moin, "Optic disc localization in retinal images using histogram matching," *EURASIP Journal on Image and Video Processing,* vol. 19, pp. 1-11, October 2012.

[65] P. C. Siddalingaswamy, "Automatic Detection of Retinal Features for Screening of Diabetic Retinopathy using Image Processing Techniques," 2011.

[66] M. Park, J. S. Jin and S. Luo, "Locating the Optic Disc in Retinal Images," in *Proceedings of the 3rd International Conference on Computer Graphics, Imaging and Visualization*, Sydney, Australia, 2006.

[67] R. Chrástek, M. Wolf, K. Donath, G. Michelson and Niemann, "Optic Disc Segmentation in Retinal Images," in *Bildverarbeitung für die Medizin 2002,* Springer Berlin Heidelberg, 2002, pp. 263-266.

[68] T. Walter and J. Klein, "Segmentation of Color Fundus Images of the Human Retina: Detection of the Optic Disc and the Vascular Tree Using Morphological Techniques," in *Proceedings of the 2nd International Symposium on Medical Data Analysis (ISMDA '01)*, 2001.

[69] A. D. Abdel-Ghafar and T. Morris, "Progress towards automated detection and characterization of the optic disc in glaucoma and diabetic retinopathy," *Medical Informatics and the Internet in Medicine,* vol. 32, no. 1, pp. 19-25, March 2007.

[70] X. Zhu, R. M. Rangayyan and A. L. Ells, "Detection of the Optic Nerve Head in Fundus Images of the Retina Using the Hough Transform for Circles," *Journal of Digital Imaging,* vol. 23, no. 3, pp. 332-341, June 2010.

[71] M. Zubair, A. Yamin and S. A. Khan, "Automated Detection of Optic Disc for the Analysis of Retina Using Color Fundus Image," in *IEEE International Conference on Imaging Systems and Techniques*, Beijing, 2013.

[72] C.-Y. Yu and S.-S. Yu, "Automatic Localization of the Optic Disc Based on Iterative Brightest Pixels Extraction," in *2014 International Symposium on Computer, Consumer and Control*, 2014.

[73] A. D. Fleming, K. A. Goatman, S. Philip, J. A. Olson and P. F. Sharp, "Automatic detection of retinal anatomy to assist diabetic retinopathy screening," *Physics in Medicine and Biology,* vol. 52, no. 2, pp. 331-345, January 2007.

[74] H. Ying, M. Zhang and J. Liu, "Fractal-based Automatic Localization and Segmentation of Optic Disc in Retinal Images," in *Proceedings of the 29th Annual International Conference of the IEEE EMBS*, 2007.

[75] R. M. Rangayyan, X. Zhu, F. J. Ayres and A. L. Ells, "Detection of the Optic Nerve Head in Fundus Images of the Retina with Gabor Filters and Phase Portrait Analysis," *Journal of Digital Imaging,* vol. 23, no. 4, pp. 438-453, August 2010.

[76] A. Osareh, M. Mirmehdi, B. Thomas and R. Markham, "Comparison of Colour Spaces for Optic Disc Localisation in Retinal Images," in *Proceedings of the 16th International Conference on Pattern Recognition,* 2002.

[77] H. Li and O. Chutatape, "Automated Feature Extraction in Color Retinal Images by a Model Based Approach," *IEEE Transactions on Biomedical Engineering,* vol. 51, no. 2, pp. 246-254, February 2004.

[78] M. Foracchia, E. Grisan and A. Ruggeri, "Detection of Optic Disc in Retinal Images by Means of a Geometrical Model of Vessel Structure," *IEEE Transactions on Medical Imaging,* vol. 23, no. 10, pp. 1189-1195, October 2004.

[79] S. Lu, "Automatic Optic Disc Detection using Retinal Background and Retinal Blood Vessels," in *2010 3rd International Confernce on Biomedical Engineering and Informatics*, Yantai, 2010.

[80] D. Zhang and Y. Zhao, "Novel Accurate and Fast Optic Disc Detection in Retinal Images with Vessel Distribution and Directional Characteristics," *IEEE Journal of Biomedical Health Informatics,* no. 99, 28 October 2014.

[81] The World Health Organization (WHO), "Fact sheet of visual impairment and blindness," [Online]. Available: http://www.who.int/mediacentre/factsheets/fs282/en/. [Accessed 30 June 2015].

[82] H. A. Quigley and A. T. Broman, "The number of people with glaucoma worldwide in 2010 and 2020," *British Journal of Ophthalmology,* vol. 90, no. 3, pp. 262-267, 2006.

[83] The Egyptian Society for the Glaucomas, [Online]. Available: http://www.glaucoma-egypt.org/. [Accessed 30 June 2015].

[84] The American Academy of Ophthalmology, 2014.

[85] M. Fingeret, F. A. Medeiros, R. Susanna and R. N. Weinreb, "Five rules to evaluate the optic disc and retinal nerve fiber layer for glaucoma," *Optometry,* vol. 76, no. 11, pp. 661-668, November 2005.

[86] R. Thomas, K. Loibl and R. Parikh, "Evaluation of a Glaucoma patient," *Indian Journal of Opthalmology,* vol. 59, no. 7, pp. 43-52, 2011.

[87] R. Sihota, G. Srinivasan, T. Dada, V. Gupta, D. Ghate and A. Sharma, "Is the ISNT rule violated in early primary open-angle glaucoma - a scanning laser tomography study," *Eye,* vol. 22, pp. 819-824, 2008.

[88] L. G. Nyul, "Retinal Image Analysis for Automated Glaucoma Risk Evaluation," *Proceedings of SPIE: Medical Imaging, Parallel Processing of Images and Optimization Techniques,* vol. 7497, pp. 1-9, October 2009.

[89] R. R. A. Bourne, "The Optic Nerve Head in Glaucoma," *Community Eye Health Journal,* vol. 19, no. 59, pp. 44-45, 2006.

[90] Z. Zhang, C. K. Kwoh, J. Liu, C. Y. L. Cheung, T. Aung and T. Y. Wong, "Automatic Glaucoma Diagnosis with mRMR-based Feature Selection," *Journal of Biometrics & Biostatisics*, pp. 1-8, 2012.

[91] Japan Glaucoma Society, "Guidelines for Glaucoma," Japan Glaucoma Society, Tokyo, 2006.

[92] C. Muramatsu, Y. Hayashi, A. Sawada, Y. Hatanaka, T. Hara, T. Yamamoto and H. Fujita, "Detection of retinal nerve fiber layer defects on retinal fundus images for early diagnosis of glaucoma," *Journal of Biomedical Optics*, vol. 15, no. 1, pp. 1-7, February 2010.

[93] T. Kubena, M. Kofronova and P. Cernosek, "Nerve Fiber Layer Defects Imaging in Glaucoma," in *The Mystery of Glaucoma*, T. Kubena, Ed., InTech, 2011, pp. 187-198.

[94] European Glaucoma Society (EGS), Terminology and Guidelines for Glaucoma, 4th ed., PubliComm, 2014.

[95] X. Song, K. Song and Y. Chen, "A Computer-based Diagnosis System for Early Glaucoma Screening," in *27th Annual Conference of Engineering in Medicine and Biology*, Shanghai, 2005.

[96] Y. Hayashi, T. Nakagawa, Y. Hatanaka, A. Aoyama, M. Kakogawa, T. Hara, H. Fujita and T. Yamamoto, "Detection of Retinal Nerve Fiber Layer Defects in Retinal Fundus Images using Gabor Filtering," in *Proceedings of SPIE 6514, Medical Imaging 2007: Computer-Aided Diagnosis*, 2007.

[97] C. Muramatsu, Y. Hatanaka, A. Sawada, T. Yamamoto and H. Fujita, "Computerized Detection of Peripapillary Chorioretinal Atrophy by Texture Analysis," in *33rd Annual International Conference of the IEEE EMBS*, Boston, 2011.

[98] J. Liu, D. W. K. Wong, J. H. Lim, H. Li, N. M. Tan, Z. Zhang, T. Y. Wong and R. Lavanya, "ARGALI: An Automatic Cup-to-Disc Ratio Measurement System for Glaucoma Analysis Using Level-set Image Processing," in *13th International Conference on Biomedical Engineering (ICBME)*, 2009.

[99] C. Burana-Anusorn, W. Kongprawechnon, T. Kondo, S. Sintuwong and K. Tungpimolrut, "Image Processing Techniques for GLaucoma Detection Using the Cup-to-Disc Ratio," *Thammasat International Journal of Science and Technology*, vol. 18, no. 1, pp. 22-34, 2013.

[100] J. Nayak, A. U. R., P. S. Bhat, N. Shetty and T.-C. Lim, "Automated Diagnosis of Glaucoma using Digital Fundus Images," *Journal of Medical Systems*, vol. 33, pp. 337-346, 2009.

[101] G. D. Joshi, J. Sivaswamy and S. R. Krishnadas, "Optic Disk and Cup Segmentation from Monocular Color Retinal Images for Glaucoma Assessment," *IEEE Transactions on Medical Imaging*, vol. 30, no. 6, pp. 1192-1205, 2011.

[102] G. D. Joshi, J. Sivaswamy, P. Reddy and Krishnadas, "Detection of Peri-papillary Atrophy and RNFL Defect from Retinal Images," in *International Conference on Image Analysis and Recognition*, Hyderabad, 2012.

[103] M. Madhusudhan, N. Malay, S. R. Nirmala and D. Samerendra, "Image Processing Techniques for Glaucoma Detection," in *Proceedings of 1st International Conference of Advances in Computing and Communications*, Kochi, 2011.

[104] J. Cheng, Y. Xu, F. Yin, D. W. K. Wong, N.-M. Tan, D. Tao, C.-Y. Cheng, T. Aung and T. Y. Wong, "Superpixel Classification Based Optic Dsic and Optic Cup Segmentation for Glaucoma Screening," *IEEE Transactions on Medical Imaging,* vol. 32, no. 6, pp. 1019-1032, 2013.

[105] The World Health Organization (WHO), "Fact sheet of diabetes," [Online]. Available: http://www.who.int/mediacentre/factsheets/fs312/en/.

[106] C. P. Wilkinson, F. L. Ferris, R. E. Klein, P. P. Lee, C. D. Agardh, M. Davis, D. Dills, A. Kampik, R. Pararajasegaram and J. T. Verdaguer, "Proposed International Clinical Diabetic Retinopathy and Diabetic Macular Edema Disease Severity Scales," *Ophthalmology,* vol. 110, no. 9, pp. 1677-1682, September 2003.

[107] B. Harangi, B. Antal and A. Hajdu, "Automatic Exudate Detection with Improved Naïve-Bayes Classifier," in *2012 25th International Symposium on Computer-Based Medical Systems (CBMS)*, Rome, 2012.

[108] H. F. Jaafar, A. K. Nandi and W. Al-Nuaimy, "Automated Detection and Grading of Hard Exudates from Retinal Fundus Images," in *19th European Signal Processing Conference*, Barcelona, 2011.

[109] S. Kumar, R. Kumar, A. Sathar and V. Sahasranamam, "Automatic Detection of Exudates in Retinal Images Using Histogram Analysis," *2013 IEEE Recent Advances in Intelligent Computational Systems,* pp. 277-281, 2013.

[110] A. Sopharak, K. T. Nwe, Y. A. Moe, M. N. Dailey and B. Uyyanonvara, "Automatic Exudate Detection with a Naive Bayes Classifier," *International Conference on Embedded Systems and Intelligent Technology,* pp. 139-142, 2008.

[111] S. Sreng, J. Takada, N. Maneerat, D. Isarakorn, B. Pasaya, R. Panjaphongse and R. Varakulsiripunth, "Automatic Exudate Extraction for Early Detection of Diabetic Retinopathy," *2013 International Conference on Information Technology and Electrical Engineering,* pp. 31-35, 7-8 October 2013.

[112] M. G. F. Eadgahi and H. Pourreza, "Localization of Hard Exudates in Retinal Fundus Image by Mathematical Morphology Operations," in *2nd International eConference on Computer and Knowledge Engineering*, 2012.

[113] C. Sinthanayothin, J. F. Boyce, T. H. Williamson, H. L. Cook, E. Mensah, S. Lal and D. Usher, "Automated detection of diabetic retinopathy on digital fundus images," *Diabetic Medicine,* vol. 19, no. 2, pp. 105-112, 2002.

[114] A. Osareh, M. Mirmehdi, B. Thomas and R. Markham, "Automated Identification of Diabetic Retinal Exudates in Digital Colour Images," *British Journal of Ophthalmology,* pp. 1220-1223, 2003.

[115] S. W. Franklin and S. E. Rajan, "Diagnosis of diabetic retinopathy by employing image processing technique to detect exudates in retinal images," *IET Image Processing*, vol. 8, no. 10, pp. 601-609, 2014.

[116] A. Singh, N. Sengar, M. K. Dutta, K. Riha and J. Minar, "Automatic Exudates Detection in Fundus Image using Intensity Thresholding and Morphology," in *2015 7th International Congress on Ultra Modern Telecommunications and Control Systems and Workshops (ICUMT)*, 2015.

[117] S. Roychowdhury, D. D. Koozekanani and K. K. Parhi, "DREAM: Diabetic Retinopathy Analysis Using Machine Learning," *IEEE Journal of Biomedical and Health Informatics*, vol. 18, no. 5, pp. 1717-1728, 2014.

[118] S. Rajan, T. Das and R. Krishnakumar, "An Analytical Method for the Detection of Exudates in Retinal Images Using Invertible Orientation Scores," in *Proceedings of the World Congress on Engineering 2016*, London, 2016.

[119] P. Prentasic and S. Loncaric, "Detection of exudates in fundus photographs using deep neural networks and anatomical landmark detection fusion," *Computer Methods and Programs in Biomedicine*, vol. 137, pp. 281-292, 2016.

[120] Q. Liu, B. Zoua, J. Chen, W. Ke, K. Yue, Z. Chen and G. Zhao, "A location-to-segmentation strategy for automatic exudate segmentation in colour retinal fundus images," *Computerized Medical Imaging and Graphics*, vol. 55, pp. 78-86, 2017.

[121] A. D. Fleming, S. Philip, K. A. Goatman, J. A. Olson and P. F. Sharp, "Automated Microaneurysm Detection Using Local Contrast Normalization and Local Vessel Detection," *IEEE TRANSACTIONS ON MEDICAL IMAGING*, vol. 25, no. 9, pp. 1223-1232, 2006.

[122] M. Niemeijer, B. van Ginneken, M. J. Cree, A. Mizutani, G. Quellec, C. I. Sánchez, B. Zhang, R. Hornero, M. Lamard, C. Muramatsu, X. Muramatsu, G. Cazuguel, J. You, A. Mayo, Q. Li, Y. Hatanaka, B. Cochener, C. Roux and F. Karray, "Retinopathy Online Challenge: Automatic Detection of Microaneurysms in Digital Color Fundus Photographs," *IEEE Transactions on Medical Imaging*, vol. 29, no. 1, pp. 185-194, January 2010.

[123] S. Wang, H. L. Tang, L. I. Al turk, Y. Hu, S. Sanei, G. M. Saleh and T. Peto, "Localising Microaneurysms in Fundus Images Through Singular Spectrum Analysis," *IEEE Transactions on Biomedical Engineering*, pp. 1-12, 2016.

[124] B. Antal and A. Hajdu, "An Ensemble-Based System for Microaneurysm Detection and Diabetic Retinopathy Grading," *1720 IEEE Transactions on Biomedical Engineering*, vol. 59, no. 6, pp. 1720-1726, 2012.

[125] B. Dai, X. Wu and W. Bu, "Retinal Microaneurysms Detection Using Gradient Vector Analysis and Class Imbalance Classification," *PLoS ONE*, vol. 11, no. 8, pp. 1-23, 2016.

[126] I. Lazar and A. Hajdu, "Retinal Microaneurysm Detection Through Local Rotating Cross-Section Profile Analysis," *IEEE Transactions on Medical Imaging*, vol. 32, no. 2, pp. 400-407, 2013.

[127] Z. Fegyver, "A Gradient Based Microaneurysm Detector," Budapest University of Technology and Economics, 2012.

[128] A. M. N. Allam, A. A. Youssif and A. Z. Ghalwash, "Optic Disc Segmentation by Weighting the Vessels Density within the Strongest Candidates," in *Proceedings of 2016 SAI Computing Conference*, London, 2016.

[129] A. M. N. Allam, A. A. Youssif and A. Z. Ghalwash, "Segmentation of Exudates via Color-based K-means Clustering and Statistical-based Thresholding," *Journal of Computer Science,* vol. 13, no. 10, pp. 524-536, 2017.

# Appendices

## Appendix A. Presence of Abnormalities of Diabetic Retinopathy

### A.1. Ground Truth of DIARETDB0

| Filename | MA | HM | HE | CWS | NV |
|---|---|---|---|---|---|
| image001 | ✓ | ✓ | ✓ | × | × |
| image002 | ✓ | ✓ | ✓ | × | × |
| image003 | ✓ | ✓ | ✓ | ✓ | × |
| image004 | ✓ | ✓ | ✓ | × | × |
| image005 | ✓ | ✓ | ✓ | × | × |
| image006 | ✓ | ✓ | ✓ | × | × |
| image007 | ✓ | ✓ | ✓ | × | × |
| image008 | ✓ | ✓ | ✓ | × | × |
| image009 | ✓ | ✓ | ✓ | ✓ | × |
| image010 | ✓ | ✓ | ✓ | ✓ | × |
| image011 | ✓ | ✓ | ✓ | ✓ | × |
| image012 | ✓ | ✓ | ✓ | × | × |
| image013 | ✓ | ✓ | ✓ | × | × |
| image014 | ✓ | ✓ | ✓ | ✓ | × |
| image015 | ✓ | ✓ | ✓ | × | × |
| image016 | ✓ | ✓ | ✓ | × | × |
| image017 | ✓ | ✓ | ✓ | × | × |
| image018 | ✓ | ✓ | ✓ | × | × |
| image019 | ✓ | ✓ | ✓ | × | × |
| image020 | × | × | ✓ | × | × |
| image021 | ✓ | ✓ | ✓ | × | × |
| image022 | ✓ | ✓ | ✓ | × | × |
| image023 | ✓ | ✓ | ✓ | × | × |
| image024 | ✓ | ✓ | ✓ | × | × |
| image025 | ✓ | ✓ | ✓ | ✓ | × |
| image026 | ✓ | ✓ | ✓ | ✓ | × |
| image027 | ✓ | ✓ | ✓ | ✓ | × |
| image028 | ✓ | ✓ | ✓ | × | × |
| image029 | ✓ | ✓ | ✓ | × | × |
| image030 | ✓ | ✓ | ✓ | × | × |
| image031 | ✓ | ✓ | ✓ | ✓ | ✓ |
| image032 | ✓ | ✓ | ✓ | ✓ | ✓ |
| image033 | ✓ | ✓ | ✓ | × | ✓ |
| image034 | ✓ | ✓ | ✓ | × | ✓ |
| image035 | ✓ | ✓ | ✓ | × | ✓ |
| image036 | ✓ | ✓ | × | ✓ | ✓ |
| image037 | ✓ | ✓ | × | ✓ | ✓ |
| image038 | ✓ | ✓ | × | ✓ | ✓ |
| image039 | ✓ | ✓ | × | ✓ | ✓ |
| image040 | ✓ | ✓ | × | × | ✓ |
| image041 | ✓ | ✓ | ✓ | × | ✓ |
| image042 | ✓ | ✓ | × | × | ✓ |

## A.1 Ground truth of DIARETDB0 (continued)

| Filename | MA | HM | HE | CWS | NV |
|---|---|---|---|---|---|
| image043 | ✓ | ✓ | ✓ | ✓ | ✓ |
| image044 | ✓ | ✓ | ✓ | ✓ | ✓ |
| image045 | ✓ | ✓ | × | ✓ | ✓ |
| image046 | ✓ | ✓ | ✓ | ✓ | ✓ |
| image047 | ✓ | ✓ | ✓ | × | ✓ |
| image048 | ✓ | ✓ | ✓ | × | ✓ |
| image049 | ✓ | ✓ | × | × | ✓ |
| image050 | × | × | × | × | ✓ |
| image051 | ✓ | ✓ | ✓ | ✓ | × |
| image052 | ✓ | ✓ | ✓ | ✓ | × |
| image053 | ✓ | × | ✓ | × | × |
| image054 | ✓ | × | ✓ | × | × |
| image055 | ✓ | ✓ | ✓ | × | × |
| image056 | ✓ | × | ✓ | × | × |
| image057 | ✓ | ✓ | × | ✓ | × |
| image058 | ✓ | × | × | ✓ | × |
| image059 | ✓ | × | ✓ | × | × |
| image060 | ✓ | × | × | × | × |
| image061 | ✓ | × | × | × | × |
| image062 | ✓ | × | × | × | × |
| image063 | ✓ | × | × | × | × |
| image064 | ✓ | × | × | × | × |
| image065 | ✓ | × | × | × | × |
| image066 | ✓ | ✓ | ✓ | × | × |
| image067 | ✓ | × | × | × | × |
| image068 | ✓ | × | × | × | × |
| image069 | ✓ | ✓ | ✓ | × | × |
| image070 | ✓ | ✓ | × | × | × |
| image071 | ✓ | ✓ | ✓ | ✓ | × |
| image072 | ✓ | ✓ | ✓ | ✓ | × |
| image073 | ✓ | ✓ | × | ✓ | × |
| image074 | ✓ | ✓ | ✓ | ✓ | × |
| image075 | ✓ | ✓ | × | × | × |
| image076 | ✓ | ✓ | × | × | × |
| image077 | ✓ | ✓ | ✓ | ✓ | × |
| image078 | ✓ | ✓ | ✓ | ✓ | × |
| image079 | ✓ | ✓ | ✓ | × | × |
| image080 | ✓ | ✓ | × | × | × |
| image081 | ✓ | ✓ | × | × | × |
| image082 | × | × | × | × | × |
| image083 | ✓ | ✓ | ✓ | × | × |
| image084 | ✓ | ✓ | × | ✓ | × |
| image085 | ✓ | × | × | × | × |
| image086 | ✓ | × | × | × | × |
| image087 | ✓ | × | × | × | × |
| image088 | ✓ | × | × | × | × |
| image089 | ✓ | × | × | × | × |
| image090 | ✓ | × | × | × | × |
| image091 | ✓ | × | × | × | × |

## A.1 Ground truth of DIARETDB0 (continued)

| Filename | MA | HM | HE | CWS | NV |
|---|---|---|---|---|---|
| image092 | ✓ | × | × | ✓ | × |
| image093 | ✓ | ✓ | ✓ | × | × |
| image094 | ✓ | × | × | × | × |
| image095 | × | × | × | × | × |
| image096 | ✓ | × | ✓ | × | × |
| image097 | ✓ | × | × | × | × |
| image098 | ✓ | × | × | ✓ | × |
| image099 | ✓ | × | × | × | × |
| image100 | ✓ | ✓ | ✓ | ✓ | × |
| image101 | ✓ | ✓ | ✓ | ✓ | × |
| image102 | ✓ | ✓ | ✓ | ✓ | × |
| image103 | ✓ | ✓ | ✓ | ✓ | × |
| image104 | ✓ | ✓ | ✓ | × | × |
| image105 | ✓ | ✓ | ✓ | × | × |
| image106 | ✓ | ✓ | ✓ | ✓ | × |
| image107 | ✓ | ✓ | ✓ | ✓ | × |
| image108 | ✓ | ✓ | ✓ | ✓ | × |
| image109 | ✓ | ✓ | ✓ | ✓ | × |
| image110 | ✓ | ✓ | ✓ | ✓ | × |
| image111 | × | × | × | × | × |
| image112 | × | × | × | × | × |
| image113 | × | × | × | × | × |
| image114 | × | × | × | × | × |
| image115 | × | × | × | × | × |
| image116 | × | × | × | × | × |
| image117 | × | × | × | × | × |
| image118 | × | × | × | × | × |
| image119 | × | × | × | × | × |
| image120 | × | × | × | × | × |
| image121 | × | × | × | × | × |
| image122 | × | × | × | × | × |
| image123 | × | × | × | × | × |
| image124 | × | × | × | × | × |
| image125 | × | × | × | × | × |
| image126 | × | × | × | × | × |
| image127 | × | × | × | × | × |
| image128 | × | × | × | × | × |
| image129 | × | × | × | × | × |
| image130 | × | × | × | × | × |

## A.2. Ground Truth of DIARETDB1

| Filename | Experts | MA | HM | HE | CWS | NV |
|---|---|---|---|---|---|---|
| image001 | Expert 1 | ✓ | ✓ | ✓ | ✗ | ✗ |
| | Expert 2 | ✓ | ✓ | ✓ | ✗ | ✗ |
| | Expert 3 | ✓ | ✓ | ✓ | ✗ | ✗ |
| | Expert 4 | ✓ | ✓ | ✓ | ✗ | ✗ |
| image002 | Expert 1 | ✓ | ✓ | ✗ | ✗ | ✗ |
| | Expert 2 | ✗ | ✓ | ✓ | ✗ | ✗ |
| | Expert 3 | ✓ | ✓ | ✓ | ✗ | ✗ |
| | Expert 4 | ✓ | ✓ | ✓ | ✗ | ✗ |
| image003 | Expert 1 | ✓ | ✓ | ✗ | ✓ | ✓ |
| | Expert 2 | ✓ | ✓ | ✓ | ✓ | ✓ |
| | Expert 3 | ✓ | ✓ | ✓ | ✗ | ✗ |
| | Expert 4 | ✓ | ✓ | ✓ | ✓ | ✗ |
| image004 | Expert 1 | ✓ | ✓ | ✓ | ✗ | ✗ |
| | Expert 2 | ✓ | ✓ | ✓ | ✓ | ✗ |
| | Expert 3 | ✓ | ✓ | ✓ | ✗ | ✗ |
| | Expert 4 | ✓ | ✓ | ✓ | ✓ | ✗ |
| image005 | Expert 1 | ✓ | ✓ | ✓ | ✓ | ✗ |
| | Expert 2 | ✓ | ✓ | ✓ | ✓ | ✗ |
| | Expert 3 | ✗ | ✓ | ✓ | ✓ | ✗ |
| | Expert 4 | ✓ | ✓ | ✓ | ✓ | ✗ |
| image006 | Expert 1 | ✓ | ✓ | ✓ | ✗ | ✗ |
| | Expert 2 | ✓ | ✓ | ✓ | ✓ | ✗ |
| | Expert 3 | ✓ | ✓ | ✓ | ✗ | ✗ |
| | Expert 4 | ✓ | ✓ | ✓ | ✓ | ✗ |
| image007 | Expert 1 | ✓ | ✓ | ✓ | ✓ | ✓ |
| | Expert 2 | ✓ | ✓ | ✓ | ✓ | ✓ |
| | Expert 3 | ✓ | ✓ | ✓ | ✗ | ✗ |
| | Expert 4 | ✓ | ✓ | ✓ | ✓ | ✗ |
| image008 | Expert 1 | ✓ | ✓ | ✓ | ✓ | ✓ |
| | Expert 2 | ✓ | ✓ | ✓ | ✓ | ✗ |
| | Expert 3 | ✗ | ✓ | ✓ | ✓ | ✗ |
| | Expert 4 | ✓ | ✓ | ✓ | ✓ | ✗ |
| image009 | Expert 1 | ✓ | ✓ | ✓ | ✓ | ✓ |
| | Expert 2 | ✗ | ✗ | ✗ | ✗ | ✗ |
| | Expert 3 | ✓ | ✓ | ✓ | ✓ | ✗ |
| | Expert 4 | ✓ | ✓ | ✓ | ✓ | ✗ |
| image010 | Expert 1 | ✓ | ✓ | ✓ | ✗ | ✗ |
| | Expert 2 | ✓ | ✓ | ✓ | ✓ | ✗ |
| | Expert 3 | ✓ | ✓ | ✓ | ✓ | ✗ |
| | Expert 4 | ✓ | ✓ | ✓ | ✓ | ✗ |
| image011 | Expert 1 | ✓ | ✓ | ✓ | ✓ | ✗ |
| | Expert 2 | ✓ | ✓ | ✓ | ✓ | ✗ |
| | Expert 3 | ✓ | ✓ | ✓ | ✓ | ✗ |
| | Expert 4 | ✓ | ✓ | ✓ | ✓ | ✗ |

## A.2 Ground truth of DIARETDB1 (continued)

| Filename | Experts | MA | HM | HE | CWS | NV |
|---|---|---|---|---|---|---|
| image012 | Expert 1 | ✓ | ✓ | ✓ | × | × |
| | Expert 2 | ✓ | × | ✓ | × | × |
| | Expert 3 | ✓ | ✓ | ✓ | × | × |
| | Expert 4 | ✓ | ✓ | ✓ | × | × |
| image013 | Expert 1 | ✓ | ✓ | ✓ | × | × |
| | Expert 2 | ✓ | ✓ | ✓ | × | × |
| | Expert 3 | ✓ | ✓ | ✓ | ✓ | ✓ |
| | Expert 4 | ✓ | ✓ | ✓ | ✓ | × |
| image014 | Expert 1 | ✓ | ✓ | ✓ | × | × |
| | Expert 2 | ✓ | ✓ | ✓ | ✓ | × |
| | Expert 3 | ✓ | ✓ | ✓ | ✓ | × |
| | Expert 4 | ✓ | ✓ | ✓ | ✓ | × |
| image015 | Expert 1 | ✓ | ✓ | ✓ | ✓ | × |
| | Expert 2 | ✓ | ✓ | ✓ | ✓ | × |
| | Expert 3 | ✓ | ✓ | ✓ | ✓ | × |
| | Expert 4 | ✓ | ✓ | ✓ | ✓ | × |
| image016 | Expert 1 | ✓ | ✓ | ✓ | ✓ | ✓ |
| | Expert 2 | ✓ | ✓ | ✓ | ✓ | ✓ |
| | Expert 3 | ✓ | ✓ | ✓ | ✓ | ✓ |
| | Expert 4 | ✓ | ✓ | ✓ | × | ✓ |
| image017 | Expert 1 | ✓ | ✓ | ✓ | × | × |
| | Expert 2 | × | ✓ | ✓ | ✓ | ✓ |
| | Expert 3 | ✓ | ✓ | ✓ | ✓ | × |
| | Expert 4 | ✓ | ✓ | ✓ | × | × |
| image018 | Expert 1 | ✓ | ✓ | ✓ | ✓ | × |
| | Expert 2 | ✓ | ✓ | ✓ | ✓ | × |
| | Expert 3 | ✓ | ✓ | ✓ | ✓ | × |
| | Expert 4 | ✓ | ✓ | ✓ | ✓ | × |
| image019 | Expert 1 | ✓ | ✓ | ✓ | × | × |
| | Expert 2 | ✓ | ✓ | ✓ | × | × |
| | Expert 3 | ✓ | ✓ | ✓ | ✓ | × |
| | Expert 4 | ✓ | ✓ | ✓ | ✓ | × |
| image020 | Expert 1 | ✓ | ✓ | ✓ | ✓ | × |
| | Expert 2 | ✓ | ✓ | ✓ | ✓ | × |
| | Expert 3 | ✓ | ✓ | ✓ | ✓ | × |
| | Expert 4 | ✓ | ✓ | ✓ | ✓ | × |
| image021 | Expert 1 | ✓ | ✓ | ✓ | × | × |
| | Expert 2 | ✓ | ✓ | ✓ | ✓ | × |
| | Expert 3 | ✓ | ✓ | ✓ | ✓ | × |
| | Expert 4 | ✓ | ✓ | ✓ | ✓ | × |
| image022 | Expert 1 | ✓ | ✓ | ✓ | ✓ | ✓ |
| | Expert 2 | ✓ | ✓ | ✓ | ✓ | × |
| | Expert 3 | ✓ | ✓ | ✓ | ✓ | ✓ |
| | Expert 4 | ✓ | ✓ | ✓ | ✓ | × |

## A.2 Ground truth of DIARETDB1 (continued)

| Filename | Experts | MA | HM | HE | CWS | NV |
|---|---|---|---|---|---|---|
| image023 | Expert 1 | ✓ | ✓ | ✓ | × | × |
| | Expert 2 | ✓ | ✓ | ✓ | ✓ | × |
| | Expert 3 | × | ✓ | ✓ | ✓ | × |
| | Expert 4 | ✓ | ✓ | ✓ | ✓ | × |
| image024 | Expert 1 | × | ✓ | ✓ | × | × |
| | Expert 2 | ✓ | ✓ | ✓ | ✓ | × |
| | Expert 3 | × | ✓ | ✓ | ✓ | × |
| | Expert 4 | ✓ | ✓ | ✓ | ✓ | × |
| image025 | Expert 1 | ✓ | ✓ | ✓ | × | ✓ |
| | Expert 2 | ✓ | ✓ | ✓ | ✓ | × |
| | Expert 3 | × | ✓ | ✓ | ✓ | × |
| | Expert 4 | ✓ | ✓ | ✓ | ✓ | ✓ |
| image026 | Expert 1 | ✓ | ✓ | × | × | ✓ |
| | Expert 2 | ✓ | ✓ | ✓ | × | ✓ |
| | Expert 3 | ✓ | ✓ | ✓ | ✓ | ✓ |
| | Expert 4 | ✓ | ✓ | ✓ | × | ✓ |
| image027 | Expert 1 | ✓ | ✓ | × | × | ✓ |
| | Expert 2 | × | ✓ | ✓ | × | ✓ |
| | Expert 3 | ✓ | ✓ | ✓ | × | ✓ |
| | Expert 4 | ✓ | ✓ | ✓ | × | ✓ |
| image028 | Expert 1 | × | ✓ | × | ✓ | ✓ |
| | Expert 2 | × | × | × | ✓ | ✓ |
| | Expert 3 | × | × | × | × | ✓ |
| | Expert 4 | × | × | × | ✓ | ✓ |
| image029 | Expert 1 | ✓ | ✓ | × | × | × |
| | Expert 2 | ✓ | ✓ | × | × | ✓ |
| | Expert 3 | ✓ | ✓ | ✓ | × | × |
| | Expert 4 | ✓ | ✓ | × | × | ✓ |
| image030 | Expert 1 | × | × | × | × | × |
| | Expert 2 | ✓ | × | ✓ | × | × |
| | Expert 3 | × | × | × | × | × |
| | Expert 4 | ✓ | × | ✓ | × | × |
| image031 | Expert 1 | ✓ | × | × | × | × |
| | Expert 2 | × | × | × | × | × |
| | Expert 3 | × | × | ✓ | × | × |
| | Expert 4 | × | × | × | × | × |
| image032 | Expert 1 | ✓ | × | × | × | × |
| | Expert 2 | × | ✓ | × | × | × |
| | Expert 3 | × | × | × | × | × |
| | Expert 4 | ✓ | × | × | × | × |
| image033 | Expert 1 | × | × | × | × | × |
| | Expert 2 | × | × | × | ✓ | × |
| | Expert 3 | × | × | ✓ | × | × |
| | Expert 4 | × | × | ✓ | × | × |

## A.2 Ground truth of DIARETDB1 (continued)

| Filename | Experts | MA | HM | HE | CWS | NV |
|---|---|---|---|---|---|---|
| image034 | Expert 1 | × | × | × | × | × |
| | Expert 2 | × | × | × | × | × |
| | Expert 3 | ✓ | × | ✓ | × | × |
| | Expert 4 | × | × | ✓ | × | × |
| image035 | Expert 1 | ✓ | ✓ | ✓ | × | × |
| | Expert 2 | × | ✓ | ✓ | × | × |
| | Expert 3 | × | ✓ | ✓ | × | × |
| | Expert 4 | ✓ | ✓ | ✓ | × | × |
| image036 | Expert 1 | ✓ | ✓ | × | × | × |
| | Expert 2 | ✓ | ✓ | × | × | × |
| | Expert 3 | ✓ | ✓ | × | × | × |
| | Expert 4 | × | ✓ | × | × | × |
| image037 | Expert 1 | ✓ | × | × | × | × |
| | Expert 2 | ✓ | × | × | × | × |
| | Expert 3 | ✓ | × | × | × | × |
| | Expert 4 | ✓ | × | × | × | × |
| image038 | Expert 1 | ✓ | × | ✓ | × | × |
| | Expert 2 | ✓ | × | ✓ | × | ✓ |
| | Expert 3 | ✓ | × | ✓ | × | × |
| | Expert 4 | ✓ | × | ✓ | × | × |
| image039 | Expert 1 | ✓ | × | × | × | × |
| | Expert 2 | ✓ | × | × | × | × |
| | Expert 3 | ✓ | × | × | × | × |
| | Expert 4 | ✓ | × | × | × | × |
| image040 | Expert 1 | ✓ | × | × | × | × |
| | Expert 2 | × | × | × | × | × |
| | Expert 3 | × | × | ✓ | × | × |
| | Expert 4 | × | × | ✓ | × | × |
| image041 | Expert 1 | ✓ | ✓ | × | × | ✓ |
| | Expert 2 | ✓ | ✓ | × | × | × |
| | Expert 3 | ✓ | ✓ | × | × | × |
| | Expert 4 | ✓ | ✓ | × | × | × |
| image042 | Expert 1 | ✓ | ✓ | × | × | × |
| | Expert 2 | ✓ | ✓ | × | × | × |
| | Expert 3 | ✓ | ✓ | × | × | × |
| | Expert 4 | ✓ | ✓ | × | × | × |
| image043 | Expert 1 | ✓ | × | × | × | ✓ |
| | Expert 2 | ✓ | × | × | × | × |
| | Expert 3 | ✓ | ✓ | × | × | × |
| | Expert 4 | ✓ | ✓ | × | × | × |
| image044 | Expert 1 | ✓ | × | × | × | × |
| | Expert 2 | ✓ | ✓ | ✓ | × | × |
| | Expert 3 | ✓ | ✓ | ✓ | × | × |
| | Expert 4 | ✓ | ✓ | ✓ | × | × |

## A.2 Ground truth of DIARETDB1 (continued)

| Filename | Experts | MA | HM | HE | CWS | NV |
|---|---|---|---|---|---|---|
| image045 | Expert 1 | ✓ | × | × | × | × |
| | Expert 2 | ✓ | × | × | × | × |
| | Expert 3 | ✓ | ✓ | × | × | × |
| | Expert 4 | ✓ | × | × | × | × |
| image046 | Expert 1 | ✓ | × | × | × | × |
| | Expert 2 | × | × | × | × | × |
| | Expert 3 | × | × | × | × | × |
| | Expert 4 | × | × | × | × | × |
| image047 | Expert 1 | × | ✓ | × | × | × |
| | Expert 2 | × | × | × | × | × |
| | Expert 3 | × | × | × | × | × |
| | Expert 4 | × | × | × | × | × |
| image048 | Expert 1 | ✓ | × | × | × | × |
| | Expert 2 | × | × | × | × | × |
| | Expert 3 | × | × | × | × | × |
| | Expert 4 | ✓ | ✓ | × | × | × |
| image049 | Expert 1 | × | × | × | × | × |
| | Expert 2 | × | × | × | × | × |
| | Expert 3 | × | × | × | × | × |
| | Expert 4 | × | × | × | × | × |
| image050 | Expert 1 | ✓ | × | × | × | × |
| | Expert 2 | × | × | × | × | × |
| | Expert 3 | × | × | × | × | × |
| | Expert 4 | × | × | × | × | × |
| image051 | Expert 1 | ✓ | × | × | × | × |
| | Expert 2 | × | × | × | × | × |
| | Expert 3 | × | × | × | × | × |
| | Expert 4 | × | × | × | × | × |
| image052 | Expert 1 | ✓ | ✓ | ✓ | ✓ | × |
| | Expert 2 | ✓ | ✓ | ✓ | ✓ | × |
| | Expert 3 | ✓ | ✓ | ✓ | ✓ | × |
| | Expert 4 | ✓ | ✓ | ✓ | ✓ | × |
| image053 | Expert 1 | ✓ | ✓ | ✓ | ✓ | × |
| | Expert 2 | ✓ | ✓ | ✓ | ✓ | × |
| | Expert 3 | ✓ | ✓ | ✓ | ✓ | × |
| | Expert 4 | ✓ | ✓ | ✓ | ✓ | × |
| image054 | Expert 1 | ✓ | ✓ | × | ✓ | × |
| | Expert 2 | ✓ | ✓ | ✓ | ✓ | × |
| | Expert 3 | ✓ | ✓ | ✓ | ✓ | × |
| | Expert 4 | ✓ | ✓ | ✓ | ✓ | × |
| image055 | Expert 1 | ✓ | ✓ | × | × | ✓ |
| | Expert 2 | ✓ | ✓ | × | × | × |
| | Expert 3 | ✓ | ✓ | × | × | × |
| | Expert 4 | ✓ | ✓ | × | × | × |

## A.2 Ground truth of DIARETDB1 (continued)

| Filename | Experts | MA | HM | HE | CWS | NV |
|---|---|---|---|---|---|---|
| image056 | Expert 1 | ✓ | × | ✓ | × | × |
| | Expert 2 | ✓ | × | × | × | × |
| | Expert 3 | ✓ | × | × | × | × |
| | Expert 4 | ✓ | × | ✓ | × | × |
| image057 | Expert 1 | × | × | × | × | × |
| | Expert 2 | × | × | × | × | × |
| | Expert 3 | × | × | × | × | × |
| | Expert 4 | × | × | × | × | × |
| image058 | Expert 1 | ✓ | × | × | × | × |
| | Expert 2 | ✓ | ✓ | × | × | × |
| | Expert 3 | ✓ | × | × | × | × |
| | Expert 4 | × | ✓ | × | × | × |
| image059 | Expert 1 | ✓ | × | × | × | × |
| | Expert 2 | ✓ | × | × | × | × |
| | Expert 3 | ✓ | × | × | × | × |
| | Expert 4 | ✓ | × | × | × | × |
| image060 | Expert 1 | × | × | × | × | × |
| | Expert 2 | × | × | × | × | × |
| | Expert 3 | × | × | × | × | × |
| | Expert 4 | × | × | × | × | × |
| image061 | Expert 1 | ✓ | × | × | × | × |
| | Expert 2 | × | × | × | × | ✓ |
| | Expert 3 | ✓ | × | × | × | × |
| | Expert 4 | × | × | × | × | × |
| image062 | Expert 1 | × | × | × | × | × |
| | Expert 2 | × | × | × | × | × |
| | Expert 3 | × | × | × | × | × |
| | Expert 4 | × | × | × | × | × |
| image063 | Expert 1 | ✓ | × | × | × | × |
| | Expert 2 | ✓ | ✓ | × | × | × |
| | Expert 3 | ✓ | × | × | × | × |
| | Expert 4 | ✓ | ✓ | × | × | × |
| image064 | Expert 1 | ✓ | ✓ | × | ✓ | ✓ |
| | Expert 2 | ✓ | ✓ | × | ✓ | × |
| | Expert 3 | ✓ | ✓ | × | ✓ | ✓ |
| | Expert 4 | ✓ | ✓ | × | ✓ | × |
| image065 | Expert 1 | ✓ | ✓ | × | ✓ | ✓ |
| | Expert 2 | ✓ | ✓ | × | ✓ | × |
| | Expert 3 | ✓ | ✓ | × | ✓ | ✓ |
| | Expert 4 | ✓ | ✓ | × | ✓ | × |
| image066 | Expert 1 | ✓ | ✓ | ✓ | ✓ | ✓ |
| | Expert 2 | ✓ | ✓ | ✓ | ✓ | × |
| | Expert 3 | × | ✓ | ✓ | ✓ | × |
| | Expert 4 | ✓ | ✓ | ✓ | ✓ | × |

## A.2 Ground truth of DIARETDB1 (continued)

| Filename | Experts | MA | HM | HE | CWS | NV |
|---|---|---|---|---|---|---|
| image067 | Expert 1 | ✓ | ✓ | ✓ | ✓ | ✓ |
| | Expert 2 | ✓ | ✓ | ✓ | ✓ | × |
| | Expert 3 | ✓ | ✓ | ✓ | ✓ | × |
| | Expert 4 | ✓ | ✓ | ✓ | ✓ | × |
| image068 | Expert 1 | ✓ | × | × | × | × |
| | Expert 2 | × | × | × | × | × |
| | Expert 3 | × | × | × | × | × |
| | Expert 4 | × | × | × | × | × |
| image069 | Expert 1 | ✓ | × | × | × | × |
| | Expert 2 | × | × | × | × | × |
| | Expert 3 | × | × | × | × | × |
| | Expert 4 | × | ✓ | × | × | × |
| image070 | Expert 1 | ✓ | × | × | × | × |
| | Expert 2 | × | × | × | × | × |
| | Expert 3 | × | × | × | × | × |
| | Expert 4 | × | × | × | ✓ | × |
| image071 | Expert 1 | ✓ | × | ✓ | × | × |
| | Expert 2 | × | × | ✓ | × | × |
| | Expert 3 | × | × | ✓ | × | × |
| | Expert 4 | × | × | ✓ | × | × |
| image072 | Expert 1 | × | × | × | × | × |
| | Expert 2 | × | × | × | × | × |
| | Expert 3 | × | × | × | × | × |
| | Expert 4 | × | × | × | × | × |
| image073 | Expert 1 | ✓ | × | × | × | × |
| | Expert 2 | × | × | × | × | × |
| | Expert 3 | × | × | × | × | × |
| | Expert 4 | × | × | × | ✓ | × |
| image074 | Expert 1 | ✓ | × | × | × | × |
| | Expert 2 | × | × | × | × | × |
| | Expert 3 | × | × | × | × | × |
| | Expert 4 | × | × | × | × | × |
| image075 | Expert 1 | ✓ | × | × | × | × |
| | Expert 2 | × | × | × | × | × |
| | Expert 3 | × | × | × | × | × |
| | Expert 4 | × | × | × | × | × |
| image076 | Expert 1 | ✓ | × | × | × | × |
| | Expert 2 | × | × | × | × | × |
| | Expert 3 | × | × | × | × | × |
| | Expert 4 | × | × | × | × | × |
| image077 | Expert 1 | ✓ | × | × | × | × |
| | Expert 2 | × | × | × | × | × |
| | Expert 3 | × | × | × | × | × |
| | Expert 4 | × | × | × | × | × |

## A.2 Ground truth of DIARETDB1 (continued)

| Filename | Experts | MA | HM | HE | CWS | NV |
|---|---|---|---|---|---|---|
| image078 | Expert 1 | ✓ | × | × | × | × |
| | Expert 2 | × | × | ✓ | × | × |
| | Expert 3 | × | ✓ | ✓ | × | × |
| | Expert 4 | ✓ | × | ✓ | × | × |
| image079 | Expert 1 | ✓ | × | × | × | × |
| | Expert 2 | × | × | × | × | × |
| | Expert 3 | × | × | × | × | × |
| | Expert 4 | ✓ | × | × | × | × |
| image080 | Expert 1 | × | × | × | × | × |
| | Expert 2 | × | × | × | × | × |
| | Expert 3 | ✓ | × | × | × | × |
| | Expert 4 | × | × | × | × | × |
| image081 | Expert 1 | ✓ | × | × | × | × |
| | Expert 2 | × | × | × | × | × |
| | Expert 3 | × | × | × | × | × |
| | Expert 4 | × | × | × | × | × |
| image082 | Expert 1 | ✓ | × | × | × | × |
| | Expert 2 | × | × | × | × | × |
| | Expert 3 | × | × | × | × | × |
| | Expert 4 | ✓ | × | ✓ | × | × |
| image083 | Expert 1 | ✓ | × | × | × | × |
| | Expert 2 | × | × | × | × | × |
| | Expert 3 | × | × | × | × | × |
| | Expert 4 | × | × | × | × | × |
| image084 | Expert 1 | × | ✓ | ✓ | × | × |
| | Expert 2 | × | ✓ | ✓ | ✓ | × |
| | Expert 3 | × | ✓ | ✓ | × | × |
| | Expert 4 | × | ✓ | ✓ | ✓ | × |
| image085 | Expert 1 | ✓ | ✓ | ✓ | × | × |
| | Expert 2 | ✓ | ✓ | ✓ | × | × |
| | Expert 3 | × | ✓ | ✓ | × | × |
| | Expert 4 | ✓ | ✓ | ✓ | ✓ | × |
| image086 | Expert 1 | ✓ | ✓ | × | × | × |
| | Expert 2 | ✓ | ✓ | × | × | × |
| | Expert 3 | × | ✓ | ✓ | × | × |
| | Expert 4 | ✓ | ✓ | ✓ | × | × |
| image087 | Expert 1 | ✓ | × | × | × | × |
| | Expert 2 | ✓ | × | × | × | × |
| | Expert 3 | × | × | × | × | × |
| | Expert 4 | ✓ | × | × | × | × |
| image088 | Expert 1 | ✓ | × | × | × | × |
| | Expert 2 | × | × | × | × | × |
| | Expert 3 | × | × | × | × | × |
| | Expert 4 | ✓ | × | × | × | × |

## A.2 Ground truth of DIARETDB1 (continued)

| Filename | Experts | MA | HM | HE | CWS | NV |
|---|---|---|---|---|---|---|
| image089 | Expert 1 | ✓ | × | × | × | × |
| | Expert 2 | ✓ | × | × | × | × |
| | Expert 3 | × | × | × | × | × |
| | Expert 4 | × | × | × | × | × |

## A.3. Ground Truth of MESSIDOR

| Image Title | Filename | MA/ HM | HE |
|---|---|---|---|
| im (1) | 20051019_38557_0100_PP | ✓ | ✓ |
| im (2) | 20051020_43808_0100_PP | × | × |
| im (3) | 20051020_43832_0100_PP | ✓ | × |
| im (4) | 20051020_43882_0100_PP | ✓ | × |
| im (5) | 20051020_43906_0100_PP | ✓ | ✓ |
| im (6) | 20051020_44261_0100_PP | × | × |
| im (7) | 20051020_44284_0100_PP | × | × |
| im (8) | 20051020_44338_0100_PP | × | × |
| im (9) | 20051020_44349_0100_PP | ✓ | ✓ |
| im (10) | 20051020_44400_0100_PP | × | × |
| im (11) | 20051020_44431_0100_PP | × | × |
| im (12) | 20051020_44598_0100_PP | ✓ | ✓ |
| im (13) | 20051020_44636_0100_PP | ✓ | × |
| im (14) | 20051020_44692_0100_PP | × | × |
| im (15) | 20051020_44714_0100_PP | × | × |
| im (16) | 20051020_44762_0100_PP | × | × |
| im (17) | 20051020_44782_0100_PP | ✓ | × |
| im (18) | 20051020_44843_0100_PP | ✓ | ✓ |
| im (19) | 20051020_44901_0100_PP | ✓ | ✓ |
| im (20) | 20051020_44923_0100_PP | ✓ | ✓ |
| im (21) | 20051020_44982_0100_PP | × | × |
| im (22) | 20051020_45004_0100_PP | ✓ | ✓ |
| im (23) | 20051020_45050_0100_PP | ✓ | ✓ |
| im (24) | 20051020_45068_0100_PP | ✓ | ✓ |
| im (25) | 20051020_45110_0100_PP | ✓ | ✓ |
| im (26) | 20051020_45137_0100_PP | ✓ | ✓ |
| im (27) | 20051020_52801_0100_PP | ✓ | ✓ |
| im (28) | 20051020_53062_0100_PP | ✓ | ✓ |
| im (29) | 20051020_53178_0100_PP | ✓ | ✓ |
| im (30) | 20051020_53997_0100_PP | ✓ | ✓ |
| im (31) | 20051020_54209_0100_PP | ✓ | ✓ |
| im (32) | 20051020_55346_0100_PP | ✓ | ✓ |
| im (33) | 20051020_55701_0100_PP | ✓ | × |
| im (34) | 20051020_56592_0100_PP | ✓ | × |
| im (35) | 20051020_56791_0100_PP | × | × |
| im (36) | 20051020_57157_0100_PP | × | × |
| im (37) | 20051020_57566_0100_PP | ✓ | ✓ |
| im (38) | 20051020_57622_0100_PP | ✓ | ✓ |
| im (39) | 20051020_57761_0100_PP | ✓ | ✓ |
| im (40) | 20051020_57844_0100_PP | ✓ | ✓ |
| im (41) | 20051020_57967_0100_PP | × | × |
| im (42) | 20051020_58065_0100_PP | × | × |
| im (43) | 20051020_58214_0100_PP | ✓ | ✓ |
| im (44) | 20051020_58276_0100_PP | ✓ | ✓ |
| im (45) | 20051020_61557_0100_PP | ✓ | ✓ |
| im (46) | 20051020_61757_0100_PP | × | × |
| im (47) | 20051020_61804_0100_PP | × | × |
| im (48) | 20051020_61907_0100_PP | × | × |
| im (49) | 20051020_61998_0100_PP | ✓ | × |
| im (50) | 20051020_62014_0100_PP | ✓ | × |
| im (51) | 20051020_62337_0100_PP | ✓ | ✓ |
| im (52) | 20051020_62385_0100_PP | ✓ | ✓ |
| im (53) | 20051020_62461_0100_PP | ✓ | × |
| im (54) | 20051020_62510_0100_PP | × | × |
| im (55) | 20051020_62577_0100_PP | ✓ | × |
| im (56) | 20051020_62615_0100_PP | ✓ | × |
| im (57) | 20051020_62709_0100_PP | ✓ | × |
| im (58) | 20051020_62802_0100_PP | ✓ | × |
| im (59) | 20051020_62878_0100_PP | ✓ | × |
| im (60) | 20051020_63045_0100_PP | × | × |
| im (61) | 20051020_63141_0100_PP | ✓ | ✓ |
| im (62) | 20051020_63269_0100_PP | × | × |
| im (63) | 20051020_63337_0100_PP | ✓ | × |
| im (64) | 20051020_63711_0100_PP | ✓ | × |
| im (65) | 20051020_63829_0100_PP | ✓ | × |
| im (66) | 20051020_63936_0100_PP | ✓ | ✓ |
| im (67) | 20051020_64007_0100_PP | ✓ | ✓ |
| im (68) | 20051020_64249_0100_PP | × | × |
| im (69) | 20051020_64388_0100_PP | × | × |
| im (70) | 20051020_64518_0100_PP | ✓ | ✓ |
| im (71) | 20051020_64570_0100_PP | ✓ | ✓ |
| im (72) | 20051020_64653_0100_PP | × | × |
| im (73) | 20051020_64703_0100_PP | × | × |
| im (74) | 20051020_64775_0100_PP | × | × |
| im (75) | 20051020_64836_0100_PP | × | × |
| im (76) | 20051020_64945_0100_PP | ✓ | × |
| im (77) | 20051020_64993_0100_PP | ✓ | × |
| im (78) | 20051020_65166_0100_PP | ✓ | × |
| im (79) | 20051020_65230_0100_PP | ✓ | × |
| im (80) | 20051021_36097_0100_PP | ✓ | ✓ |
| im (81) | 20051021_36208_0100_PP | ✓ | ✓ |
| im (82) | 20051021_36380_0100_PP | ✓ | × |
| im (83) | 20051021_36476_0100_PP | × | × |
| im (84) | 20051021_39222_0100_PP | ✓ | ✓ |
| im (85) | 20051021_39314_0100_PP | ✓ | ✓ |
| im (86) | 20051021_39482_0100_PP | × | × |
| im (87) | 20051021_39552_0100_PP | ✓ | × |
| im (88) | 20051021_39661_0100_PP | ✓ | ✓ |
| im (89) | 20051021_39719_0100_PP | ✓ | ✓ |
| im (90) | 20051021_39845_0100_PP | × | × |
| im (91) | 20051021_39914_0100_PP | × | ✓ |
| im (92) | 20051021_40018_0100_PP | × | × |
| im (93) | 20051021_40074_0100_PP | ✓ | × |
| im (94) | 20051021_40180_0100_PP | ✓ | × |
| im (95) | 20051021_40248_0100_PP | ✓ | ✓ |
| im (96) | 20051021_40377_0100_PP | ✓ | ✓ |
| im (97) | 20051021_40450_0100_PP | ✓ | ✓ |
| im (98) | 20051021_51418_0100_PP | × | × |
| im (99) | 20051021_51476_0100_PP | × | × |
| im (100) | 20051021_51561_0100_PP | ✓ | × |

## A.3 Ground truth of MESSIDOR (continued)

| Image Title | Filename | MA/ HM | HE |
|---|---|---|---|
| im (101) | 20051021_51625_0100_PP | ✓ | × |
| im (102) | 20051021_51748_0100_PP | ✓ | ✓ |
| im (103) | 20051021_51804_0100_PP | ✓ | ✓ |
| im (104) | 20051021_51936_0100_PP | × | × |
| im (105) | 20051021_51994_0100_PP | × | × |
| im (106) | 20051021_52075_0100_PP | ✓ | × |
| im (107) | 20051021_52127_0100_PP | ✓ | ✓ |
| im (108) | 20051021_57798_0100_PP | × | × |
| im (109) | 20051021_57862_0100_PP | × | × |
| im (110) | 20051021_57975_0100_PP | × | × |
| im (111) | 20051021_58035_0100_PP | × | ✓ |
| im (112) | 20051021_58178_0100_PP | ✓ | × |
| im (113) | 20051021_58316_0100_PP | × | × |
| im (114) | 20051021_58388_0100_PP | ✓ | × |
| im (115) | 20051021_58522_0100_PP | × | × |
| im (116) | 20051021_58683_0100_PP | ✓ | ✓ |
| im (117) | 20051021_58802_0100_PP | ✓ | ✓ |
| im (118) | 20051021_59136_0100_PP | ✓ | ✓ |
| im (119) | 20051021_59243_0100_PP | ✓ | ✓ |
| im (120) | 20051021_59459_0100_PP | ✓ | ✓ |
| im (121) | 20051021_59504_0100_PP | ✓ | ✓ |
| im (122) | 20051021_59589_0100_PP | × | × |
| im (123) | 20051213_61406_0100_PP | × | × |
| im (124) | 20051213_61802_0100_PP | × | × |
| im (125) | 20051213_61892_0100_PP | × | × |
| im (126) | 20051213_61951_0100_PP | × | × |
| im (127) | 20051213_62046_0100_PP | ✓ | × |
| im (128) | 20051213_62188_0100_PP | ✓ | × |
| im (129) | 20051213_62251_0100_PP | × | × |
| im (130) | 20051213_62314_0100_PP | × | × |
| im (131) | 20051213_62383_0100_PP | ✓ | ✓ |
| im (132) | 20051213_62437_0100_PP | ✓ | ✓ |
| im (133) | 20051213_62518_0100_PP | ✓ | × |
| im (134) | 20051213_62572_0100_PP | ✓ | × |
| im (135) | 20051213_62648_0100_PP | ✓ | ✓ |
| im (136) | 20051213_62705_0100_PP | ✓ | × |
| im (137) | 20051214_40361_0100_PP | ✓ | × |
| im (138) | 20051214_40456_0100_PP | ✓ | × |
| im (139) | 20051214_40529_0100_PP | × | × |
| im (140) | 20051214_40596_0100_PP | ✓ | × |
| im (141) | 20051214_40719_0100_PP | ✓ | × |
| im (142) | 20051214_40767_0100_PP | ✓ | × |
| im (143) | 20051214_40849_0100_PP | ✓ | ✓ |
| im (144) | 20051214_40912_0100_PP | ✓ | ✓ |
| im (145) | 20051214_40994_0100_PP | × | × |
| im (146) | 20051214_41055_0100_PP | × | × |
| im (147) | 20051214_41289_0100_PP | ✓ | × |
| im (148) | 20051214_41358_0100_PP | ✓ | × |
| im (149) | 20051214_41429_0100_PP | ✓ | ✓ |
| im (150) | 20051214_41490_0100_PP | ✓ | × |
| im (151) | 20051214_41582_0100_PP | ✓ | ✓ |
| im (152) | 20051214_41949_0100_PP | ✓ | × |
| im (153) | 20051214_42133_0100_PP | × | × |
| im (154) | 20051214_42197_0100_PP | × | × |
| im (155) | 20051214_42323_0100_PP | × | × |
| im (156) | 20051214_42363_0100_PP | × | × |
| im (157) | 20051214_50812_0100_PP | ✓ | × |
| im (158) | 20051214_50895_0100_PP | ✓ | × |
| im (159) | 20051214_50933_0100_PP | ✓ | × |
| im (160) | 20051214_51039_0100_PP | ✓ | × |
| im (161) | 20051214_51071_0100_PP | ✓ | × |
| im (162) | 20051214_51178_0100_PP | × | × |
| im (163) | 20051214_51211_0100_PP | × | × |
| im (164) | 20051214_51308_0100_PP | × | × |
| im (165) | 20051214_51342_0100_PP | × | × |
| im (166) | 20051214_51442_0100_PP | ✓ | × |
| im (167) | 20051214_51469_0100_PP | ✓ | × |
| im (168) | 20051214_51569_0100_PP | ✓ | ✓ |
| im (169) | 20051214_51609_0100_PP | ✓ | ✓ |
| im (170) | 20051214_51701_0100_PP | ✓ | ✓ |
| im (171) | 20051214_51733_0100_PP | ✓ | ✓ |
| im (172) | 20051214_51811_0100_PP | ✓ | ✓ |
| im (173) | 20051214_51840_0100_PP | ✓ | ✓ |
| im (174) | 20051214_51921_0100_PP | ✓ | ✓ |
| im (175) | 20051214_51953_0100_PP | ✓ | ✓ |
| im (176) | 20051214_52115_0100_PP | × | × |
| im (177) | 20051214_52204_0100_PP | ✓ | × |
| im (178) | 20051214_52242_0100_PP | ✓ | × |
| im (179) | 20051214_52349_0100_PP | ✓ | × |
| im (180) | 20051214_52492_0100_PP | ✓ | × |
| im (181) | 20051214_52611_0100_PP | ✓ | × |
| im (182) | 20051214_52695_0100_PP | ✓ | × |
| im (183) | 20051214_52707_0100_PP | ✓ | ✓ |
| im (184) | 20051214_53168_0100_PP | ✓ | ✓ |
| im (185) | 20051214_56169_0100_PP | ✓ | ✓ |
| im (186) | 20051214_56242_0100_PP | × | × |
| im (187) | 20051214_56269_0100_PP | ✓ | ✓ |
| im (188) | 20051214_56392_0100_PP | × | × |
| im (189) | 20051214_56438_0100_PP | × | × |
| im (190) | 20051214_56534_0100_PP | ✓ | × |
| im (191) | 20051214_56565_0100_PP | ✓ | × |
| im (192) | 20051214_56636_0100_PP | × | × |
| im (193) | 20051214_56688_0100_PP | × | × |
| im (194) | 20051214_56778_0100_PP | ✓ | ✓ |
| im (195) | 20051214_56821_0100_PP | ✓ | ✓ |
| im (196) | 20051214_56944_0100_PP | ✓ | ✓ |
| im (197) | 20051214_56971_0100_PP | ✓ | ✓ |
| im (198) | 20051214_57125_0100_PP | ✓ | ✓ |
| im (199) | 20051214_57154_0100_PP | ✓ | ✓ |
| im (200) | 20051214_57230_0100_PP | ✓ | ✓ |

## A.3 Ground truth of MESSIDOR (continued)

| Image Title | Filename | MA/ HM | HE |
|---|---|---|---|
| im (201) | 20051214_57260_0100_PP | ✓ | ✓ |
| im (202) | 20051214_57377_0100_PP | ✓ | ✓ |
| im (203) | 20051214_57404_0100_PP | ✓ | ✓ |
| im (204) | 20051214_57761_0100_PP | × | × |
| im (205) | 20051214_57817_0100_PP | × | × |
| im (206) | 20051214_57940_0100_PP | ✓ | ✓ |
| im (207) | 20060522_43643_0100_PP | × | × |
| im (208) | 20060522_43758_0100_PP | × | × |
| im (209) | 20060522_45069_0100_PP | × | × |
| im (210) | 20060522_45111_0100_PP | × | × |
| im (211) | 20060522_45212_0100_PP | ✓ | ✓ |
| im (212) | 20060522_45248_0100_PP | ✓ | ✓ |
| im (213) | 20060522_45402_0100_PP | ✓ | × |
| im (214) | 20060522_45455_0100_PP | ✓ | × |
| im (215) | 20060522_45541_0100_PP | ✓ | ✓ |
| im (216) | 20060522_45583_0100_PP | ✓ | ✓ |
| im (217) | 20060522_45691_0100_PP | ✓ | ✓ |
| im (218) | 20060522_45718_0100_PP | ✓ | ✓ |
| im (219) | 20060522_45777_0100_PP | × | × |
| im (220) | 20060522_45796_0100_PP | × | × |
| im (221) | 20060522_45853_0100_PP | × | × |
| im (222) | 20060522_45873_0100_PP | × | × |
| im (223) | 20060522_45935_0100_PP | ✓ | × |
| im (224) | 20060522_45967_0100_PP | ✓ | × |
| im (225) | 20060522_46104_0100_PP | × | × |
| im (226) | 20060522_46149_0100_PP | × | × |
| im (227) | 20060522_46266_0100_PP | ✓ | × |
| im (228) | 20060522_46379_0100_PP | × | ✓ |
| im (229) | 20060522_46400_0100_PP | × | ✓ |
| im (230) | 20060522_46454_0100_PP | × | × |
| im (231) | 20060523_42953_0100_PP | × | × |
| im (232) | 20060523_43016_0100_PP | ✓ | × |
| im (233) | 20060523_43038_0100_PP | ✓ | × |
| im (234) | 20060523_43105_0100_PP | × | × |
| im (235) | 20060523_43123_0100_PP | × | × |
| im (236) | 20060523_43174_0100_PP | ✓ | × |
| im (237) | 20060523_43196_0100_PP | ✓ | × |
| im (238) | 20060523_43248_0100_PP | × | × |
| im (239) | 20060523_43267_0100_PP | ✓ | ✓ |
| im (240) | 20060523_43333_0100_PP | × | × |
| im (241) | 20060523_43354_0100_PP | × | × |
| im (242) | 20060523_45216_0100_PP | ✓ | × |
| im (243) | 20060523_45235_0100_PP | ✓ | ✓ |
| im (244) | 20060523_45300_0100_PP | × | × |
| im (245) | 20060523_45316_0100_PP | × | × |
| im (246) | 20060523_45369_0100_PP | ✓ | ✓ |
| im (247) | 20060523_45389_0100_PP | ✓ | ✓ |
| im (248) | 20060523_45449_0100_PP | × | × |
| im (249) | 20060523_45467_0100_PP | × | × |
| im (250) | 20060523_45524_0100_PP | × | × |
| im (251) | 20060523_45548_0100_PP | × | × |
| im (252) | 20060523_45662_0100_PP | ✓ | ✓ |
| im (253) | 20060523_45697_0100_PP | ✓ | ✓ |
| im (254) | 20060523_45787_0100_PP | ✓ | × |
| im (255) | 20060523_45812_0100_PP | ✓ | ✓ |
| im (256) | 20060523_47987_0100_PP | × | × |
| im (257) | 20060523_48005_0100_PP | × | × |
| im (258) | 20060523_48028_0100_PP | ✓ | ✓ |
| im (259) | 20060523_48102_0100_PP | ✓ | ✓ |
| im (260) | 20060523_48136_0100_PP | × | × |
| im (261) | 20060523_48161_0100_PP | × | × |
| im (262) | 20060523_48182_0100_PP | ✓ | × |
| im (263) | 20060523_48199_0100_PP | ✓ | × |
| im (264) | 20060523_48357_0100_PP | × | × |
| im (265) | 20060523_48406_0100_PP | × | × |
| im (266) | 20060523_48425_0100_PP | ✓ | × |
| im (267) | 20060523_48477_0100_PP | ✓ | × |
| im (268) | 20060523_48499_0100_PP | ✓ | ✓ |
| im (269) | 20060523_48572_0100_PP | ✓ | × |
| im (270) | 20060523_48591_0100_PP | × | × |
| im (271) | 20060523_48643_0100_PP | × | × |
| im (272) | 20060523_48659_0100_PP | × | × |
| im (273) | 20060523_48709_0100_PP | × | × |
| im (274) | 20060523_48728_0100_PP | × | × |
| im (275) | 20060523_48787_0100_PP | ✓ | × |
| im (276) | 20060523_48816_0100_PP | ✓ | × |
| im (277) | 20060523_48890_0100_PP | × | × |
| im (278) | 20060523_48931_0100_PP | × | × |
| im (279) | 20060523_48990_0100_PP | ✓ | × |
| im (280) | 20060523_49010_0100_PP | ✓ | × |
| im (281) | 20060523_49100_0100_PP | × | × |
| im (282) | 20060523_49120_0100_PP | × | × |
| im (283) | 20060523_49176_0100_PP | × | × |
| im (284) | 20060523_49191_0100_PP | × | × |
| im (285) | 20060523_49269_0100_PP | ✓ | × |
| im (286) | 20060523_49288_0100_PP | ✓ | × |
| im (287) | 20060523_49449_0100_PP | × | × |
| im (288) | 20060523_49515_0100_PP | × | × |
| im (289) | 20060523_49573_0100_PP | × | × |
| im (290) | 20060523_49591_0100_PP | × | × |
| im (291) | 20060523_49663_0100_PP | × | × |
| im (292) | 20060523_49681_0100_PP | × | × |
| im (293) | 20060523_49726_0100_PP | × | × |
| im (294) | 20060523_49745_0100_PP | × | × |
| im (295) | 20060523_49791_0100_PP | ✓ | ✓ |
| im (296) | 20060523_49809_0100_PP | ✓ | ✓ |
| im (297) | 20060523_49859_0100_PP | ✓ | × |
| im (298) | 20060523_49875_0100_PP | ✓ | × |
| im (299) | 20060523_49928_0100_PP | ✓ | ✓ |
| im (300) | 20060523_49942_0100_PP | ✓ | ✓ |

## A.3 Ground truth of MESSIDOR (continued)

| Image Title | Filename | MA/ HM | HE |
|---|---|---|---|
| im (301) | 20060523_50003_0100_PP | ✓ | ✓ |
| im (302) | 20060523_50019_0100_PP | ✓ | ✓ |
| im (303) | 20060523_50135_0100_PP | ✓ | × |
| im (304) | 20060523_50153_0100_PP | × | × |
| im (305) | 20060523_50234_0100_PP | ✓ | ✓ |
| im (306) | 20060523_50262_0100_PP | ✓ | ✓ |
| im (307) | 20060523_50325_0100_PP | × | × |
| im (308) | 20060523_50342_0100_PP | × | × |
| im (309) | 20060523_50392_0100_PP | ✓ | ✓ |
| im (310) | 20060523_50408_0100_PP | ✓ | ✓ |
| im (311) | 20060523_50469_0100_PP | ✓ | × |
| im (312) | 20060523_50489_0100_PP | ✓ | × |
| im (313) | 20060523_50539_0100_PP | ✓ | ✓ |
| im (314) | 20060523_50556_0100_PP | ✓ | ✓ |
| im (315) | 20060523_50616_0100_PP | × | × |
| im (316) | 20060523_50631_0100_PP | × | × |
| im (317) | 20060523_50707_0100_PP | ✓ | × |
| im (318) | 20060523_50730_0100_PP | ✓ | × |
| im (319) | 20060523_50790_0100_PP | ✓ | ✓ |
| im (320) | 20060523_50806_0100_PP | ✓ | ✓ |
| im (321) | 20060529_56013_0100_PP | × | ✓ |
| im (322) | 20060529_56039_0100_PP | × | × |
| im (323) | 20060529_56255_0100_PP | ✓ | × |
| im (324) | 20060529_56338_0100_PP | ✓ | × |
| im (325) | 20060529_56420_0100_PP | × | × |
| im (326) | 20060529_56442_0100_PP | × | × |
| im (327) | 20060529_56563_0100_PP | × | × |
| im (328) | 20060529_56592_0100_PP | × | × |
| im (329) | 20060529_56700_0100_PP | ✓ | × |
| im (330) | 20060529_56730_0100_PP | ✓ | × |
| im (331) | 20060529_56834_0100_PP | ✓ | ✓ |
| im (332) | 20060529_56853_0100_PP | ✓ | × |
| im (333) | 20060529_56948_0100_PP | × | × |
| im (334) | 20060529_56968_0100_PP | × | × |
| im (335) | 20060529_57030_0100_PP | ✓ | ✓ |
| im (336) | 20060529_57063_0100_PP | ✓ | ✓ |
| im (337) | 20060529_57156_0100_PP | ✓ | × |
| im (338) | 20060529_57174_0100_PP | ✓ | ✓ |
| im (339) | 20060529_57261_0100_PP | × | × |
| im (340) | 20060529_57287_0100_PP | × | × |
| im (341) | 20060529_57351_0100_PP | × | × |
| im (342) | 20060529_57372_0100_PP | × | × |
| im (343) | 20060529_57430_0100_PP | ✓ | ✓ |
| im (344) | 20060529_57447_0100_PP | ✓ | ✓ |
| im (345) | 20060530_36788_0100_PP | ✓ | ✓ |
| im (346) | 20060530_36860_0100_PP | ✓ | ✓ |
| im (347) | 20060530_36895_0100_PP | ✓ | ✓ |
| im (348) | 20060530_51254_0100_PP | × | × |
| im (349) | 20060530_51279_0100_PP | × | × |
| im (350) | 20060530_51377_0100_PP | ✓ | ✓ |

| Image Title | Filename | MA/ HM | HE |
|---|---|---|---|
| im (351) | 20060530_51399_0100_PP | ✓ | ✓ |
| im (352) | 20060530_52988_0100_PP | ✓ | × |
| im (353) | 20060530_53042_0100_PP | × | × |
| im (354) | 20060530_53062_0100_PP | × | × |
| im (355) | 20060530_53132_0100_PP | × | × |
| im (356) | 20060530_53152_0100_PP | × | × |
| im (357) | 20060530_53233_0100_PP | ✓ | × |
| im (358) | 20060530_53271_0100_PP | ✓ | × |
| im (359) | 20060530_53421_0100_PP | ✓ | ✓ |
| im (360) | 20060530_53455_0100_PP | ✓ | ✓ |
| im (361) | 20060530_53522_0100_PP | ✓ | ✓ |
| im (362) | 20060530_53540_0100_PP | ✓ | ✓ |
| im (363) | 20060530_53597_0100_PP | × | × |
| im (364) | 20060530_53617_0100_PP | × | × |
| im (365) | 20060530_53702_0100_PP | ✓ | ✓ |
| im (366) | 20060530_53742_0100_PP | × | × |
| im (367) | 20060530_53761_0100_PP | × | × |
| im (368) | 20060530_53816_0100_PP | × | × |
| im (369) | 20060530_53836_0100_PP | × | × |
| im (370) | 20060530_53928_0100_PP | × | × |
| im (371) | 20060530_53954_0100_PP | × | × |
| im (372) | 20060530_54011_0100_PP | ✓ | × |
| im (373) | 20060530_54030_0100_PP | ✓ | × |
| im (374) | 20060530_54107_0100_PP | ✓ | ✓ |
| im (375) | 20060530_54117_0100_PP | ✓ | ✓ |
| im (376) | 20060530_54223_0100_PP | ✓ | × |
| im (377) | 20060530_54242_0100_PP | ✓ | × |
| im (378) | 20060530_54312_0100_PP | ✓ | ✓ |
| im (379) | 20060530_54332_0100_PP | ✓ | ✓ |
| im (380) | 20060530_54390_0100_PP | ✓ | × |
| im (381) | 20060530_54443_0100_PP | ✓ | × |
| im (382) | 20060530_54485_0100_PP | × | × |
| im (383) | 20060530_54529_0100_PP | ✓ | ✓ |
| im (384) | 20060530_54556_0100_PP | ✓ | ✓ |
| im (385) | 20060530_54632_0100_PP | ✓ | × |
| im (386) | 20060530_54653_0100_PP | ✓ | × |
| im (387) | 20060530_54718_0100_PP | ✓ | ✓ |
| im (388) | 20060530_55180_0100_PP | × | × |
| im (389) | 20060530_55203_0100_PP | ✓ | × |
| im (390) | 20060530_55304_0100_PP | ✓ | ✓ |
| im (391) | 20060530_55370_0100_PP | ✓ | × |
| im (392) | 20060530_55390_0100_PP | ✓ | × |
| im (393) | 20060530_55451_0100_PP | ✓ | × |
| im (394) | 20060530_55468_0100_PP | ✓ | ✓ |
| im (395) | 20060530_55607_0100_PP | × | × |
| im (396) | 20060530_55628_0100_PP | × | × |
| im (397) | 20060530_55724_0100_PP | ✓ | × |
| im (398) | 20060530_55746_0100_PP | ✓ | × |
| im (399) | 20060530_55816_0100_PP | ✓ | ✓ |
| im (400) | 20060530_55837_0100_PP | ✓ | ✓ |

## A.3 Ground truth of MESSIDOR (continued)

| Image Title | Filename | MA/HM | HE |
|---|---|---|---|
| im (401) | 20051216_43814_0200_PP | × | × |
| im (402) | 20051216_43913_0200_PP | × | × |
| im (403) | 20051216_44066_0200_PP | × | ✓ |
| im (404) | 20051216_44092_0200_PP | × | ✓ |
| im (405) | 20051216_44221_0200_PP | × | × |
| im (406) | 20051216_44252_0200_PP | × | × |
| im (407) | 20051216_44398_0200_PP | × | × |
| im (408) | 20051216_44420_0200_PP | × | × |
| im (409) | 20051216_44635_0200_PP | × | × |
| im (410) | 20051216_44660_0200_PP | × | × |
| im (411) | 20051216_44811_0200_PP | × | × |
| im (412) | 20051216_44832_0200_PP | × | × |
| im (413) | 20051216_44939_0200_PP | ✓ | ✓ |
| im (414) | 20051216_44961_0200_PP | ✓ | ✓ |
| im (415) | 20051216_45076_0200_PP | × | × |
| im (416) | 20051216_45100_0200_PP | ✓ | × |
| im (417) | 20051216_45226_0200_PP | ✓ | ✓ |
| im (418) | 20051216_45245_0200_PP | ✓ | ✓ |
| im (419) | 20051216_45351_0200_PP | ✓ | × |
| im (420) | 20051216_45375_0200_PP | ✓ | × |
| im (421) | 20051216_45478_0200_PP | × | × |
| im (422) | 20051216_45499_0200_PP | × | × |
| im (423) | 20051216_45595_0200_PP | × | × |
| im (424) | 20051216_45619_0200_PP | × | × |
| im (425) | 20051216_45757_0200_PP | ✓ | × |
| im (426) | 20051216_45781_0200_PP | × | × |
| im (427) | 20051216_45873_0200_PP | × | × |
| im (428) | 20051216_45899_0200_PP | ✓ | × |
| im (429) | 20051216_45992_0200_PP | × | × |
| im (430) | 20051216_46018_0200_PP | × | × |
| im (431) | 20051216_46156_0200_PP | × | ✓ |
| im (432) | 20051216_46183_0200_PP | × | × |
| im (433) | 20051216_46624_0200_PP | ✓ | × |
| im (434) | 20051216_46660_0200_PP | ✓ | × |
| im (435) | 20051216_46827_0200_PP | ✓ | ✓ |
| im (436) | 20051216_46847_0200_PP | ✓ | ✓ |
| im (437) | 20051216_47000_0200_PP | ✓ | ✓ |
| im (438) | 20051216_47024_0200_PP | ✓ | ✓ |
| im (439) | 20051216_47383_0200_PP | ✓ | × |
| im (440) | 20051216_47420_0200_PP | ✓ | × |
| im (441) | 20051216_47514_0200_PP | × | × |
| im (442) | 20051216_47536_0200_PP | × | × |
| im (443) | 20051216_47668_0200_PP | ✓ | ✓ |
| im (444) | 20051216_47703_0200_PP | ✓ | ✓ |
| im (445) | 20060119_41191_0200_PP | ✓ | × |
| im (446) | 20060407_38711_0200_PP | × | × |
| im (447) | 20060407_38970_0200_PP | × | × |
| im (448) | 20060407_39155_0200_PP | × | × |
| im (449) | 20060407_39184_0200_PP | × | × |
| im (450) | 20060407_39306_0200_PP | × | × |
| im (451) | 20060407_39328_0200_PP | × | × |
| im (452) | 20060407_39402_0200_PP | × | × |
| im (453) | 20060407_39435_0200_PP | × | × |
| im (454) | 20060407_39546_0200_PP | × | × |
| im (455) | 20060407_39567_0200_PP | × | × |
| im (456) | 20060407_39667_0200_PP | × | ✓ |
| im (457) | 20060407_39687_0200_PP | × | × |
| im (458) | 20060407_39761_0200_PP | × | × |
| im (459) | 20060407_39780_0200_PP | × | × |
| im (460) | 20060407_40582_0200_PP | ✓ | × |
| im (461) | 20060407_40624_0200_PP | ✓ | × |
| im (462) | 20060407_40740_0200_PP | × | ✓ |
| im (463) | 20060407_40761_0200_PP | × | × |
| im (464) | 20060407_40937_0200_PP | ✓ | × |
| im (465) | 20060407_40957_0200_PP | ✓ | × |
| im (466) | 20060407_41149_0200_PP | × | × |
| im (467) | 20060407_41177_0200_PP | × | × |
| im (468) | 20060407_41312_0200_PP | × | × |
| im (469) | 20060407_41330_0200_PP | × | × |
| im (470) | 20060407_41809_0200_PP | ✓ | × |
| im (471) | 20060407_41831_0200_PP | ✓ | ✓ |
| im (472) | 20060407_41937_0200_PP | ✓ | ✓ |
| im (473) | 20060407_41980_0200_PP | × | × |
| im (474) | 20060407_42099_0200_PP | × | × |
| im (475) | 20060407_42133_0200_PP | × | × |
| im (476) | 20060407_42290_0200_PP | × | × |
| im (477) | 20060407_42308_0200_PP | × | × |
| im (478) | 20060407_43223_0200_PP | × | ✓ |
| im (479) | 20060407_43258_0200_PP | × | × |
| im (480) | 20060407_43436_0200_PP | ✓ | × |
| im (481) | 20060407_43460_0200_PP | ✓ | × |
| im (482) | 20060407_43594_0200_PP | × | × |
| im (483) | 20060407_43618_0200_PP | × | × |
| im (484) | 20060407_43726_0200_PP | × | × |
| im (485) | 20060407_43746_0200_PP | × | × |
| im (486) | 20060407_43834_0200_PP | × | × |
| im (487) | 20060407_43856_0200_PP | × | × |
| im (488) | 20060407_44042_0200_PP | × | × |
| im (489) | 20060407_44061_0200_PP | × | × |
| im (490) | 20060407_44173_0200_PP | × | × |
| im (491) | 20060407_44192_0200_PP | × | × |
| im (492) | 20060407_44285_0200_PP | ✓ | × |
| im (493) | 20060407_44304_0200_PP | ✓ | ✓ |
| im (494) | 20060407_44400_0200_PP | × | × |
| im (495) | 20060407_44422_0200_PP | × | × |
| im (496) | 20060407_44510_0200_PP | × | × |
| im (497) | 20060407_44529_0200_PP | × | × |
| im (498) | 20060407_44617_0200_PP | ✓ | ✓ |
| im (499) | 20060407_44636_0200_PP | ✓ | ✓ |
| im (500) | 20060407_44743_0200_PP | × | × |

## A.3 Ground truth of MESSIDOR (continued)

| Image Title | Filename | MA/ HM | HE |
|---|---|---|---|
| im (501) | 20060407_44766_0200_PP | × | × |
| im (502) | 20060407_44866_0200_PP | × | × |
| im (503) | 20060407_44889_0200_PP | × | × |
| im (504) | 20060407_45087_0200_PP | × | × |
| im (505) | 20060407_45107_0200_PP | × | × |
| im (506) | 20060407_45230_0200_PP | × | × |
| im (507) | 20060407_45247_0200_PP | × | × |
| im (508) | 20060407_45362_0200_PP | × | × |
| im (509) | 20060407_45379_0200_PP | × | × |
| im (510) | 20060407_45477_0200_PP | ✓ | ✓ |
| im (511) | 20060407_45494_0200_PP | ✓ | × |
| im (512) | 20060407_45592_0200_PP | ✓ | × |
| im (513) | 20060407_45611_0200_PP | ✓ | × |
| im (514) | 20060407_45718_0200_PP | × | × |
| im (515) | 20060407_45737_0200_PP | × | × |
| im (516) | 20060407_45834_0200_PP | × | × |
| im (517) | 20060407_45852_0200_PP | × | × |
| im (518) | 20060407_45932_0200_PP | × | × |
| im (519) | 20060407_45949_0200_PP | × | × |
| im (520) | 20060407_46050_0200_PP | × | × |
| im (521) | 20060407_46070_0200_PP | × | × |
| im (522) | 20060407_46235_0200_PP | × | × |
| im (523) | 20060407_46257_0200_PP | × | × |
| im (524) | 20060407_46394_0200_PP | ✓ | × |
| im (525) | 20060407_46422_0200_PP | ✓ | × |
| im (526) | 20060410_39047_0200_PP | × | × |
| im (527) | 20060410_39075_0200_PP | × | × |
| im (528) | 20060410_39203_0200_PP | × | × |
| im (529) | 20060410_39229_0200_PP | × | × |
| im (530) | 20060410_39334_0200_PP | × | × |
| im (531) | 20060410_39355_0200_PP | ✓ | × |
| im (532) | 20060410_39476_0200_PP | × | × |
| im (533) | 20060410_39500_0200_PP | × | × |
| im (534) | 20060410_39586_0200_PP | × | × |
| im (535) | 20060410_39606_0200_PP | ✓ | × |
| im (536) | 20060410_39695_0200_PP | × | × |
| im (537) | 20060410_39726_0200_PP | × | × |
| im (538) | 20060410_39859_0200_PP | × | × |
| im (539) | 20060410_39879_0200_PP | × | × |
| im (540) | 20060410_39976_0200_PP | × | × |
| im (541) | 20060410_39994_0200_PP | × | × |
| im (542) | 20060410_40146_0200_PP | ✓ | × |
| im (543) | 20060410_40165_0200_PP | ✓ | ✓ |
| im (544) | 20060410_40254_0200_PP | ✓ | × |
| im (545) | 20060410_40274_0200_PP | ✓ | × |
| im (546) | 20060410_40381_0200_PP | × | × |
| im (547) | 20060410_40403_0200_PP | × | × |
| im (548) | 20060410_40481_0200_PP | ✓ | × |
| im (549) | 20060410_40499_0200_PP | × | × |
| im (550) | 20060410_40605_0200_PP | ✓ | ✓ |
| im (551) | 20060410_40633_0200_PP | × | × |
| im (552) | 20060410_40830_0200_PP | ✓ | × |
| im (553) | 20060410_40846_0200_PP | × | × |
| im (554) | 20060410_40953_0200_PP | × | × |
| im (555) | 20060410_40979_0200_PP | × | × |
| im (556) | 20060410_41077_0200_PP | × | × |
| im (557) | 20060410_41098_0200_PP | × | × |
| im (558) | 20060410_41191_0200_PP | ✓ | × |
| im (559) | 20060410_41209_0200_PP | × | × |
| im (560) | 20060410_41330_0200_PP | × | × |
| im (561) | 20060410_41356_0200_PP | ✓ | × |
| im (562) | 20060410_41603_0200_PP | × | × |
| im (563) | 20060410_41626_0200_PP | ✓ | × |
| im (564) | 20060410_41747_0200_PP | ✓ | ✓ |
| im (565) | 20060410_41767_0200_PP | ✓ | × |
| im (566) | 20060410_41880_0200_PP | × | × |
| im (567) | 20060410_41901_0200_PP | × | × |
| im (568) | 20060410_43675_0200_PP | ✓ | ✓ |
| im (569) | 20060410_43698_0200_PP | ✓ | ✓ |
| im (570) | 20060410_43847_0200_PP | × | × |
| im (571) | 20060410_43868_0200_PP | × | × |
| im (572) | 20060410_43959_0200_PP | × | × |
| im (573) | 20060410_43979_0200_PP | × | × |
| im (574) | 20060410_44106_0200_PP | ✓ | ✓ |
| im (575) | 20060410_44124_0200_PP | ✓ | × |
| im (576) | 20060410_44224_0200_PP | ✓ | × |
| im (577) | 20060410_44248_0200_PP | ✓ | ✓ |
| im (578) | 20060410_44345_0200_PP | × | × |
| im (579) | 20060410_44364_0200_PP | × | × |
| im (580) | 20060410_44464_0200_PP | × | × |
| im (581) | 20060410_44504_0200_PP | × | × |
| im (582) | 20060410_44601_0200_PP | × | × |
| im (583) | 20060410_44623_0200_PP | ✓ | × |
| im (584) | 20060410_44770_0200_PP | × | × |
| im (585) | 20060410_44802_0200_PP | × | × |
| im (586) | 20060410_44934_0200_PP | × | × |
| im (587) | 20060410_44953_0200_PP | ✓ | × |
| im (588) | 20060410_45167_0200_PP | × | × |
| im (589) | 20060410_45188_0200_PP | × | × |
| im (590) | 20060410_46874_0200_PP | ✓ | ✓ |
| im (591) | 20060410_46893_0200_PP | ✓ | × |
| im (592) | 20060410_47016_0200_PP | ✓ | × |
| im (593) | 20060410_47042_0200_PP | × | × |
| im (594) | 20060410_47166_0200_PP | ✓ | × |
| im (595) | 20060410_47186_0200_PP | × | × |
| im (596) | 20060410_47331_0200_PP | ✓ | × |
| im (597) | 20060410_47351_0200_PP | ✓ | × |
| im (598) | 20060411_51958_0200_PP | ✓ | ✓ |
| im (599) | 20060411_51985_0200_PP | ✓ | ✓ |
| im (600) | 20060411_57853_0200_PP | ✓ | ✓ |

## A.3 Ground truth of MESSIDOR (continued)

| Image Title | Filename | MA/ HM | HE |
|---|---|---|---|
| im (601) | 20060411_57879_0200_PP | ✓ | ✓ |
| im (602) | 20060411_57962_0200_PP | ✓ | × |
| im (603) | 20060411_57986_0200_PP | ✓ | × |
| im (604) | 20060411_58051_0200_PP | ✓ | × |
| im (605) | 20060411_58071_0200_PP | × | × |
| im (606) | 20060411_58134_0200_PP | ✓ | × |
| im (607) | 20060411_58155_0200_PP | ✓ | × |
| im (608) | 20060411_58221_0200_PP | ✓ | ✓ |
| im (609) | 20060411_58238_0200_PP | ✓ | ✓ |
| im (610) | 20060411_58303_0200_PP | ✓ | × |
| im (611) | 20060411_58328_0200_PP | ✓ | × |
| im (612) | 20060411_58392_0200_PP | × | × |
| im (613) | 20060411_58413_0200_PP | × | × |
| im (614) | 20060411_58469_0200_PP | × | × |
| im (615) | 20060411_58494_0200_PP | × | × |
| im (616) | 20060411_58550_0200_PP | × | × |
| im (617) | 20060411_58571_0200_PP | × | × |
| im (618) | 20060411_58624_0200_PP | ✓ | × |
| im (619) | 20060411_58644_0200_PP | × | × |
| im (620) | 20060411_58718_0200_PP | ✓ | × |
| im (621) | 20060411_58736_0200_PP | ✓ | × |
| im (622) | 20060411_58808_0200_PP | × | × |
| im (623) | 20060411_58829_0200_PP | × | × |
| im (624) | 20060411_58891_0200_PP | × | × |
| im (625) | 20060411_58913_0200_PP | × | × |
| im (626) | 20060411_58971_0200_PP | ✓ | × |
| im (627) | 20060411_58993_0200_PP | ✓ | × |
| im (628) | 20060411_59062_0200_PP | ✓ | × |
| im (629) | 20060411_59087_0200_PP | ✓ | × |
| im (630) | 20060411_59176_0200_PP | ✓ | ✓ |
| im (631) | 20060411_59190_0200_PP | ✓ | ✓ |
| im (632) | 20060411_59549_0200_PP | ✓ | × |
| im (633) | 20060411_59587_0200_PP | ✓ | × |
| im (634) | 20060411_59638_0200_PP | ✓ | × |
| im (635) | 20060411_59657_0200_PP | ✓ | × |
| im (636) | 20060411_59728_0200_PP | ✓ | ✓ |
| im (637) | 20060411_59747_0200_PP | ✓ | × |
| im (638) | 20060411_59812_0200_PP | ✓ | ✓ |
| im (639) | 20060411_59859_0200_PP | ✓ | ✓ |
| im (640) | 20060411_59919_0200_PP | ✓ | × |
| im (641) | 20060411_59941_0200_PP | ✓ | × |
| im (642) | 20060411_60009_0200_PP | ✓ | × |
| im (643) | 20060411_60028_0200_PP | ✓ | × |
| im (644) | 20060411_60263_0200_PP | ✓ | ✓ |
| im (645) | 20060411_60283_0200_PP | ✓ | × |
| im (646) | 20060411_60347_0200_PP | × | × |
| im (647) | 20060411_60368_0200_PP | × | × |
| im (648) | 20060411_60426_0200_PP | ✓ | × |
| im (649) | 20060411_60446_0200_PP | ✓ | × |
| im (650) | 20060411_60511_0200_PP | × | × |
| im (651) | 20060411_60533_0200_PP | ✓ | ✓ |
| im (652) | 20060411_61029_0200_PP | × | ✓ |
| im (653) | 20060411_61060_0200_PP | ✓ | × |
| im (654) | 20060411_61196_0200_PP | ✓ | × |
| im (655) | 20060411_61214_0200_PP | ✓ | × |
| im (656) | 20060411_61402_0200_PP | ✓ | × |
| im (657) | 20060411_61419_0200_PP | ✓ | × |
| im (658) | 20060411_61478_0200_PP | ✓ | × |
| im (659) | 20060411_61494_0200_PP | ✓ | × |
| im (660) | 20060411_61548_0200_PP | ✓ | × |
| im (661) | 20060411_61564_0200_PP | × | ✓ |
| im (662) | 20060411_61624_0200_PP | ✓ | × |
| im (663) | 20060411_61641_0200_PP | ✓ | × |
| im (664) | 20060411_61687_0200_PP | ✓ | × |
| im (665) | 20060411_61702_0200_PP | × | × |
| im (666) | 20060411_61781_0200_PP | ✓ | ✓ |
| im (667) | 20060411_61808_0200_PP | ✓ | ✓ |
| im (668) | 20060411_61869_0200_PP | × | × |
| im (669) | 20060411_61901_0200_PP | × | × |
| im (670) | 20060411_61952_0200_PP | ✓ | ✓ |
| im (671) | 20060411_61979_0200_PP | ✓ | ✓ |
| im (672) | 20060411_62036_0200_PP | × | × |
| im (673) | 20060411_62058_0200_PP | × | × |
| im (674) | 20060411_62142_0200_PP | × | ✓ |
| im (675) | 20060411_62162_0200_PP | × | × |
| im (676) | 20060411_62228_0200_PP | ✓ | × |
| im (677) | 20060411_62250_0200_PP | ✓ | × |
| im (678) | 20060411_62298_0200_PP | ✓ | × |
| im (679) | 20060411_62319_0200_PP | ✓ | × |
| im (680) | 20060411_62373_0200_PP | ✓ | ✓ |
| im (681) | 20060411_62390_0200_PP | ✓ | × |
| im (682) | 20060412_51656_0200_PP | ✓ | × |
| im (683) | 20060412_51677_0200_PP | ✓ | × |
| im (684) | 20060412_51746_0200_PP | ✓ | ✓ |
| im (685) | 20060412_51775_0200_PP | ✓ | ✓ |
| im (686) | 20060412_51835_0200_PP | × | × |
| im (687) | 20060412_51860_0200_PP | × | × |
| im (688) | 20060412_51932_0200_PP | ✓ | ✓ |
| im (689) | 20060412_51952_0200_PP | ✓ | ✓ |
| im (690) | 20060412_52020_0200_PP | ✓ | × |
| im (691) | 20060412_52038_0200_PP | ✓ | × |
| im (692) | 20060412_52098_0200_PP | × | × |
| im (693) | 20060412_52122_0200_PP | ✓ | × |
| im (694) | 20060412_52174_0200_PP | ✓ | × |
| im (695) | 20060412_52194_0200_PP | ✓ | ✓ |
| im (696) | 20060412_52245_0200_PP | ✓ | ✓ |
| im (697) | 20060412_52271_0200_PP | ✓ | ✓ |
| im (698) | 20060412_52351_0200_PP | × | × |
| im (699) | 20060412_52371_0200_PP | × | × |
| im (700) | 20060412_52425_0200_PP | × | × |

## A.3 Ground truth of MESSIDOR (continued)

| Image Title | Filename | MA/ HM | HE |
|---|---|---|---|
| im (701) | 20060412_52446_0200_PP | × | × |
| im (702) | 20060412_52497_0200_PP | ✓ | ✓ |
| im (703) | 20060412_52520_0200_PP | ✓ | × |
| im (704) | 20060412_52587_0200_PP | ✓ | × |
| im (705) | 20060412_52606_0200_PP | × | × |
| im (706) | 20060412_52668_0200_PP | ✓ | × |
| im (707) | 20060412_52685_0200_PP | ✓ | ✓ |
| im (708) | 20060412_52758_0200_PP | ✓ | × |
| im (709) | 20060412_52777_0200_PP | ✓ | × |
| im (710) | 20060412_52840_0200_PP | ✓ | × |
| im (711) | 20060412_52860_0200_PP | ✓ | ✓ |
| im (712) | 20060412_52910_0200_PP | ✓ | ✓ |
| im (713) | 20060412_52931_0200_PP | ✓ | ✓ |
| im (714) | 20060412_52978_0200_PP | ✓ | × |
| im (715) | 20060412_52997_0200_PP | ✓ | × |
| im (716) | 20060412_53045_0200_PP | ✓ | ✓ |
| im (717) | 20060412_57650_0200_PP | ✓ | × |
| im (718) | 20060412_57680_0200_PP | ✓ | × |
| im (719) | 20060412_57846_0200_PP | ✓ | × |
| im (720) | 20060412_57874_0200_PP | × | × |
| im (721) | 20060412_57952_0200_PP | × | × |
| im (722) | 20060412_57974_0200_PP | × | × |
| im (723) | 20060412_58032_0200_PP | × | × |
| im (724) | 20060412_58054_0200_PP | × | × |
| im (725) | 20060412_58137_0200_PP | × | × |
| im (726) | 20060412_58171_0200_PP | ✓ | × |
| im (727) | 20060412_58287_0200_PP | ✓ | ✓ |
| im (728) | 20060412_58314_0200_PP | ✓ | ✓ |
| im (729) | 20060412_58368_0200_PP | × | × |
| im (730) | 20060412_58387_0200_PP | ✓ | × |
| im (731) | 20060412_58471_0200_PP | ✓ | ✓ |
| im (732) | 20060412_58497_0200_PP | ✓ | ✓ |
| im (733) | 20060412_58548_0200_PP | ✓ | × |
| im (734) | 20060412_58563_0200_PP | ✓ | ✓ |
| im (735) | 20060412_58638_0200_PP | ✓ | × |
| im (736) | 20060412_58668_0200_PP | ✓ | × |
| im (737) | 20060412_58723_0200_PP | × | × |
| im (738) | 20060412_58747_0200_PP | ✓ | × |
| im (739) | 20060412_58802_0200_PP | × | × |
| im (740) | 20060412_58819_0200_PP | × | × |
| im (741) | 20060412_58869_0200_PP | ✓ | ✓ |
| im (742) | 20060412_58889_0200_PP | ✓ | ✓ |
| im (743) | 20060412_58945_0200_PP | ✓ | × |
| im (744) | 20060412_58965_0200_PP | ✓ | × |
| im (745) | 20060412_59012_0200_PP | ✓ | ✓ |
| im (746) | 20060412_59037_0200_PP | ✓ | × |
| im (747) | 20060412_59100_0200_PP | ✓ | ✓ |
| im (748) | 20060412_59124_0200_PP | ✓ | × |
| im (749) | 20060412_59175_0200_PP | × | × |
| im (750) | 20060412_59196_0200_PP | × | × |
| im (751) | 20060412_59242_0200_PP | ✓ | × |
| im (752) | 20060412_59259_0200_PP | × | × |
| im (753) | 20060412_59338_0200_PP | × | × |
| im (754) | 20060412_59355_0200_PP | × | × |
| im (755) | 20060412_59400_0200_PP | ✓ | × |
| im (756) | 20060412_59423_0200_PP | × | ✓ |
| im (757) | 20060412_59636_0200_PP | ✓ | × |
| im (758) | 20060412_59658_0200_PP | ✓ | × |
| im (759) | 20060412_59717_0200_PP | ✓ | × |
| im (760) | 20060412_59735_0200_PP | ✓ | × |
| im (761) | 20060412_60337_0200_PP | ✓ | ✓ |
| im (762) | 20060412_60396_0200_PP | ✓ | × |
| im (763) | 20060412_60454_0200_PP | ✓ | ✓ |
| im (764) | 20060412_60475_0200_PP | ✓ | × |
| im (765) | 20060412_60545_0200_PP | ✓ | ✓ |
| im (766) | 20060412_60573_0200_PP | ✓ | × |
| im (767) | 20060412_60751_0200_PP | × | × |
| im (768) | 20060412_60773_0200_PP | × | × |
| im (769) | 20060412_60825_0200_PP | ✓ | × |
| im (770) | 20060412_60845_0200_PP | ✓ | × |
| im (771) | 20060412_60895_0200_PP | ✓ | ✓ |
| im (772) | 20060412_60913_0200_PP | ✓ | × |
| im (773) | 20060412_60978_0200_PP | ✓ | × |
| im (774) | 20060412_61000_0200_PP | ✓ | × |
| im (775) | 20060412_61064_0200_PP | ✓ | × |
| im (776) | 20060412_61081_0200_PP | ✓ | × |
| im (777) | 20060412_61151_0200_PP | ✓ | × |
| im (778) | 20060412_61169_0200_PP | ✓ | ✓ |
| im (779) | 20060412_61222_0200_PP | ✓ | × |
| im (780) | 20060412_61251_0200_PP | ✓ | × |
| im (781) | 20060412_61299_0200_PP | ✓ | × |
| im (782) | 20060412_61316_0200_PP | ✓ | × |
| im (783) | 20060412_61365_0200_PP | × | × |
| im (784) | 20060412_61383_0200_PP | × | × |
| im (785) | 20060412_61433_0200_PP | × | × |
| im (786) | 20060412_61450_0200_PP | × | × |
| im (787) | 20060412_61501_0200_PP | ✓ | × |
| im (788) | 20060412_61525_0200_PP | × | × |
| im (789) | 20060412_61593_0200_PP | ✓ | × |
| im (790) | 20060412_61615_0200_PP | ✓ | × |
| im (791) | 20060412_61665_0200_PP | × | × |
| im (792) | 20060412_61681_0200_PP | ✓ | × |
| im (793) | 20060412_61790_0200_PP | ✓ | × |
| im (794) | 20060412_61808_0200_PP | ✓ | ✓ |
| im (795) | 20060412_62936_0200_PP | ✓ | ✓ |
| im (796) | 20060412_62960_0200_PP | ✓ | ✓ |
| im (797) | 20060412_63009_0200_PP | ✓ | × |
| im (798) | 20060412_63032_0200_PP | ✓ | × |
| im (799) | 20060412_63088_0200_PP | ✓ | × |
| im (800) | 20060412_63104_0200_PP | ✓ | × |

## A.3 Ground truth of MESSIDOR (continued)

| Image Title | Filename | MA/ HM | HE |
|---|---|---|---|
| im (801) | 20051109_57451_0400_PP | × | × |
| im (802) | 20051109_57843_0400_PP | × | × |
| im (803) | 20051109_59582_0400_PP | × | × |
| im (804) | 20051109_59751_0400_PP | × | × |
| im (805) | 20051109_59864_0400_PP | × | × |
| im (806) | 20051109_59969_0400_PP | × | × |
| im (807) | 20051109_60031_0400_PP | × | × |
| im (808) | 20051109_60136_0400_PP | × | × |
| im (809) | 20051110_33960_0400_PP | × | × |
| im (810) | 20051110_34013_0400_PP | × | × |
| im (811) | 20051110_34071_0400_PP | × | × |
| im (812) | 20051110_34493_0400_PP | × | × |
| im (813) | 20051110_35239_0400_PP | × | × |
| im (814) | 20051110_35279_0400_PP | × | × |
| im (815) | 20051110_35332_0400_PP | × | × |
| im (816) | 20051110_35926_0400_PP | × | × |
| im (817) | 20051110_37992_0400_PP | × | × |
| im (818) | 20051110_38111_0400_PP | × | × |
| im (819) | 20051110_38156_0400_PP | × | × |
| im (820) | 20051110_38194_0400_PP | × | × |
| im (821) | 20051110_38239_0400_PP | × | × |
| im (822) | 20051110_38280_0400_PP | × | × |
| im (823) | 20051110_38313_0400_PP | × | × |
| im (824) | 20051110_38352_0400_PP | × | × |
| im (825) | 20051110_38372_0400_PP | × | × |
| im (826) | 20051110_38411_0400_PP | × | × |
| im (827) | 20051110_38442_0400_PP | × | × |
| im (828) | 20051110_38472_0400_PP | × | × |
| im (829) | 20051110_38507_0400_PP | × | × |
| im (830) | 20051110_38644_0400_PP | × | × |
| im (831) | 20051110_38702_0400_PP | × | × |
| im (832) | 20051116_43388_0400_PP | × | × |
| im (833) | 20051116_43585_0400_PP | × | × |
| im (834) | 20051116_43679_0400_PP | × | × |
| im (835) | 20051116_43710_0400_PP | × | × |
| im (836) | 20051116_43721_0400_PP | × | × |
| im (837) | 20051116_43785_0400_PP | × | × |
| im (838) | 20051116_43801_0400_PP | × | × |
| im (839) | 20051116_43954_0400_PP | ✓ | × |
| im (840) | 20051116_43995_0400_PP | ✓ | × |
| im (841) | 20051116_44026_0400_PP | ✓ | × |
| im (842) | 20051116_44051_0400_PP | ✓ | × |
| im (843) | 20051116_44070_0400_PP | ✓ | × |
| im (844) | 20051116_44083_0400_PP | ✓ | × |
| im (845) | 20051116_44126_0400_PP | ✓ | × |
| im (846) | 20051116_44482_0400_PP | ✓ | × |
| im (847) | 20051116_44586_0400_PP | ✓ | × |
| im (848) | 20051116_44615_0400_PP | ✓ | × |
| im (849) | 20051116_44648_0400_PP | ✓ | × |
| im (850) | 20051116_44690_0400_PP | ✓ | × |
| im (851) | 20051116_44718_0400_PP | ✓ | × |
| im (852) | 20051116_44750_0400_PP | ✓ | × |
| im (853) | 20051116_44785_0400_PP | ✓ | × |
| im (854) | 20051116_44804_0400_PP | ✓ | × |
| im (855) | 20051116_44816_0400_PP | ✓ | × |
| im (856) | 20051116_54343_0400_PP | ✓ | × |
| im (857) | 20051116_54429_0400_PP | ✓ | × |
| im (858) | 20051116_54454_0400_PP | ✓ | ✓ |
| im (859) | 20051116_54484_0400_PP | ✓ | × |
| im (860) | 20051116_54587_0400_PP | ✓ | × |
| im (861) | 20051116_54642_0400_PP | ✓ | × |
| im (862) | 20051116_54663_0400_PP | ✓ | × |
| im (863) | 20051116_54692_0400_PP | ✓ | × |
| im (864) | 20051116_54825_0400_PP | ✓ | × |
| im (865) | 20051116_54832_0400_PP | ✓ | × |
| im (866) | 20051116_54839_0400_PP | ✓ | × |
| im (867) | 20051116_54865_0400_PP | ✓ | × |
| im (868) | 20051116_55573_0400_PP | ✓ | × |
| im (869) | 20051116_55593_0400_PP | ✓ | ✓ |
| im (870) | 20051116_55617_0400_PP | ✓ | × |
| im (871) | 20051116_55643_0400_PP | ✓ | × |
| im (872) | 20051116_55649_0400_PP | ✓ | × |
| im (873) | 20051116_55656_0400_PP | ✓ | × |
| im (874) | 20051116_58804_0400_PP | ✓ | × |
| im (875) | 20051116_58816_0400_PP | ✓ | × |
| im (876) | 20051116_58828_0400_PP | ✓ | ✓ |
| im (877) | 20051116_58835_0400_PP | ✓ | ✓ |
| im (878) | 20051116_58850_0400_PP | ✓ | × |
| im (879) | 20051116_58864_0400_PP | ✓ | ✓ |
| im (880) | 20051116_58872_0400_PP | ✓ | × |
| im (881) | 20051116_59150_0400_PP | ✓ | × |
| im (882) | 20051116_59168_0400_PP | ✓ | ✓ |
| im (883) | 20051116_59193_0400_PP | ✓ | ✓ |
| im (884) | 20051116_59201_0400_PP | ✓ | ✓ |
| im (885) | 20051116_59229_0400_PP | ✓ | ✓ |
| im (886) | 20051116_59248_0400_PP | ✓ | ✓ |
| im (887) | 20051116_59273_0400_PP | ✓ | × |
| im (888) | 20051116_59294_0400_PP | ✓ | × |
| im (889) | 20051116_59319_0400_PP | ✓ | × |
| im (890) | 20051117_37042_0400_PP | × | × |
| im (891) | 20051117_37051_0400_PP | × | × |
| im (892) | 20051117_37078_0400_PP | × | × |
| im (893) | 20051117_37100_0400_PP | × | × |
| im (894) | 20051117_37130_0400_PP | × | × |
| im (895) | 20051130_53623_0400_PP | × | × |
| im (896) | 20051130_53663_0400_PP | × | × |
| im (897) | 20051130_53991_0400_PP | × | × |
| im (898) | 20051130_54030_0400_PP | × | × |
| im (899) | 20051130_54077_0400_PP | × | × |
| im (900) | 20051130_54121_0400_PP | × | × |

## A.3 Ground truth of MESSIDOR (continued)

| Image Title | Filename | MA/ HM | HE |
|---|---|---|---|
| im (901) | 20051130_54257_0400_PP | × | × |
| im (902) | 20051130_54301_0400_PP | × | × |
| im (903) | 20051130_54323_0400_PP | × | × |
| im (904) | 20051130_54333_0400_PP | × | × |
| im (905) | 20051130_54364_0400_PP | × | × |
| im (906) | 20051130_54401_0400_PP | × | × |
| im (907) | 20051130_54476_0400_PP | × | × |
| im (908) | 20051130_54498_0400_PP | × | × |
| im (909) | 20051130_54595_0400_PP | × | × |
| im (910) | 20051130_54616_0400_PP | × | × |
| im (911) | 20051130_54802_0400_PP | × | × |
| im (912) | 20051130_54846_0400_PP | × | × |
| im (913) | 20051130_54943_0400_PP | × | × |
| im (914) | 20051130_54956_0400_PP | × | × |
| im (915) | 20051130_55004_0400_PP | × | × |
| im (916) | 20051130_55012_0400_PP | × | × |
| im (917) | 20051130_55037_0400_PP | × | × |
| im (918) | 20051130_55048_0400_PP | × | × |
| im (919) | 20051130_55074_0400_PP | × | × |
| im (920) | 20051130_55086_0400_PP | × | × |
| im (921) | 20051130_55107_0400_PP | × | × |
| im (922) | 20051130_55124_0400_PP | × | × |
| im (923) | 20051130_55160_0400_PP | × | × |
| im (924) | 20051130_55269_0400_PP | × | × |
| im (925) | 20051130_55311_0400_PP | × | × |
| im (926) | 20051130_55323_0400_PP | × | × |
| im (927) | 20051130_55381_0400_PP | × | × |
| im (928) | 20051130_55393_0400_PP | × | × |
| im (929) | 20051130_58716_0400_PP | × | × |
| im (930) | 20051130_58824_0400_PP | × | × |
| im (931) | 20051130_58874_0400_PP | × | × |
| im (932) | 20051130_58888_0400_PP | × | × |
| im (933) | 20051130_58921_0400_PP | × | × |
| im (934) | 20051130_58962_0400_PP | × | × |
| im (935) | 20051130_58998_0400_PP | × | × |
| im (936) | 20051130_59029_0400_PP | × | × |
| im (937) | 20051130_59092_0400_PP | × | × |
| im (938) | 20051130_59186_0400_PP | × | × |
| im (939) | 20051130_59284_0400_PP | × | × |
| im (940) | 20051130_59374_0400_PP | × | × |
| im (941) | 20051130_59404_0400_PP | × | × |
| im (942) | 20051130_59432_0400_PP | × | × |
| im (943) | 20051130_59457_0400_PP | × | × |
| im (944) | 20051130_59464_0400_PP | × | × |
| im (945) | 20051130_59749_0400_PP | × | × |
| im (946) | 20051130_59775_0400_PP | × | × |
| im (947) | 20051130_59793_0400_PP | × | × |
| im (948) | 20051130_59802_0400_PP | × | × |
| im (949) | 20051130_59825_0400_PP | × | × |
| im (950) | 20051130_59850_0400_PP | × | × |
| im (951) | 20051130_59869_0400_PP | × | × |
| im (952) | 20051130_59916_0400_PP | × | × |
| im (953) | 20051130_59930_0400_PP | × | × |
| im (954) | 20051130_59964_0400_PP | × | × |
| im (955) | 20051130_59993_0400_PP | × | × |
| im (956) | 20051130_60040_0400_PP | × | × |
| im (957) | 20051130_60066_0400_PP | × | × |
| im (958) | 20051130_60140_0400_PP | × | × |
| im (959) | 20051130_60186_0400_PP | × | × |
| im (960) | 20051130_60234_0400_PP | × | × |
| im (961) | 20051130_60448_0400_PP | × | × |
| im (962) | 20051130_60490_0400_PP | × | × |
| im (963) | 20051130_60532_0400_PP | × | × |
| im (964) | 20051130_60562_0400_PP | × | × |
| im (965) | 20051130_60585_0400_PP | × | × |
| im (966) | 20051130_60601_0400_PP | × | × |
| im (967) | 20051130_60630_0400_PP | × | × |
| im (968) | 20051130_60658_0400_PP | × | × |
| im (969) | 20051130_60691_0400_PP | × | × |
| im (970) | 20051130_60715_0400_PP | × | × |
| im (971) | 20051130_60740_0400_PP | × | × |
| im (972) | 20051130_60760_0400_PP | × | × |
| im (973) | 20051130_60794_0400_PP | × | × |
| im (974) | 20051130_60822_0400_PP | × | × |
| im (975) | 20051201_37312_0400_PP | × | × |
| im (976) | 20051201_37337_0400_PP | × | × |
| im (977) | 20051201_37362_0400_PP | × | × |
| im (978) | 20051201_37382_0400_PP | × | × |
| im (979) | 20051201_37390_0400_PP | × | × |
| im (980) | 20051201_37409_0400_PP | × | × |
| im (981) | 20051201_37462_0400_PP | × | × |
| im (982) | 20051201_37534_0400_PP | × | × |
| im (983) | 20051201_37557_0400_PP | × | × |
| im (984) | 20051201_38041_0400_PP | × | × |
| im (985) | 20051201_38081_0400_PP | × | × |
| im (986) | 20051201_38103_0400_PP | × | × |
| im (987) | 20051201_38137_0400_PP | × | × |
| im (988) | 20051201_38155_0400_PP | × | × |
| im (989) | 20051201_38164_0400_PP | × | × |
| im (990) | 20051201_38182_0400_PP | × | × |
| im (991) | 20051201_38199_0400_PP | × | × |
| im (992) | 20051201_38211_0400_PP | × | × |
| im (993) | 20051201_38246_0400_PP | × | × |
| im (994) | 20051201_38262_0400_PP | × | × |
| im (995) | 20051201_38280_0400_PP | × | × |
| im (996) | 20051201_38291_0400_PP | × | × |
| im (997) | 20051201_38321_0400_PP | × | × |
| im (998) | 20051201_38349_0400_PP | × | × |
| im (999) | 20051201_38411_0400_PP | × | × |
| im (1000) | 20051201_38466_0400_PP | × | × |

## A.3 Ground truth of MESSIDOR (continued)

| Image Title | Filename | MA/ HM | HE |
|---|---|---|---|
| im (1001) | 20051201_38475_0400_PP | × | × |
| im (1002) | 20051201_38506_0400_PP | × | × |
| im (1003) | 20051201_38537_0400_PP | × | × |
| im (1004) | 20051202_36970_0400_PP | ✓ | × |
| im (1005) | 20051202_37003_0400_PP | ✓ | × |
| im (1006) | 20051202_37011_0400_PP | ✓ | × |
| im (1007) | 20051202_37162_0400_PP | ✓ | × |
| im (1008) | 20051202_37199_0400_PP | ✓ | ✓ |
| im (1009) | 20051202_37227_0400_PP | ✓ | × |
| im (1010) | 20051202_37349_0400_PP | ✓ | × |
| im (1011) | 20051202_38513_0400_PP | ✓ | × |
| im (1012) | 20051202_39630_0400_PP | ✓ | × |
| im (1013) | 20051202_39708_0400_PP | ✓ | ✓ |
| im (1014) | 20051202_39797_0400_PP | ✓ | × |
| im (1015) | 20051202_40508_0400_PP | ✓ | ✓ |
| im (1016) | 20051202_41034_0400_PP | ✓ | × |
| im (1017) | 20051202_41076_0400_PP | ✓ | ✓ |
| im (1018) | 20051202_41143_0400_PP | ✓ | ✓ |
| im (1019) | 20051202_41238_0400_PP | ✓ | × |
| im (1020) | 20051202_41260_0400_PP | ✓ | × |
| im (1021) | 20051202_48232_0400_PP | ✓ | × |
| im (1022) | 20051202_48264_0400_PP | ✓ | × |
| im (1023) | 20051202_48287_0400_PP | ✓ | × |
| im (1024) | 20051202_48310_0400_PP | ✓ | × |
| im (1025) | 20051202_48329_0400_PP | ✓ | ✓ |
| im (1026) | 20051202_48393_0400_PP | ✓ | × |
| im (1027) | 20051202_48421_0400_PP | ✓ | × |
| im (1028) | 20051202_48443_0400_PP | ✓ | ✓ |
| im (1029) | 20051202_48575_0400_PP | ✓ | × |
| im (1030) | 20051202_48586_0400_PP | ✓ | × |
| im (1031) | 20051202_51488_0400_PP | ✓ | ✓ |
| im (1032) | 20051202_51518_0400_PP | ✓ | × |
| im (1033) | 20051202_51574_0400_PP | ✓ | × |
| im (1034) | 20051202_51599_0400_PP | ✓ | × |
| im (1035) | 20051202_51616_0400_PP | ✓ | × |
| im (1036) | 20051202_51655_0400_PP | ✓ | × |
| im (1037) | 20051202_51677_0400_PP | ✓ | ✓ |
| im (1038) | 20051202_54197_0400_PP | ✓ | × |
| im (1039) | 20051202_54208_0400_PP | ✓ | × |
| im (1040) | 20051202_54477_0400_PP | ✓ | × |
| im (1041) | 20051202_54498_0400_PP | ✓ | ✓ |
| im (1042) | 20051202_54530_0400_PP | ✓ | ✓ |
| im (1043) | 20051202_54547_0400_PP | ✓ | × |
| im (1044) | 20051202_54555_0400_PP | ✓ | × |
| im (1045) | 20051202_54576_0400_PP | ✓ | ✓ |
| im (1046) | 20051202_54611_0400_PP | ✓ | ✓ |
| im (1047) | 20051202_54744_0400_PP | ✓ | × |
| im (1048) | 20051202_54783_0400_PP | ✓ | ✓ |
| im (1049) | 20051202_55457_0400_PP | ✓ | ✓ |
| im (1050) | 20051202_55484_0400_PP | ✓ | × |
| im (1051) | 20051202_55498_0400_PP | ✓ | × |
| im (1052) | 20051202_55525_0400_PP | ✓ | ✓ |
| im (1053) | 20051202_55562_0400_PP | ✓ | × |
| im (1054) | 20051202_55582_0400_PP | ✓ | × |
| im (1055) | 20051202_55607_0400_PP | ✓ | ✓ |
| im (1056) | 20051202_55626_0400_PP | ✓ | × |
| im (1057) | 20051202_55650_0400_PP | ✓ | × |
| im (1058) | 20051202_55669_0400_PP | ✓ | × |
| im (1059) | 20051202_55697_0400_PP | ✓ | × |
| im (1060) | 20051202_55735_0400_PP | ✓ | × |
| im (1061) | 20051202_55742_0400_PP | ✓ | × |
| im (1062) | 20051202_55767_0400_PP | ✓ | × |
| im (1063) | 20051202_55777_0400_PP | ✓ | × |
| im (1064) | 20051202_55797_0400_PP | ✓ | × |
| im (1065) | 20051202_55816_0400_PP | ✓ | × |
| im (1066) | 20051202_55834_0400_PP | ✓ | × |
| im (1067) | 20051202_55846_0400_PP | ✓ | × |
| im (1068) | 20051202_55869_0400_PP | ✓ | × |
| im (1069) | 20051202_55883_0400_PP | ✓ | × |
| im (1070) | 20051202_55921_0400_PP | ✓ | ✓ |
| im (1071) | 20051202_55944_0400_PP | ✓ | ✓ |
| im (1072) | 20051202_55969_0400_PP | ✓ | × |
| im (1073) | 20051202_55984_0400_PP | ✓ | ✓ |
| im (1074) | 20051202_56000_0400_PP | ✓ | ✓ |
| im (1075) | 20051202_56012_0400_PP | ✓ | ✓ |
| im (1076) | 20051202_56028_0400_PP | ✓ | ✓ |
| im (1077) | 20051202_56050_0400_PP | ✓ | ✓ |
| im (1078) | 20051205_31388_0400_PP | ✓ | ✓ |
| im (1079) | 20051205_31396_0400_PP | ✓ | × |
| im (1080) | 20051205_31934_0400_PP | ✓ | ✓ |
| im (1081) | 20051205_31949_0400_PP | ✓ | × |
| im (1082) | 20051205_31994_0400_PP | ✓ | × |
| im (1083) | 20051205_32966_0400_PP | ✓ | ✓ |
| im (1084) | 20051205_32981_0400_PP | ✓ | × |
| im (1085) | 20051205_33006_0400_PP | ✓ | ✓ |
| im (1086) | 20051205_33012_0400_PP | ✓ | ✓ |
| im (1087) | 20051205_33025_0400_PP | ✓ | × |
| im (1088) | 20051205_35099_0400_PP | ✓ | ✓ |
| im (1089) | 20051205_35110_0400_PP | ✓ | × |
| im (1090) | 20051205_35142_0400_PP | ✓ | ✓ |
| im (1091) | 20051205_35162_0400_PP | ✓ | × |
| im (1092) | 20051205_35201_0400_PP | ✓ | ✓ |
| im (1093) | 20051205_35224_0400_PP | ✓ | × |
| im (1094) | 20051205_35246_0400_PP | ✓ | ✓ |
| im (1095) | 20051205_35276_0400_PP | ✓ | × |
| im (1096) | 20051205_35305_0400_PP | ✓ | × |
| im (1097) | 20051205_35323_0400_PP | ✓ | ✓ |
| im (1098) | 20051205_35339_0400_PP | ✓ | ✓ |
| im (1099) | 20051205_35354_0400_PP | ✓ | ✓ |
| im (1100) | 20051205_35392_0400_PP | ✓ | ✓ |

## A.3 Ground truth of MESSIDOR (continued)

| Image Title | Filename | MA/ HM | HE |
|---|---|---|---|
| im (1101) | 20051205_35408_0400_PP | ✓ | × |
| im (1102) | 20051205_35417_0400_PP | ✓ | ✓ |
| im (1103) | 20051205_35432_0400_PP | ✓ | ✓ |
| im (1104) | 20051205_57548_0400_PP | × | × |
| im (1105) | 20051205_57651_0400_PP | × | × |
| im (1106) | 20051205_57704_0400_PP | × | × |
| im (1107) | 20051205_57723_0400_PP | × | × |
| im (1108) | 20051205_57757_0400_PP | × | × |
| im (1109) | 20051205_57780_0400_PP | × | × |
| im (1110) | 20051205_57799_0400_PP | × | × |
| im (1111) | 20051205_57809_0400_PP | × | × |
| im (1112) | 20051205_57838_0400_PP | × | × |
| im (1113) | 20051205_57879_0400_PP | × | × |
| im (1114) | 20051205_57942_0400_PP | × | × |
| im (1115) | 20051205_57988_0400_PP | × | × |
| im (1116) | 20051205_58010_0400_PP | × | × |
| im (1117) | 20051205_58037_0400_PP | × | × |
| im (1118) | 20051205_58060_0400_PP | × | × |
| im (1119) | 20051205_58080_0400_PP | × | × |
| im (1120) | 20051205_58091_0400_PP | × | × |
| im (1121) | 20051205_58109_0400_PP | × | × |
| im (1122) | 20051205_58125_0400_PP | × | × |
| im (1123) | 20051205_58150_0400_PP | × | × |
| im (1124) | 20051205_58177_0400_PP | × | × |
| im (1125) | 20051205_58354_0400_PP | × | × |
| im (1126) | 20051205_58373_0400_PP | × | × |
| im (1127) | 20051205_58409_0400_PP | × | × |
| im (1128) | 20051205_58431_0400_PP | × | × |
| im (1129) | 20051205_58458_0400_PP | × | × |
| im (1130) | 20051205_58502_0400_PP | × | × |
| im (1131) | 20051205_58577_0400_PP | × | × |
| im (1132) | 20051205_58613_0400_PP | × | × |
| im (1133) | 20051205_59240_0400_PP | × | × |
| im (1134) | 20051205_59300_0400_PP | × | × |
| im (1135) | 20051205_59337_0400_PP | × | × |
| im (1136) | 20051205_59351_0400_PP | × | × |
| im (1137) | 20051205_59367_0400_PP | × | × |
| im (1138) | 20051205_59379_0400_PP | × | × |
| im (1139) | 20051205_59510_0400_PP | × | × |
| im (1140) | 20051205_59538_0400_PP | × | × |
| im (1141) | 20051205_59617_0400_PP | × | × |
| im (1142) | 20051205_59651_0400_PP | × | × |
| im (1143) | 20051205_59702_0400_PP | × | × |
| im (1144) | 20051205_59715_0400_PP | × | × |
| im (1145) | 20051205_59738_0400_PP | × | × |
| im (1146) | 20051205_59754_0400_PP | × | × |
| im (1147) | 20051205_59804_0400_PP | × | × |
| im (1148) | 20051205_59833_0400_PP | × | × |
| im (1149) | 20051205_59858_0400_PP | × | × |
| im (1150) | 20051205_59879_0400_PP | × | × |
| im (1151) | 20051205_59901_0400_PP | × | × |
| im (1152) | 20051205_59923_0400_PP | × | × |
| im (1153) | 20051205_60093_0400_PP | × | × |
| im (1154) | 20051205_60119_0400_PP | × | × |
| im (1155) | 20051207_54614_0400_PP | ✓ | ✓ |
| im (1156) | 20051207_55266_0400_PP | ✓ | ✓ |
| im (1157) | 20051207_56219_0400_PP | ✓ | ✓ |
| im (1158) | 20051207_56227_0400_PP | ✓ | ✓ |
| im (1159) | 20051207_62252_0400_PP | ✓ | × |
| im (1160) | 20051207_62266_0400_PP | ✓ | × |
| im (1161) | 20051207_62275_0400_PP | ✓ | × |
| im (1162) | 20051207_62320_0400_PP | ✓ | × |
| im (1163) | 20051208_39243_0400_PP | ✓ | ✓ |
| im (1164) | 20051208_39254_0400_PP | ✓ | × |
| im (1165) | 20051208_39297_0400_PP | ✓ | ✓ |
| im (1166) | 20051208_39404_0400_PP | ✓ | × |
| im (1167) | 20051208_39438_0400_PP | ✓ | ✓ |
| im (1168) | 20051208_39462_0400_PP | ✓ | × |
| im (1169) | 20051208_39484_0400_PP | ✓ | × |
| im (1170) | 20051208_39498_0400_PP | ✓ | ✓ |
| im (1171) | 20051208_39524_0400_PP | ✓ | × |
| im (1172) | 20051208_39532_0400_PP | ✓ | × |
| im (1173) | 20051208_39546_0400_PP | ✓ | × |
| im (1174) | 20051208_39572_0400_PP | ✓ | × |
| im (1175) | 20051208_40972_0400_PP | ✓ | ✓ |
| im (1176) | 20051208_41318_0400_PP | ✓ | ✓ |
| im (1177) | 20051208_41373_0400_PP | ✓ | ✓ |
| im (1178) | 20051208_41570_0400_PP | ✓ | × |
| im (1179) | 20051208_41707_0400_PP | ✓ | × |
| im (1180) | 20051208_42314_0400_PP | ✓ | × |
| im (1181) | 20051208_42322_0400_PP | ✓ | ✓ |
| im (1182) | 20051208_42546_0400_PP | ✓ | ✓ |
| im (1183) | 20051208_42552_0400_PP | ✓ | × |
| im (1184) | 20051209_38404_0400_PP | ✓ | × |
| im (1185) | 20051212_36525_0400_PP | ✓ | × |
| im (1186) | 20051212_36548_0400_PP | ✓ | × |
| im (1187) | 20051212_36605_0400_PP | ✓ | × |
| im (1188) | 20051212_36640_0400_PP | ✓ | × |
| im (1189) | 20051212_37442_0400_PP | ✓ | × |
| im (1190) | 20051212_38000_0400_PP | ✓ | × |
| im (1191) | 20051212_38043_0400_PP | ✓ | × |
| im (1192) | 20051212_38076_0400_PP | ✓ | ✓ |
| im (1193) | 20051212_38106_0400_PP | ✓ | ✓ |
| im (1194) | 20051212_38130_0400_PP | ✓ | × |
| im (1195) | 20051212_38161_0400_PP | ✓ | × |
| im (1196) | 20051212_40940_0400_PP | ✓ | ✓ |
| im (1197) | 20051212_41009_0400_PP | ✓ | ✓ |
| im (1198) | 20051212_41144_0400_PP | ✓ | ✓ |
| im (1199) | 20051212_41169_0400_PP | ✓ | × |
| im (1200) | 20051212_41432_0400_PP | ✓ | ✓ |

# Appendix B. Quantitative Results of Segmenting the Optic Disc

## B.1. Results on ARIA

| Image Title | Response |
|---|---|
| im (1) | ✓ |
| im (2) | ✓ |
| im (3) | ✓ |
| im (4) | ✓ |
| im (5) | ✓ |
| im (6) | × |
| im (7) | ✓ |
| im (8) | × |
| im (9) | ✓ |
| im (10) | × |
| im (11) | ✓ |
| im (12) | × |
| im (13) | × |
| im (14) | × |
| im (15) | ✓ |
| im (16) | × |
| im (17) | ✓ |
| im (18) | ✓ |
| im (19) | ✓ |
| im (20) | ✓ |
| im (21) | ✓ |
| im (22) | ✓ |
| im (23) | ✓ |
| im (24) | ✓ |
| im (25) | × |
| im (26) | ✓ |
| im (27) | ✓ |
| im (28) | ✓ |
| im (29) | ✓ |
| im (30) | ✓ |
| im (31) | ✓ |
| im (32) | ✓ |
| im (33) | ✓ |
| im (34) | ✓ |
| im (35) | ✓ |
| im (36) | ✓ |
| im (37) | ✓ |
| im (38) | ✓ |
| im (39) | ✓ |
| im (40) | ✓ |
| im (41) | ✓ |
| im (42) | ✓ |
| im (43) | ✓ |
| im (44) | ✓ |
| im (45) | ✓ |
| im (46) | ✓ |
| im (47) | ✓ |
| im (48) | ✓ |
| im (49) | ✓ |
| im (50) | ✓ |
| im (51) | ✓ |
| im (52) | ✓ |
| im (53) | ✓ |
| im (54) | ✓ |
| im (55) | ✓ |
| im (56) | ✓ |
| im (57) | ✓ |
| im (58) | ✓ |
| im (59) | ✓ |
| im (60) | ✓ |
| im (61) | × |
| im (62) | ✓ |
| im (63) | ✓ |
| im (64) | ✓ |
| im (65) | ✓ |
| im (66) | ✓ |
| im (67) | ✓ |
| im (68) | ✓ |
| im (69) | ✓ |
| im (70) | ✓ |
| im (71) | × |
| im (72) | ✓ |
| im (73) | ✓ |
| im (74) | ✓ |
| im (75) | ✓ |
| im (76) | × |
| im (77) | ✓ |
| im (78) | ✓ |
| im (79) | ✓ |
| im (80) | ✓ |
| im (81) | ✓ |
| im (82) | ✓ |
| im (83) | ✓ |
| im (84) | ✓ |
| im (85) | × |
| im (86) | ✓ |
| im (87) | ✓ |
| im (88) | × |
| im (89) | ✓ |
| im (90) | ✓ |
| im (91) | ✓ |
| im (92) | ✓ |
| im (93) | ✓ |
| im (94) | ✓ |
| im (95) | ✓ |
| im (96) | ✓ |
| im (97) | ✓ |
| im (98) | ✓ |
| im (99) | ✓ |
| im (100) | ✓ |
| im (101) | ✓ |
| im (102) | ✓ |
| im (103) | × |
| im (104) | ✓ |
| im (105) | ✓ |
| im (106) | × |
| im (107) | ✓ |
| im (108) | ✓ |
| im (109) | ✓ |
| im (110) | × |
| im (111) | × |
| im (112) | × |
| im (113) | ✓ |
| im (114) | ✓ |
| im (115) | ✓ |
| im (116) | ✓ |
| im (117) | ✓ |
| im (118) | × |
| im (119) | ✓ |
| im (120) | ✓ |
| im (121) | × |
| im (122) | × |
| im (123) | × |
| im (124) | ✓ |
| im (125) | ✓ |
| im (126) | ✓ |
| im (127) | ✓ |
| im (128) | ✓ |
| im (129) | ✓ |

## B.1. Results on ARIA (continued)

| Image Title | Response |
|---|---|
| im (130) | ✓ |
| im (131) | ✓ |
| im (132) | ✓ |
| im (133) | ✓ |
| im (134) | ✓ |
| im (135) | ✓ |
| im (136) | ✓ |
| im (137) | ✓ |
| im (138) | ✓ |
| im (139) | ✓ |
| im (140) | ✓ |
| im (141) | ✓ |
| im (142) | ✓ |
| im (143) | ✓ |
| **Sensitivity** | **0.8462** |

## B.2. Results on DIARETDB0

| Image Title | Response |
|---|---|
| im (1) | ✓ |
| im (2) | ✓ |
| im (3) | ✓ |
| im (4) | ✓ |
| im (5) | ✓ |
| im (6) | ✓ |
| im (7) | ✓ |
| im (8) | ✓ |
| im (9) | ✓ |
| im (10) | ✓ |
| im (11) | ✓ |
| im (12) | ✓ |
| im (13) | ✓ |
| im (14) | ✓ |
| im (15) | ✓ |
| im (16) | ✓ |
| im (17) | ✓ |
| im (18) | ✓ |
| im (19) | × |
| im (20) | × |
| im (21) | ✓ |
| im (22) | × |
| im (23) | ✓ |
| im (24) | × |
| im (25) | ✓ |
| im (26) | ✓ |
| im (27) | ✓ |
| im (28) | ✓ |
| im (29) | ✓ |
| im (30) | × |
| im (31) | ✓ |
| im (32) | ✓ |
| im (33) | ✓ |
| im (34) | ✓ |
| im (35) | × |
| im (36) | × |
| im (37) | ✓ |
| im (38) | ✓ |
| im (39) | ✓ |
| im (40) | ✓ |
| im (41) | ✓ |
| im (42) | ✓ |
| im (43) | ✓ |
| im (44) | ✓ |
| im (45) | ✓ |
| im (46) | ✓ |
| im (47) | ✓ |
| im (48) | ✓ |
| im (49) | ✓ |
| im (50) | ✓ |
| im (51) | ✓ |
| im (52) | ✓ |
| im (53) | ✓ |
| im (54) | ✓ |
| im (55) | ✓ |
| im (56) | ✓ |
| im (57) | ✓ |
| im (58) | ✓ |
| im (59) | × |
| im (60) | ✓ |
| im (61) | ✓ |
| im (62) | ✓ |
| im (63) | ✓ |
| im (64) | ✓ |
| im (65) | ✓ |
| im (66) | ✓ |
| im (67) | ✓ |
| im (68) | ✓ |
| im (69) | ✓ |
| im (70) | ✓ |
| im (71) | ✓ |
| im (72) | ✓ |
| im (73) | ✓ |
| im (74) | ✓ |
| im (75) | ✓ |
| im (76) | ✓ |
| im (77) | ✓ |
| im (78) | ✓ |
| im (79) | ✓ |
| im (80) | ✓ |
| im (81) | ✓ |
| im (82) | ✓ |
| im (83) | ✓ |
| im (84) | ✓ |
| im (85) | ✓ |
| im (86) | ✓ |
| im (87) | ✓ |
| im (88) | ✓ |
| im (89) | ✓ |
| im (90) | ✓ |
| im (91) | ✓ |
| im (92) | ✓ |
| im (93) | ✓ |
| im (94) | ✓ |
| im (95) | ✓ |
| im (96) | × |
| im (97) | ✓ |
| im (98) | ✓ |
| im (99) | ✓ |
| im (100) | ✓ |
| im (101) | ✓ |
| im (102) | × |
| im (103) | ✓ |
| im (104) | ✓ |
| im (105) | ✓ |
| im (106) | ✓ |
| im (107) | ✓ |
| im (108) | ✓ |
| im (109) | ✓ |
| im (110) | × |
| im (111) | ✓ |
| im (112) | ✓ |
| im (113) | ✓ |
| im (114) | ✓ |
| im (115) | ✓ |
| im (116) | ✓ |
| im (117) | × |
| im (118) | ✓ |
| im (119) | ✓ |
| im (120) | ✓ |
| im (121) | ✓ |
| im (122) | ✓ |
| im (123) | ✓ |
| im (124) | ✓ |
| im (125) | ✓ |
| im (126) | ✓ |
| im (127) | ✓ |
| im (128) | ✓ |
| im (129) | × |
| im (130) | ✓ |
| **Sensitivity** | **0.9000** |

## B.3. Results on DIARETDB1

| Image Title | Response |
|---|---|
| im (1) | ✓ |
| im (2) | ✓ |
| im (3) | ✓ |
| im (4) | × |
| im (5) | ✓ |
| im (6) | ✓ |
| im (7) | ✓ |
| im (8) | ✓ |
| im (9) | ✓ |
| im (10) | ✓ |
| im (11) | ✓ |
| im (12) | × |
| im (13) | ✓ |
| im (14) | ✓ |
| im (15) | ✓ |
| im (16) | ✓ |
| im (17) | ✓ |
| im (18) | ✓ |
| im (19) | ✓ |
| im (20) | ✓ |
| im (21) | × |
| im (22) | ✓ |
| im (23) | × |
| im (24) | ✓ |
| im (25) | ✓ |
| im (26) | ✓ |
| im (27) | ✓ |
| im (28) | ✓ |
| im (29) | ✓ |
| im (30) | ✓ |
| im (31) | ✓ |
| im (32) | ✓ |
| im (33) | ✓ |
| im (34) | ✓ |
| im (35) | ✓ |
| im (36) | ✓ |
| im (37) | × |
| im (38) | ✓ |
| im (39) | ✓ |
| im (40) | ✓ |
| im (41) | ✓ |
| im (42) | ✓ |
| im (43) | ✓ |
| im (44) | ✓ |
| im (45) | ✓ |
| im (46) | ✓ |
| im (47) | ✓ |
| im (48) | ✓ |
| im (49) | ✓ |
| im (50) | ✓ |
| im (51) | ✓ |
| im (52) | ✓ |
| im (53) | ✓ |
| im (54) | ✓ |
| im (55) | ✓ |
| im (56) | ✓ |
| im (57) | ✓ |
| im (58) | ✓ |
| im (59) | × |
| im (60) | ✓ |
| im (61) | ✓ |
| im (62) | ✓ |
| im (63) | ✓ |
| im (64) | × |
| im (65) | ✓ |
| im (66) | ✓ |
| im (67) | ✓ |
| im (68) | ✓ |
| im (69) | ✓ |
| im (70) | ✓ |
| im (71) | ✓ |
| im (72) | ✓ |
| im (73) | ✓ |
| im (74) | ✓ |
| im (75) | ✓ |
| im (76) | ✓ |
| im (77) | ✓ |
| im (78) | ✓ |
| im (79) | ✓ |
| im (80) | ✓ |
| im (81) | ✓ |
| im (82) | ✓ |
| im (83) | ✓ |
| im (84) | ✓ |
| im (85) | ✓ |
| im (86) | × |
| im (87) | × |
| im (88) | ✓ |
| im (89) | × |
| **Sensitivity** | **0.8876** |

## B.4. Results on DRIONS-DB

| Image Title | Response |
|---|---|
| im (1) | ✓ |
| im (2) | ✓ |
| im (3) | ✓ |
| im (4) | ✓ |
| im (5) | ✓ |
| im (6) | ✓ |
| im (7) | ✓ |
| im (8) | ✓ |
| im (9) | ✓ |
| im (10) | ✓ |
| im (11) | ✓ |
| im (12) | ✓ |
| im (13) | ✓ |
| im (14) | ✓ |
| im (15) | ✓ |
| im (16) | ✓ |
| im (17) | ✓ |
| im (18) | ✓ |
| im (19) | ✓ |
| im (20) | ✓ |
| im (21) | ✓ |
| im (22) | ✓ |
| im (23) | ✓ |
| im (24) | ✓ |
| im (25) | ✓ |
| im (26) | ✓ |
| im (27) | ✓ |
| im (28) | ✓ |
| im (29) | ✓ |
| im (30) | ✓ |
| im (31) | ✓ |
| im (32) | ✓ |
| im (33) | ✓ |
| im (34) | ✓ |
| im (35) | ✓ |
| im (36) | ✓ |
| im (37) | ✓ |
| im (38) | ✓ |
| im (39) | ✓ |
| im (40) | ✓ |
| im (41) | ✓ |
| im (42) | ✓ |
| im (43) | ✓ |
| im (44) | ✓ |
| im (45) | ✓ |
| im (46) | ✓ |
| im (47) | ✓ |
| im (48) | ✓ |
| im (49) | ✓ |
| im (50) | ✓ |
| im (51) | ✓ |
| im (52) | ✓ |
| im (53) | ✓ |
| im (54) | ✓ |
| im (55) | ✓ |
| im (56) | ✓ |
| im (57) | ✓ |
| im (58) | ✓ |
| im (59) | ✓ |
| im (60) | ✓ |
| im (61) | ✓ |
| im (62) | ✓ |
| im (63) | ✓ |
| im (64) | ✓ |
| im (65) | ✓ |
| im (66) | ✓ |
| im (67) | ✓ |
| im (68) | ✓ |
| im (69) | ✓ |
| im (70) | ✓ |
| im (71) | ✓ |
| im (72) | ✓ |
| im (73) | ✓ |
| im (74) | ✓ |
| im (75) | ✓ |
| im (76) | ✓ |
| im (77) | ✓ |
| im (78) | ✓ |
| im (79) | ✓ |
| im (80) | ✓ |
| im (81) | ✓ |
| im (82) | ✓ |
| im (83) | ✓ |
| im (84) | ✓ |
| im (85) | ✓ |
| im (86) | ✓ |
| im (87) | ✓ |
| im (88) | ✓ |
| im (89) | ✓ |
| im (90) | ✓ |
| im (91) | ✓ |
| im (92) | ✓ |
| im (93) | ✓ |
| im (94) | ✓ |
| im (95) | ✓ |
| im (96) | ✓ |
| im (97) | ✓ |
| im (98) | ✓ |
| im (99) | ✓ |
| im (100) | ✓ |
| im (101) | ✓ |
| im (102) | ✓ |
| im (103) | ✓ |
| im (104) | ✓ |
| im (105) | ✓ |
| im (106) | ✓ |
| im (107) | ✓ |
| im (108) | ✓ |
| im (109) | ✓ |
| im (110) | ✓ |
| **Sensitivity** | **1.0000** |

## B.5. Results on DRIVE

| Image Title | Response |
|---|---|
| im (1) | ✓ |
| im (2) | ✓ |
| im (3) | ✓ |
| im (4) | ✓ |
| im (5) | ✓ |
| im (6) | ✓ |
| im (7) | ✓ |
| im (8) | ✓ |
| im (9) | ✓ |
| im (10) | ✓ |
| im (11) | ✓ |
| im (12) | ✓ |
| im (13) | ✓ |
| im (14) | ✓ |
| im (15) | ✓ |
| im (16) | ✓ |
| im (17) | ✓ |
| im (18) | ✓ |
| im (19) | ✓ |
| im (20) | ✓ |
| im (21) | ✓ |
| im (22) | ✓ |
| im (23) | ✓ |
| im (24) | ✓ |
| im (25) | ✓ |
| im (26) | ✓ |
| im (27) | ✓ |
| im (28) | ✓ |
| im (29) | ✓ |
| im (30) | ✓ |
| im (31) | ✓ |
| im (32) | ✓ |
| im (33) | ✓ |
| im (34) | × |
| im (35) | ✓ |
| im (36) | ✓ |
| im (37) | ✓ |
| im (38) | ✓ |
| im (39) | ✓ |
| im (40) | ✓ |
| **Sensitivity** | **0.9750** |

## B.6. Results on HRF

| Image Title | Response |
|---|---|
| im (1) | ✓ |
| im (2) | ✓ |
| im (3) | ✓ |
| im (4) | ✓ |
| im (5) | ✓ |
| im (6) | ✓ |
| im (7) | ✓ |
| im (8) | ✓ |
| im (9) | ✓ |
| im (10) | ✓ |
| im (11) | ✓ |
| im (12) | ✓ |
| im (13) | ✓ |
| im (14) | ✓ |
| im (15) | ✓ |
| im (16) | ✓ |
| im (17) | ✓ |
| im (18) | ✓ |
| im (19) | ✓ |
| im (20) | ✓ |
| im (21) | ✓ |
| im (22) | ✓ |
| im (23) | ✓ |
| im (24) | ✗ |
| im (25) | ✓ |
| im (26) | ✓ |
| im (27) | ✓ |
| im (28) | ✓ |
| im (29) | ✓ |
| im (30) | ✓ |
| im (31) | ✓ |
| im (32) | ✓ |
| im (33) | ✓ |
| im (34) | ✓ |
| im (35) | ✓ |
| im (36) | ✓ |
| im (37) | ✗ |
| im (38) | ✓ |
| im (39) | ✓ |
| im (40) | ✓ |
| im (41) | ✓ |
| im (42) | ✓ |
| im (43) | ✓ |
| im (44) | ✓ |
| im (45) | ✓ |
| **Sensitivity** | **0.9556** |

## B.7. Results on MESSIDOR

| Image Title | Response |
|---|---|
| im (1) | ✓ |
| im (2) | ✓ |
| im (3) | ✓ |
| im (4) | ✓ |
| im (5) | ✓ |
| im (6) | ✓ |
| im (7) | ✓ |
| im (8) | ✓ |
| im (9) | ✓ |
| im (10) | ✓ |
| im (11) | ✓ |
| im (12) | ✓ |
| im (13) | ✓ |
| im (14) | ✓ |
| im (15) | ✓ |
| im (16) | ✓ |
| im (17) | ✓ |
| im (18) | ✓ |
| im (19) | ✓ |
| im (20) | ✓ |
| im (21) | ✓ |
| im (22) | ✓ |
| im (23) | ✓ |
| im (24) | ✓ |
| im (25) | ✓ |
| im (26) | ✓ |
| im (27) | ✓ |
| im (28) | ✓ |
| im (29) | ✓ |
| im (30) | ✓ |
| im (31) | ✓ |
| im (32) | ✓ |
| im (33) | ✓ |
| im (34) | ✓ |
| im (35) | ✓ |
| im (36) | ✓ |
| im (37) | ✓ |
| im (38) | ✓ |
| im (39) | ✓ |
| im (40) | ✓ |
| im (41) | ✓ |
| im (42) | ✓ |
| im (43) | ✓ |
| im (44) | ✓ |
| im (45) | ✓ |
| im (46) | ✓ |
| im (47) | ✓ |
| im (48) | ✓ |
| im (49) | ✓ |
| im (50) | ✓ |
| im (51) | ✓ |
| im (52) | ✓ |
| im (53) | ✓ |
| im (54) | ✓ |
| im (55) | ✓ |
| im (56) | ✓ |
| im (57) | ✓ |
| im (58) | ✓ |
| im (59) | ✓ |
| im (60) | ✓ |
| im (61) | ✓ |
| im (62) | ✓ |
| im (63) | ✓ |
| im (64) | ✓ |
| im (65) | ✓ |
| im (66) | ✓ |
| im (67) | ✓ |
| im (68) | ✓ |
| im (69) | ✓ |
| im (70) | ✓ |
| im (71) | ✓ |
| im (72) | ✓ |
| im (73) | ✓ |
| im (74) | ✓ |
| im (75) | ✓ |
| im (76) | ✓ |
| im (77) | × |
| im (78) | ✓ |
| im (79) | ✓ |
| im (80) | ✓ |
| im (81) | ✓ |
| im (82) | ✓ |
| im (83) | ✓ |
| im (84) | ✓ |
| im (85) | ✓ |
| im (86) | ✓ |
| im (87) | ✓ |
| im (88) | ✓ |
| im (89) | ✓ |
| im (90) | ✓ |
| im (91) | ✓ |
| im (92) | ✓ |
| im (93) | ✓ |
| im (94) | ✓ |
| im (95) | ✓ |
| im (96) | ✓ |
| im (97) | ✓ |
| im (98) | ✓ |
| im (99) | × |
| im (100) | ✓ |
| im (101) | ✓ |
| im (102) | ✓ |
| im (103) | ✓ |
| im (104) | ✓ |
| im (105) | ✓ |
| im (106) | ✓ |
| im (107) | ✓ |
| im (108) | ✓ |
| im (109) | ✓ |
| im (110) | ✓ |
| im (111) | ✓ |
| im (112) | ✓ |
| im (113) | ✓ |
| im (114) | ✓ |
| im (115) | ✓ |
| im (116) | ✓ |
| im (117) | ✓ |
| im (118) | ✓ |
| im (119) | ✓ |
| im (120) | ✓ |
| im (121) | ✓ |
| im (122) | ✓ |
| im (123) | ✓ |
| im (124) | ✓ |
| im (125) | ✓ |
| im (126) | ✓ |
| im (127) | ✓ |
| im (128) | ✓ |
| im (129) | ✓ |
| im (130) | ✓ |
| im (131) | ✓ |
| im (132) | ✓ |

## B.7. Results on MESSIDOR (continued)

| Image Title | Response |
|---|---|
| im (133) | ✓ |
| im (134) | ✓ |
| im (135) | ✓ |
| im (136) | ✓ |
| im (137) | ✓ |
| im (138) | ✓ |
| im (139) | ✓ |
| im (140) | ✓ |
| im (141) | ✓ |
| im (142) | ✓ |
| im (143) | ✓ |
| im (144) | ✓ |
| im (145) | ✓ |
| im (146) | ✓ |
| im (147) | ✓ |
| im (148) | ✓ |
| im (149) | ✓ |
| im (150) | ✓ |
| im (151) | ✓ |
| im (152) | ✓ |
| im (153) | ✓ |
| im (154) | ✓ |
| im (155) | ✓ |
| im (156) | ✓ |
| im (157) | ✓ |
| im (158) | ✓ |
| im (159) | ✓ |
| im (160) | ✓ |
| im (161) | ✓ |
| im (162) | ✓ |
| im (163) | ✓ |
| im (164) | ✓ |
| im (165) | ✓ |
| im (166) | ✓ |
| im (167) | ✓ |
| im (168) | ✓ |
| im (169) | ✓ |
| im (170) | ✓ |
| im (171) | ✓ |
| im (172) | ✓ |
| im (173) | ✓ |
| im (174) | ✓ |
| im (175) | ✓ |
| im (176) | ✓ |
| im (177) | ✓ |
| im (178) | ✓ |
| im (179) | ✓ |
| im (180) | ✓ |
| im (181) | ✓ |
| im (182) | ✓ |
| im (183) | ✓ |
| im (184) | ✓ |
| im (185) | ✓ |
| im (186) | ✓ |
| im (187) | ✓ |
| im (188) | ✓ |
| im (189) | ✓ |
| im (190) | ✓ |
| im (191) | ✓ |
| im (192) | ✓ |
| im (193) | ✓ |
| im (194) | ✓ |
| im (195) | ✓ |
| im (196) | ✓ |
| im (197) | ✓ |
| im (198) | ✓ |
| im (199) | ✓ |
| im (200) | ✓ |
| im (201) | ✓ |
| im (202) | ✓ |
| im (203) | ✓ |
| im (204) | ✓ |
| im (205) | ✓ |
| im (206) | ✓ |
| im (207) | ✓ |
| im (208) | ✓ |
| im (209) | ✓ |
| im (210) | ✓ |
| im (211) | ✓ |
| im (212) | ✓ |
| im (213) | ✓ |
| im (214) | ✓ |
| im (215) | ✓ |
| im (216) | ✓ |
| im (217) | ✓ |
| im (218) | ✓ |
| im (219) | ✓ |
| im (220) | ✓ |
| im (221) | ✓ |
| im (222) | ✓ |
| im (223) | ✓ |
| im (224) | ✓ |
| im (225) | ✓ |
| im (226) | ✓ |
| im (227) | ✓ |
| im (228) | ✓ |
| im (229) | ✓ |
| im (230) | ✓ |
| im (231) | ✓ |
| im (232) | ✓ |
| im (233) | ✓ |
| im (234) | ✓ |
| im (235) | ✓ |
| im (236) | ✓ |
| im (237) | ✓ |
| im (238) | ✓ |
| im (239) | ✓ |
| im (240) | ✓ |
| im (241) | ✓ |
| im (242) | ✓ |
| im (243) | ✓ |
| im (244) | ✓ |
| im (245) | ✓ |
| im (246) | ✓ |
| im (247) | ✓ |
| im (248) | × |
| im (249) | × |
| im (250) | ✓ |
| im (251) | ✓ |
| im (252) | ✓ |
| im (253) | ✓ |
| im (254) | ✓ |
| im (255) | ✓ |
| im (256) | ✓ |
| im (257) | ✓ |
| im (258) | ✓ |
| im (259) | ✓ |
| im (260) | ✓ |
| im (261) | ✓ |
| im (262) | ✓ |
| im (263) | ✓ |
| im (264) | ✓ |

## B.7. Results on MESSIDOR (continued)

| Image Title | Response |
|---|---|
| im (265) | ✓ |
| im (266) | ✓ |
| im (267) | ✓ |
| im (268) | ✓ |
| im (269) | ✓ |
| im (270) | ✓ |
| im (271) | ✓ |
| im (272) | ✓ |
| im (273) | ✓ |
| im (274) | ✓ |
| im (275) | ✓ |
| im (276) | ✓ |
| im (277) | ✓ |
| im (278) | ✓ |
| im (279) | ✓ |
| im (280) | ✓ |
| im (281) | ✓ |
| im (282) | ✓ |
| im (283) | ✓ |
| im (284) | ✓ |
| im (285) | ✓ |
| im (286) | ✓ |
| im (287) | ✓ |
| im (288) | ✓ |
| im (289) | ✓ |
| im (290) | ✓ |
| im (291) | ✓ |
| im (292) | ✓ |
| im (293) | ✓ |
| im (294) | ✓ |
| im (295) | ✓ |
| im (296) | ✓ |
| im (297) | ✓ |
| im (298) | ✓ |
| im (299) | ✓ |
| im (300) | ✓ |
| im (301) | ✓ |
| im (302) | ✓ |
| im (303) | ✓ |
| im (304) | ✓ |
| im (305) | ✓ |
| im (306) | ✓ |
| im (307) | ✓ |
| im (308) | ✓ |
| im (309) | ✓ |
| im (310) | ✓ |
| im (311) | ✓ |
| im (312) | ✓ |
| im (313) | ✓ |
| im (314) | ✓ |
| im (315) | ✓ |
| im (316) | ✓ |
| im (317) | ✓ |
| im (318) | ✓ |
| im (319) | ✓ |
| im (320) | ✓ |
| im (321) | ✓ |
| im (322) | ✓ |
| im (323) | ✓ |
| im (324) | ✓ |
| im (325) | ✓ |
| im (326) | ✓ |
| im (327) | ✓ |
| im (328) | ✓ |
| im (329) | ✓ |
| im (330) | ✓ |
| im (331) | ✓ |
| im (332) | ✓ |
| im (333) | ✓ |
| im (334) | ✓ |
| im (335) | ✓ |
| im (336) | ✓ |
| im (337) | ✓ |
| im (338) | ✓ |
| im (339) | ✓ |
| im (340) | ✓ |
| im (341) | ✓ |
| im (342) | ✓ |
| im (343) | ✓ |
| im (344) | ✓ |
| im (345) | ✓ |
| im (346) | ✓ |
| im (347) | ✓ |
| im (348) | ✓ |
| im (349) | ✓ |
| im (350) | ✓ |
| im (351) | ✓ |
| im (352) | ✓ |
| im (353) | ✓ |
| im (354) | ✓ |
| im (355) | ✓ |
| im (356) | ✓ |
| im (357) | ✓ |
| im (358) | ✓ |
| im (359) | ✓ |
| im (360) | ✓ |
| im (361) | ✓ |
| im (362) | ✓ |
| im (363) | ✓ |
| im (364) | ✓ |
| im (365) | ✓ |
| im (366) | ✓ |
| im (367) | × |
| im (368) | ✓ |
| im (369) | ✓ |
| im (370) | ✓ |
| im (371) | ✓ |
| im (372) | ✓ |
| im (373) | ✓ |
| im (374) | ✓ |
| im (375) | ✓ |
| im (376) | ✓ |
| im (377) | ✓ |
| im (378) | ✓ |
| im (379) | ✓ |
| im (380) | ✓ |
| im (381) | ✓ |
| im (382) | ✓ |
| im (383) | ✓ |
| im (384) | ✓ |
| im (385) | ✓ |
| im (386) | ✓ |
| im (387) | ✓ |
| im (388) | ✓ |
| im (389) | × |
| im (390) | ✓ |
| im (391) | ✓ |
| im (392) | ✓ |
| im (393) | ✓ |
| im (394) | ✓ |
| im (395) | ✓ |
| im (396) | ✓ |

## B.7. Results on MESSIDOR (continued)

| Image Title | Response |
|---|---|
| im (397) | ✓ |
| im (398) | ✓ |
| im (399) | ✓ |
| im (400) | ✓ |
| im (401) | ✓ |
| im (402) | ✓ |
| im (403) | ✓ |
| im (404) | ✓ |
| im (405) | ✓ |
| im (406) | ✓ |
| im (407) | ✓ |
| im (408) | ✓ |
| im (409) | ✓ |
| im (410) | ✓ |
| im (411) | ✓ |
| im (412) | ✓ |
| im (413) | ✓ |
| im (414) | ✓ |
| im (415) | × |
| im (416) | × |
| im (417) | ✓ |
| im (418) | ✓ |
| im (419) | ✓ |
| im (420) | ✓ |
| im (421) | ✓ |
| im (422) | ✓ |
| im (423) | ✓ |
| im (424) | × |
| im (425) | ✓ |
| im (426) | ✓ |
| im (427) | ✓ |
| im (428) | ✓ |
| im (429) | ✓ |
| im (430) | ✓ |
| im (431) | ✓ |
| im (432) | ✓ |
| im (433) | ✓ |
| im (434) | ✓ |
| im (435) | ✓ |
| im (436) | ✓ |
| im (437) | ✓ |
| im (438) | ✓ |
| im (439) | ✓ |
| im (440) | ✓ |
| im (441) | ✓ |
| im (442) | ✓ |
| im (443) | ✓ |
| im (444) | ✓ |
| im (445) | ✓ |
| im (446) | ✓ |
| im (447) | ✓ |
| im (448) | ✓ |
| im (449) | ✓ |
| im (450) | ✓ |
| im (451) | ✓ |
| im (452) | ✓ |
| im (453) | ✓ |
| im (454) | ✓ |
| im (455) | ✓ |
| im (456) | ✓ |
| im (457) | ✓ |
| im (458) | ✓ |
| im (459) | ✓ |
| im (460) | ✓ |
| im (461) | ✓ |
| im (462) | ✓ |
| im (463) | ✓ |
| im (464) | ✓ |
| im (465) | ✓ |
| im (466) | ✓ |
| im (467) | ✓ |
| im (468) | ✓ |
| im (469) | ✓ |
| im (470) | ✓ |
| im (471) | ✓ |
| im (472) | ✓ |
| im (473) | ✓ |
| im (474) | ✓ |
| im (475) | ✓ |
| im (476) | ✓ |
| im (477) | ✓ |
| im (478) | ✓ |
| im (479) | ✓ |
| im (480) | ✓ |
| im (481) | ✓ |
| im (482) | ✓ |
| im (483) | ✓ |
| im (484) | ✓ |
| im (485) | ✓ |
| im (486) | ✓ |
| im (487) | ✓ |
| im (488) | ✓ |
| im (489) | ✓ |
| im (490) | ✓ |
| im (491) | ✓ |
| im (492) | ✓ |
| im (493) | ✓ |
| im (494) | ✓ |
| im (495) | ✓ |
| im (496) | ✓ |
| im (497) | ✓ |
| im (498) | ✓ |
| im (499) | ✓ |
| im (500) | ✓ |
| im (501) | ✓ |
| im (502) | ✓ |
| im (503) | ✓ |
| im (504) | ✓ |
| im (505) | ✓ |
| im (506) | ✓ |
| im (507) | ✓ |
| im (508) | ✓ |
| im (509) | ✓ |
| im (510) | ✓ |
| im (511) | ✓ |
| im (512) | ✓ |
| im (513) | ✓ |
| im (514) | ✓ |
| im (515) | ✓ |
| im (516) | ✓ |
| im (517) | ✓ |
| im (518) | ✓ |
| im (519) | ✓ |
| im (520) | ✓ |
| im (521) | ✓ |
| im (522) | ✓ |
| im (523) | ✓ |
| im (524) | ✓ |
| im (525) | ✓ |
| im (526) | ✓ |
| im (527) | ✓ |
| im (528) | ✓ |

## B.7. Results on MESSIDOR (continued)

| Image Title | Response |
|---|---|
| im (529) | ✓ |
| im (530) | ✓ |
| im (531) | ✓ |
| im (532) | ✓ |
| im (533) | × |
| im (534) | ✓ |
| im (535) | ✓ |
| im (536) | ✓ |
| im (537) | ✓ |
| im (538) | ✓ |
| im (539) | ✓ |
| im (540) | ✓ |
| im (541) | ✓ |
| im (542) | ✓ |
| im (543) | ✓ |
| im (544) | ✓ |
| im (545) | ✓ |
| im (546) | ✓ |
| im (547) | ✓ |
| im (548) | ✓ |
| im (549) | ✓ |
| im (550) | ✓ |
| im (551) | ✓ |
| im (552) | ✓ |
| im (553) | ✓ |
| im (554) | ✓ |
| im (555) | ✓ |
| im (556) | ✓ |
| im (557) | ✓ |
| im (558) | ✓ |
| im (559) | ✓ |
| im (560) | ✓ |
| im (561) | ✓ |
| im (562) | ✓ |
| im (563) | ✓ |
| im (564) | ✓ |
| im (565) | ✓ |
| im (566) | ✓ |
| im (567) | ✓ |
| im (568) | ✓ |
| im (569) | ✓ |
| im (570) | ✓ |
| im (571) | ✓ |
| im (572) | ✓ |
| im (573) | ✓ |
| im (574) | ✓ |
| im (575) | ✓ |
| im (576) | ✓ |
| im (577) | ✓ |
| im (578) | ✓ |
| im (579) | ✓ |
| im (580) | ✓ |
| im (581) | ✓ |
| im (582) | ✓ |
| im (583) | ✓ |
| im (584) | × |
| im (585) | × |
| im (586) | ✓ |
| im (587) | ✓ |
| im (588) | ✓ |
| im (589) | ✓ |
| im (590) | ✓ |
| im (591) | ✓ |
| im (592) | × |
| im (593) | ✓ |
| im (594) | ✓ |
| im (595) | ✓ |
| im (596) | ✓ |
| im (597) | ✓ |
| im (598) | ✓ |
| im (599) | ✓ |
| im (600) | ✓ |
| im (601) | × |
| im (602) | ✓ |
| im (603) | ✓ |
| im (604) | ✓ |
| im (605) | ✓ |
| im (606) | ✓ |
| im (607) | ✓ |
| im (608) | ✓ |
| im (609) | ✓ |
| im (610) | ✓ |
| im (611) | ✓ |
| im (612) | ✓ |
| im (613) | ✓ |
| im (614) | ✓ |
| im (615) | ✓ |
| im (616) | ✓ |
| im (617) | ✓ |
| im (618) | ✓ |
| im (619) | × |
| im (620) | ✓ |
| im (621) | ✓ |
| im (622) | ✓ |
| im (623) | ✓ |
| im (624) | ✓ |
| im (625) | ✓ |
| im (626) | ✓ |
| im (627) | ✓ |
| im (628) | ✓ |
| im (629) | ✓ |
| im (630) | ✓ |
| im (631) | ✓ |
| im (632) | ✓ |
| im (633) | ✓ |
| im (634) | ✓ |
| im (635) | ✓ |
| im (636) | ✓ |
| im (637) | ✓ |
| im (638) | ✓ |
| im (639) | × |
| im (640) | ✓ |
| im (641) | ✓ |
| im (642) | ✓ |
| im (643) | ✓ |
| im (644) | ✓ |
| im (645) | ✓ |
| im (646) | ✓ |
| im (647) | ✓ |
| im (648) | ✓ |
| im (649) | ✓ |
| im (650) | ✓ |
| im (651) | ✓ |
| im (652) | ✓ |
| im (653) | ✓ |
| im (654) | ✓ |
| im (655) | ✓ |
| im (656) | ✓ |
| im (657) | ✓ |
| im (658) | ✓ |
| im (659) | ✓ |
| im (660) | ✓ |

## B.7. Results on MESSIDOR (continued)

| Image Title | Response |
|---|---|
| im (661) | ✓ |
| im (662) | ✓ |
| im (663) | ✓ |
| im (664) | ✓ |
| im (665) | ✓ |
| im (666) | ✓ |
| im (667) | ✓ |
| im (668) | ✓ |
| im (669) | ✓ |
| im (670) | ✓ |
| im (671) | ✓ |
| im (672) | ✓ |
| im (673) | ✓ |
| im (674) | ✓ |
| im (675) | ✓ |
| im (676) | ✓ |
| im (677) | ✓ |
| im (678) | ✓ |
| im (679) | ✓ |
| im (680) | ✓ |
| im (681) | ✓ |
| im (682) | ✓ |
| im (683) | ✓ |
| im (684) | ✓ |
| im (685) | ✓ |
| im (686) | ✓ |
| im (687) | ✓ |
| im (688) | ✓ |
| im (689) | ✓ |
| im (690) | ✓ |
| im (691) | ✓ |
| im (692) | ✓ |
| im (693) | ✓ |
| im (694) | ✗ |
| im (695) | ✓ |
| im (696) | ✓ |
| im (697) | ✓ |
| im (698) | ✓ |
| im (699) | ✓ |
| im (700) | ✓ |
| im (701) | ✓ |
| im (702) | ✓ |
| im (703) | ✓ |
| im (704) | ✓ |
| im (705) | ✓ |
| im (706) | ✓ |
| im (707) | ✓ |
| im (708) | ✓ |
| im (709) | ✓ |
| im (710) | ✓ |
| im (711) | ✓ |
| im (712) | ✓ |
| im (713) | ✓ |
| im (714) | ✓ |
| im (715) | ✓ |
| im (716) | ✓ |
| im (717) | ✓ |
| im (718) | ✓ |
| im (719) | ✓ |
| im (720) | ✓ |
| im (721) | ✓ |
| im (722) | ✓ |
| im (723) | ✓ |
| im (724) | ✓ |
| im (725) | ✓ |
| im (726) | ✓ |
| im (727) | ✓ |
| im (728) | ✓ |
| im (729) | ✓ |
| im (730) | ✓ |
| im (731) | ✓ |
| im (732) | ✓ |
| im (733) | ✓ |
| im (734) | ✓ |
| im (735) | ✓ |
| im (736) | ✓ |
| im (737) | ✓ |
| im (738) | ✓ |
| im (739) | ✓ |
| im (740) | ✓ |
| im (741) | ✓ |
| im (742) | ✓ |
| im (743) | ✓ |
| im (744) | ✓ |
| im (745) | ✓ |
| im (746) | ✓ |
| im (747) | ✓ |
| im (748) | ✓ |
| im (749) | ✓ |
| im (750) | ✓ |
| im (751) | ✓ |
| im (752) | ✓ |
| im (753) | ✓ |
| im (754) | ✓ |
| im (755) | ✓ |
| im (756) | ✓ |
| im (757) | ✓ |
| im (758) | ✓ |
| im (759) | ✓ |
| im (760) | ✓ |
| im (761) | ✓ |
| im (762) | ✓ |
| im (763) | ✓ |
| im (764) | ✓ |
| im (765) | ✓ |
| im (766) | ✓ |
| im (767) | ✓ |
| im (768) | ✓ |
| im (769) | ✓ |
| im (770) | ✓ |
| im (771) | ✓ |
| im (772) | ✓ |
| im (773) | ✓ |
| im (774) | ✓ |
| im (775) | ✓ |
| im (776) | ✓ |
| im (777) | ✓ |
| im (778) | ✓ |
| im (779) | ✓ |
| im (780) | ✓ |
| im (781) | ✓ |
| im (782) | ✓ |
| im (783) | ✓ |
| im (784) | ✓ |
| im (785) | ✓ |
| im (786) | ✓ |
| im (787) | ✓ |
| im (788) | ✓ |
| im (789) | ✓ |
| im (790) | ✓ |
| im (791) | ✓ |
| im (792) | ✓ |

## B.7. Results on MESSIDOR (continued)

| Image Title | Response |
|---|---|
| im (793) | ✓ |
| im (794) | ✓ |
| im (795) | ✓ |
| im (796) | ✓ |
| im (797) | ✓ |
| im (798) | ✓ |
| im (799) | ✓ |
| im (800) | ✓ |
| im (801) | ✓ |
| im (802) | ✓ |
| im (803) | ✓ |
| im (804) | ✓ |
| im (805) | ✓ |
| im (806) | ✓ |
| im (807) | ✓ |
| im (808) | ✓ |
| im (809) | ✓ |
| im (810) | ✓ |
| im (811) | ✓ |
| im (812) | ✓ |
| im (813) | ✓ |
| im (814) | ✓ |
| im (815) | ✓ |
| im (816) | ✓ |
| im (817) | ✓ |
| im (818) | ✓ |
| im (819) | ✓ |
| im (820) | ✓ |
| im (821) | ✓ |
| im (822) | ✓ |
| im (823) | ✓ |
| im (824) | × |
| im (825) | ✓ |
| im (826) | ✓ |
| im (827) | ✓ |
| im (828) | ✓ |
| im (829) | ✓ |
| im (830) | ✓ |
| im (831) | ✓ |
| im (832) | ✓ |
| im (833) | ✓ |
| im (834) | ✓ |
| im (835) | ✓ |
| im (836) | ✓ |
| im (837) | ✓ |
| im (838) | ✓ |
| im (839) | ✓ |
| im (840) | ✓ |
| im (841) | ✓ |
| im (842) | ✓ |
| im (843) | ✓ |
| im (844) | ✓ |
| im (845) | ✓ |
| im (846) | ✓ |
| im (847) | ✓ |
| im (848) | ✓ |
| im (849) | ✓ |
| im (850) | ✓ |
| im (851) | ✓ |
| im (852) | ✓ |
| im (853) | ✓ |
| im (854) | ✓ |
| im (855) | ✓ |
| im (856) | ✓ |
| im (857) | ✓ |
| im (858) | ✓ |
| im (859) | ✓ |
| im (860) | ✓ |
| im (861) | ✓ |
| im (862) | ✓ |
| im (863) | ✓ |
| im (864) | ✓ |
| im (865) | ✓ |
| im (866) | ✓ |
| im (867) | ✓ |
| im (868) | ✓ |
| im (869) | ✓ |
| im (870) | ✓ |
| im (871) | ✓ |
| im (872) | ✓ |
| im (873) | ✓ |
| im (874) | ✓ |
| im (875) | ✓ |
| im (876) | ✓ |
| im (877) | ✓ |
| im (878) | ✓ |
| im (879) | ✓ |
| im (880) | ✓ |
| im (881) | ✓ |
| im (882) | ✓ |
| im (883) | ✓ |
| im (884) | ✓ |
| im (885) | ✓ |
| im (886) | ✓ |
| im (887) | ✓ |
| im (888) | ✓ |
| im (889) | ✓ |
| im (890) | ✓ |
| im (891) | ✓ |
| im (892) | ✓ |
| im (893) | ✓ |
| im (894) | ✓ |
| im (895) | ✓ |
| im (896) | ✓ |
| im (897) | ✓ |
| im (898) | ✓ |
| im (899) | ✓ |
| im (900) | ✓ |
| im (901) | ✓ |
| im (902) | ✓ |
| im (903) | ✓ |
| im (904) | ✓ |
| im (905) | ✓ |
| im (906) | ✓ |
| im (907) | ✓ |
| im (908) | ✓ |
| im (909) | ✓ |
| im (910) | ✓ |
| im (911) | ✓ |
| im (912) | ✓ |
| im (913) | ✓ |
| im (914) | ✓ |
| im (915) | ✓ |
| im (916) | ✓ |
| im (917) | ✓ |
| im (918) | ✓ |
| im (919) | ✓ |
| im (920) | × |
| im (921) | ✓ |
| im (922) | ✓ |
| im (923) | ✓ |
| im (924) | ✓ |

## B.7. Results on MESSIDOR (continued)

| Image Title | Response |
|---|---|
| im (925) | ✓ |
| im (926) | ✓ |
| im (927) | ✓ |
| im (928) | ✓ |
| im (929) | ✓ |
| im (930) | ✓ |
| im (931) | ✓ |
| im (932) | ✓ |
| im (933) | ✓ |
| im (934) | ✓ |
| im (935) | ✓ |
| im (936) | ✓ |
| im (937) | ✓ |
| im (938) | ✓ |
| im (939) | ✓ |
| im (940) | ✓ |
| im (941) | ✓ |
| im (942) | ✓ |
| im (943) | ✓ |
| im (944) | ✓ |
| im (945) | ✓ |
| im (946) | ✓ |
| im (947) | ✓ |
| im (948) | ✓ |
| im (949) | ✓ |
| im (950) | ✓ |
| im (951) | ✓ |
| im (952) | ✓ |
| im (953) | ✓ |
| im (954) | ✓ |
| im (955) | ✓ |
| im (956) | ✓ |
| im (957) | ✓ |
| im (958) | ✓ |
| im (959) | ✓ |
| im (960) | ✓ |
| im (961) | ✓ |
| im (962) | ✓ |
| im (963) | ✓ |
| im (964) | ✓ |
| im (965) | ✓ |
| im (966) | ✓ |
| im (967) | ✓ |
| im (968) | ✓ |
| im (969) | ✓ |
| im (970) | ✓ |
| im (971) | ✓ |
| im (972) | ✓ |
| im (973) | ✓ |
| im (974) | ✓ |
| im (975) | ✓ |
| im (976) | ✓ |
| im (977) | ✓ |
| im (978) | ✓ |
| im (979) | ✓ |
| im (980) | ✓ |
| im (981) | ✓ |
| im (982) | ✓ |
| im (983) | ✓ |
| im (984) | ✓ |
| im (985) | ✓ |
| im (986) | ✓ |
| im (987) | ✓ |
| im (988) | ✓ |
| im (989) | ✓ |
| im (990) | ✓ |
| im (991) | ✓ |
| im (992) | ✓ |
| im (993) | ✓ |
| im (994) | ✓ |
| im (995) | ✓ |
| im (996) | ✓ |
| im (997) | ✓ |
| im (998) | ✓ |
| im (999) | ✓ |
| im (1000) | ✓ |
| im (1001) | ✓ |
| im (1002) | ✓ |
| im (1003) | ✓ |
| im (1004) | ✓ |
| im (1005) | ✓ |
| im (1006) | ✓ |
| im (1007) | ✓ |
| im (1008) | ✓ |
| im (1009) | ✓ |
| im (1010) | ✓ |
| im (1011) | ✓ |
| im (1012) | ✓ |
| im (1013) | ✓ |
| im (1014) | ✓ |
| im (1015) | ✓ |
| im (1016) | ✓ |
| im (1017) | ✓ |
| im (1018) | ✓ |
| im (1019) | ✓ |
| im (1020) | ✓ |
| im (1021) | ✓ |
| im (1022) | ✓ |
| im (1023) | ✓ |
| im (1024) | ✓ |
| im (1025) | ✓ |
| im (1026) | ✓ |
| im (1027) | ✓ |
| im (1028) | ✓ |
| im (1029) | ✓ |
| im (1030) | ✓ |
| im (1031) | ✓ |
| im (1032) | ✓ |
| im (1033) | ✓ |
| im (1034) | ✓ |
| im (1035) | ✓ |
| im (1036) | ✓ |
| im (1037) | ✓ |
| im (1038) | ✓ |
| im (1039) | ✓ |
| im (1040) | ✓ |
| im (1041) | ✓ |
| im (1042) | ✓ |
| im (1043) | ✓ |
| im (1044) | ✓ |
| im (1045) | ✓ |
| im (1046) | ✓ |
| im (1047) | ✓ |
| im (1048) | ✓ |
| im (1049) | ✓ |
| im (1050) | ✓ |
| im (1051) | ✓ |
| im (1052) | ✓ |
| im (1053) | ✓ |
| im (1054) | ✓ |
| im (1055) | ✓ |
| im (1056) | ✓ |

## B.7. Results on MESSIDOR (continued)

| Image Title | Response |
|---|---|
| im (1057) | ✓ |
| im (1058) | ✓ |
| im (1059) | ✓ |
| im (1060) | × |
| im (1061) | × |
| im (1062) | ✓ |
| im (1063) | ✓ |
| im (1064) | ✓ |
| im (1065) | ✓ |
| im (1066) | ✓ |
| im (1067) | ✓ |
| im (1068) | ✓ |
| im (1069) | ✓ |
| im (1070) | ✓ |
| im (1071) | ✓ |
| im (1072) | ✓ |
| im (1073) | ✓ |
| im (1074) | ✓ |
| im (1075) | ✓ |
| im (1076) | ✓ |
| im (1077) | ✓ |
| im (1078) | ✓ |
| im (1079) | ✓ |
| im (1080) | ✓ |
| im (1081) | ✓ |
| im (1082) | ✓ |
| im (1083) | ✓ |
| im (1084) | ✓ |
| im (1085) | ✓ |
| im (1086) | ✓ |
| im (1087) | ✓ |
| im (1088) | ✓ |
| im (1089) | ✓ |
| im (1090) | ✓ |
| im (1091) | ✓ |
| im (1092) | ✓ |
| im (1093) | ✓ |
| im (1094) | ✓ |
| im (1095) | ✓ |
| im (1096) | ✓ |
| im (1097) | ✓ |
| im (1098) | ✓ |
| im (1099) | ✓ |
| im (1100) | ✓ |

| Image Title | Response |
|---|---|
| im (1101) | ✓ |
| im (1102) | ✓ |
| im (1103) | ✓ |
| im (1104) | ✓ |
| im (1105) | ✓ |
| im (1106) | ✓ |
| im (1107) | ✓ |
| im (1108) | ✓ |
| im (1109) | ✓ |
| im (1110) | ✓ |
| im (1111) | ✓ |
| im (1112) | ✓ |
| im (1113) | ✓ |
| im (1114) | ✓ |
| im (1115) | ✓ |
| im (1116) | ✓ |
| im (1117) | ✓ |
| im (1118) | ✓ |
| im (1119) | ✓ |
| im (1120) | ✓ |
| im (1121) | ✓ |
| im (1122) | ✓ |
| im (1123) | ✓ |
| im (1124) | ✓ |
| im (1125) | ✓ |
| im (1126) | ✓ |
| im (1127) | ✓ |
| im (1128) | ✓ |
| im (1129) | ✓ |
| im (1130) | ✓ |
| im (1131) | ✓ |
| im (1132) | ✓ |
| im (1133) | ✓ |
| im (1134) | ✓ |
| im (1135) | ✓ |
| im (1136) | ✓ |
| im (1137) | ✓ |
| im (1138) | ✓ |
| im (1139) | ✓ |
| im (1140) | ✓ |
| im (1141) | ✓ |
| im (1142) | ✓ |
| im (1143) | ✓ |
| im (1144) | ✓ |

| Image Title | Response |
|---|---|
| im (1145) | ✓ |
| im (1146) | ✓ |
| im (1147) | ✓ |
| im (1148) | ✓ |
| im (1149) | ✓ |
| im (1150) | ✓ |
| im (1151) | ✓ |
| im (1152) | ✓ |
| im (1153) | ✓ |
| im (1154) | ✓ |
| im (1155) | ✓ |
| im (1156) | ✓ |
| im (1157) | × |
| im (1158) | ✓ |
| im (1159) | ✓ |
| im (1160) | ✓ |
| im (1161) | ✓ |
| im (1162) | ✓ |
| im (1163) | ✓ |
| im (1164) | ✓ |
| im (1165) | ✓ |
| im (1166) | ✓ |
| im (1167) | ✓ |
| im (1168) | ✓ |
| im (1169) | ✓ |
| im (1170) | ✓ |
| im (1171) | ✓ |
| im (1172) | × |
| im (1173) | × |
| im (1174) | ✓ |
| im (1175) | × |
| im (1176) | ✓ |
| im (1177) | ✓ |
| im (1178) | × |
| im (1179) | ✓ |
| im (1180) | ✓ |
| im (1181) | ✓ |
| im (1182) | ✓ |
| im (1183) | ✓ |
| im (1184) | ✓ |
| im (1185) | ✓ |
| im (1186) | ✓ |
| im (1187) | ✓ |
| im (1188) | ✓ |

## B.7. Results on MESSIDOR (continued)

| Image Title | Response |
|---|---|
| im (1189) | ✓ |
| im (1190) | ✓ |
| im (1191) | ✓ |
| im (1192) | ✓ |
| im (1193) | ✓ |
| im (1194) | ✓ |
| im (1195) | × |
| im (1196) | ✓ |
| im (1197) | ✓ |
| im (1198) | ✓ |
| im (1199) | ✓ |
| im (1200) | ✓ |
| **Sensitivity** | **0.9775** |

## B.8. Results on ONHSD

| Image Title | Response |
|---|---|
| im (1) | ✓ |
| im (2) | ✓ |
| im (3) | ✓ |
| im (4) | ✓ |
| im (5) | ✓ |
| im (6) | ✓ |
| im (7) | ✓ |
| im (8) | ✓ |
| im (9) | ✓ |
| im (10) | ✓ |
| im (11) | ✓ |
| im (12) | ✓ |
| im (13) | ✓ |
| im (14) | ✓ |
| im (15) | ✓ |
| im (16) | ✓ |
| im (17) | ✓ |
| im (18) | ✓ |
| im (19) | ✓ |
| im (20) | ✓ |
| im (21) | ✓ |
| im (22) | ✓ |
| im (23) | ✓ |
| im (24) | ✓ |
| im (25) | ✗ |
| im (26) | ✓ |
| im (27) | ✓ |
| im (28) | ✓ |
| im (29) | ✓ |
| im (30) | ✓ |
| im (31) | ✓ |
| im (32) | ✓ |
| im (33) | ✓ |
| im (34) | ✓ |
| im (35) | ✓ |
| im (36) | ✗ |
| im (37) | ✓ |
| im (38) | ✓ |
| im (39) | ✗ |
| im (40) | ✓ |
| im (41) | ✓ |
| im (42) | ✓ |
| im (43) | ✓ |
| im (44) | ✓ |

| Image Title | Response |
|---|---|
| im (45) | ✓ |
| im (46) | ✓ |
| im (47) | ✓ |
| im (48) | ✓ |
| im (49) | ✓ |
| im (50) | ✓ |
| im (51) | ✓ |
| im (52) | ✓ |
| im (53) | ✓ |
| im (54) | ✓ |
| im (55) | ✓ |
| im (56) | ✓ |
| im (57) | ✓ |
| im (58) | ✓ |
| im (59) | ✓ |
| im (60) | ✓ |
| im (61) | ✓ |
| im (62) | ✓ |
| im (63) | ✓ |
| im (64) | ✓ |
| im (65) | ✓ |
| im (66) | ✓ |
| im (67) | ✓ |
| im (68) | ✓ |
| im (69) | ✓ |
| im (70) | ✓ |
| im (71) | ✓ |
| im (72) | ✓ |
| im (73) | ✓ |
| im (74) | ✗ |
| im (75) | ✗ |
| im (76) | ✓ |
| im (77) | ✓ |
| im (78) | ✓ |
| im (79) | ✓ |
| im (80) | ✓ |
| im (81) | ✓ |
| im (82) | ✓ |
| im (83) | ✓ |
| im (84) | ✓ |
| im (85) | ✓ |
| im (86) | ✓ |
| im (87) | ✓ |
| im (88) | ✓ |

| Image Title | Response |
|---|---|
| im (89) | ✓ |
| im (90) | ✓ |
| im (91) | ✓ |
| im (92) | ✓ |
| im (93) | ✓ |
| im (94) | ✓ |
| im (95) | ✓ |
| im (96) | ✓ |
| im (97) | ✓ |
| im (98) | ✓ |
| im (99) | ✓ |
| **Sensitivity** | **0.9495** |

## B.9. Results on STARE

| Image Title | Response |
|---|---|
| im (1) | × |
| im (2) | ✓ |
| im (3) | × |
| im (4) | × |
| im (5) | × |
| im (6) | × |
| im (7) | ✓ |
| im (8) | ✓ |
| im (9) | ✓ |
| im (10) | ✓ |
| im (11) | ✓ |
| im (12) | × |
| im (13) | × |
| im (14) | ✓ |
| im (15) | ✓ |
| im (16) | ✓ |
| im (17) | × |
| im (18) | ✓ |
| im (19) | × |
| im (20) | × |
| im (21) | × |
| im (22) | ✓ |
| im (23) | ✓ |
| im (24) | ✓ |
| im (25) | ✓ |
| im (26) | × |
| im (27) | × |
| im (28) | ✓ |
| im (29) | ✓ |
| im (30) | ✓ |
| im (31) | ✓ |
| im (32) | ✓ |
| im (33) | ✓ |
| im (34) | × |
| im (35) | × |
| im (36) | ✓ |
| im (37) | × |
| im (38) | ✓ |
| im (39) | ✓ |
| im (40) | ✓ |
| im (41) | ✓ |
| im (42) | × |
| im (43) | ✓ |
| im (44) | × |
| im (45) | ✓ |
| im (46) | ✓ |
| im (47) | ✓ |
| im (48) | × |
| im (49) | ✓ |
| im (50) | ✓ |
| im (51) | ✓ |
| im (52) | ✓ |
| im (53) | ✓ |
| im (54) | ✓ |
| im (55) | ✓ |
| im (56) | ✓ |
| im (57) | ✓ |
| im (58) | ✓ |
| im (59) | ✓ |
| im (60) | ✓ |
| im (61) | ✓ |
| im (62) | ✓ |
| im (63) | × |
| im (64) | ✓ |
| im (65) | ✓ |
| im (66) | ✓ |
| im (67) | ✓ |
| im (68) | ✓ |
| im (69) | ✓ |
| im (70) | × |
| im (71) | ✓ |
| im (72) | ✓ |
| im (73) | ✓ |
| im (74) | ✓ |
| im (75) | ✓ |
| im (76) | ✓ |
| im (77) | ✓ |
| im (78) | ✓ |
| im (79) | ✓ |
| im (80) | × |
| im (81) | ✓ |
| **Sensitivity** | **0.7284** |

# Appendix C. Quantitative Results of Segmenting the Bright Abnormalities

## C.1. Results on DIARETDB0

| Image Title | Bright Lesions | Positive Response | Negative Response |
|---|---|---|---|
| im (1) | Present | ✓ | |
| im (2) | Present | ✗ | |
| im (3) | Present | ✓ | |
| im (4) | Present | ✗ | |
| im (5) | Present | ✓ | |
| im (6) | Present | ✗ | |
| im (7) | Present | ✓ | |
| im (8) | Present | ✓ | |
| im (9) | Present | ✓ | |
| im (10) | Present | ✓ | |
| im (11) | Present | ✓ | |
| im (12) | Present | ✓ | |
| im (13) | Present | ✓ | |
| im (14) | Present | ✓ | |
| im (15) | Present | ✓ | |
| im (16) | Present | ✓ | |
| im (17) | Present | ✓ | |
| im (18) | Present | ✓ | |
| im (19) | Present | ✓ | |
| im (20) | Present | ✓ | |
| im (21) | Present | ✓ | |
| im (22) | Present | ✓ | |
| im (23) | Present | ✗ | |
| im (24) | Present | ✓ | |
| im (25) | Present | ✓ | |
| im (26) | Present | ✓ | |
| im (27) | Present | ✓ | |
| im (28) | Present | ✓ | |
| im (29) | Present | ✓ | |
| im (30) | Present | ✓ | |
| im (31) | Present | ✓ | |
| im (32) | Present | ✓ | |
| im (33) | Present | ✓ | |
| im (34) | Present | ✓ | |
| im (35) | Present | ✓ | |
| im (36) | Present | ✓ | |
| im (37) | Present | ✓ | |
| im (38) | Present | ✓ | |
| im (39) | Present | ✓ | |
| im (40) | Present | ✓ | |
| im (41) | Present | ✓ | |
| im (42) | Present | ✓ | |
| im (43) | Present | ✓ | |
| im (44) | Present | ✓ | |
| im (45) | Present | ✓ | |
| im (46) | Present | ✓ | |
| im (47) | Present | ✓ | |
| im (48) | Present | ✓ | |
| im (49) | Absent | | ✓ |
| im (50) | Present | ✓ | |
| im (51) | Present | ✗ | |
| im (52) | Present | ✓ | |
| im (53) | Present | ✓ | |
| im (54) | Present | ✗ | |
| im (55) | Present | ✗ | |
| im (56) | Present | ✓ | |
| im (57) | Present | ✗ | |
| im (58) | Present | ✓ | |
| im (59) | Present | ✓ | |
| im (60) | Present | ✓ | |
| im (61) | Absent | | ✓ |
| im (62) | Absent | | ✗ |
| im (63) | Absent | | ✗ |
| im (64) | Absent | | ✓ |
| im (65) | Absent | | ✓ |
| im (66) | Present | ✗ | |
| im (67) | Absent | | ✗ |
| im (68) | Absent | | ✗ |
| im (69) | Present | ✓ | |
| im (70) | Absent | | ✗ |
| im (71) | Present | ✓ | |
| im (72) | Present | ✓ | |
| im (73) | Present | ✗ | |
| im (74) | Present | ✓ | |
| im (75) | Absent | | ✗ |
| im (76) | Absent | | ✗ |
| im (77) | Present | ✗ | |
| im (78) | Present | ✗ | |
| im (79) | Present | ✗ | |
| im (80) | Absent | | ✗ |
| im (81) | Present | ✓ | |
| im (82) | Absent | | ✓ |
| im (83) | Present | ✗ | |
| im (84) | Present | ✗ | |
| im (85) | Absent | | ✓ |
| im (86) | Absent | | ✗ |
| im (87) | Absent | | ✓ |
| im (88) | Absent | | ✗ |
| im (89) | Absent | | ✓ |
| im (90) | Absent | | ✓ |
| im (91) | Absent | | ✓ |
| im (92) | Present | ✗ | |
| im (93) | Present | ✓ | |
| im (94) | Absent | | ✓ |

## C.1. Results on DIARETDB0 (continued)

| Image Title | Bright Lesions | Positive Response | Negative Response |
|---|---|---|---|
| im (95) | Absent | | ✓ |
| im (96) | Present | × | |
| im (97) | Absent | | × |
| im (98) | Present | ✓ | |
| im (99) | Absent | | ✓ |
| im (100) | Present | ✓ | |
| im (101) | Present | ✓ | |
| im (102) | Present | ✓ | |
| im (103) | Present | ✓ | |
| im (104) | Present | ✓ | |
| im (105) | Present | ✓ | |
| im (106) | Present | ✓ | |
| im (107) | Present | ✓ | |
| im (108) | Present | × | |
| im (109) | Present | ✓ | |
| im (110) | Present | ✓ | |
| im (111) | Absent | | × |
| im (112) | Absent | | ✓ |
| im (113) | Absent | | ✓ |
| im (114) | Absent | | ✓ |
| im (115) | Absent | | ✓ |
| im (116) | Absent | | ✓ |
| im (117) | Absent | | × |
| im (118) | Absent | | ✓ |
| im (119) | Absent | | ✓ |
| im (120) | Absent | | ✓ |
| im (121) | Absent | | ✓ |
| im (122) | Absent | | ✓ |
| im (123) | Absent | | ✓ |
| im (124) | Absent | | ✓ |
| im (125) | Absent | | ✓ |
| im (126) | Absent | | ✓ |
| im (127) | Absent | | × |
| im (128) | Absent | | ✓ |
| im (129) | Absent | | × |
| im (130) | Absent | | × |
| **Sensitivity** | | **0.7907** | |
| **Specificity** | | **0.6364** | |

## C.2. Results on DIARETDB1

| Image Title | Bright Lesions | Positive Response | Negative Response |
|---|---|---|---|
| im (1) | Present | ✓ | |
| im (2) | Present | ✓ | |
| im (3) | Present | ✓ | |
| im (4) | Present | ✓ | |
| im (5) | Present | ✓ | |
| im (6) | Present | ✓ | |
| im (7) | Present | ✓ | |
| im (8) | Present | ✓ | |
| im (9) | Present | ✓ | |
| im (10) | Present | ✓ | |
| im (11) | Present | ✓ | |
| im (12) | Present | ✓ | |
| im (13) | Present | ✓ | |
| im (14) | Present | ✓ | |
| im (15) | Present | ✓ | |
| im (16) | Present | ✓ | |
| im (17) | Present | ✓ | |
| im (18) | Present | ✓ | |
| im (19) | Present | ✓ | |
| im (20) | Present | ✓ | |
| im (21) | Present | ✓ | |
| im (22) | Present | ✓ | |
| im (23) | Present | ✓ | |
| im (24) | Present | ✓ | |
| im (25) | Present | ✓ | |
| im (26) | Present | ✓ | |
| im (27) | Present | ✓ | |
| im (28) | Present | ✓ | |
| im (29) | Present | ✓ | |
| im (30) | Present | ✗ | |
| im (31) | Absent | | ✗ |
| im (32) | Absent | | ✓ |
| im (33) | Present | ✓ | |
| im (34) | Present | ✗ | |
| im (35) | Present | ✓ | |
| im (36) | Absent | | ✓ |
| im (37) | Absent | | ✗ |
| im (38) | Present | ✓ | |
| im (39) | Absent | | ✓ |
| im (40) | Present | ✗ | |
| im (41) | Absent | | ✓ |
| im (42) | Absent | | ✓ |
| im (43) | Absent | | ✓ |
| im (44) | Present | ✓ | |
| im (45) | Absent | | ✓ |
| im (46) | Absent | | ✓ |
| im (47) | Absent | | ✗ |
| im (48) | Absent | | ✓ |
| im (49) | Absent | | ✓ |
| im (50) | Absent | | ✓ |
| im (51) | Absent | | ✗ |
| im (52) | Present | ✓ | |
| im (53) | Present | ✓ | |
| im (54) | Present | ✗ | |
| im (55) | Absent | | ✓ |
| im (56) | Present | ✗ | |
| im (57) | Absent | | ✓ |
| im (58) | Absent | | ✓ |
| im (59) | Absent | | ✗ |
| im (60) | Absent | | ✗ |
| im (61) | Absent | | ✓ |
| im (62) | Absent | | ✓ |
| im (63) | Absent | | ✓ |
| im (64) | Present | ✓ | |
| im (65) | Present | ✓ | |
| im (66) | Present | ✓ | |
| im (67) | Present | ✓ | |
| im (68) | Absent | | ✗ |
| im (69) | Absent | | ✓ |
| im (70) | Absent | | ✓ |
| im (71) | Present | ✗ | |
| im (72) | Absent | | ✓ |
| im (73) | Absent | | ✓ |
| im (74) | Absent | | ✓ |
| im (75) | Absent | | ✓ |
| im (76) | Absent | | ✗ |
| im (77) | Absent | | ✗ |
| im (78) | Present | ✗ | |
| im (79) | Absent | | ✓ |
| im (80) | Absent | | ✓ |
| im (81) | Absent | | ✓ |
| im (82) | Absent | | ✓ |
| im (83) | Absent | | ✓ |
| im (84) | Present | ✓ | |
| im (85) | Present | ✗ | |
| im (86) | Present | ✗ | |
| im (87) | Absent | | ✗ |
| im (88) | Absent | | ✓ |
| im (89) | Absent | | ✗ |
| **Sensitivity** | | **0.8163** | |
| **Specificity** | | **0.7250** | |

## C.3. Results on MESSIDOR

| Image Title | Bright Lesions | Positive Response | Negative Response |
|---|---|---|---|
| im (1) | Present | ✓ | |
| im (2) | Absent | | ✓ |
| im (3) | Absent | | ✓ |
| im (4) | Absent | | ✓ |
| im (5) | Present | ✗ | |
| im (6) | Absent | | ✗ |
| im (7) | Absent | | ✗ |
| im (8) | Absent | | ✗ |
| im (9) | Present | ✓ | |
| im (10) | Absent | | ✗ |
| im (11) | Absent | | ✗ |
| im (12) | Present | ✗ | |
| im (13) | Absent | | ✓ |
| im (14) | Absent | | ✗ |
| im (15) | Absent | | ✓ |
| im (16) | Absent | | ✓ |
| im (17) | Absent | | ✓ |
| im (18) | Present | ✓ | |
| im (19) | Present | ✓ | |
| im (20) | Present | ✓ | |
| im (21) | Absent | | ✓ |
| im (22) | Present | ✓ | |
| im (23) | Present | ✓ | |
| im (24) | Present | ✓ | |
| im (25) | Present | ✓ | |
| im (26) | Present | ✓ | |
| im (27) | Present | ✗ | |
| im (28) | Present | ✓ | |
| im (29) | Present | ✓ | |
| im (30) | Present | ✓ | |
| im (31) | Present | ✓ | |
| im (32) | Present | ✓ | |
| im (33) | Absent | | ✓ |
| im (34) | Absent | | ✓ |
| im (35) | Absent | | ✓ |
| im (36) | Absent | | ✓ |
| im (37) | Present | ✓ | |
| im (38) | Present | ✓ | |
| im (39) | Present | ✓ | |
| im (40) | Present | ✓ | |
| im (41) | Absent | | ✓ |
| im (42) | Absent | | ✓ |
| im (43) | Present | ✓ | |
| im (44) | Present | ✓ | |
| im (45) | Present | ✓ | |
| im (46) | Absent | | ✓ |
| im (47) | Absent | | ✓ |
| im (48) | Absent | | ✗ |
| im (49) | Absent | | ✓ |
| im (50) | Absent | | ✓ |
| im (51) | Present | ✓ | |
| im (52) | Present | ✓ | |
| im (53) | Absent | | ✓ |
| im (54) | Absent | | ✓ |
| im (55) | Absent | | ✓ |
| im (56) | Absent | | ✓ |
| im (57) | Present | ✓ | |
| im (58) | Present | ✓ | |
| im (59) | Absent | | ✓ |
| im (60) | Absent | | ✓ |
| im (61) | Present | ✓ | |
| im (62) | Absent | | ✗ |
| im (63) | Absent | | ✓ |
| im (64) | Absent | | ✗ |
| im (65) | Absent | | ✓ |
| im (66) | Present | ✓ | |
| im (67) | Present | ✓ | |
| im (68) | Absent | | ✓ |
| im (69) | Absent | | ✓ |
| im (70) | Present | ✗ | |
| im (71) | Present | ✓ | |
| im (72) | Absent | | ✓ |
| im (73) | Absent | | ✓ |
| im (74) | Absent | | ✗ |
| im (75) | Absent | | ✗ |
| im (76) | Absent | | ✓ |
| im (77) | Absent | | ✓ |
| im (78) | Absent | | ✗ |
| im (79) | Absent | | ✓ |
| im (80) | Present | ✓ | |
| im (81) | Present | ✓ | |
| im (82) | Absent | | ✓ |
| im (83) | Absent | | ✓ |
| im (84) | Present | ✓ | |
| im (85) | Present | ✓ | |
| im (86) | Absent | | ✗ |
| im (87) | Absent | | ✗ |
| im (88) | Present | ✓ | |
| im (89) | Present | ✓ | |
| im (90) | Absent | | ✓ |
| im (91) | Present | ✓ | |
| im (92) | Absent | | ✓ |
| im (93) | Absent | | ✓ |
| im (94) | Absent | | ✓ |
| im (95) | Present | ✗ | |
| im (96) | Present | ✓ | |
| im (97) | Present | ✗ | |
| im (98) | Absent | | ✗ |
| im (99) | Absent | | ✓ |
| im (100) | Absent | | ✗ |

## C.3. Results on MESSIDOR (continued)

| Image Title | Bright Lesions | Positive Response | Negative Response |
|---|---|---|---|
| im (101) | Absent | | × |
| im (102) | Present | ✓ | |
| im (103) | Present | × | |
| im (104) | Absent | | × |
| im (105) | Absent | | × |
| im (106) | Absent | | × |
| im (107) | Present | ✓ | |
| im (108) | Absent | | ✓ |
| im (109) | Absent | | × |
| im (110) | Absent | | ✓ |
| im (111) | Present | ✓ | |
| im (112) | Absent | | × |
| im (113) | Absent | | ✓ |
| im (114) | Absent | | × |
| im (115) | Absent | | ✓ |
| im (116) | Present | ✓ | |
| im (117) | Present | ✓ | |
| im (118) | Present | ✓ | |
| im (119) | Present | ✓ | |
| im (120) | Present | ✓ | |
| im (121) | Present | ✓ | |
| im (122) | Absent | | × |
| im (123) | Absent | | ✓ |
| im (124) | Absent | | ✓ |
| im (125) | Absent | | ✓ |
| im (126) | Absent | | ✓ |
| im (127) | Absent | | × |
| im (128) | Absent | | × |
| im (129) | Absent | | ✓ |
| im (130) | Absent | | ✓ |
| im (131) | Present | ✓ | |
| im (132) | Present | ✓ | |
| im (133) | Absent | | ✓ |
| im (134) | Absent | | ✓ |
| im (135) | Present | ✓ | |
| im (136) | Absent | | ✓ |
| im (137) | Absent | | ✓ |
| im (138) | Absent | | ✓ |
| im (139) | Absent | | ✓ |
| im (140) | Absent | | ✓ |
| im (141) | Absent | | ✓ |
| im (142) | Absent | | ✓ |
| im (143) | Present | ✓ | |
| im (144) | Present | ✓ | |
| im (145) | Absent | | ✓ |
| im (146) | Absent | | ✓ |
| im (147) | Absent | | ✓ |
| im (148) | Absent | | ✓ |
| im (149) | Present | ✓ | |
| im (150) | Absent | | × |
| im (151) | Present | ✓ | |
| im (152) | Present | × | |
| im (153) | Absent | | ✓ |
| im (154) | Absent | | ✓ |
| im (155) | Absent | | ✓ |
| im (156) | Absent | | ✓ |
| im (157) | Absent | | × |
| im (158) | Absent | | ✓ |
| im (159) | Absent | | × |
| im (160) | Absent | | × |
| im (161) | Absent | | × |
| im (162) | Absent | | ✓ |
| im (163) | Absent | | ✓ |
| im (164) | Absent | | ✓ |
| im (165) | Absent | | × |
| im (166) | Absent | | ✓ |
| im (167) | Absent | | ✓ |
| im (168) | Present | ✓ | |
| im (169) | Present | ✓ | |
| im (170) | Present | ✓ | |
| im (171) | Present | ✓ | |
| im (172) | Present | ✓ | |
| im (173) | Present | ✓ | |
| im (174) | Present | ✓ | |
| im (175) | Present | ✓ | |
| im (176) | Absent | | ✓ |
| im (177) | Absent | | ✓ |
| im (178) | Absent | | ✓ |
| im (179) | Absent | | ✓ |
| im (180) | Absent | | × |
| im (181) | Absent | | × |
| im (182) | Absent | | × |
| im (183) | Present | × | |
| im (184) | Present | × | |
| im (185) | Present | ✓ | |
| im (186) | Absent | | × |
| im (187) | Present | ✓ | |
| im (188) | Absent | | ✓ |
| im (189) | Absent | | ✓ |
| im (190) | Absent | | × |
| im (191) | Absent | | × |
| im (192) | Absent | | × |
| im (193) | Absent | | ✓ |
| im (194) | Present | ✓ | |
| im (195) | Present | ✓ | |
| im (196) | Present | ✓ | |
| im (197) | Present | ✓ | |
| im (198) | Present | ✓ | |
| im (199) | Present | ✓ | |
| im (200) | Present | ✓ | |

## C.3. Results on MESSIDOR (continued)

| Image Title | Bright Lesions | Positive Response | Negative Response |
|---|---|---|---|
| im (201) | Present | ✓ | |
| im (202) | Present | ✓ | |
| im (203) | Present | ✓ | |
| im (204) | Absent | | ✗ |
| im (205) | Absent | | ✗ |
| im (206) | Present | ✓ | |
| im (207) | Absent | | ✗ |
| im (208) | Absent | | ✗ |
| im (209) | Absent | | ✗ |
| im (210) | Absent | | ✗ |
| im (211) | Present | ✗ | |
| im (212) | Present | ✓ | |
| im (213) | Absent | | ✓ |
| im (214) | Absent | | ✓ |
| im (215) | Present | ✓ | |
| im (216) | Present | ✓ | |
| im (217) | Present | ✓ | |
| im (218) | Present | ✓ | |
| im (219) | Absent | | ✗ |
| im (220) | Absent | | ✓ |
| im (221) | Absent | | ✓ |
| im (222) | Absent | | ✓ |
| im (223) | Absent | | ✗ |
| im (224) | Absent | | ✓ |
| im (225) | Absent | | ✓ |
| im (226) | Absent | | ✓ |
| im (227) | Absent | | ✗ |
| im (228) | Present | ✓ | |
| im (229) | Present | ✓ | |
| im (230) | Absent | | ✗ |
| im (231) | Absent | | ✗ |
| im (232) | Absent | | ✗ |
| im (233) | Absent | | ✗ |
| im (234) | Absent | | ✓ |
| im (235) | Absent | | ✓ |
| im (236) | Absent | | ✗ |
| im (237) | Absent | | ✓ |
| im (238) | Absent | | ✗ |
| im (239) | Present | ✗ | |
| im (240) | Absent | | ✗ |
| im (241) | Absent | | ✗ |
| im (242) | Absent | | ✓ |
| im (243) | Present | ✓ | |
| im (244) | Absent | | ✓ |
| im (245) | Absent | | ✓ |
| im (246) | Present | ✓ | |
| im (247) | Present | ✓ | |
| im (248) | Absent | | ✗ |
| im (249) | Absent | | ✗ |
| im (250) | Absent | | ✓ |
| im (251) | Absent | | ✓ |
| im (252) | Present | ✓ | |
| im (253) | Present | ✓ | |
| im (254) | Absent | | ✓ |
| im (255) | Present | ✗ | |
| im (256) | Absent | | ✗ |
| im (257) | Absent | | ✗ |
| im (258) | Present | ✓ | |
| im (259) | Present | ✓ | |
| im (260) | Absent | | ✗ |
| im (261) | Absent | | ✓ |
| im (262) | Absent | | ✗ |
| im (263) | Absent | | ✓ |
| im (264) | Absent | | ✓ |
| im (265) | Absent | | ✓ |
| im (266) | Absent | | ✓ |
| im (267) | Absent | | ✗ |
| im (268) | Present | ✓ | |
| im (269) | Absent | | ✗ |
| im (270) | Absent | | ✗ |
| im (271) | Absent | | ✓ |
| im (272) | Absent | | ✓ |
| im (273) | Absent | | ✗ |
| im (274) | Absent | | ✓ |
| im (275) | Absent | | ✗ |
| im (276) | Absent | | ✓ |
| im (277) | Absent | | ✓ |
| im (278) | Absent | | ✗ |
| im (279) | Absent | | ✗ |
| im (280) | Absent | | ✗ |
| im (281) | Absent | | ✗ |
| im (282) | Absent | | ✗ |
| im (283) | Absent | | ✗ |
| im (284) | Absent | | ✓ |
| im (285) | Absent | | ✓ |
| im (286) | Absent | | ✗ |
| im (287) | Absent | | ✓ |
| im (288) | Absent | | ✗ |
| im (289) | Absent | | ✓ |
| im (290) | Absent | | ✓ |
| im (291) | Absent | | ✗ |
| im (292) | Absent | | ✗ |
| im (293) | Absent | | ✓ |
| im (294) | Absent | | ✓ |
| im (295) | Present | ✓ | |
| im (296) | Present | ✓ | |
| im (297) | Absent | | ✓ |
| im (298) | Absent | | ✓ |
| im (299) | Present | ✓ | |
| im (300) | Present | ✓ | |

## C.3. Results on MESSIDOR (continued)

| Image Title | Bright Lesions | Positive Response | Negative Response |
|---|---|---|---|
| im (301) | Present | ✓ | |
| im (302) | Present | ✓ | |
| im (303) | Absent | | × |
| im (304) | Absent | | × |
| im (305) | Present | ✓ | |
| im (306) | Present | ✓ | |
| im (307) | Absent | | ✓ |
| im (308) | Absent | | ✓ |
| im (309) | Present | ✓ | |
| im (310) | Present | ✓ | |
| im (311) | Absent | | × |
| im (312) | Absent | | × |
| im (313) | Present | ✓ | |
| im (314) | Present | ✓ | |
| im (315) | Absent | | × |
| im (316) | Absent | | × |
| im (317) | Absent | | × |
| im (318) | Absent | | × |
| im (319) | Present | ✓ | |
| im (320) | Present | ✓ | |
| im (321) | Present | ✓ | |
| im (322) | Absent | | ✓ |
| im (323) | Absent | | × |
| im (324) | Absent | | × |
| im (325) | Absent | | × |
| im (326) | Absent | | ✓ |
| im (327) | Absent | | ✓ |
| im (328) | Absent | | × |
| im (329) | Absent | | × |
| im (330) | Absent | | × |
| im (331) | Present | ✓ | |
| im (332) | Absent | | ✓ |
| im (333) | Absent | | × |
| im (334) | Absent | | × |
| im (335) | Present | ✓ | |
| im (336) | Present | ✓ | |
| im (337) | Absent | | ✓ |
| im (338) | Present | ✓ | |
| im (339) | Absent | | × |
| im (340) | Absent | | ✓ |
| im (341) | Absent | | ✓ |
| im (342) | Absent | | ✓ |
| im (343) | Present | ✓ | |
| im (344) | Present | ✓ | |
| im (345) | Present | ✓ | |
| im (346) | Present | ✓ | |
| im (347) | Present | × | |
| im (348) | Absent | | ✓ |
| im (349) | Absent | | ✓ |
| im (350) | Present | ✓ | |
| im (351) | Present | ✓ | |
| im (352) | Absent | | × |
| im (353) | Absent | | × |
| im (354) | Absent | | ✓ |
| im (355) | Absent | | × |
| im (356) | Absent | | ✓ |
| im (357) | Absent | | ✓ |
| im (358) | Absent | | ✓ |
| im (359) | Present | ✓ | |
| im (360) | Present | ✓ | |
| im (361) | Present | ✓ | |
| im (362) | Present | ✓ | |
| im (363) | Absent | | ✓ |
| im (364) | Absent | | × |
| im (365) | Present | ✓ | |
| im (366) | Absent | | × |
| im (367) | Absent | | × |
| im (368) | Absent | | ✓ |
| im (369) | Absent | | ✓ |
| im (370) | Absent | | × |
| im (371) | Absent | | ✓ |
| im (372) | Absent | | × |
| im (373) | Absent | | × |
| im (374) | Present | ✓ | |
| im (375) | Present | ✓ | |
| im (376) | Absent | | ✓ |
| im (377) | Absent | | × |
| im (378) | Present | ✓ | |
| im (379) | Present | ✓ | |
| im (380) | Absent | | × |
| im (381) | Absent | | × |
| im (382) | Absent | | ✓ |
| im (383) | Present | ✓ | |
| im (384) | Present | ✓ | |
| im (385) | Absent | | × |
| im (386) | Absent | | × |
| im (387) | Present | × | |
| im (388) | Absent | | × |
| im (389) | Absent | | ✓ |
| im (390) | Present | ✓ | |
| im (391) | Absent | | ✓ |
| im (392) | Absent | | × |
| im (393) | Absent | | ✓ |
| im (394) | Present | ✓ | |
| im (395) | Absent | | × |
| im (396) | Absent | | ✓ |
| im (397) | Absent | | ✓ |
| im (398) | Absent | | × |
| im (399) | Present | ✓ | |
| im (400) | Present | ✓ | |

## C.3. Results on MESSIDOR (continued)

| Image Title | Bright Lesions | Positive Response | Negative Response |
|---|---|---|---|
| im (401) | Absent | | ✗ |
| im (402) | Absent | | ✗ |
| im (403) | Present | ✓ | |
| im (404) | Present | ✓ | |
| im (405) | Absent | | ✓ |
| im (406) | Absent | | ✓ |
| im (407) | Absent | | ✗ |
| im (408) | Absent | | ✓ |
| im (409) | Absent | | ✗ |
| im (410) | Absent | | ✗ |
| im (411) | Absent | | ✗ |
| im (412) | Absent | | ✗ |
| im (413) | Present | ✓ | |
| im (414) | Present | ✓ | |
| im (415) | Absent | | ✗ |
| im (416) | Absent | | ✗ |
| im (417) | Present | ✓ | |
| im (418) | Present | ✓ | |
| im (419) | Absent | | ✗ |
| im (420) | Absent | | ✗ |
| im (421) | Absent | | ✓ |
| im (422) | Absent | | ✗ |
| im (423) | Absent | | ✗ |
| im (424) | Absent | | ✓ |
| im (425) | Absent | | ✗ |
| im (426) | Absent | | ✓ |
| im (427) | Absent | | ✗ |
| im (428) | Absent | | ✓ |
| im (429) | Absent | | ✗ |
| im (430) | Absent | | ✗ |
| im (431) | Present | ✓ | |
| im (432) | Absent | | ✗ |
| im (433) | Absent | | ✓ |
| im (434) | Absent | | ✓ |
| im (435) | Present | ✓ | |
| im (436) | Present | ✓ | |
| im (437) | Present | ✓ | |
| im (438) | Present | ✓ | |
| im (439) | Absent | | ✓ |
| im (440) | Absent | | ✓ |
| im (441) | Absent | | ✗ |
| im (442) | Absent | | ✗ |
| im (443) | Present | ✗ | |
| im (444) | Present | ✗ | |
| im (445) | Absent | | ✗ |
| im (446) | Absent | | ✓ |
| im (447) | Absent | | ✓ |
| im (448) | Absent | | ✗ |
| im (449) | Absent | | ✓ |
| im (450) | Absent | | ✓ |
| im (451) | Absent | | ✗ |
| im (452) | Absent | | ✗ |
| im (453) | Absent | | ✗ |
| im (454) | Absent | | ✗ |
| im (455) | Absent | | ✗ |
| im (456) | Present | ✓ | |
| im (457) | Absent | | ✓ |
| im (458) | Absent | | ✗ |
| im (459) | Absent | | ✗ |
| im (460) | Absent | | ✓ |
| im (461) | Absent | | ✓ |
| im (462) | Present | ✓ | |
| im (463) | Absent | | ✗ |
| im (464) | Absent | | ✓ |
| im (465) | Absent | | ✗ |
| im (466) | Absent | | ✓ |
| im (467) | Absent | | ✗ |
| im (468) | Absent | | ✓ |
| im (469) | Absent | | ✓ |
| im (470) | Absent | | ✓ |
| im (471) | Present | ✓ | |
| im (472) | Present | ✗ | |
| im (473) | Absent | | ✓ |
| im (474) | Absent | | ✗ |
| im (475) | Absent | | ✗ |
| im (476) | Absent | | ✓ |
| im (477) | Absent | | ✓ |
| im (478) | Present | ✓ | |
| im (479) | Absent | | ✓ |
| im (480) | Absent | | ✗ |
| im (481) | Absent | | ✓ |
| im (482) | Absent | | ✓ |
| im (483) | Absent | | ✗ |
| im (484) | Absent | | ✗ |
| im (485) | Absent | | ✗ |
| im (486) | Absent | | ✗ |
| im (487) | Absent | | ✓ |
| im (488) | Absent | | ✗ |
| im (489) | Absent | | ✗ |
| im (490) | Absent | | ✗ |
| im (491) | Absent | | ✗ |
| im (492) | Absent | | ✓ |
| im (493) | Present | ✗ | |
| im (494) | Absent | | ✗ |
| im (495) | Absent | | ✗ |
| im (496) | Absent | | ✓ |
| im (497) | Absent | | ✓ |
| im (498) | Present | ✓ | |
| im (499) | Present | ✓ | |
| im (500) | Absent | | ✓ |

## C.3. Results on MESSIDOR (continued)

| Image Title | Bright Lesions | Positive Response | Negative Response |
|---|---|---|---|
| im (501) | Absent | | ✓ |
| im (502) | Absent | | × |
| im (503) | Absent | | × |
| im (504) | Absent | | ✓ |
| im (505) | Absent | | ✓ |
| im (506) | Absent | | × |
| im (507) | Absent | | × |
| im (508) | Absent | | ✓ |
| im (509) | Absent | | ✓ |
| im (510) | Present | ✓ | |
| im (511) | Absent | | ✓ |
| im (512) | Absent | | × |
| im (513) | Absent | | × |
| im (514) | Absent | | ✓ |
| im (515) | Absent | | × |
| im (516) | Absent | | × |
| im (517) | Absent | | ✓ |
| im (518) | Absent | | ✓ |
| im (519) | Absent | | ✓ |
| im (520) | Absent | | × |
| im (521) | Absent | | ✓ |
| im (522) | Absent | | × |
| im (523) | Absent | | ✓ |
| im (524) | Absent | | × |
| im (525) | Absent | | × |
| im (526) | Absent | | ✓ |
| im (527) | Absent | | ✓ |
| im (528) | Absent | | × |
| im (529) | Absent | | ✓ |
| im (530) | Absent | | ✓ |
| im (531) | Absent | | ✓ |
| im (532) | Absent | | ✓ |
| im (533) | Absent | | ✓ |
| im (534) | Absent | | ✓ |
| im (535) | Absent | | ✓ |
| im (536) | Absent | | × |
| im (537) | Absent | | × |
| im (538) | Absent | | × |
| im (539) | Absent | | ✓ |
| im (540) | Absent | | × |
| im (541) | Absent | | × |
| im (542) | Absent | | ✓ |
| im (543) | Present | ✓ | |
| im (544) | Absent | | ✓ |
| im (545) | Absent | | ✓ |
| im (546) | Absent | | ✓ |
| im (547) | Absent | | ✓ |
| im (548) | Absent | | × |
| im (549) | Absent | | × |
| im (550) | Present | × | |
| im (551) | Absent | | ✓ |
| im (552) | Absent | | ✓ |
| im (553) | Absent | | ✓ |
| im (554) | Absent | | × |
| im (555) | Absent | | ✓ |
| im (556) | Absent | | ✓ |
| im (557) | Absent | | × |
| im (558) | Absent | | × |
| im (559) | Absent | | × |
| im (560) | Absent | | × |
| im (561) | Absent | | ✓ |
| im (562) | Absent | | ✓ |
| im (563) | Absent | | ✓ |
| im (564) | Present | × | |
| im (565) | Absent | | × |
| im (566) | Absent | | ✓ |
| im (567) | Absent | | × |
| im (568) | Present | ✓ | |
| im (569) | Present | ✓ | |
| im (570) | Absent | | ✓ |
| im (571) | Absent | | ✓ |
| im (572) | Absent | | ✓ |
| im (573) | Absent | | ✓ |
| im (574) | Present | ✓ | |
| im (575) | Absent | | × |
| im (576) | Absent | | ✓ |
| im (577) | Present | ✓ | |
| im (578) | Absent | | ✓ |
| im (579) | Absent | | × |
| im (580) | Absent | | ✓ |
| im (581) | Absent | | ✓ |
| im (582) | Absent | | ✓ |
| im (583) | Absent | | ✓ |
| im (584) | Absent | | × |
| im (585) | Absent | | × |
| im (586) | Absent | | × |
| im (587) | Absent | | ✓ |
| im (588) | Absent | | × |
| im (589) | Absent | | × |
| im (590) | Present | ✓ | |
| im (591) | Absent | | ✓ |
| im (592) | Absent | | × |
| im (593) | Absent | | × |
| im (594) | Absent | | × |
| im (595) | Absent | | × |
| im (596) | Absent | | × |
| im (597) | Absent | | ✓ |
| im (598) | Present | ✓ | |
| im (599) | Present | ✓ | |
| im (600) | Present | ✓ | |

## C.3. Results on MESSIDOR (continued)

| Image Title | Bright Lesions | Positive Response | Negative Response |
|---|---|---|---|
| im (601) | Present | ✓ | |
| im (602) | Absent | | ✓ |
| im (603) | Absent | | ✓ |
| im (604) | Absent | | × |
| im (605) | Absent | | × |
| im (606) | Absent | | × |
| im (607) | Absent | | × |
| im (608) | Present | ✓ | |
| im (609) | Present | ✓ | |
| im (610) | Absent | | × |
| im (611) | Absent | | ✓ |
| im (612) | Absent | | ✓ |
| im (613) | Absent | | × |
| im (614) | Absent | | ✓ |
| im (615) | Absent | | ✓ |
| im (616) | Absent | | × |
| im (617) | Absent | | ✓ |
| im (618) | Absent | | × |
| im (619) | Absent | | ✓ |
| im (620) | Absent | | ✓ |
| im (621) | Absent | | × |
| im (622) | Absent | | × |
| im (623) | Absent | | × |
| im (624) | Absent | | ✓ |
| im (625) | Absent | | ✓ |
| im (626) | Absent | | ✓ |
| im (627) | Absent | | ✓ |
| im (628) | Absent | | ✓ |
| im (629) | Absent | | × |
| im (630) | Present | ✓ | |
| im (631) | Present | ✓ | |
| im (632) | Absent | | ✓ |
| im (633) | Absent | | ✓ |
| im (634) | Absent | | ✓ |
| im (635) | Absent | | ✓ |
| im (636) | Present | ✓ | |
| im (637) | Absent | | ✓ |
| im (638) | Present | ✓ | |
| im (639) | Present | ✓ | |
| im (640) | Absent | | × |
| im (641) | Absent | | × |
| im (642) | Absent | | ✓ |
| im (643) | Absent | | ✓ |
| im (644) | Present | × | |
| im (645) | Absent | | ✓ |
| im (646) | Absent | | ✓ |
| im (647) | Absent | | × |
| im (648) | Absent | | ✓ |
| im (649) | Absent | | ✓ |
| im (650) | Absent | | ✓ |

| Image Title | Bright Lesions | Positive Response | Negative Response |
|---|---|---|---|
| im (651) | Absent | | × |
| im (652) | Absent | | × |
| im (653) | Absent | | × |
| im (654) | Present | ✓ | |
| im (655) | Present | ✓ | |
| im (656) | Present | × | |
| im (657) | Present | × | |
| im (658) | Present | ✓ | |
| im (659) | Absent | | × |
| im (660) | Absent | | ✓ |
| im (661) | Absent | | ✓ |
| im (662) | Present | ✓ | |
| im (663) | Present | ✓ | |
| im (664) | Absent | | × |
| im (665) | Absent | | ✓ |
| im (666) | Absent | | × |
| im (667) | Present | ✓ | |
| im (668) | Absent | | ✓ |
| im (669) | Absent | | ✓ |
| im (670) | Absent | | ✓ |
| im (671) | Absent | | ✓ |
| im (672) | Absent | | × |
| im (673) | Absent | | × |
| im (674) | Present | ✓ | |
| im (675) | Absent | | ✓ |
| im (676) | Absent | | ✓ |
| im (677) | Absent | | × |
| im (678) | Present | ✓ | |
| im (679) | Absent | | ✓ |
| im (680) | Absent | | × |
| im (681) | Absent | | × |
| im (682) | Present | ✓ | |
| im (683) | Absent | | ✓ |
| im (684) | Present | ✓ | |
| im (685) | Absent | | × |
| im (686) | Absent | | ✓ |
| im (687) | Absent | | × |
| im (688) | Absent | | × |
| im (689) | Present | ✓ | |
| im (690) | Present | × | |
| im (691) | Absent | | ✓ |
| im (692) | Absent | | × |
| im (693) | Absent | | × |
| im (694) | Present | ✓ | |
| im (695) | Absent | | × |
| im (696) | Absent | | × |
| im (697) | Absent | | × |
| im (698) | Absent | | × |
| im (699) | Absent | | × |
| im (700) | Absent | | × |

## C.3. Results on MESSIDOR (continued)

| Image Title | Bright Lesions | Positive Response | Negative Response |
|---|---|---|---|
| im (701) | Absent | | × |
| im (702) | Present | ✓ | |
| im (703) | Absent | | ✓ |
| im (704) | Absent | | ✓ |
| im (705) | Absent | | ✓ |
| im (706) | Absent | | ✓ |
| im (707) | Present | ✓ | |
| im (708) | Absent | | × |
| im (709) | Absent | | × |
| im (710) | Absent | | × |
| im (711) | Present | ✓ | |
| im (712) | Present | ✓ | |
| im (713) | Present | ✓ | |
| im (714) | Absent | | ✓ |
| im (715) | Absent | | ✓ |
| im (716) | Present | ✓ | |
| im (717) | Absent | | × |
| im (718) | Absent | | ✓ |
| im (719) | Absent | | × |
| im (720) | Absent | | ✓ |
| im (721) | Absent | | ✓ |
| im (722) | Absent | | × |
| im (723) | Absent | | × |
| im (724) | Absent | | × |
| im (725) | Absent | | × |
| im (726) | Absent | | × |
| im (727) | Present | ✓ | |
| im (728) | Present | ✓ | |
| im (729) | Absent | | ✓ |
| im (730) | Absent | | × |
| im (731) | Present | ✓ | |
| im (732) | Present | ✓ | |
| im (733) | Absent | | × |
| im (734) | Present | ✓ | |
| im (735) | Absent | | ✓ |
| im (736) | Absent | | × |
| im (737) | Absent | | × |
| im (738) | Absent | | × |
| im (739) | Absent | | ✓ |
| im (740) | Absent | | ✓ |
| im (741) | Present | ✓ | |
| im (742) | Present | ✓ | |
| im (743) | Absent | | ✓ |
| im (744) | Absent | | × |
| im (745) | Present | ✓ | |
| im (746) | Absent | | × |
| im (747) | Present | ✓ | |
| im (748) | Absent | | × |
| im (749) | Absent | | × |
| im (750) | Absent | | × |

| Image Title | Bright Lesions | Positive Response | Negative Response |
|---|---|---|---|
| im (751) | Absent | | ✓ |
| im (752) | Absent | | ✓ |
| im (753) | Absent | | ✓ |
| im (754) | Absent | | ✓ |
| im (755) | Absent | | × |
| im (756) | Present | ✓ | |
| im (757) | Absent | | × |
| im (758) | Absent | | ✓ |
| im (759) | Absent | | × |
| im (760) | Absent | | ✓ |
| im (761) | Present | ✓ | |
| im (762) | Absent | | × |
| im (763) | Present | ✓ | |
| im (764) | Absent | | × |
| im (765) | Present | ✓ | |
| im (766) | Absent | | × |
| im (767) | Absent | | × |
| im (768) | Absent | | ✓ |
| im (769) | Absent | | ✓ |
| im (770) | Absent | | ✓ |
| im (771) | Present | ✓ | |
| im (772) | Absent | | × |
| im (773) | Absent | | ✓ |
| im (774) | Absent | | ✓ |
| im (775) | Absent | | ✓ |
| im (776) | Absent | | ✓ |
| im (777) | Absent | | ✓ |
| im (778) | Present | × | |
| im (779) | Absent | | × |
| im (780) | Absent | | ✓ |
| im (781) | Absent | | ✓ |
| im (782) | Absent | | ✓ |
| im (783) | Absent | | × |
| im (784) | Absent | | × |
| im (785) | Absent | | × |
| im (786) | Absent | | × |
| im (787) | Absent | | ✓ |
| im (788) | Absent | | × |
| im (789) | Absent | | ✓ |
| im (790) | Absent | | ✓ |
| im (791) | Absent | | × |
| im (792) | Absent | | × |
| im (793) | Absent | | × |
| im (794) | Present | ✓ | |
| im (795) | Present | ✓ | |
| im (796) | Present | ✓ | |
| im (797) | Absent | | ✓ |
| im (798) | Absent | | ✓ |
| im (799) | Absent | | × |
| im (800) | Absent | | ✓ |

## C.3. Results on MESSIDOR (continued)

| Image Title | Bright Lesions | Positive Response | Negative Response |
|---|---|---|---|
| im (801) | Absent | | ✓ |
| im (802) | Absent | | × |
| im (803) | Absent | | ✓ |
| im (804) | Absent | | ✓ |
| im (805) | Absent | | ✓ |
| im (806) | Absent | | × |
| im (807) | Absent | | × |
| im (808) | Absent | | ✓ |
| im (809) | Absent | | × |
| im (810) | Absent | | × |
| im (811) | Absent | | × |
| im (812) | Absent | | × |
| im (813) | Absent | | ✓ |
| im (814) | Absent | | ✓ |
| im (815) | Absent | | ✓ |
| im (816) | Absent | | ✓ |
| im (817) | Absent | | × |
| im (818) | Absent | | × |
| im (819) | Absent | | ✓ |
| im (820) | Absent | | × |
| im (821) | Absent | | ✓ |
| im (822) | Absent | | ✓ |
| im (823) | Absent | | ✓ |
| im (824) | Absent | | ✓ |
| im (825) | Absent | | × |
| im (826) | Absent | | ✓ |
| im (827) | Absent | | ✓ |
| im (828) | Absent | | ✓ |
| im (829) | Absent | | × |
| im (830) | Absent | | ✓ |
| im (831) | Absent | | ✓ |
| im (832) | Absent | | × |
| im (833) | Absent | | × |
| im (834) | Absent | | ✓ |
| im (835) | Absent | | ✓ |
| im (836) | Absent | | × |
| im (837) | Absent | | ✓ |
| im (838) | Absent | | ✓ |
| im (839) | Absent | | ✓ |
| im (840) | Absent | | ✓ |
| im (841) | Absent | | ✓ |
| im (842) | Absent | | ✓ |
| im (843) | Absent | | ✓ |
| im (844) | Absent | | × |
| im (845) | Absent | | × |
| im (846) | Absent | | × |
| im (847) | Absent | | ✓ |
| im (848) | Absent | | × |
| im (849) | Absent | | ✓ |
| im (850) | Absent | | ✓ |

| Image Title | Bright Lesions | Positive Response | Negative Response |
|---|---|---|---|
| im (851) | Absent | | ✓ |
| im (852) | Absent | | ✓ |
| im (853) | Absent | | ✓ |
| im (854) | Absent | | ✓ |
| im (855) | Absent | | × |
| im (856) | Absent | | ✓ |
| im (857) | Absent | | ✓ |
| im (858) | Present | ✓ | |
| im (859) | Absent | | ✓ |
| im (860) | Absent | | ✓ |
| im (861) | Absent | | ✓ |
| im (862) | Absent | | ✓ |
| im (863) | Absent | | ✓ |
| im (864) | Absent | | ✓ |
| im (865) | Absent | | × |
| im (866) | Absent | | ✓ |
| im (867) | Absent | | ✓ |
| im (868) | Absent | | ✓ |
| im (869) | Present | ✓ | |
| im (870) | Absent | | ✓ |
| im (871) | Absent | | ✓ |
| im (872) | Absent | | × |
| im (873) | Absent | | × |
| im (874) | Absent | | ✓ |
| im (875) | Absent | | × |
| im (876) | Present | ✓ | |
| im (877) | Present | ✓ | |
| im (878) | Absent | | ✓ |
| im (879) | Present | ✓ | |
| im (880) | Absent | | ✓ |
| im (881) | Absent | | ✓ |
| im (882) | Present | ✓ | |
| im (883) | Present | ✓ | |
| im (884) | Present | × | |
| im (885) | Present | × | |
| im (886) | Present | × | |
| im (887) | Absent | | ✓ |
| im (888) | Absent | | ✓ |
| im (889) | Absent | | ✓ |
| im (890) | Absent | | ✓ |
| im (891) | Absent | | ✓ |
| im (892) | Absent | | ✓ |
| im (893) | Absent | | × |
| im (894) | Absent | | × |
| im (895) | Absent | | × |
| im (896) | Absent | | ✓ |
| im (897) | Absent | | ✓ |
| im (898) | Absent | | ✓ |
| im (899) | Absent | | ✓ |
| im (900) | Absent | | ✓ |

## C.3. Results on MESSIDOR (continued)

| Image Title | Bright Lesions | Positive Response | Negative Response |
|---|---|---|---|
| im (901) | Absent | | ✓ |
| im (902) | Absent | | × |
| im (903) | Absent | | ✓ |
| im (904) | Absent | | × |
| im (905) | Absent | | ✓ |
| im (906) | Absent | | ✓ |
| im (907) | Absent | | ✓ |
| im (908) | Absent | | ✓ |
| im (909) | Absent | | ✓ |
| im (910) | Absent | | ✓ |
| im (911) | Absent | | × |
| im (912) | Absent | | × |
| im (913) | Absent | | × |
| im (914) | Absent | | × |
| im (915) | Absent | | × |
| im (916) | Absent | | × |
| im (917) | Absent | | × |
| im (918) | Absent | | ✓ |
| im (919) | Absent | | × |
| im (920) | Absent | | × |
| im (921) | Absent | | ✓ |
| im (922) | Absent | | × |
| im (923) | Absent | | ✓ |
| im (924) | Absent | | ✓ |
| im (925) | Absent | | ✓ |
| im (926) | Absent | | ✓ |
| im (927) | Absent | | ✓ |
| im (928) | Absent | | ✓ |
| im (929) | Absent | | ✓ |
| im (930) | Absent | | ✓ |
| im (931) | Absent | | × |
| im (932) | Absent | | × |
| im (933) | Absent | | ✓ |
| im (934) | Absent | | ✓ |
| im (935) | Absent | | × |
| im (936) | Absent | | ✓ |
| im (937) | Absent | | ✓ |
| im (938) | Absent | | × |
| im (939) | Absent | | ✓ |
| im (940) | Absent | | ✓ |
| im (941) | Absent | | ✓ |
| im (942) | Absent | | × |
| im (943) | Absent | | ✓ |
| im (944) | Absent | | ✓ |
| im (945) | Absent | | ✓ |
| im (946) | Absent | | ✓ |
| im (947) | Absent | | ✓ |
| im (948) | Absent | | ✓ |
| im (949) | Absent | | × |
| im (950) | Absent | | ✓ |
| im (951) | Absent | | ✓ |
| im (952) | Absent | | × |
| im (953) | Absent | | × |
| im (954) | Absent | | ✓ |
| im (955) | Absent | | ✓ |
| im (956) | Absent | | ✓ |
| im (957) | Absent | | ✓ |
| im (958) | Absent | | × |
| im (959) | Absent | | × |
| im (960) | Absent | | ✓ |
| im (961) | Absent | | × |
| im (962) | Absent | | × |
| im (963) | Absent | | ✓ |
| im (964) | Absent | | × |
| im (965) | Absent | | ✓ |
| im (966) | Absent | | × |
| im (967) | Absent | | ✓ |
| im (968) | Absent | | ✓ |
| im (969) | Absent | | ✓ |
| im (970) | Absent | | × |
| im (971) | Absent | | × |
| im (972) | Absent | | × |
| im (973) | Absent | | × |
| im (974) | Absent | | × |
| im (975) | Absent | | × |
| im (976) | Absent | | × |
| im (977) | Absent | | ✓ |
| im (978) | Absent | | ✓ |
| im (979) | Absent | | ✓ |
| im (980) | Absent | | × |
| im (981) | Absent | | ✓ |
| im (982) | Absent | | × |
| im (983) | Absent | | ✓ |
| im (984) | Absent | | × |
| im (985) | Absent | | × |
| im (986) | Absent | | × |
| im (987) | Absent | | × |
| im (988) | Absent | | × |
| im (989) | Absent | | × |
| im (990) | Absent | | × |
| im (991) | Absent | | ✓ |
| im (992) | Absent | | ✓ |
| im (993) | Absent | | ✓ |
| im (994) | Absent | | ✓ |
| im (995) | Absent | | ✓ |
| im (996) | Absent | | ✓ |
| im (997) | Absent | | ✓ |
| im (998) | Absent | | × |
| im (999) | Absent | | × |
| im (1000) | Absent | | × |

## C.3. Results on MESSIDOR (continued)

| Image Title | Bright Lesions | Positive Response | Negative Response |
|---|---|---|---|
| im (1001) | Absent | | ✗ |
| im (1002) | Absent | | ✓ |
| im (1003) | Absent | | ✗ |
| im (1004) | Absent | | ✗ |
| im (1005) | Absent | | ✗ |
| im (1006) | Absent | | ✗ |
| im (1007) | Absent | | ✓ |
| im (1008) | Present | ✓ | |
| im (1009) | Absent | | ✓ |
| im (1010) | Absent | | ✓ |
| im (1011) | Absent | | ✓ |
| im (1012) | Absent | | ✗ |
| im (1013) | Present | ✓ | |
| im (1014) | Absent | | ✗ |
| im (1015) | Present | ✓ | |
| im (1016) | Absent | | ✓ |
| im (1017) | Present | ✓ | |
| im (1018) | Present | ✓ | |
| im (1019) | Absent | | ✓ |
| im (1020) | Absent | | ✓ |
| im (1021) | Absent | | ✓ |
| im (1022) | Absent | | ✓ |
| im (1023) | Absent | | ✓ |
| im (1024) | Absent | | ✓ |
| im (1025) | Present | ✓ | |
| im (1026) | Absent | | ✓ |
| im (1027) | Absent | | ✓ |
| im (1028) | Present | ✓ | |
| im (1029) | Absent | | ✓ |
| im (1030) | Absent | | ✓ |
| im (1031) | Present | ✓ | |
| im (1032) | Absent | | ✓ |
| im (1033) | Absent | | ✓ |
| im (1034) | Absent | | ✓ |
| im (1035) | Absent | | ✓ |
| im (1036) | Absent | | ✗ |
| im (1037) | Present | ✓ | |
| im (1038) | Absent | | ✓ |
| im (1039) | Absent | | ✗ |
| im (1040) | Absent | | ✗ |
| im (1041) | Present | ✓ | |
| im (1042) | Present | ✗ | |
| im (1043) | Absent | | ✓ |
| im (1044) | Absent | | ✓ |
| im (1045) | Present | ✓ | |
| im (1046) | Present | ✓ | |
| im (1047) | Absent | | ✗ |
| im (1048) | Present | ✓ | |
| im (1049) | Present | ✓ | |
| im (1050) | Absent | | ✗ |

| Image Title | Bright Lesions | Positive Response | Negative Response |
|---|---|---|---|
| im (1051) | Absent | | ✓ |
| im (1052) | Present | ✓ | |
| im (1053) | Absent | | ✓ |
| im (1054) | Absent | | ✗ |
| im (1055) | Present | ✓ | |
| im (1056) | Absent | | ✓ |
| im (1057) | Absent | | ✗ |
| im (1058) | Absent | | ✓ |
| im (1059) | Absent | | ✗ |
| im (1060) | Absent | | ✗ |
| im (1061) | Absent | | ✗ |
| im (1062) | Absent | | ✗ |
| im (1063) | Absent | | ✗ |
| im (1064) | Absent | | ✓ |
| im (1065) | Absent | | ✗ |
| im (1066) | Absent | | ✗ |
| im (1067) | Absent | | ✓ |
| im (1068) | Absent | | ✓ |
| im (1069) | Absent | | ✓ |
| im (1070) | Present | ✓ | |
| im (1071) | Present | ✓ | |
| im (1072) | Absent | | ✓ |
| im (1073) | Present | ✓ | |
| im (1074) | Present | ✓ | |
| im (1075) | Present | ✓ | |
| im (1076) | Present | ✓ | |
| im (1077) | Present | ✓ | |
| im (1078) | Present | ✓ | |
| im (1079) | Absent | | ✓ |
| im (1080) | Present | ✓ | |
| im (1081) | Absent | | ✓ |
| im (1082) | Absent | | ✗ |
| im (1083) | Present | ✓ | |
| im (1084) | Absent | | ✗ |
| im (1085) | Present | ✓ | |
| im (1086) | Present | ✓ | |
| im (1087) | Absent | | ✓ |
| im (1088) | Present | ✓ | |
| im (1089) | Absent | | ✗ |
| im (1090) | Present | ✓ | |
| im (1091) | Absent | | ✓ |
| im (1092) | Present | ✓ | |
| im (1093) | Absent | | ✗ |
| im (1094) | Present | ✓ | |
| im (1095) | Absent | | ✓ |
| im (1096) | Absent | | ✗ |
| im (1097) | Present | ✓ | |
| im (1098) | Present | ✓ | |
| im (1099) | Present | ✗ | |
| im (1100) | Present | ✓ | |

## C.3. Results on MESSIDOR (continued)

| Image Title | Bright Lesions | Positive Response | Negative Response | Image Title | Bright Lesions | Positive Response | Negative Response |
|---|---|---|---|---|---|---|---|
| im (1101) | Absent | | ✓ | im (1151) | Absent | | ✓ |
| im (1102) | Present | ✗ | | im (1152) | Absent | | ✓ |
| im (1103) | Present | ✓ | | im (1153) | Absent | | ✗ |
| im (1104) | Absent | | ✗ | im (1154) | Absent | | ✓ |
| im (1105) | Absent | | ✓ | im (1155) | Present | ✓ | |
| im (1106) | Absent | | ✓ | im (1156) | Present | ✗ | |
| im (1107) | Absent | | ✓ | im (1157) | Present | ✓ | |
| im (1108) | Absent | | ✓ | im (1158) | Present | ✓ | |
| im (1109) | Absent | | ✓ | im (1159) | Absent | | ✗ |
| im (1110) | Absent | | ✗ | im (1160) | Absent | | ✓ |
| im (1111) | Absent | | ✗ | im (1161) | Absent | | ✗ |
| im (1112) | Absent | | ✓ | im (1162) | Absent | | ✗ |
| im (1113) | Absent | | ✓ | im (1163) | Present | ✗ | |
| im (1114) | Absent | | ✗ | im (1164) | Absent | | ✓ |
| im (1115) | Absent | | ✓ | im (1165) | Present | ✓ | |
| im (1116) | Absent | | ✗ | im (1166) | Absent | | ✓ |
| im (1117) | Absent | | ✓ | im (1167) | Present | ✓ | |
| im (1118) | Absent | | ✓ | im (1168) | Absent | | ✗ |
| im (1119) | Absent | | ✓ | im (1169) | Absent | | ✗ |
| im (1120) | Absent | | ✓ | im (1170) | Present | ✓ | |
| im (1121) | Absent | | ✓ | im (1171) | Absent | | ✓ |
| im (1122) | Absent | | ✓ | im (1172) | Absent | | ✗ |
| im (1123) | Absent | | ✓ | im (1173) | Absent | | ✗ |
| im (1124) | Absent | | ✓ | im (1174) | Absent | | ✓ |
| im (1125) | Absent | | ✓ | im (1175) | Present | ✓ | |
| im (1126) | Absent | | ✗ | im (1176) | Present | ✓ | |
| im (1127) | Absent | | ✓ | im (1177) | Present | ✓ | |
| im (1128) | Absent | | ✗ | im (1178) | Absent | | ✗ |
| im (1129) | Absent | | ✗ | im (1179) | Absent | | ✓ |
| im (1130) | Absent | | ✓ | im (1180) | Absent | | ✗ |
| im (1131) | Absent | | ✓ | im (1181) | Present | ✓ | |
| im (1132) | Absent | | ✓ | im (1182) | Present | ✓ | |
| im (1133) | Absent | | ✓ | im (1183) | Absent | | ✓ |
| im (1134) | Absent | | ✓ | im (1184) | Absent | | ✗ |
| im (1135) | Absent | | ✗ | im (1185) | Absent | | ✓ |
| im (1136) | Absent | | ✓ | im (1186) | Absent | | ✓ |
| im (1137) | Absent | | ✗ | im (1187) | Absent | | ✗ |
| im (1138) | Absent | | ✓ | im (1188) | Absent | | ✓ |
| im (1139) | Absent | | ✗ | im (1189) | Absent | | ✓ |
| im (1140) | Absent | | ✗ | im (1190) | Absent | | ✗ |
| im (1141) | Absent | | ✗ | im (1191) | Absent | | ✗ |
| im (1142) | Absent | | ✗ | im (1192) | Present | ✓ | |
| im (1143) | Absent | | ✓ | im (1193) | Present | ✗ | |
| im (1144) | Absent | | ✓ | im (1194) | Absent | | ✗ |
| im (1145) | Absent | | ✓ | im (1195) | Absent | | ✓ |
| im (1146) | Absent | | ✓ | im (1196) | Present | ✗ | |
| im (1147) | Absent | | ✓ | im (1197) | Present | ✓ | |
| im (1148) | Absent | | ✗ | im (1198) | Present | ✗ | |
| im (1149) | Absent | | ✓ | im (1199) | Absent | | ✗ |
| im (1150) | Absent | | ✓ | im (1200) | Present | ✓ | |
| **Sensitivity** | | **0.8741** | | **Specificity** | | **0.5574** | |